

ISTANBUL TECHNICAL UNIVERSITY ★ GRADUATE SCHOOL

**ANALYSIS AND DESIGN OF GENERAL TYPE-2 FUZZY LOGIC
CONTROLLERS**



Ph.D. THESIS

Ahmet SAKALLI

Department of Control and Automation Engineering

Control and Automation Engineering Programme

DECEMBER 2020

ISTANBUL TECHNICAL UNIVERSITY ★ GRADUATE SCHOOL

**ANALYSIS AND DESIGN OF GENERAL TYPE-2 FUZZY LOGIC
CONTROLLERS**



Ph.D. THESIS

**Ahmet SAKALLI
(504142102)**

Department of Control and Automation Engineering

Control and Automation Engineering Programme

Thesis Advisor: Assoc. Prof. Dr. Tufan KUMBASAR

DECEMBER 2020

İSTANBUL TEKNİK ÜNİVERSİTESİ ★ LİSANSÜSTÜ EĞİTİM ENSTİTÜSÜ

**GENEL TİP-2 BULANIK MANTIK KONTROLÖRLERİNİN ANALİZİ VE
TASARIMI**



DOKTORA TEZİ

**Ahmet SAKALLI
(504142102)**

Kontrol ve Otomasyon Mühendisliği Anabilim Dalı

Kontrol ve Otomasyon Mühendisliği Programı

Tez Danışmanı: Doç. Dr. Tufan KUMBASAR

ARALIK 2020

Ahmet SAKALLI, a Ph.D. student of ITU Graduate School student ID 504142102, successfully defended the thesis/dissertation entitled “ANALYSIS AND DESIGN OF GENERAL TYPE-2 FUZZY LOGIC CONTROLLERS”, which he prepared after fulfilling the requirements specified in the associated legislations, before the jury whose signatures are below.

Thesis Advisor : **Assoc. Prof. Dr. Tufan KUMBASAR**
Istanbul Technical University

Jury Members : **Prof. Dr. İbrahim EKSİN**
Istanbul Technical University

.....
Asst. Prof. Dr. İlker ÜSTOĞLU
Istanbul Technical University

.....
Prof. Dr. Şeref Naci ENGİN
Yildiz Technical University

.....
Asst. Prof. Dr. Gürkan SOYKAN
Bahcesehir University

Date of Submission : 03 November 2020

Date of Defense : 08 December 2020





To my family,



FOREWORD

I would like to thank my family who provides me a comfortable environment against the challenges that I faced during my thesis period. They have always shared the load from my back. Without their presence, I would have never found the courage to move forward and this thesis, which is dedicated to them, would not have been possible.

I would like to show my sincere gratitude to my thesis advisor Assoc. Prof. Dr. Tufan KUMBASAR for his continuous support, wise guidance, and immense knowledge. He provided a chance to work on the advanced topics of the fuzzy sets and systems in his hardworking research group.

I would like to thank the Scientific and Technological Research Council of Turkey (TUBITAK) for their support under the research project 118E807. I would like to also thank AVL Research and Engineering Turkey for their financial support.

December 2020

Ahmet SAKALLI



TABLE OF CONTENTS

	<u>Page</u>
FOREWORD	ix
TABLE OF CONTENTS.....	xi
ABBREVIATIONS	xiii
LIST OF TABLES	xv
LIST OF FIGURES	xvii
SUMMARY	xix
ÖZET.....	xxiii
1. INTRODUCTION.....	1
2. PRELIMINARIES ON FUZZY LOGIC CONTROLLERS	9
2.1 Type-1 and Interval Type-2 Fuzzy Sets	9
2.1.1 Type-1 fuzzy sets	9
2.1.2 Type-2 fuzzy sets	11
2.1.3 Interval type-2 fuzzy sets	13
2.2 Type-1 and Interval Type-2 Fuzzy Logic Controllers.....	18
2.2.1 Type-1 fuzzy logic controllers	18
2.2.2 Interval type-2 fuzzy logic controllers	19
2.3 From FLC Mapping to Fuzzy PID Controllers	23
2.4 Single-Input Fuzzy PID Controllers.....	25
2.4.1 Type-1 single-input fuzzy PID controllers.....	25
2.4.2 Interval type-2 single-input fuzzy PID controllers	26
2.5 Double-Input Fuzzy PID Controllers	27
2.5.1 Type-1 double-input fuzzy PID controllers	28
2.5.2 Interval type-2 double-input fuzzy PID controllers	28
2.6 Structural Design Recommendations	29
3. GENERAL TYPE-2 FUZZY LOGIC CONTROLLERS	33
3.1 Introduction	33
3.2 General Type-2 Fuzzy Sets	34
3.3 Secondary Membership Functions	41
3.3.1 Triangle secondary membership function.....	42
3.3.2 Trapezoid secondary membership function	44
3.4 Horizontal Slice Representation based on α -Planes	46
3.5 Computation of an α -Plane Output	53
3.6 Aggregation of α -Planes towards Fuzzy Logic Controller Output	54
3.7 Illustrative Numerical Example	55
4. TOWARDS SYSTEMATIC DESIGN OF GENERAL TYPE-2 FUZZY LOGIC CONTROLLERS.....	61
4.1 Interactions between Fuzzy Logic Controllers.....	61
4.2 Novel Representation of Trapezoid Secondary Membership Function	63
4.3 Structural Design Recommendations and Design Parameters	69
5. ANALYSIS AND DESIGN OF SHAPE DESIGN PARAMETER.....	75

5.1 Structural Change Analysis	75
5.2 Shape Analyses of Control Curves / Control Surfaces.....	76
5.2.1 Baseline FLCs used in shape analyses	78
5.2.2 Control curves of GT2-SFLCs	84
5.2.3 Control surfaces of GT2-DFLCs.....	88
5.3 Comments and Suggestions on Shape Design Parameter	93
5.4 Systematic Tuning of Shape Design Parameter	94
5.5 Online Scheduling Mechanisms for Shape Design Parameter	96
6. ANALYSIS AND DESIGN OF SENSITIVITY DESIGN PARAMETER ...	101
6.1 Sensitivity Analyses of Control Curves / Control Surfaces	101
6.2 Comments and Suggestions on the Sensitivity Design Parameter	107
6.3 Tuning of Sensitivity Design Parameter.....	108
7. SIMULATION STUDIES AND REAL-TIME APPLICATIONS.....	115
7.1 Simulation Study on a Second-Order Nonlinear System	115
7.1.1 Simulation environment	115
7.1.2 Controller design	116
7.1.3 Simulation results.....	117
7.2 Real-Time Application on Parrot Mambo Drone	118
7.2.1 Experimental setup.....	118
7.2.2 Design of the shape design parameter	119
7.2.3 Comments on the control surfaces of the designed DFCLCs	121
7.2.4 Design of the sensitivity design parameter	125
7.2.5 Experimental results	126
8. CONCLUSIONS.....	131
REFERENCES	135
CURRICULUM VITAE	141

ABBREVIATIONS

CC	: Control Curve
CS	: Control Surface
CT	: Computation Time
DFLC	: Double-Input Fuzzy Logic Controller
DFPID	: Double-Input Fuzzy PID
FLC	: Fuzzy Logic Controller
FLS	: Fuzzy Logic System
FOU	: Footprint of Uncertainty
FPID	: Fuzzy PID
FS	: Fuzzy Set
IT2	: Interval Type-2
GT2	: General Type-2
KM	: Karnik-Mendel
LMF	: Lower Membership Function
MAE	: Mean of Absolute Errors
MF	: Membership Function
MVE	: Maximum Value of Errors
NR	: Noise Ratio
NTE	: Normalized Total Energy
PID	: Proportional-Integral-Derivative
SFLC	: Single-Input Fuzzy Logic Controller
SFPID	: Single-Input Fuzzy PID
SM	: Scheduling Mechanism
SMF	: Secondary Membership Function
TSK	: Takagi-Sugeno-Kang
T1	: Type-1
T2	: Type-2
UMF	: Upper Membership Function
α -T2-FLC	: α -plane associated T2-FLC



LIST OF TABLES

	<u>Page</u>
Table 2.1 : Design parameters of T1-SFLCs.....	30
Table 2.2 : Design parameters of T1-DFLCs.....	31
Table 2.3 : Design parameters of IT2-SFLCs.	31
Table 2.4 : Design parameters of IT2-DFLCs.....	31
Table 2.5 : Summary of T1 and IT2 FLC design parameters.	32
Table 2.6 : Design parameters of T1-FPID and IT2 FPID controllers.....	32
Table 3.1 : Rule base of the illustrative GT2-FLC.....	55
Table 3.2 : Calculation steps of illustrative GT2-FLC.....	57
Table 4.1 : Design parameters of GT2-SFLCs.....	72
Table 4.2 : Design parameters of GT2-DFLCs.	72
Table 4.3 : Summary of T1, IT2, and GT2 FLC design parameters.	73
Table 5.1 : Rule base of baseline T1-SFLC.	79
Table 5.2 : Rule base of baseline IT2-SFLCs.	79
Table 5.3 : Rule base of baseline T1-DFLC.	82
Table 5.4 : Rule base of baseline IT2-DFLCs.....	82
Table 5.5 : Performance measures of shape analyses for GT2-SFLCs.....	87
Table 5.6 : Performance measures of shape analyses for GT2-DFLCs.	92
Table 5.7 : Tuning steps of the shape design parameter.	95
Table 5.8 : Design steps of the online SM-1.....	97
Table 5.9 : Rule table of fuzzy mapping of online SM-2.....	99
Table 6.1 : Sensitivity measures for GT2-SFLCs.	104
Table 6.2 : Sensitivity measures for GT2-DFLCs.....	106
Table 6.3 : Tuning algorithm of the sensitivity design parameter.	110
Table 7.1 : Performance measures of T1, IT2, and GT2 FLCs.....	118
Table 7.2 : Performance measures of the designed CSs of the DFLCs.	124
Table 7.3 : Performance measures of T1, IT2, and GT2 FLCs.....	126



LIST OF FIGURES

	<u>Page</u>
Figure 2.1 : Triangle T1-FS.	10
Figure 2.2 : Trapezoid T1-FS.....	11
Figure 2.3 : Gaussian T1-FS.	12
Figure 2.4 : Triangle IT2-FS.	14
Figure 2.5 : Trapezoid IT2-FS.	15
Figure 2.6 : Gaussian IT2-FS.....	16
Figure 2.7 : Secondary grade examples of T1 and T2 fuzzy sets.	17
Figure 2.8 : System block diagram of type-1 fuzzy logic controllers.....	18
Figure 2.9 : System block diagram of interval type-2 fuzzy logic controllers.....	20
Figure 2.10 : A triangle IT2 membership function for $M = 0.2$ setting.	22
Figure 2.11 : A triangle IT2 membership function for $M = 0.5$ setting.	22
Figure 2.12 : A triangle IT2 membership function for $M = 0.8$ setting.	22
Figure 2.13 : A triangle IT2 membership function for $M = 1$ setting.	23
Figure 2.14 : Closed-loop control block diagram of single-input FPID controllers.	25
Figure 2.15 : Closed-loop block diagram of double-input FPID controllers.	27
Figure 3.1 : System block diagram of general type-2 fuzzy logic controllers.....	33
Figure 3.2 : A triangle GT2-FS employing triangle SMF.....	35
Figure 3.3 : A triangle GT2-FS employing triangle SMF.....	36
Figure 3.4 : A trapezoid GT2-FS employing trapezoid SMF.	37
Figure 3.5 : A trapezoid GT2-FS employing trapezoid SMF.	38
Figure 3.6 : A Gaussian GT2-FS employing Gaussian SMF.....	39
Figure 3.7 : A Gaussian GT2-FS employing Gaussian SMF.....	40
Figure 3.8 : A triangle SMF and its apex point.....	43
Figure 3.9 : A triangle SMFs with different apex point settings.....	43
Figure 3.10 : A trapezoid SMF and its support and core points.	45
Figure 3.11 : A trapezoid SMF and its support and core points.	46
Figure 3.12 : An α -plane of triangle GT2-FS employing triangle SMF.	48
Figure 3.13 : An α -plane of trapezoid GT2-FS employing trapezoid SMF.....	49
Figure 3.14 : Illustration of varying FOU sizes for different α -planes.	51
Figure 3.15 : Illustration of a horizontal-sliced GT2-FS by α -plane levels.	52
Figure 3.16 : Block diagram of α -plane associated type-2 fuzzy logic controllers.	53
Figure 3.17 : Block diagram of the aggregation of α -plane based horizontal slices.	54
Figure 3.18 : Block diagram of the aggregation of α -plane based horizontal slices.	56
Figure 3.19 : Illustration of (a) antecedent MFs, (b) SMFs, (c) type-reduced sets... ..	58
Figure 4.1 : Inclusions and interactions of fuzzy sets.	61
Figure 4.2 : Illustration of novel representation of trapezoid SMF.	63
Figure 4.3 : Trapezoid SMF parameters for the design setting $\theta = -2$	66
Figure 4.4 : Trapezoid SMF parameters for the design setting $\theta = -1.5$	66
Figure 4.5 : Trapezoid SMF parameters for the design setting $\theta = -1$	66
Figure 4.6 : Trapezoid SMF parameters for the design setting $\theta = -0.5$	67

Figure 4.7 : Trapezoid SMF parameters for the design setting $\theta = 0$.	67
Figure 4.8 : Trapezoid SMF parameters for the design setting $\theta = 0.5$.	67
Figure 4.9 : Trapezoid SMF parameters for the design setting $\theta = 1$.	68
Figure 4.10 : Trapezoid SMF parameters for the design setting $\theta = 1.5$.	68
Figure 4.11 : Trapezoid SMF parameters for the design setting $\theta = 2$.	68
Figure 4.12 : Effect of shape design parameter on SMF shapes of GT2-FLCs.	70
Figure 5.1 : Baseline T1-SFLC and baseline IT2-SFLC employing FOU-1.	80
Figure 5.2 : Baseline T1-SFLC and baseline IT2-SFLC employing FOU-2.	81
Figure 5.3 : Baseline T1-DFLC and baseline IT2-DFLC employing FOU-3.	83
Figure 5.4 : Baseline T1-DFLC and baseline IT2-DFLC employing FOU-4.	84
Figure 5.5 : Effect of shape design parameter on CCs of GT2-SFLCs with FOU-1.	85
Figure 5.6 : Effect of shape design parameter on CCs of GT2-SFLCs with FOU-2.	86
Figure 5.7 : Effect of shape design parameter on CSs of GT2-DFLCs with FOU-3.	88
Figure 5.8 : Effect of shape design parameter on CSs of GT2-DFLCs with FOU-4.	89
Figure 5.9 : CS differences between GT2 and T1 FLCs with FOU-3.	90
Figure 5.10 : CS differences between GT2 and IT2 FLCs with FOU-3.	90
Figure 5.11 : CS differences between GT2 and T1 FLCs with FOU-4.	91
Figure 5.12 : CS differences between GT2 and IT2 FLCs with FOU-4.	91
Figure 5.13 : Surface of fuzzy mapping of online SM-2.	99
Figure 6.1 : Effect of sensitivity design parameter on CCs of GT2-SFLCs.	102
Figure 6.2 : CC differences between UC and UP for $P = 2, 3, 4, 10, 25, 100$.	103
Figure 6.3 : Effect of sensitivity design parameter on GT2-FLCs' ε_{PC} values.	104
Figure 6.4 : CC differences between $UP + 1$ and UP for $P = 2, 3, 4, 10, 25, 100$.	105
Figure 6.5 : Effect of sensitivity design parameter on GT2-FLCs' ε_{PP+1} values.	106
Figure 6.6 : Variation of MAE measure with respect to the P values.	111
Figure 6.7 : Variation of execution time with respect to the P values.	112
Figure 6.8 : Variation of MVE measure with respect to the P values.	112
Figure 6.9 : Output differences of GT2-FLCs with different P values.	113
Figure 7.1 : Control performances of T1, IT2, and GT2 FLCs.	117
Figure 7.2 : Illustration of Parrot Mambo drone.	119
Figure 7.3 : The CSs of the designed T1, IT2, and GT2 DFLCs.	121
Figure 7.4 : The CS differences between the designed T1, IT2, and GT2 DFLCs.	121
Figure 7.5 : OP r1: CS differences between SM-1 and (a) T1 (b) IT2 (c) GT2.	122
Figure 7.6 : OP r2: CS differences between SM-1 and (a) T1, (b) IT2, (c) GT2.	122
Figure 7.7 : OP r3: CS differences between SM-1 and (a) T1, (b) IT2, (c) GT2.	123
Figure 7.8 : OP r1: CS differences between SM-2 and (a) T1, (b) IT2, (c) GT2.	123
Figure 7.9 : OP r2: CS differences between SM-2 and (a) T1, (b) IT2, (c) GT2.	123
Figure 7.10 : OP r3: CS differences between SM-2 and (a) T1, (b) IT2, (c) GT2.	123
Figure 7.11 : Real-time experiment results of the T1, IT2 and GT2 DFLCs.	127
Figure 7.12 : Real-time experiment results of the GT2 DFLCs for r1.	128
Figure 7.13 : Real-time experiment results of the GT2 DFLCs for r2.	129
Figure 7.14 : Real-time experiment results of the GT2 DFLCs for r3.	129

ANALYSIS AND DESIGN OF GENERAL TYPE-2 FUZZY LOGIC CONTROLLERS

SUMMARY

This thesis presents new interpretations on the design parameters of the general type-2 fuzzy logic controllers by investigating their internal structures, proposes novel systematic design approaches for the general type-2 fuzzy logic controllers based on comprehensive and comparative analyses, and validates theoretical findings as well as proposed tuning methods via simulation and real-time experiments.

The fuzzy systems have been successfully realized in a wide variety of engineering areas such as controls, image processing, data processing, decision making, estimation, modeling, and robotics. The fuzzy logic systems provide complex mappings from inputs to outputs, and this benefit usually results in better performances in comparison to non-fuzzy counterparts. Due to this, the fuzzy logic controllers have been applied to numerous challenging control problems for decades. Nowadays, more attention has been given to a new research direction of the fuzzy sets and systems, the general type-2 fuzzy logic controllers, which is the main motivation of this thesis.

The internal structures of a class of Takagi-Sugeno-Kang type fuzzy logic controllers are first examined in detail. In this context, three fuzzy logic controller types (type-1, interval type-2, and general type 2) and two kinds of controller configurations (single-input and double-input) are considered. The baseline controllers, i.e. type-1 and interval type-2 fuzzy logic controllers, are presented in the preliminaries section. The fuzzy sets, fuzzy relations, fuzzy rules, fuzzy operators, and PID forms of these fuzzy logic controllers are explained in detail. The design assumptions and design parameters are given, also the most common design approaches are listed. Afterward, the general type-2 fuzzy sets and the general type-2 fuzzy logic controllers are presented. The general type-2 fuzzy logic controllers are described with α -plane associated horizontal slices because the α -plane representation provides useful advantages on the handling of the secondary membership function of the general type-2 fuzzy sets and the calculation of the general type-2 fuzzy logic controller output. It is shown that the α -plane based general type-2 fuzzy logic controller output calculation is accomplished through the well-known interval type-2 fuzzy logic computations. The secondary membership functions are further detailed in terms of their mathematical definitions and design options.

The structure analysis on the general type-2 fuzzy sets shows the interactions between non-fuzzy, type-1 fuzzy, interval type-2 fuzzy, and general type-2 fuzzy sets happen in the secondary membership function. It is shown that the general type-2 fuzzy logic controller can easily transform into interval type-2 fuzzy, or type-1 fuzzy counterparts based on the secondary membership function definitions. As an outcome of this structural analysis, a new representation of the trapezoid secondary membership function is proposed based on a novel parameterization of the parameters that form the trapezoid shape. It is shown that the parameterized trapezoid secondary membership

function is capable to construct trapezoid, triangle, interval, and singleton shapes so that the general type-2 fuzzy logic controllers are further capable to transform into interval type-2 fuzzy, or type-1 fuzzy counterparts. It is also shown that the proposed parameterization of the trapezoid secondary membership functions allows designing the control curves/surfaces of the general type-2 fuzzy logic controllers with a single tuning parameter. Moreover, the structural design suggestions are presented not only to construct fuzzy controllers in a straightforward manner but also to ease the design of the controllers with few design parameters. The design parameters of the general type-2 fuzzy logic controllers are grouped as the shape and the sensitivity design parameters with respect to their effects on the accuracy and the shape of the resulting fuzzy mapping. Accordingly, the tuning parameter of the secondary membership functions and the total number of α -planes are interpreted and as the sensitivity and shape design parameters, respectively.

The shape analyses of the general type-2 fuzzy logic controllers show the effects of the proposed shape design parameter on the control curves/surfaces. In this context, the resulting fuzzy mappings of single input and double input general type-2 fuzzy logic controller structures are compared for various design settings of the shape design parameter. The comparative analyses provide interpretable and practical explanations on the potential advances of the shape design parameter. Based on the shape analyses, novel design approaches are proposed to tune the shape design parameter in a systematic way. In this context, it is suggested constructing the general type-2 fuzzy logic controllers over their type-1 and interval type-2 baselines and tuning them via the shape design parameter by providing a tunable tradeoff between robustness and performance. Therefore, it is aimed to combine benefits of baseline type-1 (relatively more aggressive control curves/surfaces better performance measures) and interval type 2 (relatively smoother control curves/surfaces, better robustness measures) fuzzy logic controllers. To enhance the control performance, two scheduling mechanisms are also proposed for online-tuning of the shape design parameter with respect to the steady-state operating points as well as transient-state dynamics.

The sensitivity analyses of the general type-2 fuzzy logic controllers show the effects of the proposed sensitivity design parameter on the accuracy of the control curves/surfaces. In this context, the resulting fuzzy mappings of single input and double input general type-2 fuzzy logic controller structures are also compared for various design settings of the sensitivity design parameter. The comparative sensitivity analyses show interpretable and practical explanations of the sensitivity design parameter in terms of calculation accuracy and computation burden. Therefore, it is suggested tuning the sensitivity design parameter by considering the limitations of hardware components such as resolution and processing speed. To accomplish the design in accordance with a tradeoff between sensitivity and computational time, a novel iterative algorithm is proposed to tune the sensitivity design parameter.

The simulation and real-time experimental control studies validate the proposed design recommendations, systematic design approaches, and tuning methods for the general type-2 fuzzy logic controllers on benchmark control systems. In these control studies, the general type-2 fuzzy logic controllers are designed based on the proposed design methods. In order to show the performance improvements on the control systems, the general type-2 fuzzy logic controllers (tuned either online or offline) are compared with type-1 fuzzy and interval type-2 fuzzy counterparts. The performance measures clearly show that the online-tuned general type-2 fuzzy logic controllers outperform all general type-2, interval type-2, and type-1 counterparts on account of the proposed

scheduling mechanisms over the proposed systematic design rules. The results also show that the systematic design of the general type-2 fuzzy logic controllers is simply accomplished by following the proposed tuning steps of the shape and sensitivity design parameters.





GENEL TİP-2 BULANIK MANTIK KONTROLÖRLERİNİN ANALİZİ VE TASARIMI

ÖZET

Bu tez; bulanık kontrolörlerin iç yapılarını analiz ederek genel tip-2 bulanık mantık kontrolörlerinin tasarım parametreleri üzerine yeni yorumlar sunmakta; genel tip-2 bulanık mantık kontrolörler için geniş kapsamlı ve karşılaştırmalı analizlere dayanan yeni sistematik tasarım yaklaşımları önermekte; elde edilen teorik bulgular ve önerilen ayarlama yöntemlerini benzetim ve gerçek zamanlı deneyler ile doğrulamaktadır.

Bulanık mantık tabanlı sistemler, görüntü işleme, veri işleme, kontrol, karar verme, öngörü, tahmin, robotik ve modelleme gibi birçok mühendislik alanında başarıyla uygulanmaya devam etmektedir. Bulanık mantık sistemleri, girişleri ve çıkışları arasında gelişmiş üst düzey bir haritalama sağlamaktadır ve bu durum genellikle bulanık olmayan eşdeğerlerine kıyasla daha iyi performanslar ile sonuçlanmaktadır. Bu sebeple, bulanık mantık kontrolörleri, zorlu kontrol problemlerinde sıklıkla uygulanmıştır. Uzun yıllardan beri tip-1 bulanık mantık kontrolörleri birçok farklı uygulamada birçok farklı şekillerde uygulanmıştır. Yakın zamanda gösterilmiştir ki belirsizlikleri ve doğrusal olmayan sistemlerin ele alınmasında aralık değerli tip-2 bulanık mantık kontrolörler daha iyi sonuçlar vermektedir. Aralık değerli tip-2 bulanık mantık kontrolörlerinin bu kazanımı, aralık değerli tip-2 üyelik fonksiyonlarında yer alan belirsizlerin izdüşümü elamanının getirdiği yeni tasarım parametreleri, serbestlik derecesi ve geniş tasarım esnekliği ile açıklanmıştır, çünkü aralık değerli tip-2 üyelik fonksiyonları, genel tip-2 bulanık kümelerin özel bir hali olan aralık değerli tip-2 bulanık kümeler ile tanımlanmıştır. Günümüzde ise, bu tezin de ana motivasyonu olan, bulanık kümeler ve bulanık sistemlerin yeni bir araştırma alanı olan genel tip-2 bulanık mantık kontrolörlerine, daha fazla ilgi gösterilmektedir.

Bu tez kapsamında Takagi-Sugeno-Kang tipi bulanık mantık kontrolörlerinin bir sınıfının iç yapıları detaylı bir şekilde incelenmiştir. Bu bağlamda, üç farklı bulanık mantık kontrolör tipi (tip-1, aralık değerli tip-2, ve genel tip-2) ve iki farklı kontrolör yapısı (tek girişli ve iki girişli) ele alınmıştır. Temel bulanık mantık kontrolörleri, diğer bir deyişle tip-1 ve aralık değerli tip-2 bulanık mantık kontrolörleri ön bilgiler kısmında sunulmuştur. Bu temel bulanık mantık kontrolörlerinin bulanık kümeleri, bulanık ilişkileri, bulanık kuralları, bulanık operatörleri ve PID kontrolör formları detaylı bir şekilde açıklanmıştır. Tasarım varsayımları ve tasarım parametreleri detaylıca verilmiş ve en çok kullanılan tasarım yöntemleri listelenmiştir. Daha sonra genel tip-2 bulanık kümeler ve genel tip-2 bulanık mantık kontrolörleri sunulmuştur. Genel tip-2 bulanık mantık kontrolörleri α -düzlemi ile ilişkili yatay dilimler ile ifade edilmiştir, çünkü α -düzlemi gösterimi, genel tip-2 bulanık kümelerin ikincil üyelik fonksiyonunun ve genel tip-2 bulanık mantık kontrolörünün çıkış hesaplanmasının ele alınmasında birçok avantaj sunmaktadır. Ayrıca α -düzlemi tabanlı genel tip-2 bulanık mantık kontrolörü çıkış hesaplaması, iyi bilinen (ve literatürde sıklıkla kullanılan) aralık değerli tip-2 bulanık mantık kontrolörüne ait hesaplamalar ile yapılabildiği

gösterilmiştir. Ayrıca genel tip-2 bulanık kümelerinin ikincil üyelik fonksiyonları da tanımları ve tasarım seçenekleri bakımından detaylandırılmıştır.

Genel tip-2 bulanık kümelerinin yapı analizi, bulanık olmayan, tip-1 bulanık, aralık değerli tip-2 bulanık ve genel tip-2 bulanık kümeler arası etkileşimlerin (veya bir sınıftan diğerine geçişler) ikincil üyelik fonksiyonunda gerçekleştiğini göstermiştir. Genel tip-2 bulanık mantık kontrolörlerinin, ikincil üyelik fonksiyonu tanımlarına bağlı olarak, kolaylıkla aralık değerli tip-2 bulanık mantık veya tip-1 bulanık mantık kontrolörlere dönüşebilmektedir. Bu genel tip-2 bulanık kümelerinin yapı analizinin bir çıktısı olarak, yamuk şeklini oluşturan parametrelerin yeni özgün bir haritalama (diğer bir ifade ile yamuk tasarım parametrelerini eşleme) ile yamuk ikincil üyelik fonksiyonlarının yeni gösterimi önerilmiştir. Parametreleri eşlenmiş ikincil üyelik fonksiyonu yamuk, üçgen, aralık-değerli (dikdörtgen) ve tekil şekiller oluşturabildiği gösterilmiştir, ki bu sayede, genel tip-2 bulanık mantık kontrolörlerinin de aralık değerli tip-2 bulanık ve tip-1 bulanık mantık kontrolör eşdeğerlerine dönüşebildiği gösterilmiştir. Ayrıca, önerilen parametre eşlemeli ikincil üyelik fonksiyonları ile genel tip-2 bulanık mantık kontrolörlerinin kontrol eğrileri/yüzeyleri tasarımının tek bir ayarlama parametresi ile mümkün olduğu gösterilmiştir. Bu yapısal tasarım önerileri, sadece bulanık mantık kontrolörlerini açık bir biçimde oluşturmak için değil aynı zamanda daha az parametre ile bu kontrolörlerin tasarımının kolaylaştırma amacıyla da sunulmuştur. Genel tip-2 bulanık mantık kontrolörlerinin temel tasarım parametreleri, bu tasarım parametrelerin değerleri ile oluşacak olan bulanık giriş-çıkış haritalaması üzerindeki doğruluk (veya hassaslık) ve bulanık yüzey şekli üzerindeki etkilerine bağlı olarak, hassaslık ve şekil parametreleri olarak gruplanmıştır. Bu nedenle, α -düzlemlerinin toplam sayısı ve ikincil üyelik fonksiyonun tasarım parametresi, sırasıyla genel tip-2 bulanık mantık kontrolörlerinin hassaslık ve şekil tasarım parametreleri olarak adlandırılmıştır.

Genel tip-2 bulanık mantık kontrolörlerinin şekil analizleri, önerilen şekil tasarım parametresinin kontrol eğrileri/yüzeyleri üzerindeki etkilerini göstermektedir. Bu bağlamda, tek girişli ve iki girişli genel tip-2 bulanık mantık kontrolör yapılarının çıkışı olan bulanık haritalar, şekil tasarım parametresinin farklı tasarım seçenekleri için karşılaştırılmıştır. Önerilen şekil tasarım parametresi $[-2, 2]$ aralığında tanımlanmıştır ve karşılaştırmalı analizlerde adım aralıkları 0.5 olacak şekilde $[-2, 2]$ değer aralığında dokuz nokta seçilmiştir. Bu karşılaştırmalı analizler, genel tip-2 bulanık mantık kontrolörlerinin şekil tasarım parametresinin olası getirileri hakkında yorumlanabilir ve pratik açıklamalar sunmuştur. Bu analizler ışığında, genel tip-2 bulanık mantık kontrolörlerinin şekil tasarım parametresini sistematik bir şekilde ayarlamak için özgün tasarım yaklaşımları önerilmiştir. Bu bağlamda, genel tip-2 bulanık mantık kontrolörlerinin, temel tip-1 ve temel aralık değerli tip-2 eşdeğerleri üzerinden oluşturulması ve şekil tasarım parametresinin, sistemi performansı ve dayanıklılığı arasındaki ayarlanabilir bir dengeye bağlı olarak seçilmesi önerilmiştir. Böylece temel tip-1 (göreceli agresif kontrol eğrisine/yüzeyine sahip, performans ölçütleri yüksek) ve temel aralık değerli tip-2 (göreceli yumuşak kontrol eğrisine/yüzeyine sahip, dayanıklılık ölçütleri yüksek) bulanık mantık kontrolörlerinin getirilerinden faydalanılması amaçlanmıştır. Ayrıca, kontrol sisteminin performansını arttırmak amacıyla, şekil tasarım parametresinin sürekli hal çalışma noktaları ve sistemin geçici hal dinamiklerine bağlı olarak çevrimiçi güncellenmesi için iki farklı programlama mekanizması da önerilmiştir.

Genel tip-2 bulanık mantık kontrolörlerinin hassasiyet analizleri, önerilen hassasiyet tasarım parametresinin kontrol eğrileri/yüzeyleri üzerindeki hesaplama doğruluğunu

göstermektedir. Bu bağlamda, tek girişli ve iki girişli genel tip-2 bulanık mantık kontrolör yapılarının çıkışı olan bulanık haritalar, hassasiyet tasarım parametresinin farklı tasarım seçenekleri için karşılaştırılmıştır. Bu karşılaştırmalı analizler, genel tip-2 bulanık mantık kontrolörlerinin hassasiyet tasarım parametresi hakkında, hesaplama doğruluğu ve hesaplama yükü bakımından, yorumlanabilir ve pratik açıklamalar sunmuştur. Analizler ışığında, hassasiyet tasarım parametresinin sistemdeki donanın bileşenlerin ölçekleme değeri ve işlem yapma hızı gibi yapısal limitleri göz önüne alınarak ayarlanması önerilmiştir. Bu bağlamda, hesaplama doğruluğu ve hesaplama zamanı arasındaki dengeye bağlı olarak genel tip-2 bulanık mantık kontrolörlerinin hassasiyet tasarım parametresini ayarlamak için yeni iteratif bir ayarlama algoritması önerilmiştir.

Benzetim ve gerçek zamanlı deneysel kontrol çalışmaları, bu tez kapsamında önerilen genel tip-2 bulanık mantık kontrolörleri için sunulan tasarım varsayımları, sistematik tasarım yaklaşımları ve ayarlama yöntemlerini, kıyaslamaya uygun deneysel kontrol sistemleri üzerinde onaylamaktadır. Bu çalışmalarda, genel tip-2 bulanık mantık kontrolörleri tez kapsamında önerilen tasarım yöntemlerinde verilen adımlara göre oluşturulmuştur. Kontrol sisteminin performans iyileştirmelerini açıkça gösterebilmek amacıyla, çevrimiçi veya çevrimdışı ayarlanan genel tip-2 bulanık mantık kontrolörleri, tip-1 bulanık mantık ve aralık değerli tip-2 bulanık mantık eşdeğerleri ile karşılaştırılmıştır. Performans ölçümleri, çevrimiçi ayarlanan genel tip-2 bulanık mantık kontrolörlerinin, önerilen sistematik tasarım kurallarına göre belirlenen çevrimiçi programlama mekanizmaları sayesinde tüm genel tip-2, aralık tipi-2 ve tip-1 benzerlerinden daha iyi performanslar gösterdiğini göstermiştir. Ayrıca elde edilen bu sonuçlar, genel tip-2 bulanık mantık kontrolörlerinin tasarımının sistematik bir şekilde, sadece şekil ve hassasiyet tasarım parametreleri vasıtasıyla önerilen ayarlama adımlarının izlenmesiyle gerçekleştirilebildiğini göstermektedir.



1. INTRODUCTION

Fuzzy Logic Controllers (FLCs) have been successfully implemented in numerous engineering problems and applications including control, robotics, image processing, decision making, estimation, and modeling for more than 50 years [1-76]. A FLC is a complex system that provides a mapping from its input(s) to its output(s) based on fuzzy rules and fuzzy relations. That is why it is also called as Fuzzy Logic System (FLS) by researchers. A FLC computes Fuzzy Sets (FSs) instead of ordinary sets. The pioneering study on the FSs and their notations was introduced in 1965 [1] and the first study on the fuzzy rules and the FLC structure was presented in [2]. The pioneer industrial application of FLCs was accomplished in 1974. In this study, the linguistic control rules of a skilled human operator are expressed by a fuzzy inference [3-4]. The early fuzzy literature (in the 80s and 90s) focused on the theory of fuzzy logic, fuzzy sets, and fuzzy systems as well as fuzzy applications (in the 2000s) [3-21]. These studies were performed with ordinary FSs and FLCs, which are now called as Type-1 (T1) FLCs in today's fuzzy literature. After the 2000s, the fuzzy community began working on Interval Type-2 (IT2) FLCs as an extension of ordinary T1-FSs and T1-FLCs, then in the 2000s and early 2010s, the fuzzy research interest dominantly focused on the theory of IT2-FLCs and real-time applications [22-59]. Nowadays, researchers have given more attention to a new research direction of the fuzzy sets and systems, General Type-2 (GT2) FLCs, which is the main motivation of this thesis.

For more than four decades, T1-FLCs have been popular in fuzzy control applications and T1-FLCs have taken part in many studies [3-21]. In fuzzy literature, the most popular fuzzy systems are Mamdani fuzzy systems [2-3] and Takagi-Sugeno-Kang fuzzy systems [5-6]. These FLC structures are characterized by the same fuzzy IF-THEN rules and the same FSs at the antecedent part, on the other hand, they differ in the part of consequents. As mentioned in [7], a Mamdani fuzzy system uses Zadeh rules [2] and Mamdani implications [3] in computations and employs FSs sets at the consequent part, whereas a Takagi-Sugeno-Kang (TSK) system uses singletons [5] or mathematical functions [6] at the consequent part. The TSK fuzzy systems are one of

the most well-known fuzzy structures and they have been widely used in control applications as the design and analysis of the fuzzy control system is relatively more interpretable than Mamdani fuzzy systems. In this context, numerous fuzzy control and fuzzy modeling papers implemented TSK fuzzy systems for various engineering problems associated with the systems where uncertainties and nonlinearities exist [7-11]. In fuzzy control problems, the PID type fuzzy controllers, or simply Fuzzy PID (FPID) controllers are generally preferred, since, from the input-output mapping point of view, the FPID controllers are equivalent to conventional PID controllers [9-12]. The FPID controllers can be designed in many ways that the fuzzy inference either generates the control signal (which is applied to the system) [14] or tunes the PID controller gains [15]. In T1 fuzzy literature, there are also various studies that employ / present online self-tuning structures with heuristic update rules [16-18], auto-tuning mechanisms for controller design [19], and online scheduling or self-tuning structures via optimization [19-21].

In the past decades, the fuzzy research has been mainly focused on IT2-FLCs, although the concept of Type-2 (T2) FSs were first introduced in 1975 [22]. Once the T1-FLCs have reached a high level of research maturity, then the popularity of T2-FSs starts increasing and this interest is sustained for more than 20 years [7]. A complete overview of the IT2 fuzzy systems (e.g. fuzzy sets, inference, operations) was first introduced in [23] and the theory and design were further investigated in [24-25]. The first IT2 fuzzy control applications [26-28] demonstrated that T1-FLCs might have limitations on the handling uncertainties and nonlinearities while IT2-FLCs are better to handle uncertainties and nonlinearities. This limitation is mostly occurred due to crisp membership grade values. It has been stated that T2-FSs are very useful in situations where the determination of an accurate membership function is relatively difficult with a T1 fuzzy set [7, 29]. The IT2-FLCs have been also successfully implemented in various simulation studies and real-time control applications [26-45]; autonomous mobile robot control [26, 37], liquid-level control of coupled tank process [27, 28], linear system control [32, 33, 38], pH control of neutralization process [34-36], position control of magnetic levitation system [39], load frequency control of power system [40], nonlinear system control [41, 42], velocity control of electric vehicle [43], position control of spherical robot control [44], control of flying drone [45].

In the first years of the IT2-FLC studies, there were some theoretical drawbacks for applications; the computational complexity (or computational burden), and the lack of complete understanding of the internal structure of the IT2-FLCs [7, 30-31]. The computational burden bottleneck has been addressed by the type-reduction algorithms/methods. The most known algorithm is Karnik-Mendel (KM) algorithm [46]. In the KM algorithm and its enhancements [7, 47-48], the type reduced set of the IT2-FLC (lower and upper bound of interval output set) is calculated based on the optimal left and right switching points which are determined iteratively [7]. Although there are many approximations of the KM-based type-reduction algorithm, the KM-based algorithms are the most popular type-reduction and defuzzification methods, since KM algorithms calculate precise IT2-FLC outputs [7, 49]. In order to answer the lack of a deeper understanding of the IT2-FLCs, the researchers have investigated the internal structure, stability, and analytic derivations of IT2-FLCs. The internal structure of the IT2-FLCs is also investigated in further studies by providing easier representations [50], IT2-FS mathematics (based on T1-FS mathematics) [51], new geometric representations [52], notation similarities between IT2-FLC and standard mathematics [53], the relationship between FSs [54], application-independent perspectives [55] as well as comprehensive fuzzy logic books [7, 30, 31]. The stability of the IT2 fuzzy systems is also examined in various studies [41, 56, 57]. Moreover, the analytical derivations are investigated in various studies; for example, the closed-form formulation of the single input fuzzy system was determined in [36] and [41], the controller gains around the origin were obtained in [38, 43] and [58, 59] derived IT2-FLC outputs by dividing the input space to several sub-regions.

The main superiority of the IT2-FLCs is preserved in the Fingerprint of Uncertainty (FOU) in their antecedent Membership Functions (MFs) as it covers uncertainties and nonlinearities in the secondary membership function layer [7, 30-31]. It has been illustrated that IT2-FLCs are better to handle uncertainties and nonlinearities in comparison to T1-FLC counterparts [26-33]. It is demonstrated that IT2-FLCs can achieve significant control performance improvements in comparison to their T1-FLC counterpart via a FOU design by extending T1-MFs into IT2-MFs [33, 41, 42]. It has been also shown that the IT2-FLCs are potentially more robust than T1 counterparts, as their Control Curves (CCs) / Control Surfaces (CSs) are usually smooth around the steady-state [26-28, 32-33, 41-45]. In [41] (for single input structures) and [43, 44]

(for double input structures), it is shown that both smooth or aggressive CCs/CSs can be generated by tuning the parameters that define the FOU. These performance and robustness improvements of IT2-FLCs occur due to the extra degree of freedom provided by the FOU in the antecedent MFs that are defined by IT2-FSs. Thus, the FOU parameters are categorized as the design parameters of the IT2-FLCs.

Recently, in a wider perspective, [55] have sought an answer to the research question: “Why does improved performance occur as one goes from crisp, to T1, to IT2, to GT2 fuzzy systems?”. It has stated that the performance improvement usually happens when structure changes from crisp system, to T1 fuzzy systems, and to IT2 fuzzy systems, by introducing three kinds of partitions: (1) Uncertainty partitions to distinguish T1-FSs from crisp sets, and IT2-FSs from T1-FSs; (2) First-and second-order rule partitions that are results of uncertainty partitions and are associated with the rules that fired in corresponding regions of the state space and the changes in their mathematical formulae within those regions; and (3) Novelty partitions that can only occur in an IT2 fuzzy system that uses type-reduction [55]. The same research question has been also investigated for GT2-FLCs in [60] to show the first-order and second-order rule partitions and novelty partitions of GT2-FLCs and provide new perspectives for the potentials of GT2-FLCs comparing to IT2, T1, and crisp counterparts.

Nowadays, researchers have given more attention to GT2-FLCs, as it is a new research direction for the fuzzy community [7, 59-76]. A GT2-FS and a GT2-FLC are in fact a T2-FS and a T2-FLC respectively (“in the most general form”), but to distinguish them from IT2 counterparts, “General” notation is preferred by many researchers [7]. In early studies on GT2-FLCs [61-68], the internal structure of GT2-FLCs is investigated. One of the representations of GT2-FSs, α -plane representation, has been proposed in [61-62] so that the GT2-FLC calculations can be handled by existing T1 and IT2 FS mathematics. Another representation of GT2-FSs, zSlice representation, has been presented [63-64] with GT2 mathematics and one of the pioneer real-time control applications of GT2-FLCs. These two representations have been investigated further in [65-66], and as mentioned in [7, 67], these two novel representations are the same from a content point of view with a different view. These representations are quite important for further GT2-FLC studies since zSlice or α -plane representations make it possible to represent the output of GT2-FLC by aggregation of T1 and/or IT2 FLCs [7]. The studies have shown that GT2-FLCs can outperform their T1 and IT2 FLC

counterparts [7, 30, 31, 60, 62, 68-76]. This is due to the fact that GT2-FLCs have more parameters to be tuned in comparison to their IT2 and T1 counterparts, and it computes GT2-FSs, by employing zSlice or α -plane representations into Secondary MFs (SMFs) which are T1-FSs instead of interval FSs [7]. This is also connected to the FOU comment of IT2-FLCs (as it is a footprint of a collection of all SMFs at the secondary layer) since GT2-FSs differs from IT2 and T1 counterparts at the secondary layer of antecedent MFs. In [68], the impacts of the SMFs (in terms of size and shape) on the control system performance have been also investigated by employing zSlices representation. It has been marked that the design of GT2-FSs is relatively more complex than the IT2 ones due to the difficulty of tuning the parameters, on the other hand, the GT2-FLCs provide an acceptable tradeoff between system performance and robustness and by tuning the SMFs. As of 2020, the GT2-FLCs have been successfully implemented for various applications, including autonomous outdoor mobile robot control [62, 68], mobile robot control [69-70], water tank liquid level control [70, 73], control of ball and beam system [70], chaotic system control [71], traffic control [72], linear system control [74], and nonlinear system control [74, 75]. The research interest on the GT2-FLCs still continues to analyze the internal structures better and design more systematic controllers.

In this thesis, new insights on the interpretations of GT2-FLCs' design parameters and the novel systematic design and new tuning methods of GT2-FLCs are presented with comprehensive analyses, simulations, and a real-time experiment.

First, a class of TSK FLCs is examined in Chapter 2 and Chapter 3, and the internal structures of the GT2-FLCs are presented after giving the preliminaries on the T1-FSs, T1-FLCs, IT2-FSs, and IT2-FLCs. In the preliminaries part that is given in Chapter 2, the internal structures of two kinds of FLC type (single input and double input) are presented along with their FPID configurations, the design parameters of these fuzzy controllers are listed, and the most common design parameters are summarized based on the design assumptions. The GT2-FS and GT2-FLC definitions are given in Chapter 3; the GT2-FLCs are first represented with α -planes since this representation provides various benefits on the handling of the GT2-FSs, the mathematical definitions, and numerous design options for two types of T1-FSs (triangular and trapezoid) that are employed as the SMF of GT2-FLC are given, and the α -plane based output calculation

of the GT2-FLCs is explained in terms of well-known IT2-FLC computations with an illustrative numerical example.

The comprehensive analyses on the GT2-FSs, SMFs, and GT2-FLCs are presented in Chapter 4. The interactions between GT2-FSs and IT2-FSs, T1-FSs, and crisp sets are first shown in terms of the SMF definitions at the antecedent part, and a novel representation and parameterization of the trapezoid SMF are proposed. It is shown that the trapezoid SMF allows constructing trapezoid, triangle, interval, and singleton shapes so that the GT2-FLC can behave like its IT2-FLC or T1-FLC counterpart as per design. Therefore, it is suggested the usage of trapezoid SMFs with the proposed parameterization of the trapezoid SMFs that accomplish the design with a single tuning parameter. Then, the general suggestions on the structural settings of GT2-FLCs are provided not only to construct GT2-FLCs straightforwardly but also to ease the design of the GT2-FLCs with few design parameters. The main design parameters of the GT2-FLCs are presented and summarized by the given interpretations with respect to their effects on the shape and sensitivity of the resulting CCs/CSs. The total number of α -planes is called as the sensitivity design parameter and the tuning parameter of the SMFs is called as the shape design parameter.

In Chapter 5 and Chapter 6, comparative analyses/simulations on the single input and double input GT2-FLC structures (with numerous design settings) are conducted to validate the interpretations of the shape and sensitivity design parameters of the GT2-FLCs respectively. In this context, new design methods are proposed for interpretable and practical selections of the shape and sensitivity design parameters towards a systematic controller design.

The effects of the shape design parameter on the CCs/CSs are first investigated by comparing the resulting CCs/CSs of the GT2-FLCs in terms of comparison measures. These comparative studies provide a deeper understanding of the role of the shape design parameters and how this parameter improves the performance and robustness of the control system. In the light of the shape analyses, novel and systematic design recommendations are proposed on how to tune the shape design parameter by providing a tradeoff between robustness and performance. Moreover, two novel online scheduling mechanisms are proposed for online-tuning of the shape design parameter with respect to the steady-state operating points and transient-state dynamics.

The effects of the sensitivity design parameter on the CCs/CSs are also investigated by comparing the resulting CCs/CSs. These comparative studies provide practical insight on how to tune the sensitivity design parameter in terms of calculation accuracy and computation burden. Based on these analyses, it is suggested tuning the sensitivity design parameter by taking into account the limitations of hardware components such as quantization level (e.g. resolutions) and computational time (processing speed). Then, a novel iterative algorithm, which provides a compromise between sensitivity and computational time, is proposed to tune the sensitivity design parameter.

In Chapter 7, simulation and real-time experimental control studies are presented to validate the proposed design recommendations and systematic design approaches for GT2-FLCs. In these simulation and real-time studies, the GT2-FLCs (online-tuned or offline-tuned) are compared with T1-FLC and IT2-FLC counterparts. In the simulation study on a second-order nonlinear system, the proposed tuning steps for the shape design parameter are followed, and a simple scheduling mechanism (steady-state operating point-based) is employed into PID type -FLCs. The real-time experiments are performed on a real-world drone that acts as a proof-of-concept benchmark control system. The real-time experimental study presents a comprehensive design (for both shape and sensitivity design parameters) and a comparative, as well as a complete application (among T1, IT2, and GT2 FLCs) to validate the proposed systematic design approaches (the tuning steps of shape and sensitivity design parameters) for the GT2-FLCs in real-time control applications.

Chapter 8 presents the conclusions and discussions.



2. PRELIMINARIES ON FUZZY LOGIC CONTROLLERS

2.1 Type-1 and Interval Type-2 Fuzzy Sets

2.1.1 Type-1 fuzzy sets

A Type-1 Fuzzy Set (A) is defined as follows [7]:

$$A = \{(x, \mu_A(x)) \mid x \in X\} \quad (2.1)$$

where x is the input variable, X is the value set of the input variable x , and $\mu_A(x)$ is the MF of T1-FS A . In standard mathematical set notation, a T1-FS can be also described as follows [53]:

$$\mu_A: X \rightarrow [0,1] \quad (2.2)$$

In fuzzy set notation, a T1-FS (i.e. A) can be also described for the continuous universe (X) and the discrete universe (X_d) as follows [7]:

$$A = \int_{x \in X} \mu_A(x)/x \quad (2.3)$$

$$A = \sum_{x \in X_d} \mu_A(x)/x \quad (2.4)$$

in which $0 \leq \mu_A(x) \leq 1$. Here, “/ term” associates with the elements in X and X_d universes, while \int and \sum denote union over x values for X and X_d universes, respectively. The value of $\mu_A(x)$ is called as the membership degree of the input x . In the fuzzy literature, the MFs are characterized by well-known geometric shapes such as triangle, trapezoid, sigmoid, or gaussian. The membership degree is calculated based on the shape of the employed MFs. Moreover, an α -cut of T1-FS is denoted as A^α and defined based on α -cut level (i.e. $\alpha \in [0,1]$) as follows [7]:

$$A^\alpha = \{x \mid \mu_A(x) > \alpha\} \quad (2.5)$$

A triangleT1-FS is defined as follows:

$$\mu_A(x) = \begin{cases} \frac{x-a}{b-a} & a < x \leq b \\ \frac{c-x}{c-b}, & b < x \leq c \\ 0, & \text{otherwise} \end{cases} \quad (2.6)$$

where a , b , and c are left support, center, and right support points of the triangle shape, respectively. A simple illustration of a triangle T1-MF (e.g. A) is presented in Figure 2.1. A triangle T1-MF can be also defined with min and max mathematical operator functions as follows:

$$\mu_A(x) = \max\left(\min\left(\frac{x-a}{b-a}, \frac{c-x}{c-b}\right), 0\right) \quad (2.7)$$

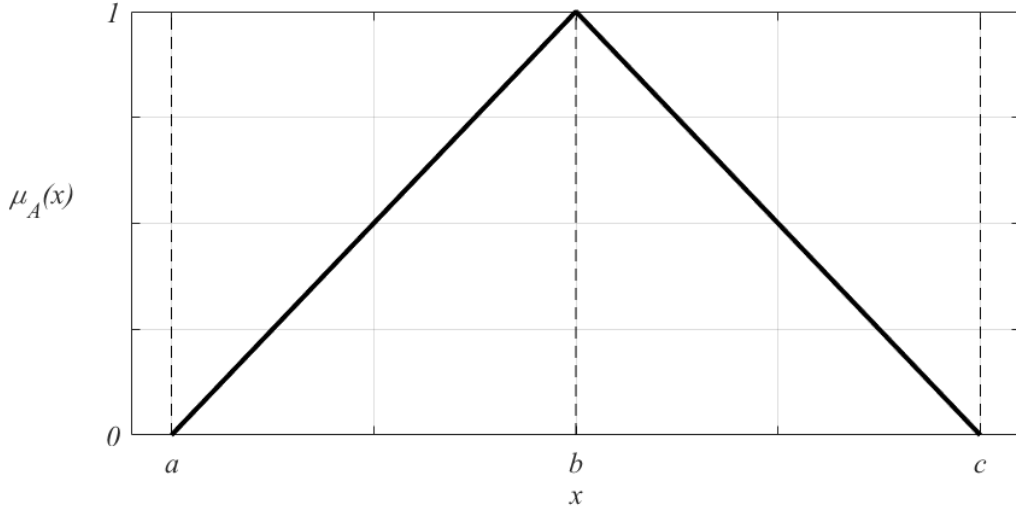


Figure 2.1 : Triangle T1-FS.

A trapezoid T1-FS is defined as follows:

$$\mu_A(x) = \begin{cases} \frac{x-a}{b-a} & a \leq x < b \\ 1 & b \leq x < c \\ \frac{d-x}{d-c} & c \leq x < d \\ 0 & \text{otherwise} \end{cases} \quad (2.8)$$

where a , b , c , and d are left support, left center, right center, and right support points of the trapezoid shape, respectively. A simple illustration of a trapezoid T1-MF is given in Figure 2.2. Alternatively, a trapezoid T1-MF (e.g. A) can be defined with min and max mathematical operator functions as follows:

$$\mu_A(x) = \max\left(\min\left(\frac{x-a}{b-a}, 1, \frac{d-x}{d-c}\right), 0\right) \quad (2.9)$$

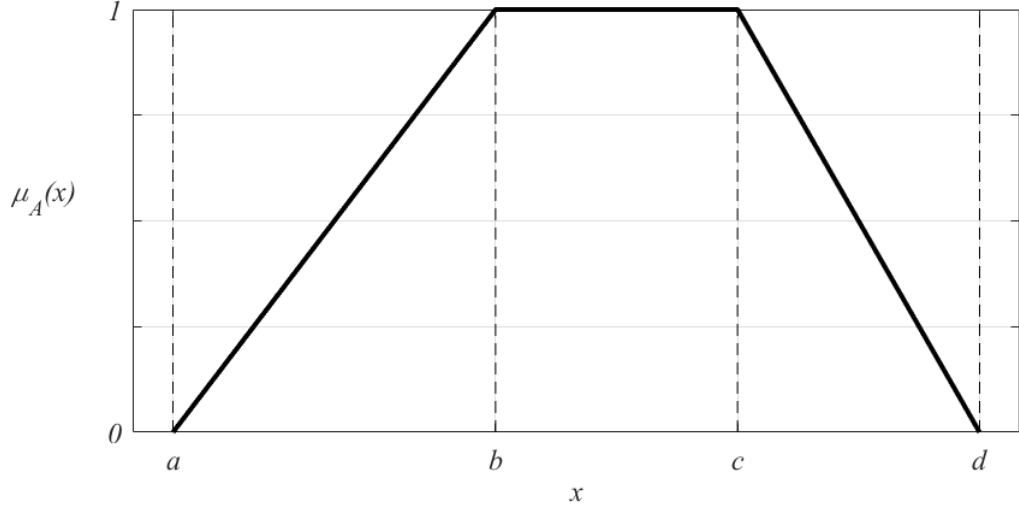


Figure 2.2 : Trapezoid T1-FS.

A Gaussian T1-FS is defined as follows:

$$\mu_A(x) = e^{-\frac{1}{2}\left(\frac{x-m}{\sigma}\right)^2} \quad (2.10)$$

where m and σ are mean and standard deviation values of the Gaussian T1-MF, respectively. An illustration of a Gaussian T1-MF (e.g. A) is presented in Figure 2.3.

2.1.2 Type-2 fuzzy sets

A Type-2 Fuzzy Set (\tilde{A}) is defined as follows [7]:

$$\tilde{A} = \{(x, u), \mu_{\tilde{A}}(x, u) \mid x \in X, u \in U\} \quad (2.11)$$

where x is the input variable (also called as the primary variable of \tilde{A}), X is the universe of the primary variable x , u is the secondary variable of \tilde{A} , $U \equiv [0, 1]$ is the universe for the secondary variable u , and $\mu_{\tilde{A}}(x, u)$ is the T2-MF of the T2-FS \tilde{A} . Here it is worth mentioning that the membership grade of T2-MF (i.e. $\mu_{\tilde{A}}(x, u)$) is defined in the three-dimensional domain ($X \times U_x$), while the membership grade of T1-MF (i.e. $\mu_A(x)$) is defined in the two-dimensional domain (X). A T2-FS is also described in standard set notation as follows [53]:

$$\mu_{\tilde{A}}: X \times U \rightarrow [0, 1] \quad (2.12)$$

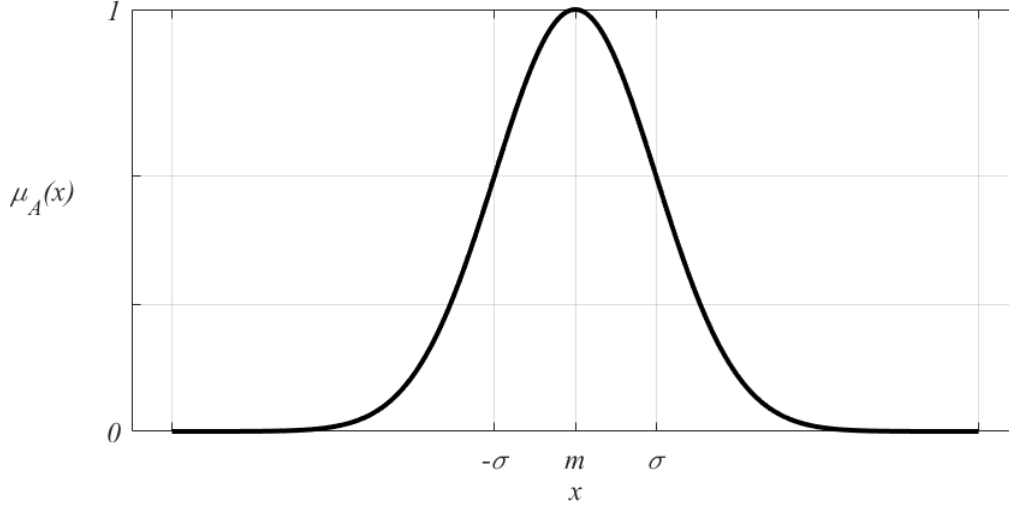


Figure 2.3 : Gaussian T1-FS.

Similar to its T1 counterpart, in fuzzy set notation, a T2-FS \tilde{A} can be defined for the continuous universe (i.e. X and U) and the discrete universe (i.e. X_d and U_d) as:

$$\tilde{A} = \int_{x \in X} \int_{u \in U} \mu_{\tilde{A}}(x, u) / (x, u) \quad \text{or} \quad \tilde{A} = \int_{x \in X} \left(\int_{u \in U} \mu_{\tilde{A}}(x, u) / u \right) / x \quad (2.13)$$

$$\tilde{A} = \sum_{x \in X_d} \sum_{u \in U_d} \mu_{\tilde{A}}(x, u) / (x, u) \quad \text{or} \quad \tilde{A} = \sum_{x \in X_d} \left(\sum_{u \in U_d} \mu_{\tilde{A}}(x, u) / u \right) / x \quad (2.14)$$

The membership grade (primary and/or secondary) of a T2-FS is described based on the primary membership of x (i.e. J_x) and the SMF ($\mu_{\tilde{A}(x)}(u)$ or $\mu_{\tilde{A}_x}(u)$) as follows:

$$\mu_{\tilde{A}(x)}(u) = \mu_{\tilde{A}(x)} = \mu_{\tilde{A}_x} = \int_{u \in [0,1]} \mu_{\tilde{A}}(x, u) / (u) \quad (2.15)$$

$$J_x = \{(x, u) | u \in [0,1], \mu_{\tilde{A}}(x, u) > 0\} \quad (2.16)$$

where $\tilde{A}(x)$ and \tilde{A}_x denote the FS of the SMF. Here, if the employed SMF support (I_x) is always closed such that $J_x \equiv \{x\} \times I_x$, then J_x is defined as follows [7]:

$$J_x = [\underline{\mu}_{\tilde{A}}(x), \bar{\mu}_{\tilde{A}}(x)] \quad (2.17)$$

where $\underline{\mu}_{\tilde{A}}(x)$ and $\bar{\mu}_{\tilde{A}}(x)$ are Lower MF (LMF) and Upper MF (UMF), respectively. Here, J_x is calculated based on the input variable x at the primary level. The difference

between T1 and T2 MFs is that a T1-MF has a single membership degree (which means that J_x is a value), while a T2-MF has uncountable membership degrees (which means that J_x is a union set of these intervals). Moreover, the SMF is the distinguishing property of the T2-FSs, since it determines the output and categorizes the type of FS (i.e. type-1, interval type-2, or general type-2) as it is defined by a set (e.g. crisp, interval or type-1) at the secondary level. In the fuzzy literature, “GT2” is preferred to distinguish T2, IT2, and GT2 terms [7]. For the T1-FS case, there is no factual SMF since secondary grades are crisp values. For the IT2-FS case, the SMF is an interval set where all secondary grades are 1. For the GT2-FS case; the SMF is a T1-FS that is denoted as $\tilde{A}(x)$ or \tilde{A}_x , as indicated in equation 2.15. Another distinguishing property of T2-FSs is preserved in the FOU which is a collection of all primary memberships of the input x . The FOU of \tilde{A} is drawn by shading the area where $\mu_{\tilde{A}}(x, u) > 0$, and defined as follows:

$$\text{FOU}(\tilde{A}) = \bigcup_{x \in X} J_x = \{(x, u) | x \in X, u \in [\underline{\mu}_{\tilde{A}}(x), \bar{\mu}_{\tilde{A}}(x)]\} \quad (2.18)$$

Here, the LMF and the UMF are also defined on the primary level and characterize the lower and upper boundaries of the $\text{FOU}(\tilde{A})$ as follows:

$$\underline{\mu}_{\tilde{A}}(x) = \inf\{u | u \in [0, 1], \mu_{\tilde{A}}(x, u) > 0\} \quad (2.19)$$

$$\bar{\mu}_{\tilde{A}}(x) = \sup\{u | u \in [0, 1], \mu_{\tilde{A}}(x, u) > 0\} \quad (2.20)$$

2.1.3 Interval type-2 fuzzy sets

As a special form of GT2-FSs, an IT2-FS is obtained when all secondary membership grades are 1 (i.e. $\mu_{\tilde{A}}(x, u) = 1$) as follows [7]:

$$\tilde{A} = \{(x, u), \mu_{\tilde{A}}(x, u) = 1 \mid x \in X, u \in U\} \quad (2.21)$$

When an IT2-MF (instead of GT2-MF) is employed, an interval set (instead of T1-FS) is used at the secondary layer of SMF, $\mu_{\tilde{A}(x)}(u)$, so that the IT2-MFs can be drawn in the 2D domain (similar to the T1 counterpart) with respect to LMF, UMF, and FOU. In this context, IT2 counterparts of T1-MF examples (triangle, trapezoid, and Gaussian) are given in Figures 2.4, 2.5, and 2.6.

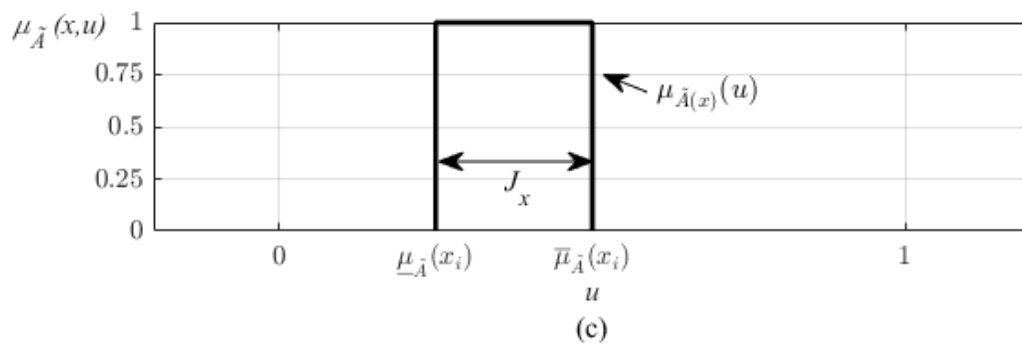
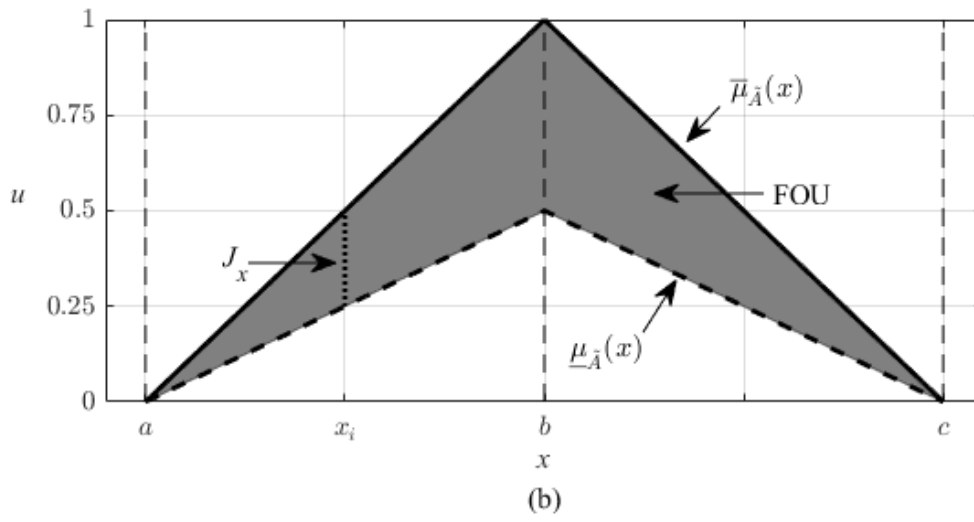
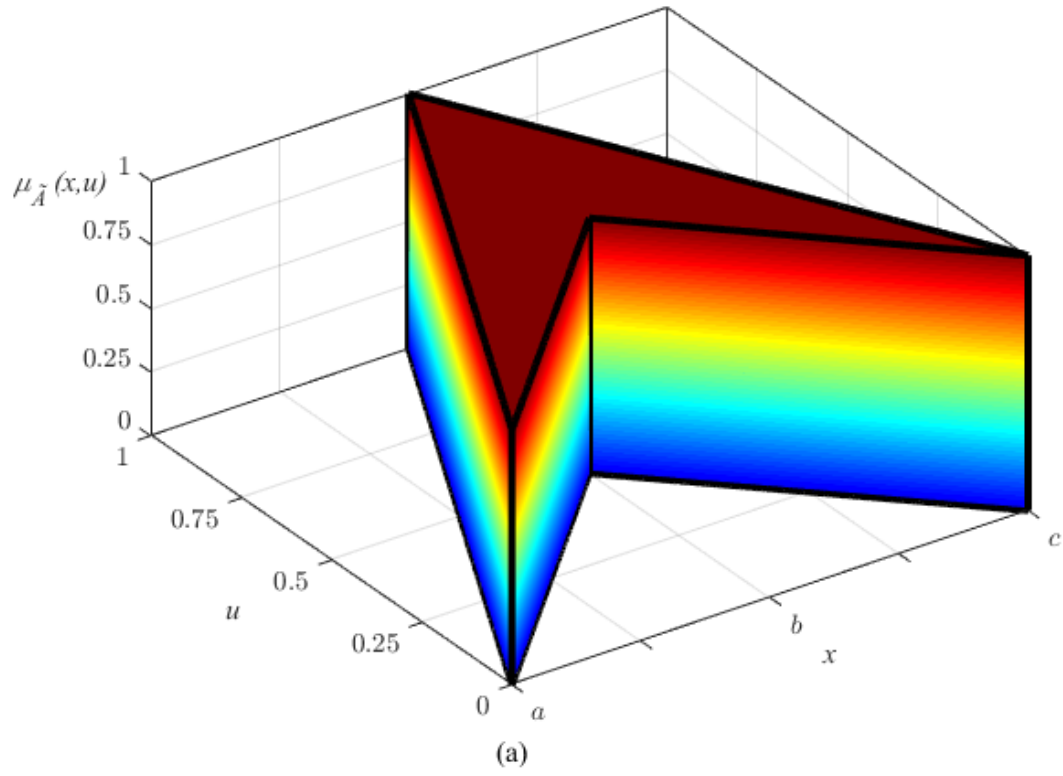


Figure 2.4 : Triangle IT2-FS.

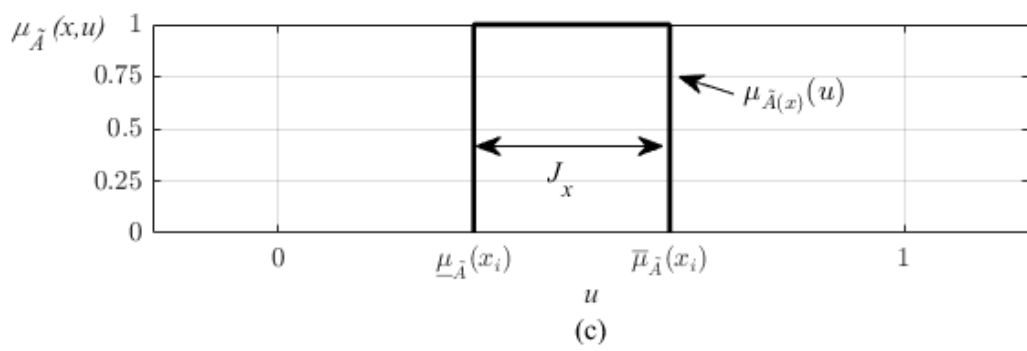
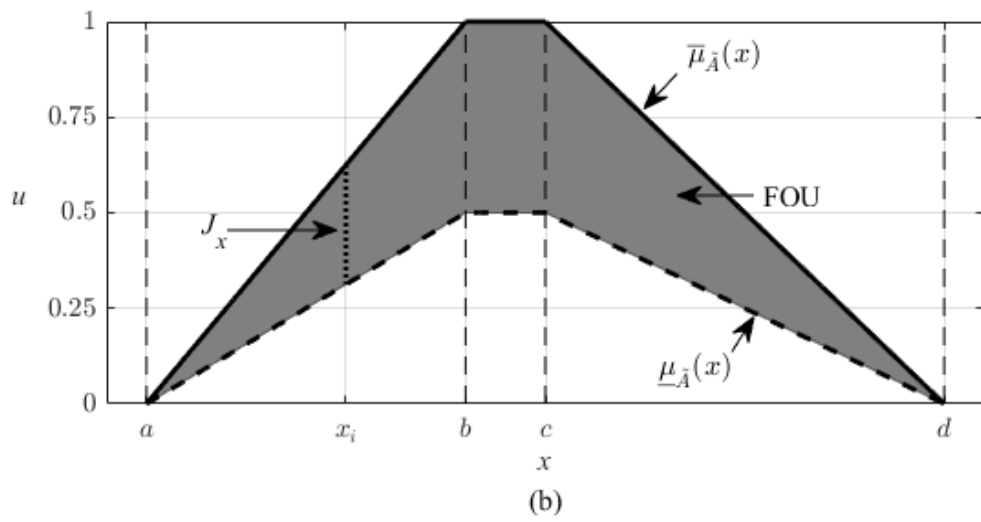
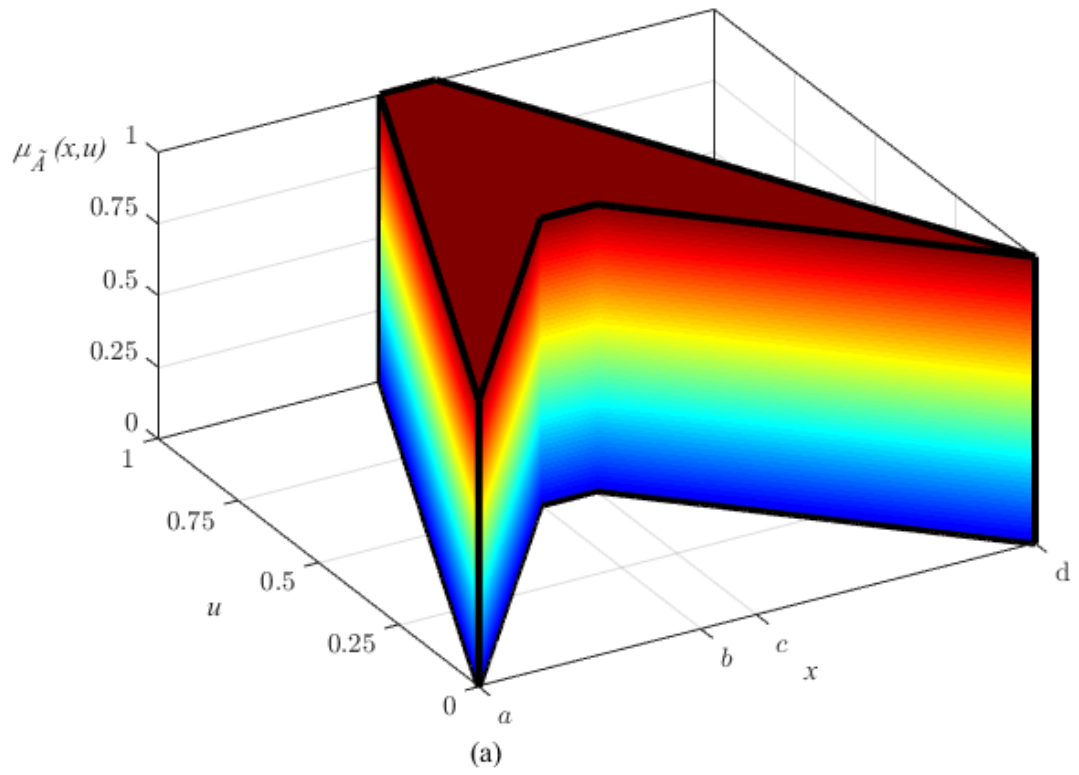


Figure 2.5 : Trapezoid IT2-FS.

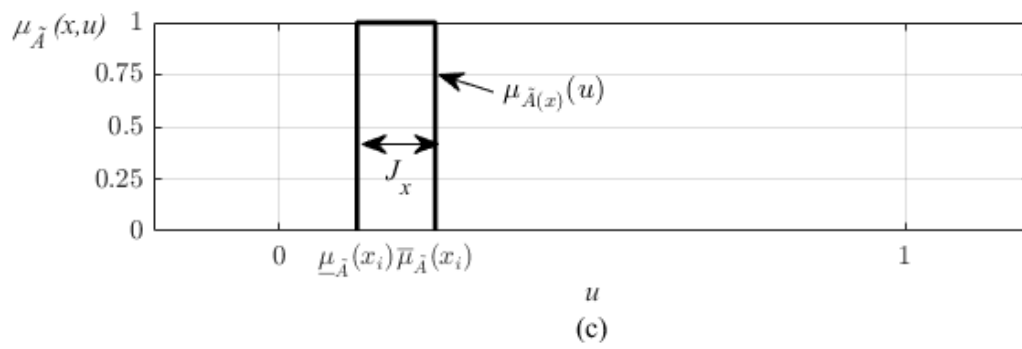
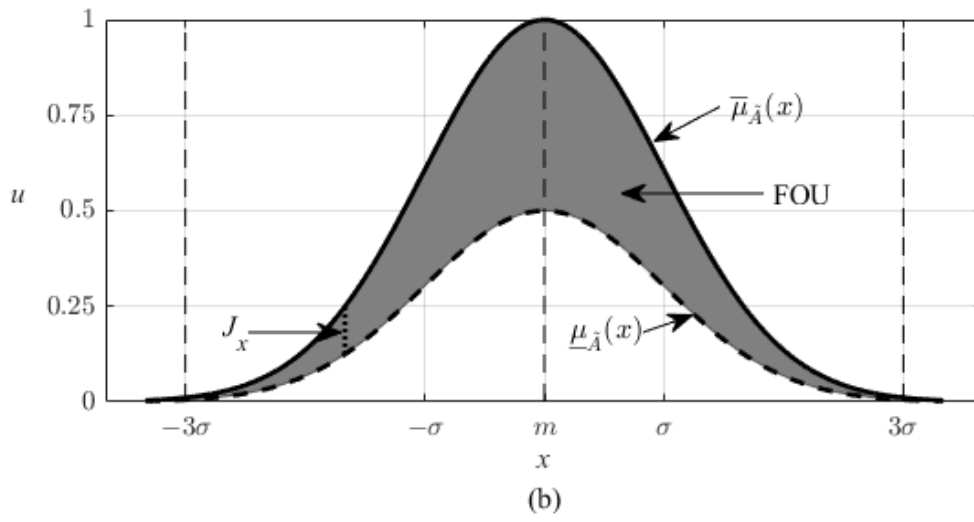
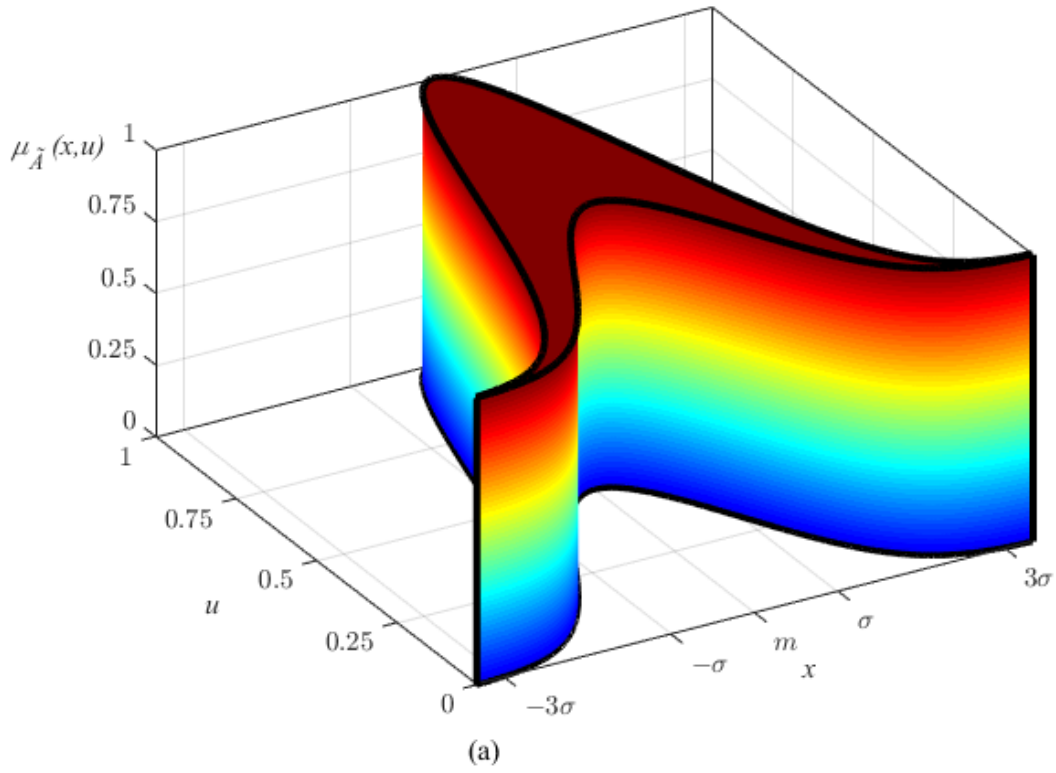


Figure 2.6 : Gaussian IT2-FS.

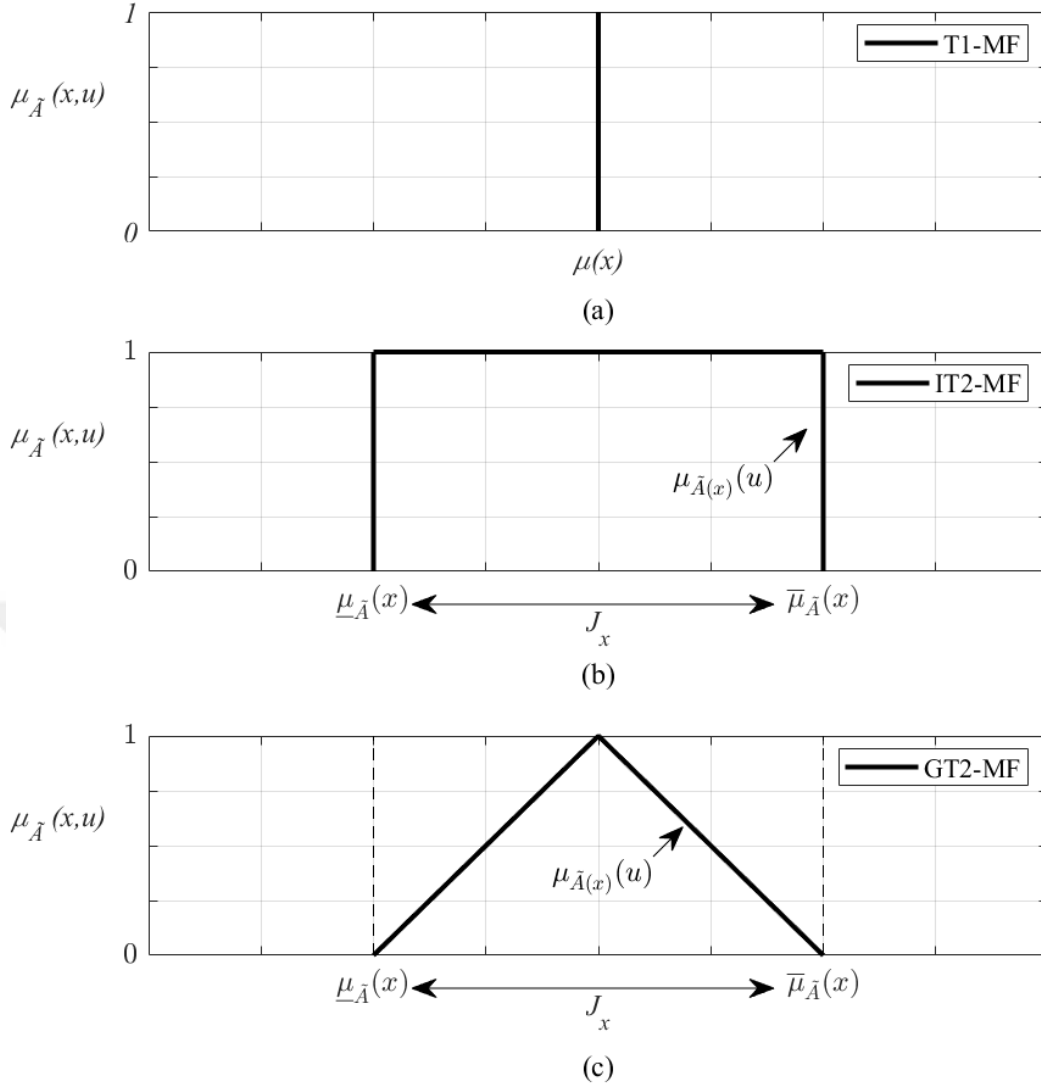


Figure 2.7 : Secondary grade examples of T1 and T2 fuzzy sets.

The differences between T1, IT2, and GT2-MFs at the secondary layer (in terms of the SMF) are illustrated in Figure 2.7. Here, the FOU does not exist for the T1-MF since the LMF and the UMF are overlapped at the value of $\mu(x)$. Accordingly, this provides a crisp secondary layer as shown in Figure 2.7a. On the other hand, the IT2-MF has a predefined interval set at the secondary layer thanks to its FOU bounded by the LMF ($\underline{\mu}_{\tilde{A}}(x)$) and the UMF ($\overline{\mu}_{\tilde{A}}(x)$). This provides additional design flexibility, whereas the SMF design is not possible as all secondary grades are 1 as shown in Figure 2.7b. On the contrary for the GT2-MF case, numerous SMF design is possible since the SMF is designed based on a T1-FS used at the secondary layer (Figure 2.7c shows only triangle example in this context). This provides extra design flexibility and opportunity to the designer. The selection of the SMFs and the effects on the controller/system performances will be investigated in the next chapters.

2.2 Type-1 and Interval Type-2 Fuzzy Logic Controllers

A FLC is a complex system that provides a mapping from its input(s) to its output based on fuzzy rules in the rule table, which is used in many applications such as reasoning, decision making, modeling, and control [30, 31]. In fuzzy literature, the most popular FLC structures are Mamdani and Takagi-Sugeno-Kang [7]. Both FLC structures are characterized by IF-THEN rules and have the same antecedent part, on the other hand, they differ in the part of consequents. The Mamdani fuzzy systems use fuzzy sets at the consequent part of the rules, whereas the TSK fuzzy systems use mathematical functions or singletons at the consequent part of the rules. As the TSK FLCs are considered in this thesis, the consequents of all FLCs are defined by singletons, while the antecedent parts are defined by T1, IT2, and GT2 FSs for T1, IT2, and GT2 FLCs, respectively.

2.2.1 Type-1 fuzzy logic controllers

The T1-FLCs are constructed by four main parts [7]: fuzzifier, fuzzy rule base, inference engine, defuzzifier as shown in Figure 2.8. Here, the fuzzifier converts the crisp input into T1 fuzzy input sets. Then, the inference engine combines these T1 fuzzy input sets through the fuzzy IF-THEN rules and accumulates T1 fuzzy output sets after calculating the corresponding firing levels of fuzzy rules. After combining these T1 output fuzzy sets, the defuzzifier generates the crisp output.

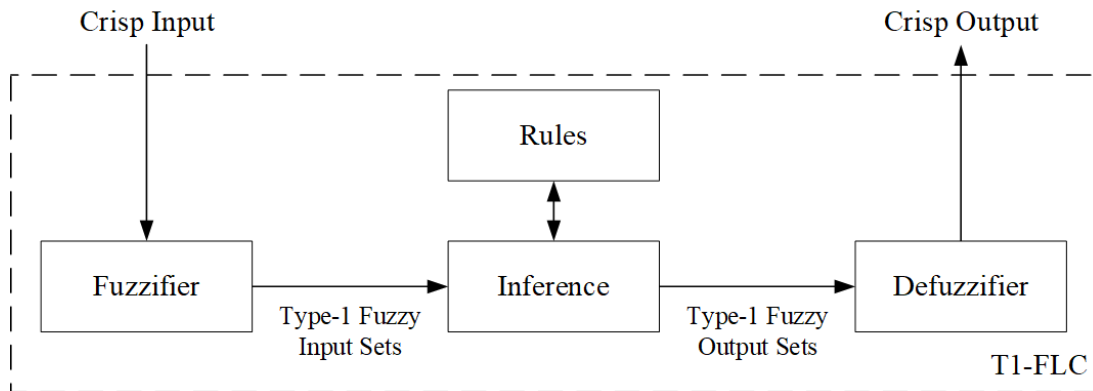


Figure 2.8 : System block diagram of type-1 fuzzy logic controllers.

A fuzzy rule of a T1-FLC is defined as follows [7]:

$$R_n: \text{ IF } x_1 \text{ is } A_{1,i} \text{ and } \dots \text{ and } x_j \text{ is } A_{j,i} \text{ THEN } y_{T1} \text{ is } C_n \quad (2.22)$$

where x_j ($j \in \{1, 2, \dots, J\}$) is an input, $A_{j,i}$ ($i \in \{1, 2, \dots, I\}$) is an antecedent MF, J is the total number of inputs, I is the total number of antecedent MFs, R_n ($n \in \{1, 2, \dots, N\}$) is the n^{th} rule of the rule table, N is the total number of rules in the rule table, y_{T1} is the output of T1-FLC, and C_n is an output singleton consequent of the rule R_n . When the weighted average center-of-sets defuzzification method is applied, then the output of a T1-FLC (y_{T1}) is defined as follows [7]:

$$y_{T1} = \frac{\sum_{n=1}^N f_n C_n}{\sum_{n=1}^N f_n} \quad (2.23)$$

where f_n is the firing strength of the rule R_n and calculated as:

$$f_n = \prod_{j=1}^J \mu_{A_{j,i}}(x_j) = \mu_{A_{1,i}}(x_1) \times \dots \times \mu_{A_{J,i}}(x_J) \quad (2.24)$$

where \times and Π terms indicate product t-norm operators. Here, $\mu_{A_{j,i}}(x_j)$ is the membership degree of the corresponding T1-MF (i.e. $\mu_A(x)$) and calculated according to T1-MF definitions and the value of the input x_j .

2.2.2 Interval type-2 fuzzy logic controllers

In addition to their T1 counterparts, the T2-FLCs have additional operation denoted as type-reduction as illustrated in Figure 2.9 [7]. The type reducer is essential for T2-FLCs; it requires a computational cost which is assumed as the main bottleneck of T2-FLCs [7], whereas it is required to complete the output calculation of T2-FLCs. The fuzzifier uses and processes the T2-FSs. The output of the inference becomes T2 fuzzy output sets. Then the type-reducer evaluates these T2 fuzzy output sets and converts them to a kind of type-1 fuzzy set denoted as type-reduced sets. The defuzzifier uses this type-reduced set for the defuzzification process. It is worth mentioning that there are several type-reduction algorithms in the literature, while the KM type reduction [46] is still the most commonly used type-reduction method [7]. Due to this reason in this thesis, the KM algorithm is employed as a type-reducer of T2-FLCs. Another remark is that the type-reduction methods are generally proposed for IT2-FLCs, where all secondary grades are 1. This is also GT2-FLC compatible from the calculation point of view since the output calculation of GT2-FLCs is handled in a way that all IT2-FLC fuzzy notations that are given in Figure 2.9 become also valid for the GT2-FLC

calculations [7]. The computation of a GT2-FLC will be explained in “Chapter 3 - General Type-2 Fuzzy Logic Controllers in detail.

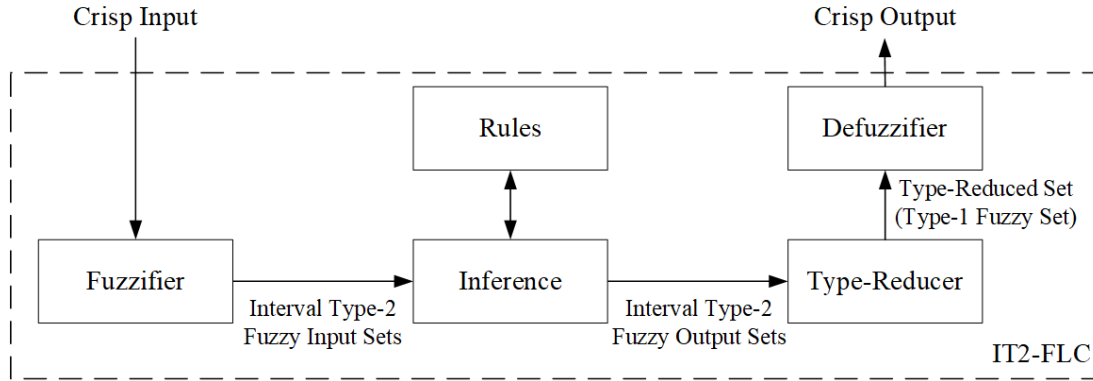


Figure 2.9 : System block diagram of interval type-2 fuzzy logic controllers.

A fuzzy rule of an IT2-FLC is defined as follows [7]:

$$R_n: \text{ IF } x_1 \text{ is } \tilde{A}_{1,i} \text{ and } \dots \text{ and } x_j \text{ is } \tilde{A}_{j,i} \text{ THEN } y_{IT2} \text{ is } C_n \quad (2.25)$$

where x_j ($j \in \{1, 2, \dots, J\}$) is an input, $\tilde{A}_{j,i}$ ($i \in \{1, 2, \dots, I\}$) is an antecedent MF, J is the total number of inputs, I is the total number of antecedents MF, R_n ($n \in \{1, 2, \dots, N\}$) is the n^{th} rule of the rule table, N is the total number of rules in the rule table, y_{IT2} is the output of IT2-FLC, and C_n is an output singleton consequent of the rule R_n . When a KM type reduction and center of set defuzzification method [46] is applied, then the output of an IT2-FLC (y_{IT2}) is defined as follows [7, 48, 49]:

$$y_{IT2} = \frac{(y_{IT2} + \bar{y}_{IT2})}{2} \quad (2.26)$$

where \underline{y}_{IT2} and \bar{y}_{IT2} are left and right endpoints of the type-reduced set (i.e. T1 interval fuzzy numbers), respectively. The left and right endpoints of the type-reduced set are calculated as follows:

$$\underline{y}_{IT2} = \frac{\sum_{n=1}^L \bar{f}_n C_n + \sum_{n=L+1}^N \underline{f}_n C_n}{\sum_{n=1}^L \bar{f}_n + \sum_{n=L+1}^N \underline{f}_n} \quad (2.27)$$

$$\bar{y}_{IT2} = \frac{\sum_{n=1}^R \underline{f}_n C_n + \sum_{n=R+1}^N \bar{f}_n C_n}{\sum_{n=1}^R \underline{f}_n + \sum_{n=R+1}^N \bar{f}_n} \quad (2.28)$$

where L and R are left and right switching points of the KM algorithm respectively [7, 48, 49], $\overline{f_n}$ and $\underline{f_n}$ are the upper and lower firing strengths of the firing interval (FI_n) associated with the rule R_n . The firing interval is calculated as follows:

$$FI_n = [\underline{f_n} \quad \overline{f_n}] \quad (2.29)$$

where lower and upper bounds of the firing interval are calculated as:

$$\underline{f_n} = \prod_{j=1}^J \underline{\mu}_{\tilde{A}_{j,i}}(x_j) = \underline{\mu}_{\tilde{A}_{1,i}}(x_1) \times \dots \times \underline{\mu}_{\tilde{A}_{J,i}}(x_J) \quad (2.30)$$

$$\overline{f_n} = \prod_{j=1}^J \overline{\mu}_{\tilde{A}_{j,i}}(x_j) = \overline{\mu}_{\tilde{A}_{1,i}}(x_1) \times \dots \times \overline{\mu}_{\tilde{A}_{J,i}}(x_J) \quad (2.31)$$

where $\underline{\mu}_{\tilde{A}_{j,i}}(x_j)$ and $\overline{\mu}_{\tilde{A}_{j,i}}(x_j)$ are the membership degrees of the corresponding LMF and UMF (i.e. $\underline{\mu}_{\tilde{A}}(x)$ and $\overline{\mu}_{\tilde{A}}(x)$), respectively. In this thesis, (as in previous works [40, 42-44, 49]), the UMFs and the LMFs are always defined with respect to their T1 baseline and the design parameter denoted by $M_{j,i}$ as follows:

$$\overline{\mu}_{\tilde{A}_{j,i}}(x_j) = \mu_{A_{j,i}}(x_j) \quad (2.32)$$

$$\underline{\mu}_{\tilde{A}_{j,i}}(x_j) = \overline{\mu}_{\tilde{A}_{j,i}}(x_j) M_{j,i} = \mu_{A_{j,i}}(x_j) M_{j,i} \quad (2.33)$$

where $M_{j,i}$ is the height of the LMF associated with the T2-FS $\tilde{A}_{j,i}$. The parameter M associated with an IT2-FLC \tilde{A} , in the most generic form, is also called as the FOU design parameter of IT2-FLCs [36-45]. This design parameter defines the size of the FOU since it changes the shaded area. As illustrated in Figures 2.10-2.13, higher M values result in a smaller FOU as the shaded area shrinks when the LMF approaches towards the UMF. In a similar manner, lower M values result in larger FOU since the shaded area enlarges. For example, the shaded FOU area of Figure 2.10 is much larger than the one for Figure 2.12, since the height values are $M = 0.2$ and $M = 0.8$, respectively. Moreover, as illustrated in Figure 2.13, when $M = 1$ for all T2-FSs, then the FOU disappears so that the IT2-FLC reduces into its T1-FLC counterpart from the structure and calculation points of view.

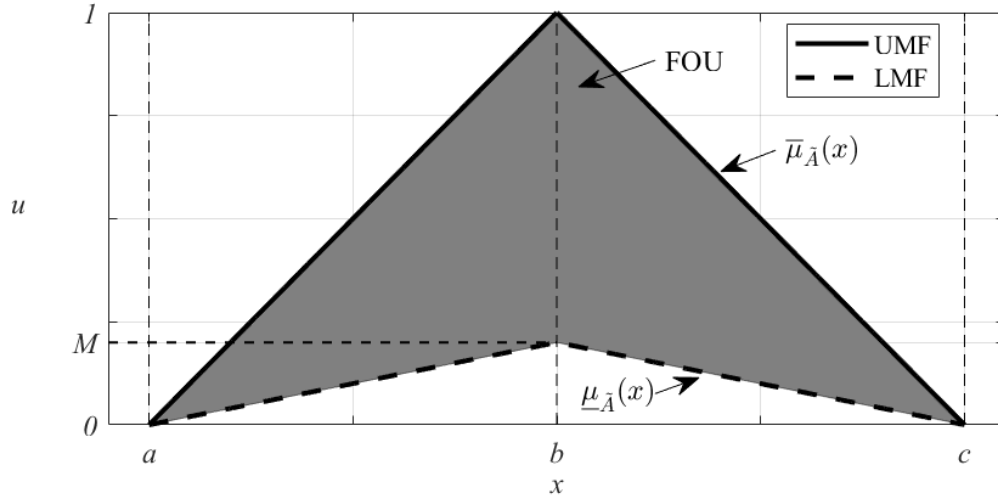


Figure 2.10 : A triangle IT2 membership function for $M = 0.2$ setting.

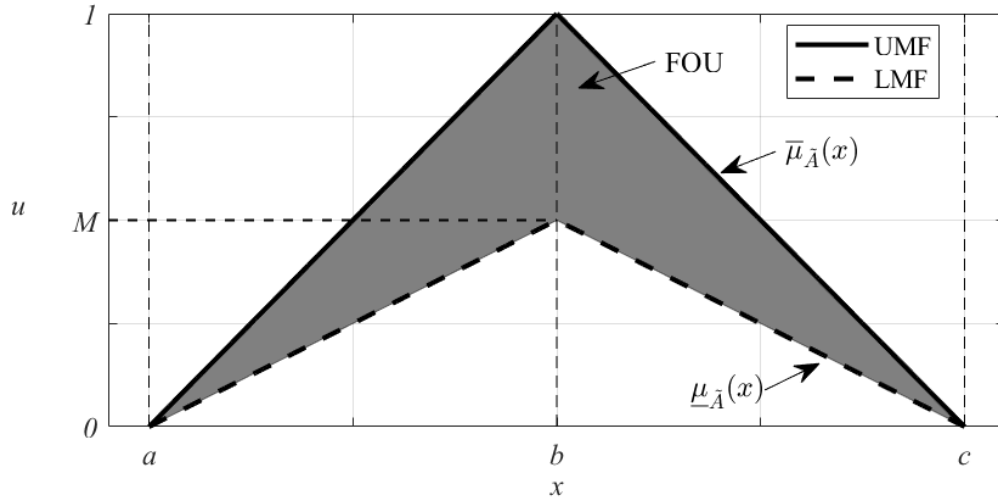


Figure 2.11 : A triangle IT2 membership function for $M = 0.5$ setting.

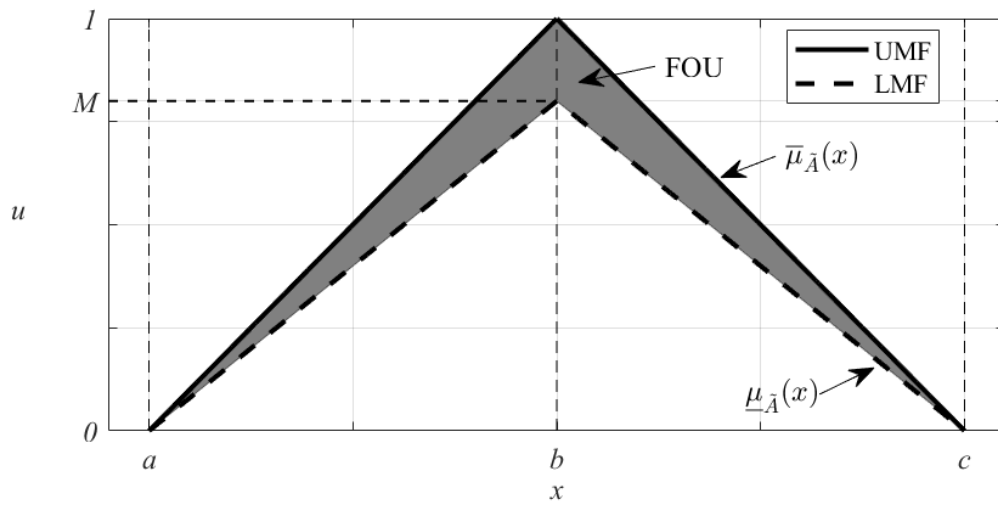


Figure 2.12 : A triangle IT2 membership function for $M = 0.8$ setting.

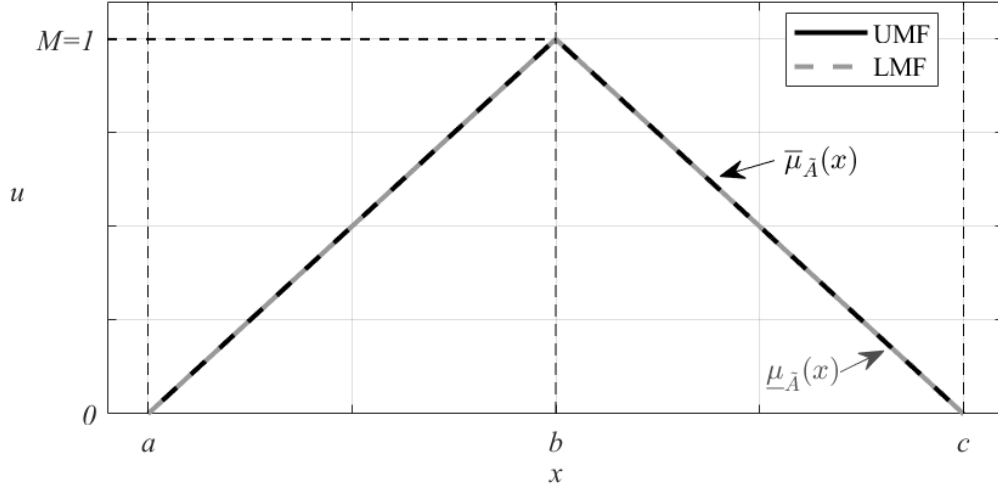


Figure 2.13 : A triangle IT2 membership function for $M = 1$ setting.

2.3 From FLC Mapping to Fuzzy PID Controllers

The PID type fuzzy logic controllers, in other words, FPID controllers, are generally cited as an alternative to the classic PID controllers, as they are analogous to their conventional counterparts from their input-output mapping perspectives [9-11, 14-16]. The main difference between conventional and fuzzy controllers is that the conventional controller provides a linear mapping from input to output, while the FPID controller provides a nonlinear mapping. In some studies, this mapping is interpreted that the FPID controller is a conventional PID controller with a varying controller gain [19]. The FPID controller structures are generally constructed by the scaling factors (input and output) and a base FLC. In literature, various fuzzy controller structures are proposed [11-21].

In this thesis; all fuzzy controllers are categorized based on their internal FLC type and the number of inputs. The generic FPID term is preferred to represent all possible configurations of FPID controllers (i.e. PID, PD, PI, and P) since this categorization happens with respect to the non-zero values of the scaling factors. Based on the FLC type, the following FPID controller structures are examined:

- T1-FPID controller that employs T1-FLC,
- IT2-FPID controller that employs IT2-FLC,
- GT2-FPID controller that employs GT2-FLC;

while these fuzzy controllers (i.e. T1, IT2, and GT2 FPID controllers) are also categorized with respect to their number of inputs as follows:

- Single-Input FLCs (SFLCs),
- Double-Input FLCs (DFLCs).

A fuzzy controller (either FLC or FPID) is generally constructed by choosing its inputs as the error signal (e) and the derivative of the error signal (\dot{e}), while its output is the control signal (u). Note that, in the fuzzy literature [14, 17, 21], inputs and outputs are sometimes defined in the discrete-time domain instead of the continuous-time domain by using the discrete error signal ($e[k]$) and the change of error signal ($\Delta e[k]$). But these expressions do not change the generic structure of the fuzzy controller since the fuzzy rule base and internal fuzzy inference calculations are the same. In this thesis, for the sake of consistency, the notion of (e , Δe) is used to represent the error signal and the change of the error signal, respectively. Hence, the inputs of a fuzzy controller are defined as follows:

$$e = r_s - y_s \cong r[k] - y_s[k] \quad (2.34)$$

$$\dot{e} = \frac{de}{dt} \cong \frac{\Delta e}{T} \quad (2.35)$$

$$\Delta e = e[k] - e[k - 1] \quad (2.36)$$

where r_s is the reference signal of the control system, y_s is the output of the system to be controlled, and T denotes the sample time of the discrete system. For all fuzzy controllers, the input scaling factors are used to normalize the inputs in the range of the universe of discourse [40]. The input scaling factors are denoted as K_e and $K_{\Delta e}$ for the error and the change of error inputs, respectively. The input scaling factors normalize the inputs as follows:

$$E = K_e e, \quad E \in [-1, 1] \quad (2.37)$$

$$\Delta E = K_{\Delta e} \Delta e, \quad \Delta E \in [-1, 1] \quad (2.38)$$

where E is the normalized error input and ΔE is the normalized change of error input. Here, the universe of discourse is defined in the range of $[-1, 1]$, so inputs E and ΔE are bounded in this value interval employed in the FLC. Here it is worth underlying

that e is the input of the conventional or fuzzy controller, while E and ΔE are the inputs of the FLC that is used in the fuzzy controller. Moreover, the output of the fuzzy controller (u), which is the control signal of the closed-loop system, is generated after the conversion of the FLC output by the output scaling factors, namely K_a and K_b . Here, the output scaling factors convert the control signal into a real-time applicable signal range as the FLC provides output only in the universe of discourse.

2.4 Single-Input Fuzzy PID Controllers

A Single-input Fuzzy PID (SFPID) controller consists of a SFLC, an input scaling factor that is K_e , an output scaling factor that is K_a , and a conventional PID controller with 3 gain terms (K_p , K_i , and K_d) [36, 41]. In the closed-loop control block diagram, the input of the SFPID controller is the error signal (e), while the output is the control signal (u) as given in Figure 2.14.

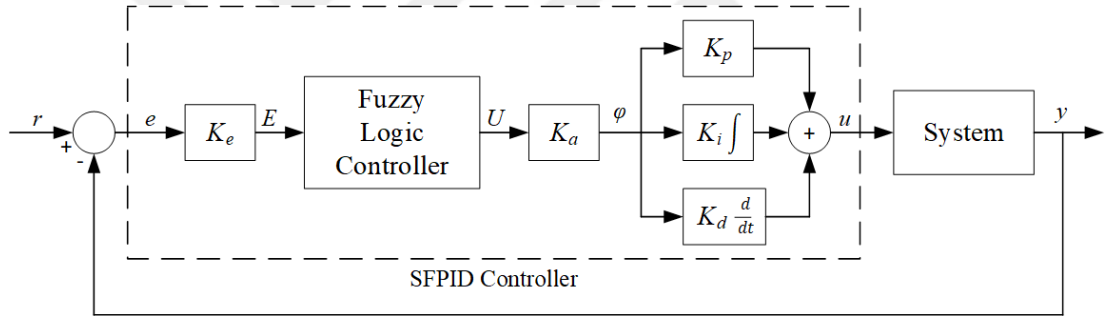


Figure 2.14 : Closed-loop control block diagram of single-input FPID controllers.

2.4.1 Type-1 single-input fuzzy PID controllers

The T1-SFLC of a SFPID controller is constructed by selecting its single input as the normalized error signal ($x_1 = E$) and the output as $y_{T1} = U_{T1}$ [36, 41]. It is worth marking that the fuzzy literature prefers “ y ” term to express the output of the fuzzy mapping (from a fuzzy input x to a fuzzy output y). In this thesis, the y terms (e.g. y_{T1} , y_{IT2} , and y_{GT2}) are used to represent a generic FLC output (like in equation (2.39)), while U terms (e.g. U_{T1} , U_{IT2} , and U_{GT2}) are used for FLC output for control applications. Therefore, the fuzzy rule in equation (2.22) is arranged for T1-SFLCs employing T1-FSs ($A_{j,i}$) as follows:

$$R_n: \text{ IF } x_1 \text{ is } A_{1,i} \text{ THEN } y_{T1} \text{ is } C_n \quad (2.39)$$

where $i \in \{1, \dots, I\}$ and $k \in \{1, \dots, K = I\}$ represent corresponding antecedent MFs that are defined in the rule R_n . Hence, the output of a T1-SFLC is calculated as given in equation (2.23), while the firing strength calculation is accomplished after redefining equation (2.24) as follows:

$$f_n = \mu_{A_{1,i}}(x_1) = \mu_{A_{1,i}}(E) \quad (2.40)$$

where $x_1 = E$ is the single input of the T1-SFLC structure. This single input signal is obtained according to equation (2.37) in where the error signal (e) is obtained as in equation (2.34). Then, the output scaling factor (K_a) converts the SFLC output (U_{T1} , also shown as U in Figure 2.14) as follows:

$$\varphi = K_a U, \quad U \in [-1,1] \quad (2.41)$$

where φ is the denormalized output of the T1-SFLC mapping. Here, the value of φ is the input of the conventional part of the SFPID controller (as replacement of the error signal) as given in Figure 2. 14. Consequently, the output of the T1-SPID controller, namely the control signal ($u = u_{T1}$), is calculated as follows:

$$u = K_p \varphi + K_i \int_0^t \varphi(\xi) d\xi + K_d \frac{d\varphi}{dt} \quad (2.42)$$

It is worth underlying that the term “ u ” is used as the control signal (for example as in equation (2.42)), in control applications as shown in Figure 2.14, while it is used as the secondary variable in T2-FS definitions (as given in equation (2.11)). Also, the U term is used as the FLC output in control applications (for example as given in equation (2.41)) as shown in Figure 2.14, while it is used as the universe of discourse of the secondary variable (as given in equation (2.11)). In this thesis, the given both “ u and U ” notations are followed for all FLC types (T1, IT2, and GT2) to have the same naming convention as in the literature.

2.4.2 Interval type-2 single-input fuzzy PID controllers

The IT2-SFLC of a SFPID controller is also constructed by selecting its single input as the normalized error signal ($x_1 = E$) and the output as $y_{IT2} = U_{IT2}$ [36, 41]. The fuzzy rule in equation (2.25) is arranged for T2-SFLCs employing T2-FSs ($\tilde{A}_{j,i}$) as:

$$R_n: \text{ IF } x_1 \text{ is } \tilde{A}_{1,i} \text{ THEN } y_{IT2} \text{ is } C_n \quad (2.43)$$

Like its T1 counterpart, the output of IT2-SFLC is calculated as given in equations (2.26), (2.27), and (2.28), while the lower and upper firing interval calculations in equations (2.30) and (2.31) are arranged, respectively as follows:

$$\underline{f}_n = \underline{\mu}_{\tilde{A}_{1,i}}(x_1) = \underline{\mu}_{\tilde{A}_{1,i}}(E) \quad (2.44)$$

$$\overline{f}_n = \overline{\mu}_{\tilde{A}_{1,i}}(x_1) = \overline{\mu}_{\tilde{A}_{1,i}}(E) \quad (2.45)$$

where $x_1 = E$ is also obtained according to equation (2.37) in where the error signal (e) is obtained as in equation (2.34). The membership degrees of LMF and UMF are calculated as given in equations (2.32) and (2.33). The output scaling factor (K_a) converts the IT2-SFLC output (U_{IT2}) as given in equation (2.41). Then the output of the IT2-SPID controller (where $u = u_{IT2}$), is calculated as given in equation (2.42). It is worth underlying that once the FLC output (i.e. U) is obtained, then the rest of the output calculations are the same for all FLCs. It only differs in the assignments of FLC output to the corresponding signals: y_{T1} , y_{IT2} , and y_{GT2} . Consequently, in the same manner, the output of the GT2-SFPID controller (where $u = u_{GT2}$), is calculated as in T1-FPID and IT2-FPID controllers. The output calculations of GT2-SFLCs will be presented in “Chapter 3 - General Type-2 Fuzzy Logic Controllers”.

2.5 Double-Input Fuzzy PID Controllers

A Double-input Fuzzy PID (DFPID) controller consists of a DFCLC cascaded to two input scaling factors (K_e for E input, and $K_{\Delta e}$ for ΔE input), and two output scaling factors (K_a and K_b with an integrator) [10, 19, 39-40, 42-44] as shown in the closed-loop block diagram in Figure 2.15.

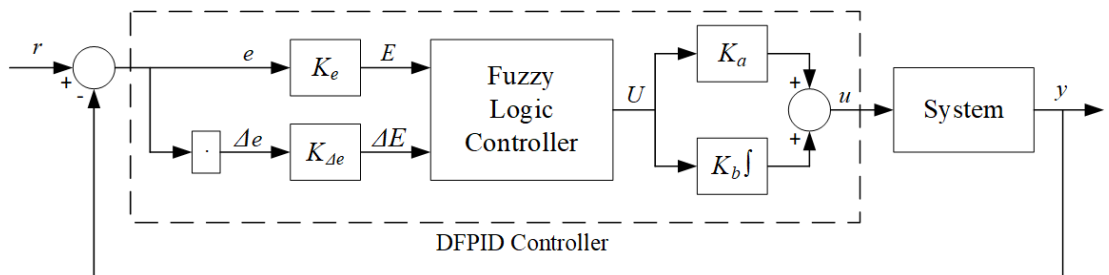


Figure 2.15 : Closed-loop block diagram of double-input FPID controllers.

2.5.1 Type-1 double-input fuzzy PID controllers

The T1-DFLC of a DFPID controller is constructed by selecting its inputs as the normalized error input ($x_1 = E$) and the normalized change of error input ($x_2 = \Delta E$) and the output as $y_{T1} = U_{T1}$ [10, 19]. Therefore, the fuzzy rule in equation (2.22) is arranged for T1-DFLCs employing T1-FSs ($A_{j,i}$) as:

$$R_n: \text{ IF } x_1 \text{ is } A_{1,i} \text{ and } x_2 \text{ is } A_{2,k} \text{ THEN } y_{T1} \text{ is } C_n \quad (2.46)$$

The output of T1-DFLC is calculated as given in equation (2.23), and the firing strength calculation in equation (2.24) is arranged as follows:

$$f_n = \mu_{A_{1,i}}(x_1) \times \mu_{A_{2,k}}(x_2) = \mu_{A_{1,i}}(E) \times \mu_{A_{2,k}}(\Delta E) \quad (2.47)$$

where the inputs of the T1-DFLC structure (E and ΔE) are obtained according to equations (2.37) and (2.38), respectively. Then, the output scaling factors convert the T1-DFLC output (U in Figure 2.15) as follows:

$$u = K_a U + K_b \int_0^t U(\xi) d\xi, \quad U \in [-1,1] \quad (2.48)$$

where u is the control signal of the closed-loop control system. Here it is also denoted as the output of the T1-SPID controller (i.e. $u = u_{T1}$).

It is worth noting again that the term “ u ” is used as the control signal (i.e. as given in equation (2.48)), in control applications as shown in Figure 2.15, while it is used as the secondary variable in T2-FS definitions (as given in equation (2.11)). Moreover, the U term is used as the FLC output in control applications (i.e. as given in equation (2.48)) as shown in Figure 2.15, while it is used as the universe of discourse of the secondary variable in T2-FS definitions (as given in equation (2.11)). In this thesis, the given both “ u and U ” notations are also followed for the sake of having the same naming convention as in the literature.

2.5.2 Interval type-2 double-input fuzzy PID controllers

The T2-DFLC of a DFPID controller is also constructed by selecting inputs as the normalized error input ($x_1 = E$) and the normalized change of error input ($x_2 = \Delta E$) and the output as $y_{IT2} = U_{IT2}$ [10, 19, 39-40, 42-44]. The fuzzy rule in equation (2.25)

is arranged for IT2-DFLCs employing T2-FSs ($\tilde{A}_{j,i}$) and accordingly, the following fuzzy rule structure is obtained:

$$R_n: \text{ IF } x_1 \text{ is } \tilde{A}_{1,i} \text{ and } x_2 \text{ is } \tilde{A}_{2,k} \text{ THEN } y_{IT2} \text{ is } C_n \quad (2.49)$$

Like its T1 counterpart, the output of IT2-SFLC is calculated as given in equations (2.26), (2.27), and (2.28), while the lower and upper firing interval calculations in equations (2.30) and (2.31) are arranged, respectively as follows:

$$\underline{f}_n = \underline{\mu}_{\tilde{A}_{1,i}}(x_1) \times \underline{\mu}_{\tilde{A}_{2,k}}(x_2) = \underline{\mu}_{\tilde{A}_{1,i}}(E) \times \underline{\mu}_{\tilde{A}_{2,k}}(\Delta E) \quad (2.50)$$

$$\overline{f}_n = \overline{\mu}_{\tilde{A}_{1,i}}(x_1) \times \overline{\mu}_{\tilde{A}_{2,k}}(x_2) = \overline{\mu}_{\tilde{A}_{1,i}}(E) \times \overline{\mu}_{\tilde{A}_{2,k}}(\Delta E) \quad (2.51)$$

where $x_1 = E$ and $x_2 = \Delta E$ are obtained according to firing interval calculations given in equations (2.37) and (2.38) respectively. Here, the membership degrees of LMF and UMF are calculated as given in equations (2.32) and (2.33), respectively. Then, the output scaling factors (K_a and K_b) convert the IT2-SFLC output (U) into the control signal u as illustrated in Figure 2.15. Therefore, the output of the IT2-SPID controller (i.e. $u = u_{IT2}$), is calculated as given in equation (2.48).

Similar to the SFPID controller case, once the FLC output (i.e. U in terms of U_{T1} , U_{IT2} , U_{GT2}) is obtained, then the rest of the output calculations are the same for all FLCs. In other words, it only differs in the assignments of FLC output to the corresponding signals, in terms of type-1, interval type-2, or general type-2. Consequently, the output of the GT2-DPID controller (i.e. $u = u_{GT2}$) is calculated in the same manner. The output calculations of GT2-DFLCs will be presented in “Chapter 3 - General Type-2 Fuzzy Logic Controllers”.

2.6 Structural Design Recommendations

Although, the FLCs provide a superior framework to handle complex/nonlinear systems thanks to their sophisticated input-output mappings, a proper or optimized design might be challenging as the design parameters can be assigned independently from each other, and the total number of the design parameters is also application-dependent. To overcome this problem of the FLC design, some assumptions/rules are

followed such that the FLC design is accomplished in a reasonable effort [7, 30, 31, 40, 41, 55]. In this thesis, the following common design assumptions are considered:

1. The antecedent MFs ($A_{j,i}$ or $\tilde{A}_{j,i}$) are uniformly distributed over the universe (X_i) of the corresponding input (x_i).
2. The antecedent MFs ($A_{j,i}$ or $\tilde{A}_{j,i}$) are constructed with triangle FSs.
3. The total number of antecedent MFs (I or K) corresponds to the total number of rules in the rule table (N). For SFLC and DFLC structures, the conditions are defined as $N = I$ and $N = I \times K$, respectively.
4. The total number of rules (N) is a structural setting parameter for all SFLC and DFLC structures.
5. The Consequent MFs (C_n) are constructed with singletons and each singleton (C_n) corresponds to the fuzzy rule (R_n) in the rule table. The output values of consequent MFs are assumed as design parameters for T1-FLCs.
6. The UMFs of the IT2 antecedent MFs ($\tilde{A}_{j,i}$) are constructed over their T1 counterparts by setting the UMFs as T1-FSs ($A_{j,i}$).
7. The LMFs of the IT2 antecedent MFs ($\tilde{A}_{j,i}$) are constructed over their T1 counterparts by weighting the T1-FSs ($A_{j,i}$) with a height variable ($M_{j,i}$). The height of the IT2 antecedent MFs ($\tilde{A}_{j,i}$) is assumed as a design parameter for IT2-FLCs.
8. The scaling factors (K_e , $K_{\Delta e}$, K_a , and K_b), although they are common for all FLC types, are mostly assumed as design parameters of T1-FLCs.

Table 2.1 : Design parameters of T1-SFLCs.

Assumptions	Total Number of Rules	Known Structural Parameters	Antecedent Design Parameters	Consequent Design Parameters	Total Number of Design Parameters
—	—	—	$A_{1,i}$	C_n	? ¹
4	N	—	$A_{1,i}$	C_n	? ²
3-5	N	$I = N$	$A_{1,i}$	C_n	? ³ + N
2-5	N	$I = N$	$A_{1,i}$	C_n	$3N + N$
1-5	N	$I = N$	—*	C_n	N^*

?¹: Rule structure is not clear, since the total number of rules is undefined.

?²: Rule structure is not clear, since the total number of antecedent MF is undefined.

?³: Antecedent MF type is not clear. (It is $3N$ for triangle case, while it is $4N$ for trapezoid case).

—* : There is no antecedent design parameter according to assumptions since all parameters are defined during distribution over the universe with respect to the total number of rules.

N^* : The number reduces if a consequent is used in multiple rules.

Table 2.2 : Design parameters of T1-DFLCs.

Assumptions	Total Number of Rules	Known Structural Parameters	Antecedent Design Parameters	Consequent Design Parameters	Total Number of Design Parameters
—	—	—	$A_{1,i}, A_{2,k}$	C_n	$?^1$
4	N	—	$A_{1,i}, A_{2,k}$	C_n	$?^2$
3-5	N	$I \times K = N$	$A_{1,i}, A_{2,k}$	C_n	$?^3 + N$
2-5	N	$I \times K = N$	$A_{1,i}, A_{2,k}$	C_n	$3(I + K) + N$
1-5	N	$I \times K = N$	—*	C_n	N^*

$?^1$: Rule structure is not clear, since the total number of rules is undefined.

$?^2$: Rule structure is not clear, since the total number of antecedent MF is undefined.

$?^3$: Antecedent MF type is not clear. (For example, it is $4(I + K)$ for trapezoid case).

—*: All parameters are defined according to assumptions.

N^* : The number reduces if a consequent is used in multiple rules.

Table 2.3 : Design parameters of IT2-SFLCs.

Assumptions	Total Number of Rules	Known Structural Parameters	Antecedent Design Parameters	Consequent Design Parameters	Total Number of Design Parameters
—	—	—	$\tilde{A}_{1,i}$	C_n	$?$
1-5	N	$I = N$	$\tilde{A}_{1,i}$	$-^{T1}$	$6I^\dagger$
1-6	N	$I = N$	$\tilde{A}_{1,i}$	$-^{T1}$	$3I^\ddagger$
1-7	N	$I = N$	$M_{1,i}$	$-^{T1}$	I^\bullet

$?$: Rule structure is not clear.

$-^{T1}$: T1-FLC baseline design. There is no IT2 design parameter.

\dagger : IT2 Antecedent MFs are designed from scratch (Separate LMF and UMF designs).

\ddagger : UMF is fixed according to assumptions. Only LMFs are designed from scratch.

\bullet : LMF and UMFs are defined according to assumptions. The parameter $M_{1,i}$ ($i \in \{1, 2, \dots, I\}$) is the FOU design parameter.

Table 2.4 : Design parameters of IT2-DFLCs.

Assumptions	Total Number of Rules	Known Structural Parameters	Antecedent Design Parameters	Consequent Design Parameters	Total Number of Design Parameters
—	—	—	$\tilde{A}_{1,i}, \tilde{A}_{2,k}$	C_n	$?$
1-5	N	$I \times K = N$	$\tilde{A}_{1,i}, \tilde{A}_{2,k}$	$-^{T1}$	$(6I + 6K)^\dagger$
1-6	N	$I \times K = N$	$\tilde{A}_{1,i}, \tilde{A}_{2,k}$	—	$(3I + 3K)^\dagger$
1-7	N	$I \times K = N$	$M_{1,i}, M_{2,k}$	—	$(I + K)^\bullet$

$?$: Rule structure is not clear.

$-^{T1}$: T1-FLC baseline design. There is no IT2 design parameter.

\dagger : IT2 Antecedent MFs are designed from scratch (Separate LMF and UMF designs).

\ddagger : UMF is fixed according to assumptions. Only LMFs are designed from scratch.

\bullet : LMF and UMFs are defined according to assumptions. The parameters $M_{1,i}$ ($i \in \{1, 2, \dots, I\}$) and $M_{2,k}$ ($k \in \{1, 2, \dots, K\}$) are the FOU design parameters.

As a comprehensive summary of various T1 and IT2-FLC design options, the settings with the least design parameters (i.e. the last rows of the above tables) are summarized in Table 2.5.

Table 2.5 : Summary of T1 and IT2 FLC design parameters.

FLC Type	Total Number of Rules	Known Structural Parameters	Antecedent Design Parameters	Consequent Design Parameters	Total Number of Design Parameters
T1-SFLC	N	$I = N$	—	C_n	N
T1-DFLC	N	$I \times K = N$	—	C_n	N
IT2-SFLC	N	$I = N$	$M_{1,i}$	—	I
IT2-SFLC	N	$I \times K = N$	$M_{1,i}, M_{2,k}$	—	$I + K$

Finally, the design parameters of T1-FPID and IT2 FPID controllers are summarized in Table 2.6. Once the design is handled in a hierarchal order (first T1 fuzzy controller, then IT2fuzzy controller), only antecedent FOU parameters are additionally tuned during the IT2-FPID controller design.

Table 2.6 : Design parameters of T1-FPID and IT2 FPID controllers.

Controller Type	Input Scaling Factors	Antecedent Design Parameters	Consequent Design Parameters	Output Scaling Factors	Additional Parameters (PID)
T1-SFPID	K_e	—	C_n	K_a	K_p, K_i, K_d
T1-DFPID	$K_e, K_{\Delta e}$	—	C_n	K_a, K_b	—
IT2-SFPID	K_e	$M_{1,i}$	C_n	K_a	K_p, K_i, K_d
IT2-DFPID	$K_e, K_{\Delta e}$	$M_{1,i}, M_{2,k}$	C_n	K_a, K_b	—

3. GENERAL TYPE-2 FUZZY LOGIC CONTROLLERS

3.1 Introduction

The GT2-FLCs are constructed by five main parts: fuzzifier, fuzzy rule base, inference engine, type-reducer, and defuzzifier [7]. As in the T1-FLC and IT2-FLC counterparts, the fuzzifier converts crisp input into GT2 fuzzy input sets, then the inference engine combines these GT2 fuzzy input sets through the fuzzy IF-THEN rules and accumulates the GT2 fuzzy output sets after calculating corresponding firing levels of each fuzzy rule. After combining these output fuzzy sets, the type reducer calculates them as type-reduced sets to be used in the defuzzification. Then the defuzzifier generates the crisp output. Although the system block diagram of GT2-FLC seems like its IT2 counterpart, the calculation steps are much more complex and additional computation operations are required to compute the GT2-FLC output. These additional operations and calculation steps will be given in the next sections. The system block diagram of GT2-FLCs is given in Figure 3.1

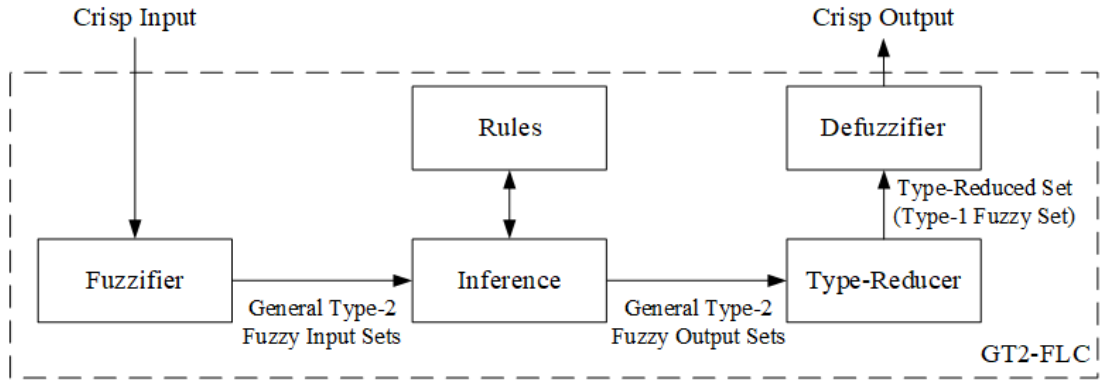


Figure 3.1 : System block diagram of general type-2 fuzzy logic controllers.

A fuzzy rule of a GT2-FLC is defined as follows [7]:

$$R_n: \text{ IF } x_1 \text{ is } \tilde{A}_{1,i} \text{ and } \dots \text{ and } x_J \text{ is } \tilde{A}_{J,i} \text{ THEN } y_{GT2} \text{ is } C_n \quad (3.1)$$

where x_j ($j \in \{1, 2, \dots, J\}$) is an input, $\tilde{A}_{j,i}$ ($i \in \{1, 2, \dots, I\}$) is an antecedent GT2-MF, J is the total number of inputs, I is the total number of antecedent GT2-MFs, R_n ($n \in$

$\{1, 2, \dots, N\}$) is the n^{th} rule of the rule table, N is the total number of rules in the rule table, and C_n is an output singleton consequent of the rule R_n , and y_{GT2} is the output of GT2-FLC.

3.2 General Type-2 Fuzzy Sets

The General Type-2 Fuzzy Set (GT2-FS) is the generic form of T2-FSs. Hence a GT2-FS is also denoted as \tilde{A} and it is defined as in equation (2.11). For completeness reasons, the definition of a GT2-FS (\tilde{A}) is also given in this section as follows [7]:

$$\tilde{A} = \{(x, u), \mu_{\tilde{A}}(x, u) \mid x \in X, u \in U\} \quad (3.2)$$

where x is the input variable (also called as the primary variable of \tilde{A}), X is the universe of the primary variable x , u is the secondary variable of \tilde{A} , U is the universe for the secondary variable u , and $\mu_{\tilde{A}}(x, u)$ is the T2-MF of the T2-FS \tilde{A} . In the continuous and the discrete domains, a GT2-FS (i.e. denoted as \tilde{A}) is defined as follows:

$$\tilde{A} = \int_{x \in X} \int_{u \in U} \mu_{\tilde{A}}(x, u) / (x, u) \quad \text{or} \quad \tilde{A} = \int_{x \in X} \left(\int_{u \in U} \mu_{\tilde{A}}(x, u) / u \right) / x \quad (3.3)$$

$$\tilde{A} = \sum_{x \in X_d} \sum_{u \in U_d} \mu_{\tilde{A}}(x, u) / (x, u) \quad \text{or} \quad \tilde{A} = \sum_{x \in X_d} \left(\sum_{u \in U_d} \mu_{\tilde{A}}(x, u) / u \right) / x \quad (3.4)$$

The membership grade (primary and/or secondary) of a GT2-FS is described based on the primary membership of x (i.e. J_x) and the SMF ($\mu_{\tilde{A}(x)}(u)$ or $\mu_{\tilde{A}(x)}$). Here, similar to the IT2 case, the SMF and the primary membership (J_x) are also defined as:

$$\mu_{\tilde{A}(x)} = \mu_{\tilde{A}(x)}(u) = \int_{u \in [0,1]} \mu_{\tilde{A}}(x, u) / (u) \quad (3.5)$$

$$J_x = \{(x, u) \mid u \in [0, 1], \mu_{\tilde{A}}(x, u) > 0\} \quad (3.6)$$

The SMF (i.e. $\mu_{\tilde{A}(x)}$) is a distinguishing property of the GT2-FSs since it determines the resulting output of the GT2-FLC [68]. The SMFs are generally defined with well-known T1-FSs (triangle, trapezoid, and gauss) at the secondary layer [7]. In this context, GT2-FS counterparts of IT2-FSs (given in Figures 2.4, 2.5, and 2.6) and T1-

FSs (given in Figures 2.1, 2.2, and 2.3) are illustrated in Figures 3.2-3.7. For easiness, the SMFs are selected as triangle, trapezoid, gaussian T1-FSs, respectively.

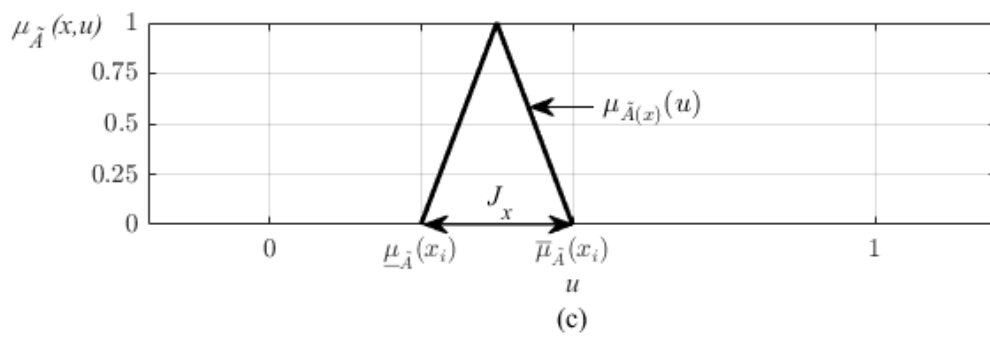
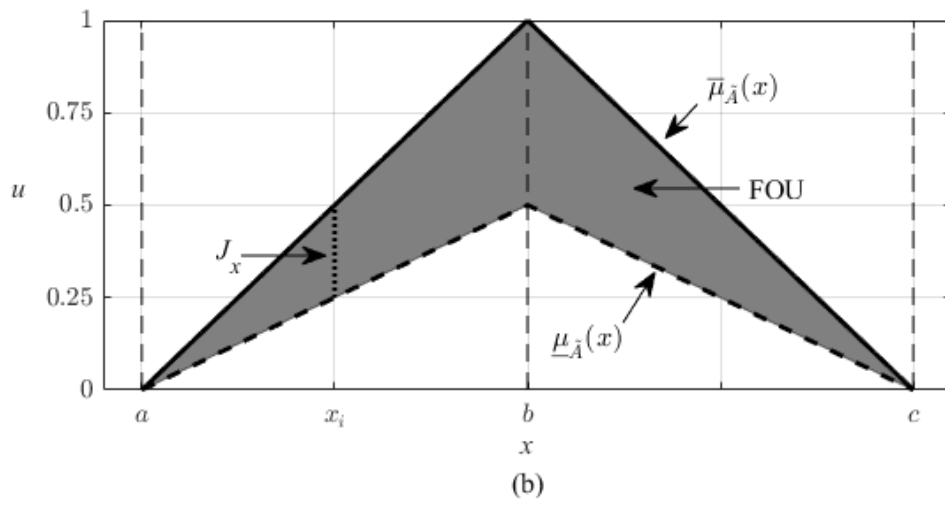
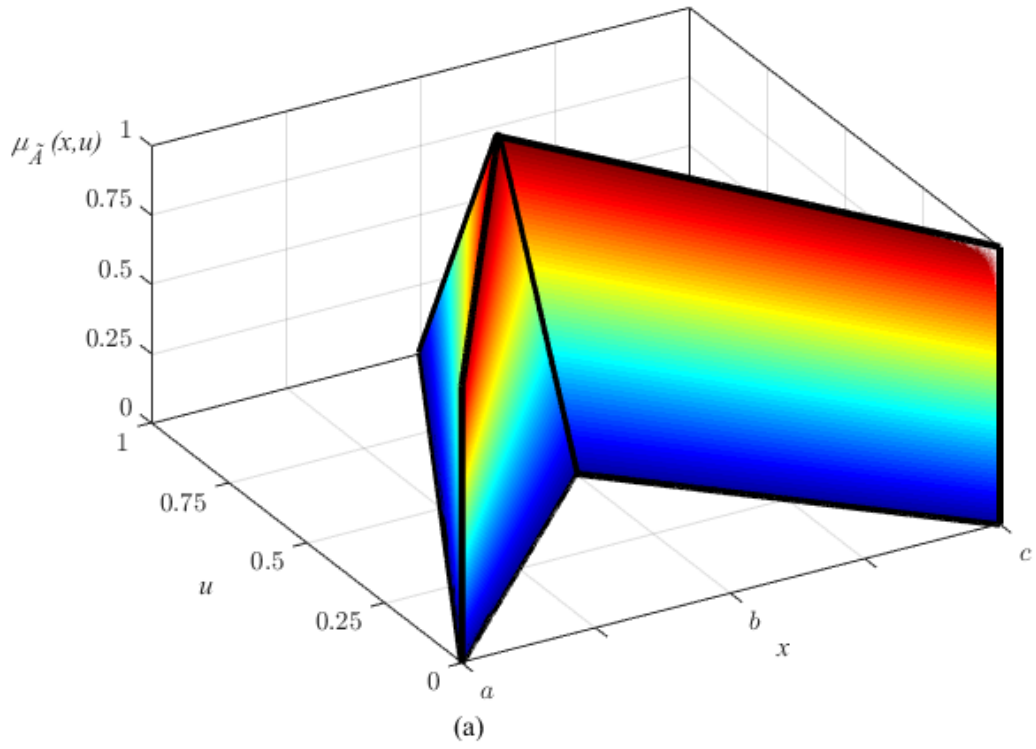


Figure 3.2 : A triangle GT2-FS employing triangle SMF.

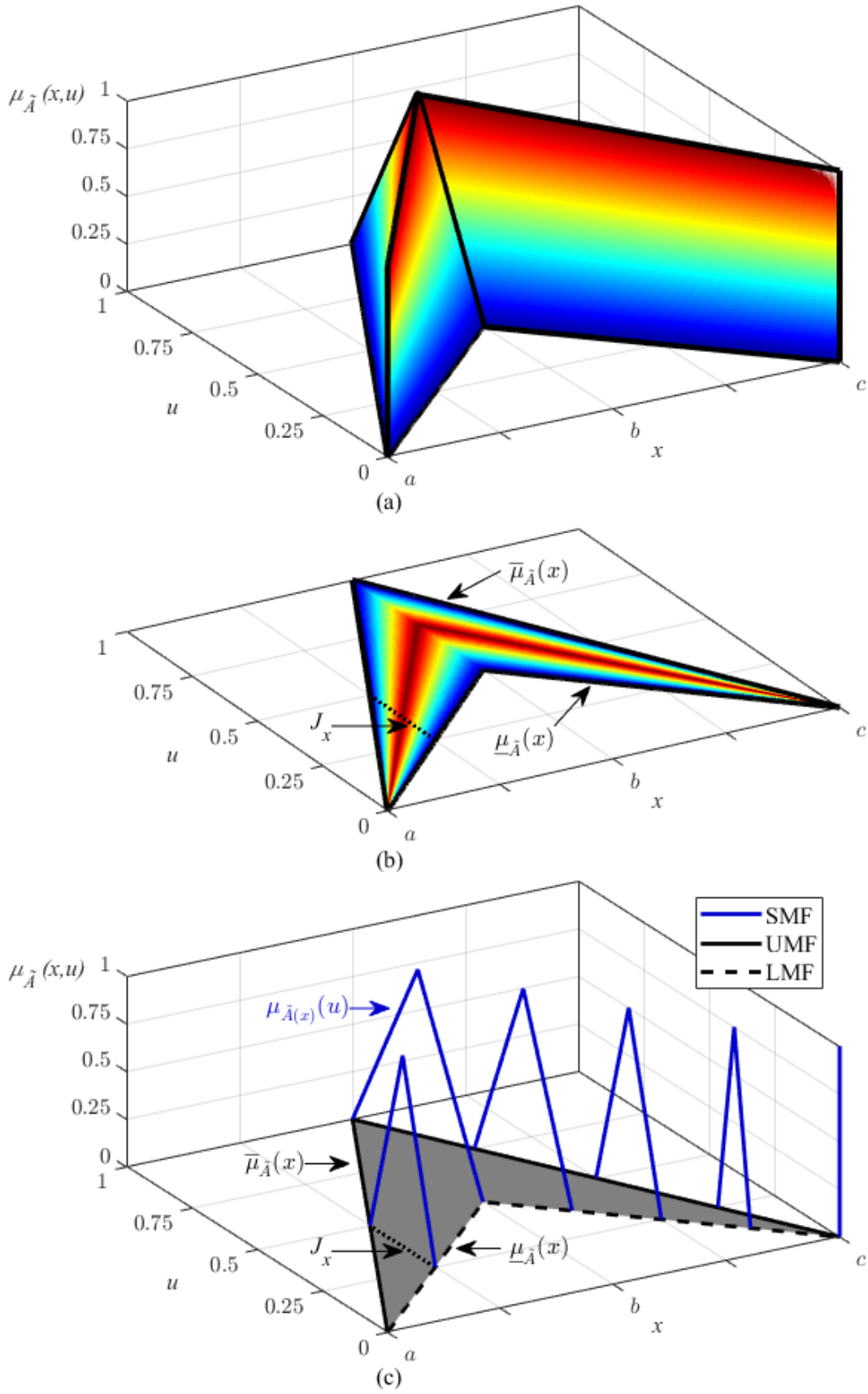


Figure 3.3 : A triangle GT2-FS employing triangle SMF.

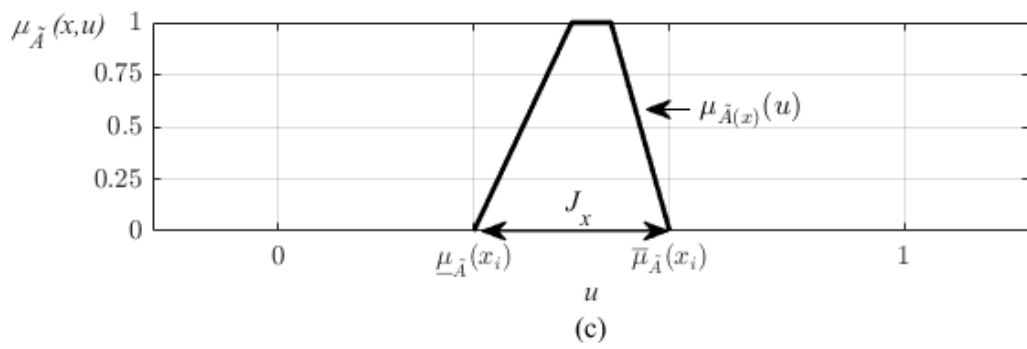
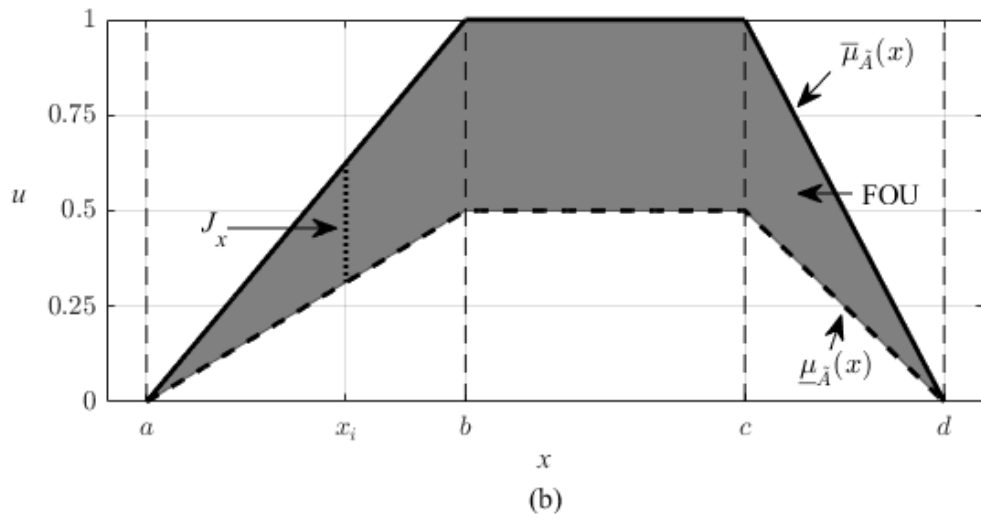
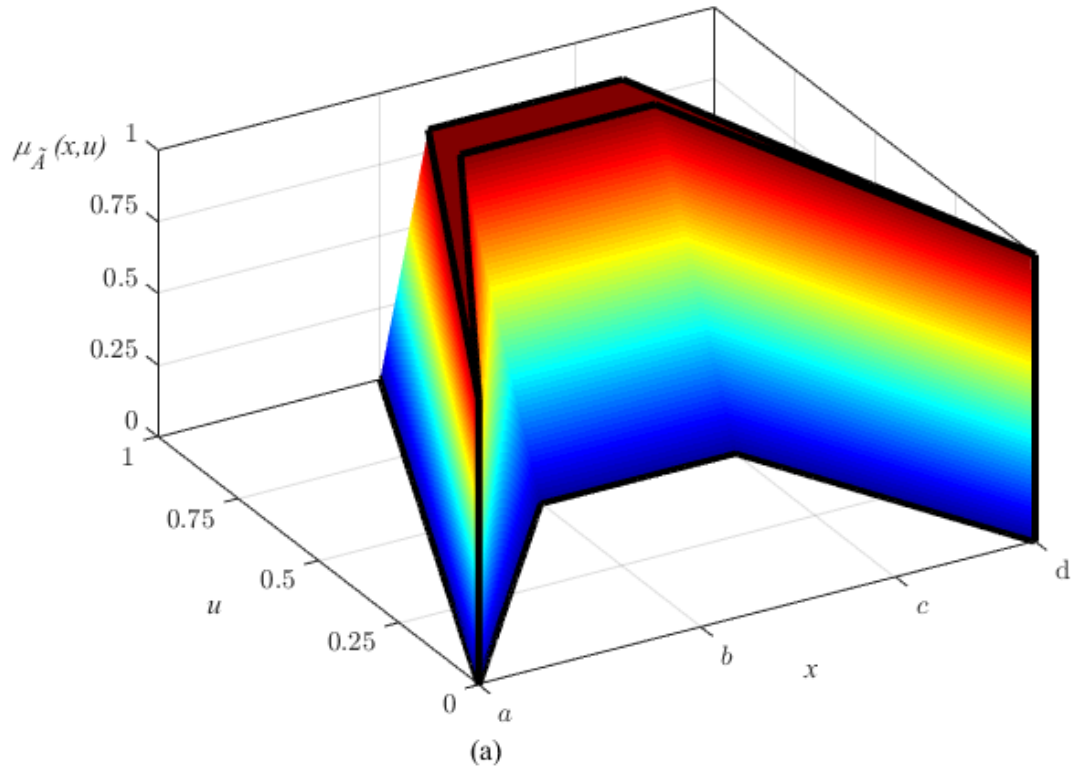


Figure 3.4 : A trapezoid GT2-FS employing trapezoid SMF.

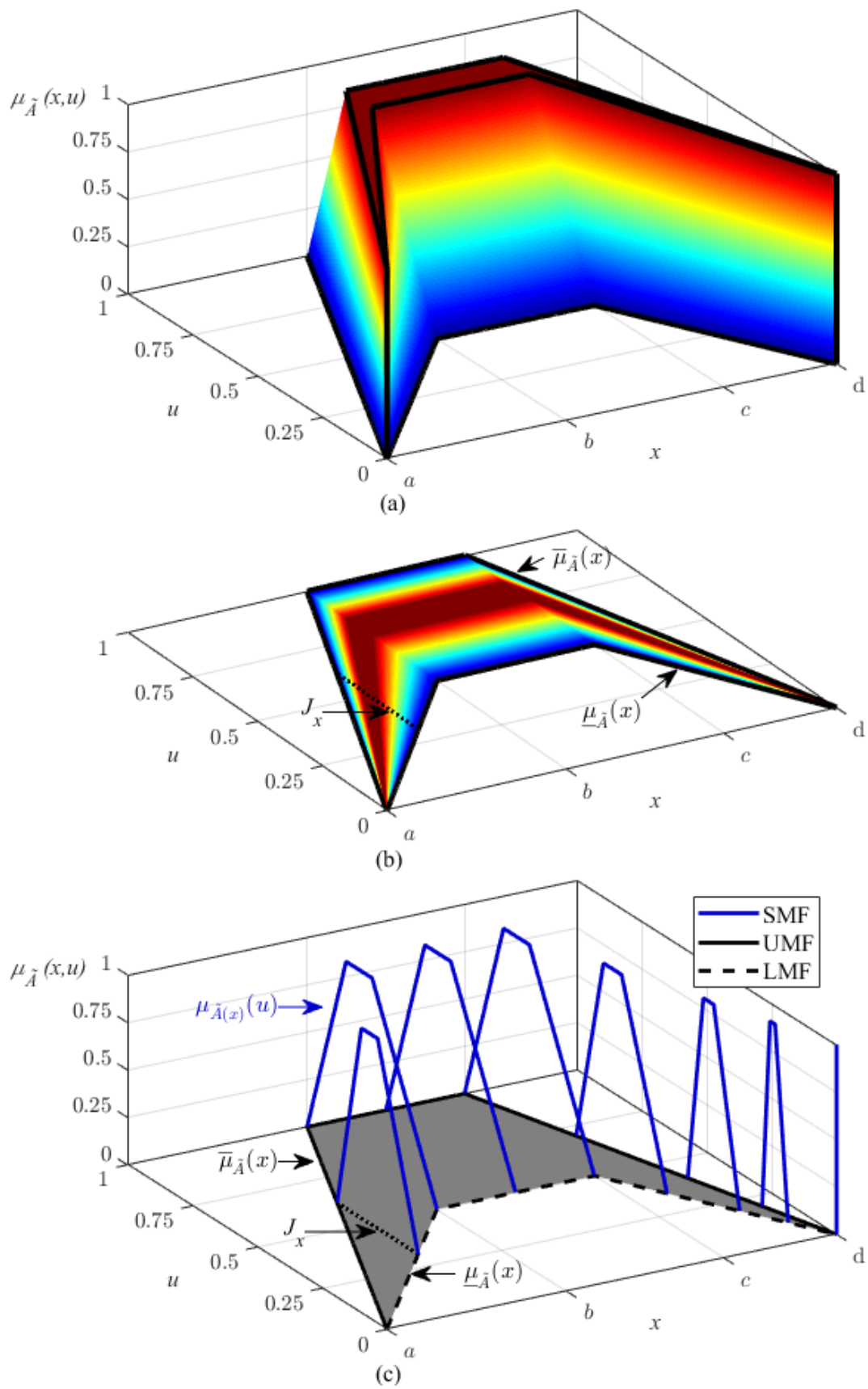


Figure 3.5 : A trapezoid GT2-FS employing trapezoid SMF.

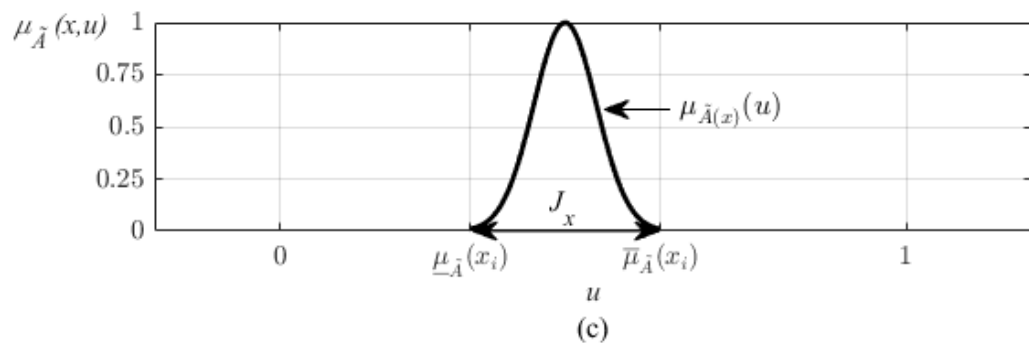
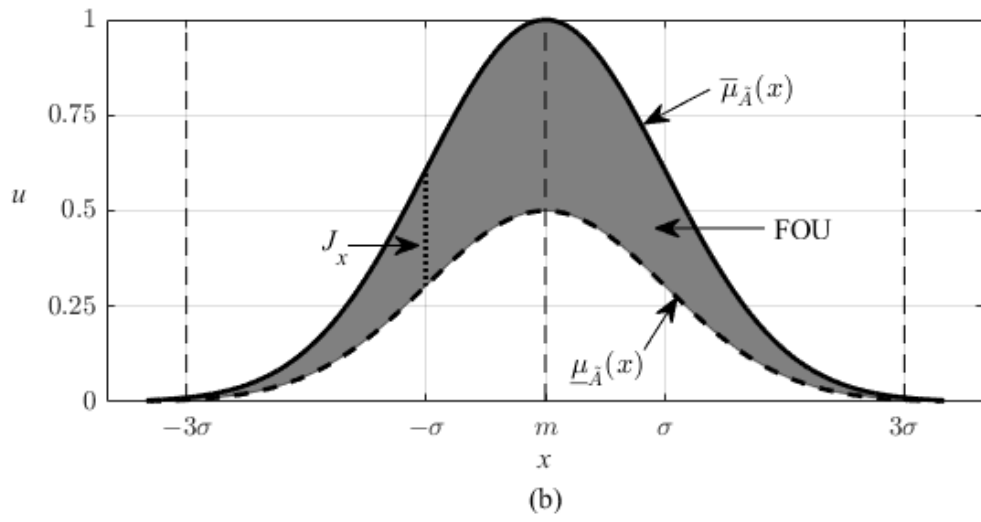
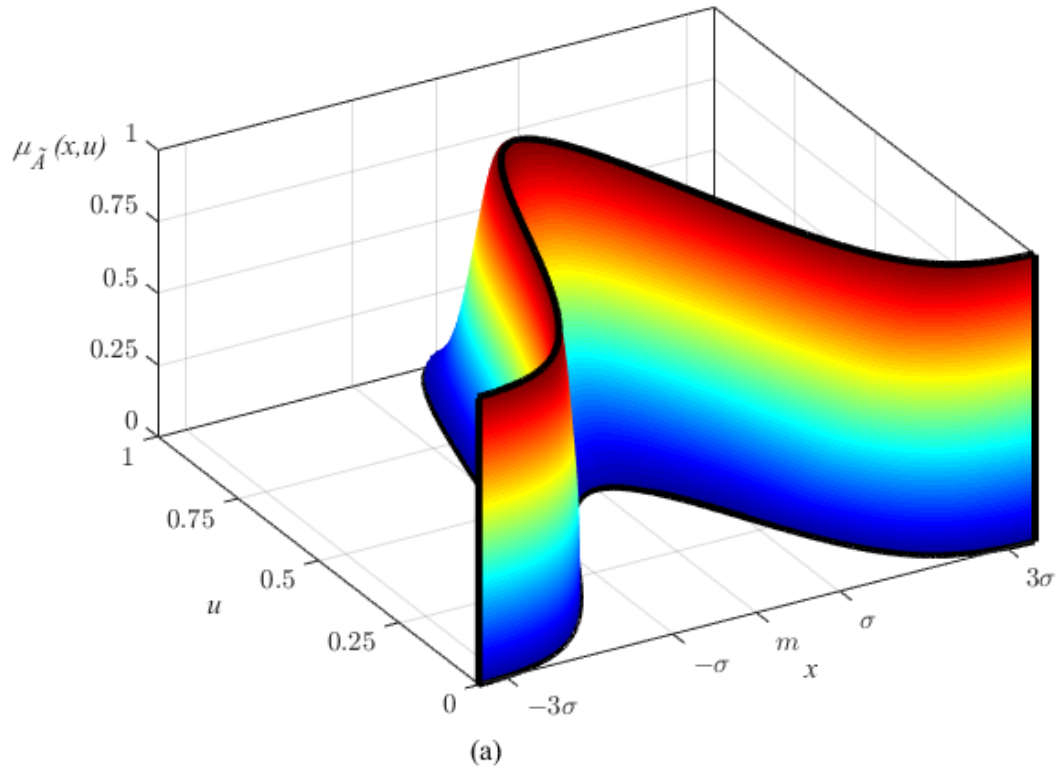


Figure 3.6 : A Gaussian GT2-FS employing Gaussian SMF.

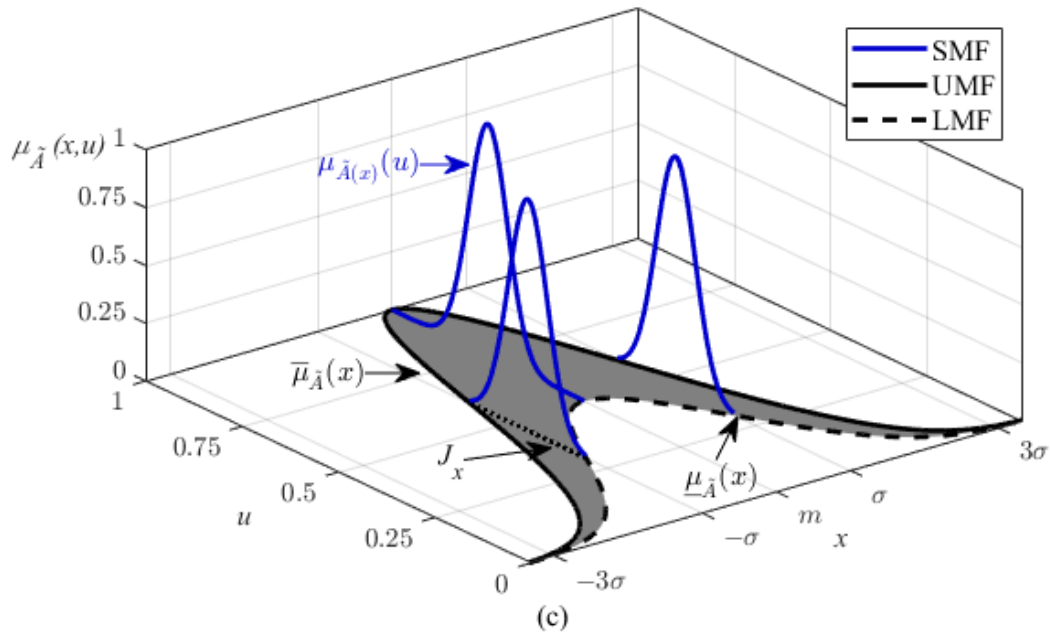
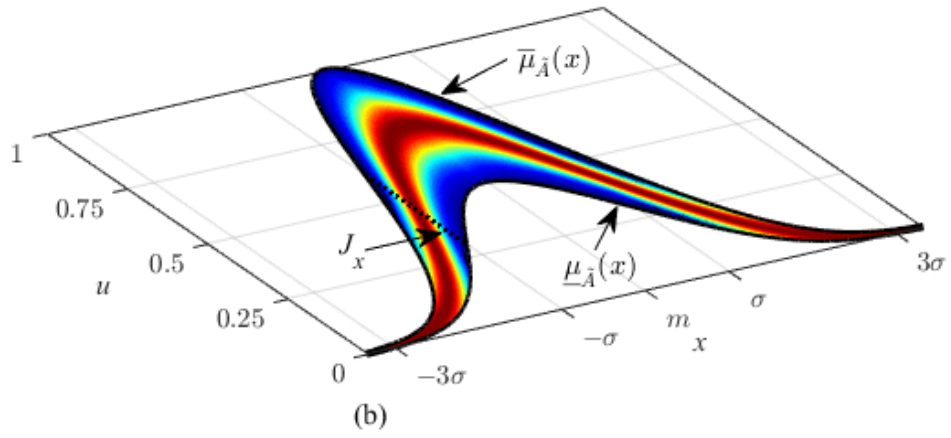
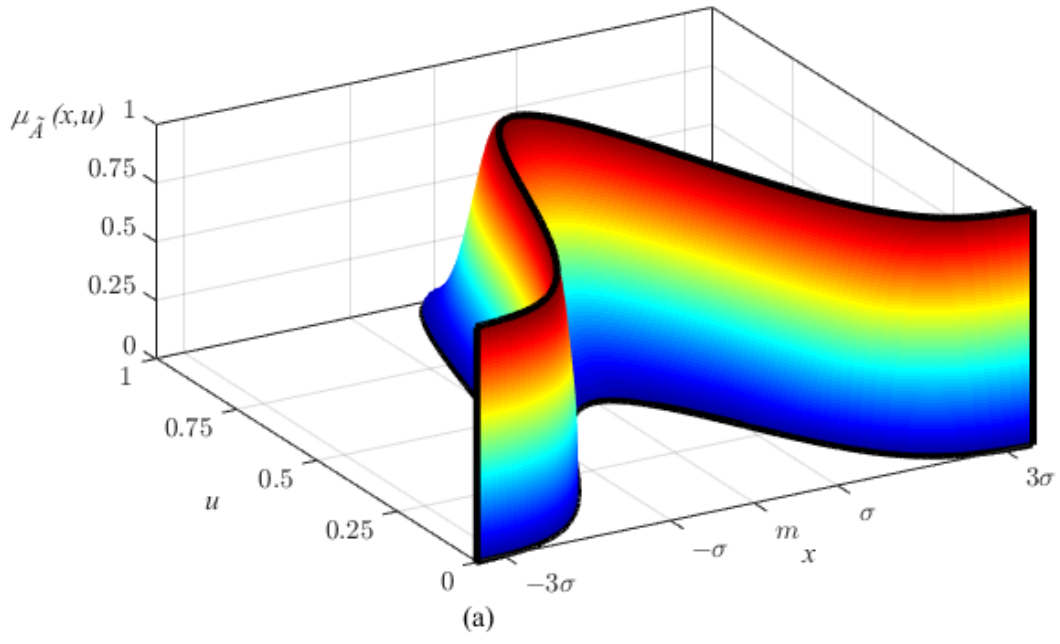


Figure 3.7 : A Gaussian GT2-FS employing Gaussian SMF.

As shown in Figures 3.2-3.7, the visual properties of the GT2-FSs are considerably more complex than their T1 and IT2 counterparts. In all figures, subplots (a) show GT2-FSs in the 3D representation domain where the x-y-z axes are defined by the primary input variable (i.e. x), the secondary variable (i.e. u), and the secondary membership grade (i.e. $\mu_{\tilde{A}}(x, u)$), respectively. The FOU, LMF, and UMF are shown in Figures 3.2b, 3.4b, and 3.6b associated with their triangle, trapezoid, Gaussian T2-FSs, respectively. In Figures 3.2c, 3.4c, and 3.6c, for a fixed input value (i.e. x_i), the resulting SMF support (i.e. J_x) and corresponding triangle, trapezoid, and Gaussian SMFs (i.e. $\mu_{\tilde{A}(x)}(u)$) are given respectively. The figure subplot pairs 3.3a-3.3b, 3.5a-3.5b, and 3.7a-3.7b are the same from the content point of view, but they differ from the view rotation of the z-axis. In these figures, all subplots (b) are rotated on the z-axis (i.e. $\mu_{\tilde{A}}(x, u)$) until the data is projected into the “ x, u ” domain. In Figures 3.3c, 3.5c, and 3.7c, a set of the resulting triangle, trapezoid, and Gaussian T1-FSs of the SMFs are illustrated with blue markers, respectively. Here it is worth mentioning again that, if a collection of all individual T1-FSs of the SMFs (marked as blue in Figures 3.3c, 3.5c, and 3.7c) are combined for all x values ($x \in X$), then the GT2-FS (i.e. \tilde{A}) is obtained over the values of SMF (i.e. $\mu_{\tilde{A}(x)}(u)$) as follows [7]:

$$\tilde{A} = \int_{x \in X} (\mu_{\tilde{A}(x)})/x, \quad \mu_{\tilde{A}(x)} = \mu_{\tilde{A}(x)}(u) = \int_{\underline{\mu}_{\tilde{A}}(x)}^{\overline{\mu}_{\tilde{A}}(x)} (f_x(u))/u \quad (3.7)$$

where $f_x(u)$ denotes the secondary grade of input variable x and it equals to $\mu_{\tilde{A}}(x, u)$. The secondary grade can be also defined by the employed T1-FSs, that depict SMFs, which are defined in the range of LMF and UMF values as follows:

$$f_x(u) = A_x, \quad A_x = \left\{ (u, \mu_{A_x}(u)) \mid u \in [\underline{\mu}_{\tilde{A}}(x), \overline{\mu}_{\tilde{A}}(x)] \right\} \quad (3.8)$$

where A_x represents an individual T1-FS of a SMF.

3.3 Secondary Membership Functions

As mentioned in the previous sections, the SMF (i.e. $\mu_{\tilde{A}(x)}(u)$) is constructed by an ordinary T1-FS, which is also called as A_x to represent the T1-FS associated with a SMF slice. Therefore, the SMF definitions can be obtained by rearranging the T1-FS definitions based on the input value universe of the secondary variable (i.e. u).

3.3.1 Triangle secondary membership function

A triangle SMF that employs triangle T1-FS is defined (after the arrangement of the triangle T1-FS definition in equation (2.6)) as follows:

$$\mu_{\tilde{A}(x)}(u) = \begin{cases} \frac{u - \rho^1}{\rho^2 - \rho^1} & \rho^1 < u \leq \rho^2 \\ \frac{\rho^3 - u}{\rho^3 - \rho^2}, & \rho^2 < u \leq \rho^3 \\ 0, & \text{otherwise} \end{cases} \quad (3.9)$$

where $\rho^s \in [0, 1]$ ($s \in \{1, 2, 3\}$) defines the shape of the triangle. Here, ρ^1 , ρ^2 , and ρ^3 are left support, apex, and right support points of the triangle shape, respectively. These $\{\rho^1, \rho^2, \rho^3\}$ parameters in equation (3.9) are corresponding counterparts of the T1-FS design parameters $\{a, b, c\}$ in equation (2.6). The SMF parameters (ρ^1 , ρ^2 , and ρ^3) are defined in increasing order as $0 \leq \rho^1 \leq \rho^2 \leq \rho^3 \leq 1$. Based on the values of these parameters, it is possible to generate numerous SMFs with different shapes and supports. In the fuzzy literature, the researchers mainly preferred to locate the supports (ρ^1 and ρ^3) on the values of LMF and UMF, such that the design of the SMF can be accomplished through a single parameter [7, 62, 65]. This design is alternatively called as the apex point design through a parameter $\text{Apex}(u|x)$.

Once the base parameters (ρ^1 , ρ^2 , and ρ^3) are replaced with corresponding values of $\{\underline{\mu}_{\tilde{A}}(x), \text{Apex}(u|x), \overline{\mu}_{\tilde{A}}(x)\}$ as follows:

$$\rho^1 = \underline{\mu}_{\tilde{A}}(x) \quad \rho^2 = \text{Apex}(u|x) \quad \rho^3 = \overline{\mu}_{\tilde{A}}(x) \quad (3.10)$$

then the triangle SMF can be defined as follows:

$$\mu_{\tilde{A}(x)}(u) = \begin{cases} \frac{u - \underline{\mu}_{\tilde{A}}(x)}{\text{Apex}(u|x) - \underline{\mu}_{\tilde{A}}(x)} & \underline{\mu}_{\tilde{A}}(x) < u \leq \text{Apex}(u|x) \\ \frac{\overline{\mu}_{\tilde{A}}(x) - u}{\overline{\mu}_{\tilde{A}}(x) - \text{Apex}(u|x)}, & \text{Apex}(u|x) < u \leq \overline{\mu}_{\tilde{A}}(x) \\ 0, & \text{otherwise} \end{cases} \quad (3.11)$$

where the apex point ($\text{Apex}(u|x)$) is designed based on a single design parameter (w) as $\underline{\mu}_{\tilde{A}}(x)$ and $\overline{\mu}_{\tilde{A}}(x)$ are straightforwardly calculated for any x input value. The apex point is mapped as a function of this design parameter (w) as follows:

$$\text{Apex}(u|x) = \underline{\mu}_{\tilde{A}}(x) + w \left(\overline{\mu}_{\tilde{A}}(x) - \underline{\mu}_{\tilde{A}}(x) \right) \quad (3.12)$$

where $w \in [0,1]$ determines the location of the apex point in the range of $[\underline{\mu}_{\tilde{A}}(x), \overline{\mu}_{\tilde{A}}(x)]$ as shown in Figure 3.8. Note that the parameter w is denoted as the design parameter of triangle SMF and it is treated as the same for all vertical slices [65].

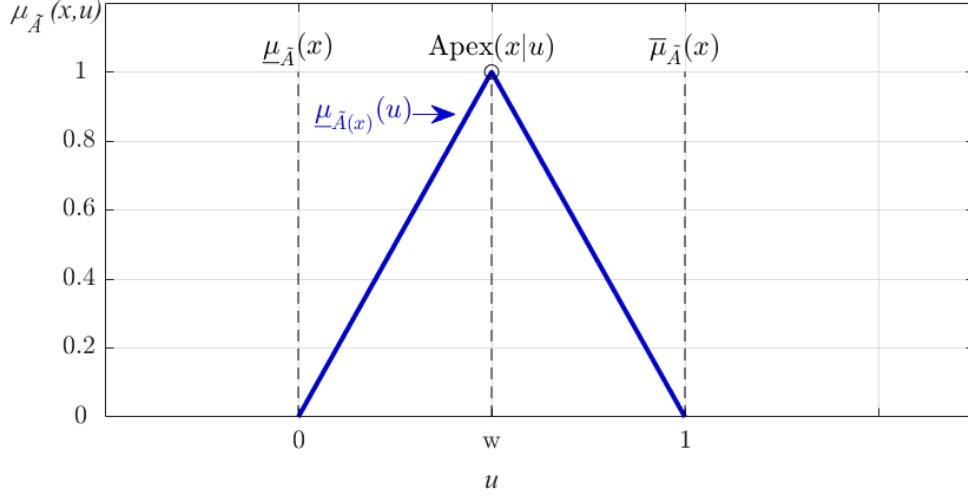


Figure 3.8 : A triangle SMF and its apex point.

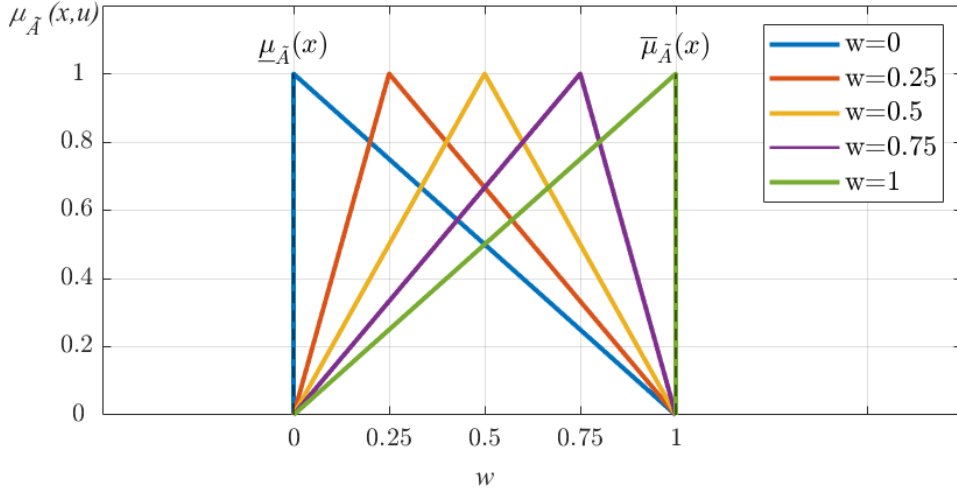


Figure 3.9 : A triangle SMFs with different apex point settings.

When the parameter is set to $w = 0$, the apex point is located on the LMF (i.e. $\underline{\mu}_{\tilde{A}}(x)$) as a left perpendicular triangle is obtained. When the parameter is set to $w = 1$, the apex point is located on the UMF (i.e. $\overline{\mu}_{\tilde{A}}(x)$) as a right perpendicular triangle is obtained. The resulting shapes of the triangle SMFs for different w design parameter settings $\{0, 0.25, 0.5, 0.75, \text{ and } 1\}$ are illustrated in Figure 3.9.

It is worth underlying that the w -based parameterization provides a simple and useful mapping for the SMF design, while the ρ -based parameterization provides more design flexibility. For example, the support of the SMF is defined on a subset of the primary membership of x (J_x), when $\rho^1 > 0$ or $\rho^3 < 1$, which can be commented as a resizing of the FOU [76]. When $\rho^1 = 0$ and $\rho^3 = 1$; the support of the SMF, in other words, the horizontal line between ρ^1 and ρ^3 , is defined on the primary membership of x $[\underline{\mu}_{\tilde{A}}(x), \bar{\mu}_{\tilde{A}}(x)]$. The ρ -based parameterization covers the w -based one per design option. The w -based parameterization has a single design parameter (w), while the ρ -based parameterization has three design parameter (ρ^1, ρ^2 , and ρ^3).

3.3.2 Trapezoid secondary membership function

A trapezoid SMF that employs trapezoid T1-FS is defined (after the arrangement of the trapezoid T1-FS definition in equation (2.8)) as follows:

$$\mu_{\tilde{A}(x)}(u) = \begin{cases} \frac{u - \delta^1}{\delta^2 - \delta^1} & \delta^1 \leq u < \delta^2 \\ 1 & \delta^2 \leq u < \delta^3 \\ \frac{\delta^4 - u}{\delta^4 - \delta^3} & \delta^3 \leq u < \delta^4 \\ 0 & \text{otherwise} \end{cases} \quad (3.13)$$

where $\delta^t \in [0, 1]$ ($t \in \{1, 2, 3, 4\}$) defines the shape of the trapezoid. Here, $\delta^1, \delta^2, \delta^3$, and δ^4 are left support, left core, right core, and right support points of the trapezoid shape, respectively. The parameters $\{\delta^1, \delta^2, \delta^3, \delta^4\}$ are corresponding counterparts of the T1-FS design parameters $\{a, b, c, d\}$ in equation (2.8). The SMF parameters ($\delta^1, \delta^2, \delta^3$, and δ^4) are defined in increasing order as $0 \leq \delta^1 \leq \delta^2 \leq \delta^3 \leq \delta^4 \leq 1$. Based on the values of these parameters, it is possible to generate numerous SMFs with different shapes and supports. In fuzzy literature, like the triangle case, researchers mainly preferred to locate the left and right supports (δ^1 and δ^4) on the values of LMF and UMF, such that the design of the SMF can be accomplished with fewer design parameters [7]. This design can be alternatively called as the core line design through $\text{Core}_L(u|x)$ and $\text{Core}_R(u|x)$. These core points can be selected as symmetrical or non-symmetrical based on design preferences [7].

Once the base parameters ($\delta^1, \delta^2, \delta^3$, and δ^4) are replaced with corresponding values of $\{\underline{\mu}_{\tilde{A}}(x), \text{Core}_L(u|x), \text{Core}_R(u|x), \bar{\mu}_{\tilde{A}}(x)\}$, the triangle SMF is defined as follows:

$$\mu_{\tilde{A}(x)}(u) = \begin{cases} \frac{u - \underline{\mu}_{\tilde{A}}(x)}{\text{Core}_L(u|x) - \underline{\mu}_{\tilde{A}}(x)} & \underline{\mu}_{\tilde{A}}(x) \leq u < \text{Core}_L(u|x) \\ 1 & \text{Core}_L(u|x) \leq u < \text{Core}_R(u|x) \\ \frac{\bar{\mu}_{\tilde{A}}(x) - u}{\bar{\mu}_{\tilde{A}}(x) - \text{Core}_R(u|x)} & \text{Core}_R(u|x) \leq u < \bar{\mu}_{\tilde{A}}(x) \\ 0 & \text{otherwise} \end{cases} \quad (3.14)$$

where

$$\delta^1 = \underline{\mu}_{\tilde{A}}(x) \quad \delta^2 = \text{Core}_L(u|x) \quad \delta^3 = \text{Core}_R(u|x) \quad \delta^4 = \bar{\mu}_{\tilde{A}}(x) \quad (3.15)$$

Here, the left and right core points (i.e. $\text{Core}_L(u|x)$ and $\text{Core}_R(u|x)$) are determined based on the symmetrical or non-symmetrical design options. The core points are treated as the same for all vertical slices [7] and they are mapped based on two design parameters (w_L and w_R) as follows:

$$\text{Core}_L(u|x) = \underline{\mu}_{\tilde{A}}(x) + w_L \left(\bar{\mu}_{\tilde{A}}(x) - \underline{\mu}_{\tilde{A}}(x) \right) \quad (3.16)$$

$$\text{Core}_R(u|x) = \underline{\mu}_{\tilde{A}}(x) + w_R \left(\bar{\mu}_{\tilde{A}}(x) - \underline{\mu}_{\tilde{A}}(x) \right) \quad (3.17)$$

where w_L and w_R determine the core points in the relative range of $[\underline{\mu}_{\tilde{A}}(x), \bar{\mu}_{\tilde{A}}(x)]$.

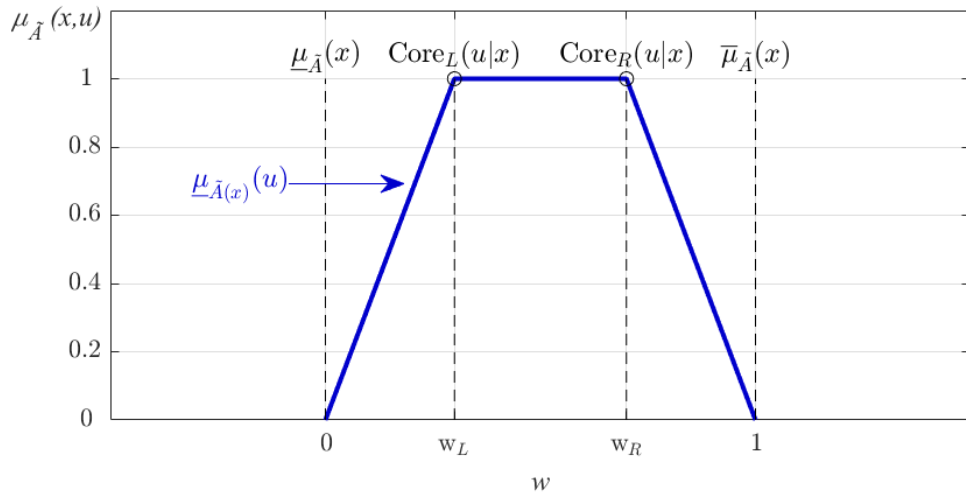


Figure 3.10 : A trapezoid SMF and its support and core points.

For the symmetrical trapezoid SMF design option, the design parameters (w_L and w_R) that determines the core points ($\text{Core}_L(u|x)$ and $\text{Core}_R(u|x)$) are mapped based on a single design parameter ($w \in [0, 0.5]$) as follows [7]:

$$w_L = w \quad w_R = 1 - w \quad (3.18)$$

For the non-symmetrical trapezoid SMF design option, the design parameters (w_L, w_R) that determine the core points ($\text{Core}_L(u|x)$ and $\text{Core}_R(u|x)$) are selected as [7]

$$0 \leq w_L \leq w_R \leq 1 \quad (3.19)$$

Symmetrical and non-symmetrical trapezoid SMF design examples are given in Figures 3.10 and 3.11, respectively. When $w_L = 0$ and $w_R = 1$, a rectangle shape is obtained, therefore GT2-FS reduces to IT2-FS. For the setting $w_L = w_R = w = 0.5$ setting, a triangle shape is obtained, therefore trapezoid SMF reduces to triangle SMF. The trapezoid SMFs will be also investigated in “Section 4.2 - Novel Representation of Trapezoid Secondary Membership Function”.

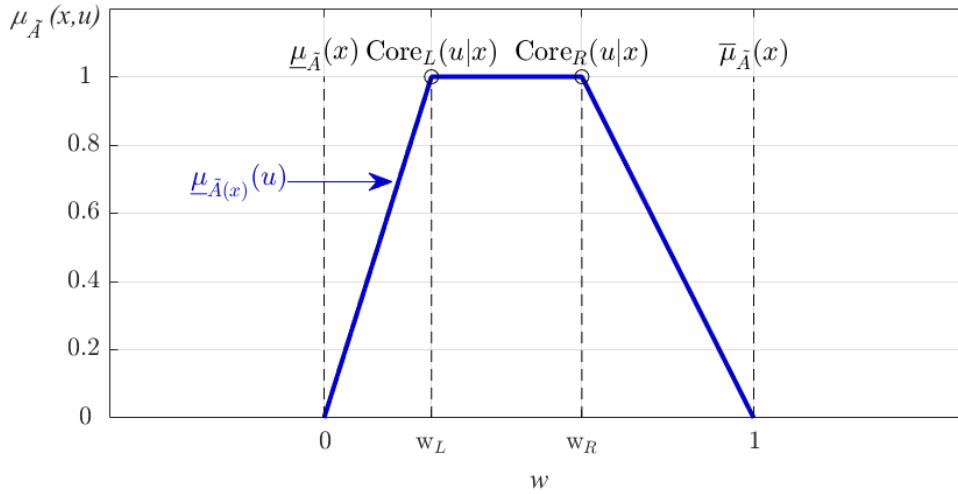


Figure 3.11 : A trapezoid SMF and its support and core points.

3.4 Horizontal Slice Representation based on α -Planes

The GT2-FSs are represented with various methods; a) collection of all points, b) union of all (vertical) slices over for all x values, c) union of wavy slices, d) union of all (horizontal) slices over the α levels (or z-slices) at the secondary layer (e.g. $\mu_{\tilde{A}}(x, u)$ axis) [7]. The collection of all points representation given in equation (3.2), is the initial definition for all other representations. The representation, namely union of all (vertical) slices over for all x values, is defined in the previous section in equation (3.7). The vertical representation provides supportive features for the visualization of GT2-FSs. The most popular representation is the union of all horizontal slices. This

representation is also called as α -plane representation [61, 62] or z-slice representation [63, 64]. Although the definitions of α -plane and z-slice representations seem to be different, the resulting outputs are the same [65, 66, 76]. In this thesis, the “ α -plane” term is used to express the horizontal slices. According to the α -plane representation, a GT2-FS (\tilde{A}) is represented as a union collection of α -planes (\tilde{A}^{α_p}) raised to the level α_p in various ways, as given in [60]:

$$\tilde{A} = \bigcup_{\alpha_p \in [0,1]} \tilde{A}^{\alpha_p} \quad (3.20)$$

$$\tilde{A}^{\alpha_p} = \{(x, u), \mu_{\tilde{A}}(x, u) > \alpha_p \mid x \in X, u \in [0,1]\} \quad (3.21)$$

$$\tilde{A}^{\alpha_p} = \int_{x \in X} \int_{u \in [0,1]} \{(x, u), \mu_{\tilde{A}}(x, u) > \alpha_p\} \quad (3.22)$$

where \tilde{A}^{α_p} is an α -plane of the GT2-FS \tilde{A} that is associated with an α -plane (α_p) (i.e. an α -plane raised to the level α_p). Here, an α -plane \tilde{A}^{α_p} also resembles an IT2-FS whose secondary grade equals to the level α_p instead of 1. An α -plane is also defined as the union of all primary memberships whose secondary grades (i.e. $\mu_{\tilde{A}}(x, u)$) are greater than or equal to the level α_p . Since the α -plane representation of T2-FSs is quite similar to the α -cut representation of T1-FSs, α -planes of GT2-FS can be obtained from α -cuts of the T1-FS employed in the SMF ($\mu_{\tilde{A}(x)}(u)$) [7]. Based on this notation, an α -plane of the GT2-FS (i.e. \tilde{A}^{α_p}) and α -cut of T1-FS employed in SMFs (i.e. $\tilde{A}_x^{\alpha_p}$) can be expressed as follows:

$$\tilde{A}_x^{\alpha_p} = \{u | \mu_{\tilde{A}(x)}(u) \geq \alpha_p\} = \{u | \mu_{\tilde{A}_x} \geq \alpha_p\} \equiv [\underline{\mu}_{\tilde{A}^{\alpha_p}}(x), \bar{\mu}_{\tilde{A}^{\alpha_p}}(x)] \quad (3.23)$$

$$\tilde{A}^{\alpha_p} = \int_{x \in X} \tilde{A}_x^{\alpha_p} / x = \int_{x \in X} [\underline{\mu}_{\tilde{A}^{\alpha_p}}(x), \bar{\mu}_{\tilde{A}^{\alpha_p}}(x)] / x \quad (3.24)$$

where $\underline{\mu}_{\tilde{A}^{\alpha_p}}(x)$ and $\bar{\mu}_{\tilde{A}^{\alpha_p}}(x)$ (or simply $\underline{\mu}_{\tilde{A}^{\alpha_p}}$ and $\bar{\mu}_{\tilde{A}^{\alpha_p}}$) are lower and upper MFs of \tilde{A}^{α_p} , also called as α -plane associated LMF and UMF, respectively. The illustrative α -plane examples for triangle and trapezoid FSs are given in Figure 3.12 and Figure 3.13, respectively.

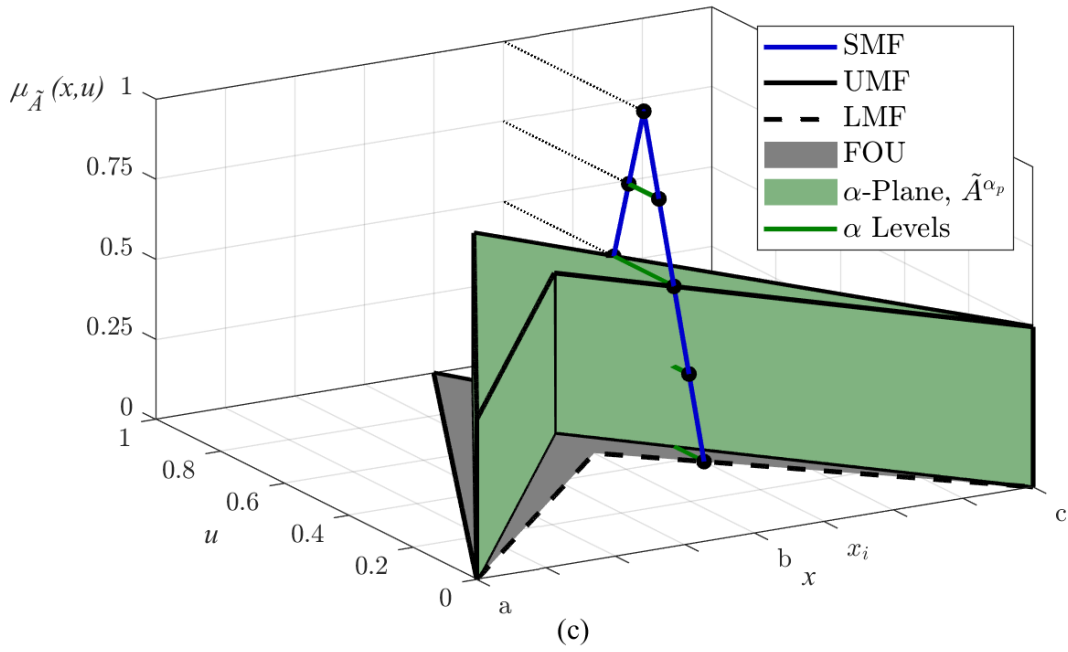
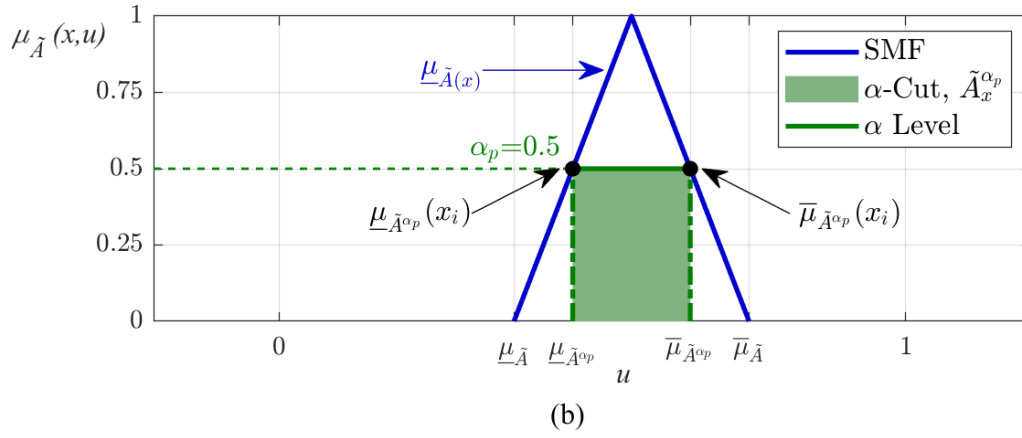
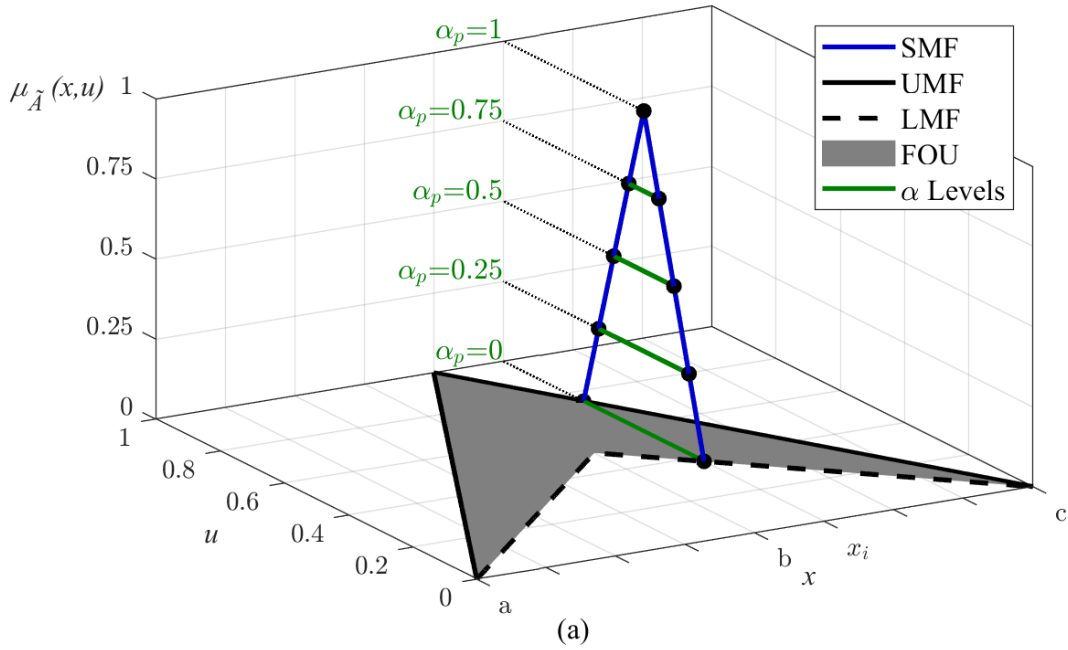


Figure 3.12 : An α -plane of triangle GT2-FS employing triangle SMF.

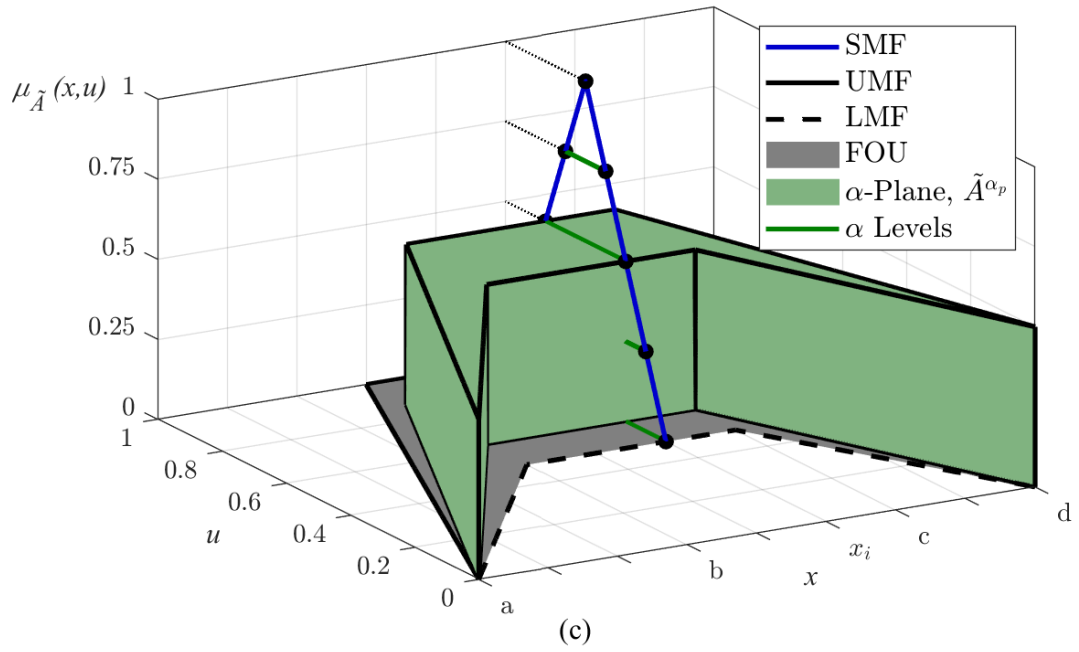
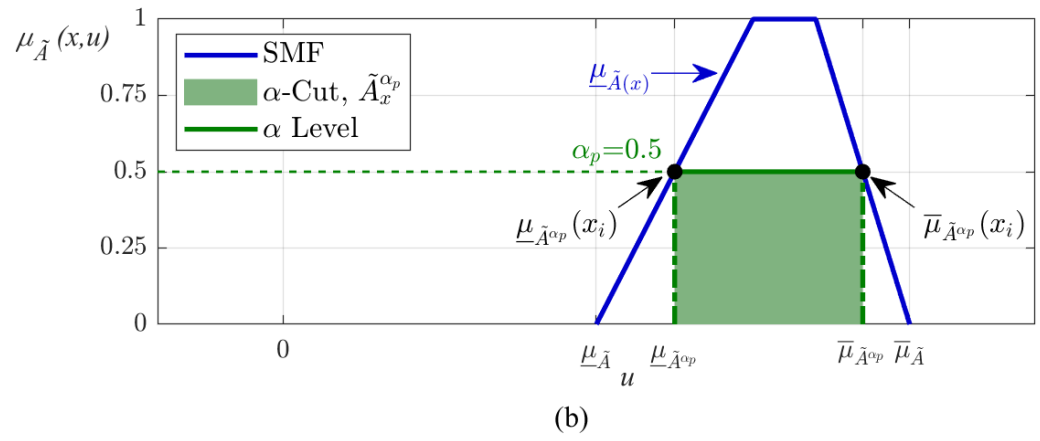
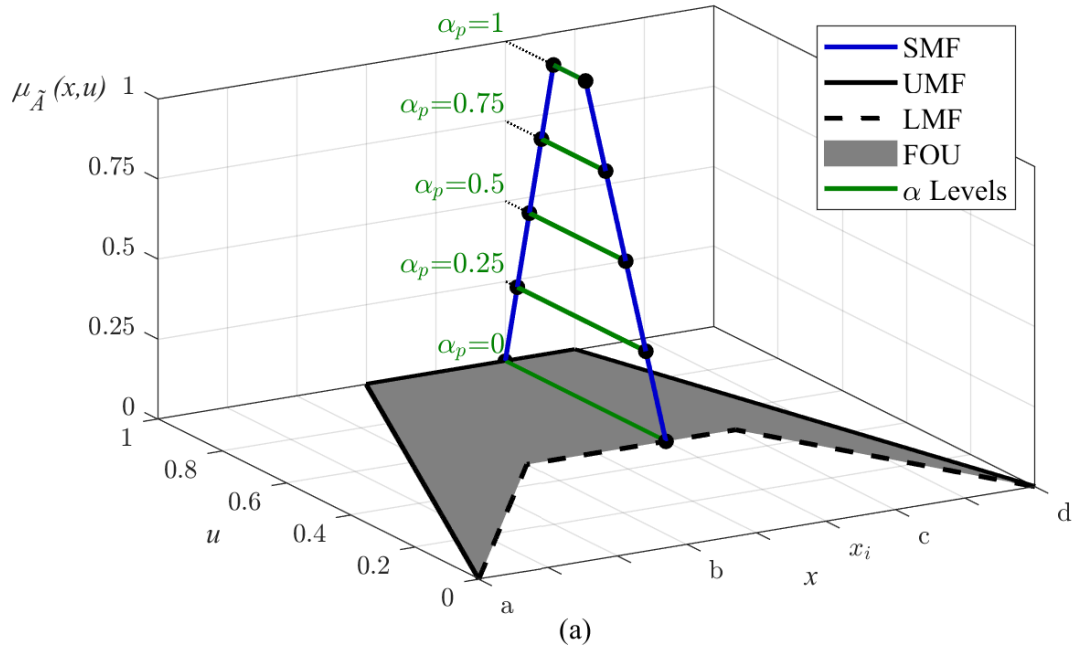


Figure 3.13 : An α -plane of trapezoid GT2-FS employing trapezoid SMF.

The α -plane representations of triangle and trapezoid GT2-FS employing triangle and trapezoid SMFs are given in Figures 3.12 and 3.13, respectively. Here, the subplot (a) shows the SMF slice (marked as blue) for a fixed input value $x = x_i$ on the FOU (marked as grey) at the α -plane level $\alpha_p = 0$. On this SMF slice, five α -plane levels $\alpha_p = \{0, 0.25, 0.5, 0.75, 1\}$ are illustrated with green lines. The bottom line, where $\alpha_p = 0$ is the support of the SMF and stands on the FOU. In the subplot (b), the SMF and the α -plane level at $\alpha_p = 0.5$ are shown on the “ $u, \mu_{\tilde{A}}(x, u)$ ” axis domain. Here, an α -plane level at $\alpha_p = 0.5$ also means an α -cut from the T1-FS of the SMF ($\underline{\mu}_{\tilde{A}_x}$, as marked with the blue triangle). In the subplot (b), based on the input value or slice value (x_i), the lower and upper membership degrees for an α -plane ($\underline{\mu}_{\tilde{A}^{\alpha_p}}(x_i)$ and $\overline{\mu}_{\tilde{A}^{\alpha_p}}(x_i)$) are illustrated. When these values are raised to the α -cut level (in other words, raised to the α level α_p), a rectangular shape, an interval set with the height $\mu_{\tilde{A}}(x, u) = \alpha_p$, is obtained as marked with light green. This interval set is important since it is the same as the secondary grade of IT2-FSs, it only differs from the height. The subplot (c) shows the union of all α -planes raised to the level of α_p over the input $x \in X$. Here, the resulting shape is a triangular prism with a fixed height of $\alpha_p = 0.5$, in other words, an IT2-FS with height $\alpha_p = 0.5$ and its LMF and UMF are defined by α -plane associated LMF and UMF ($\underline{\mu}_{\tilde{A}^{\alpha_p}}$ and $\overline{\mu}_{\tilde{A}^{\alpha_p}}$), respectively. This view of α -planes is also important as the shape is an unnormal IT2-FS where $\mu_{\tilde{A}}(x, u) < 1$. Here all IT2 properties are preserved in the α -plane (\tilde{A}^{α_p}) raised to the level of α_p .

It is worth underlying that a horizontal slice (or zSlice) is obtained when an α -plane is raised to the level α_p . The benefit of this representation based on α -planes is that the computations developed for IT2 FSs can be applied to each horizontal slice [7].

In a similar manner that the support of α -cut for T1-FS changes with respect to the α -cut level and the base support of FS, the support of α -plane for GT2-FS, or in other words the support of α -cut for the SMF, which is T1-FS ($\tilde{A}(x)$), changes with respect to the α -plane level, and the primary membership that is the support of SMF. Hence, the size and shape of the FOU change for each α -plane level as shown in Figure 3.14. This α -plane associated FOU is called as FOU^{α_p} . For example, the size of the FOU at $\alpha_p = 0$, $FOU^{\alpha_p=0}$ (or in simple notation FOU^0 , marked as grey in figures) is larger than the one at $\alpha_p = 0.5$, $FOU^{0.5}$. As the FOU is also defined by the LMF and UMF

($\underline{\mu}_{\tilde{A}}$ and $\overline{\mu}_{\tilde{A}}$), an α -plane associated FOU (FOU^{α_p}) can be defined by α -plane associated LMF ($\underline{\mu}_{\tilde{A}^{\alpha_p}}$) and UMF ($\overline{\mu}_{\tilde{A}^{\alpha_p}}$). As $J_x^{\alpha_p} = [\underline{\mu}_{\tilde{A}^{\alpha_p}}(x), \overline{\mu}_{\tilde{A}^{\alpha_p}}(x)]$, the α -plane support, changes with respect to the degrees of α -plane associated LMF and UMF ($\underline{\mu}_{\tilde{A}^{\alpha_p}}$ and $\overline{\mu}_{\tilde{A}^{\alpha_p}}$), the α -plane support also changes with respect to the input value (through $\underline{\mu}_{\tilde{A}}(x)$ and $\overline{\mu}_{\tilde{A}}(x)$) in addition to the definition of the SMF. Since this dependency is handled in LMF and UMF, α -plane associated ones are denoted as $\underline{\mu}_{\tilde{A}^{\alpha_p}}$ and $\overline{\mu}_{\tilde{A}^{\alpha_p}}$ respectively.

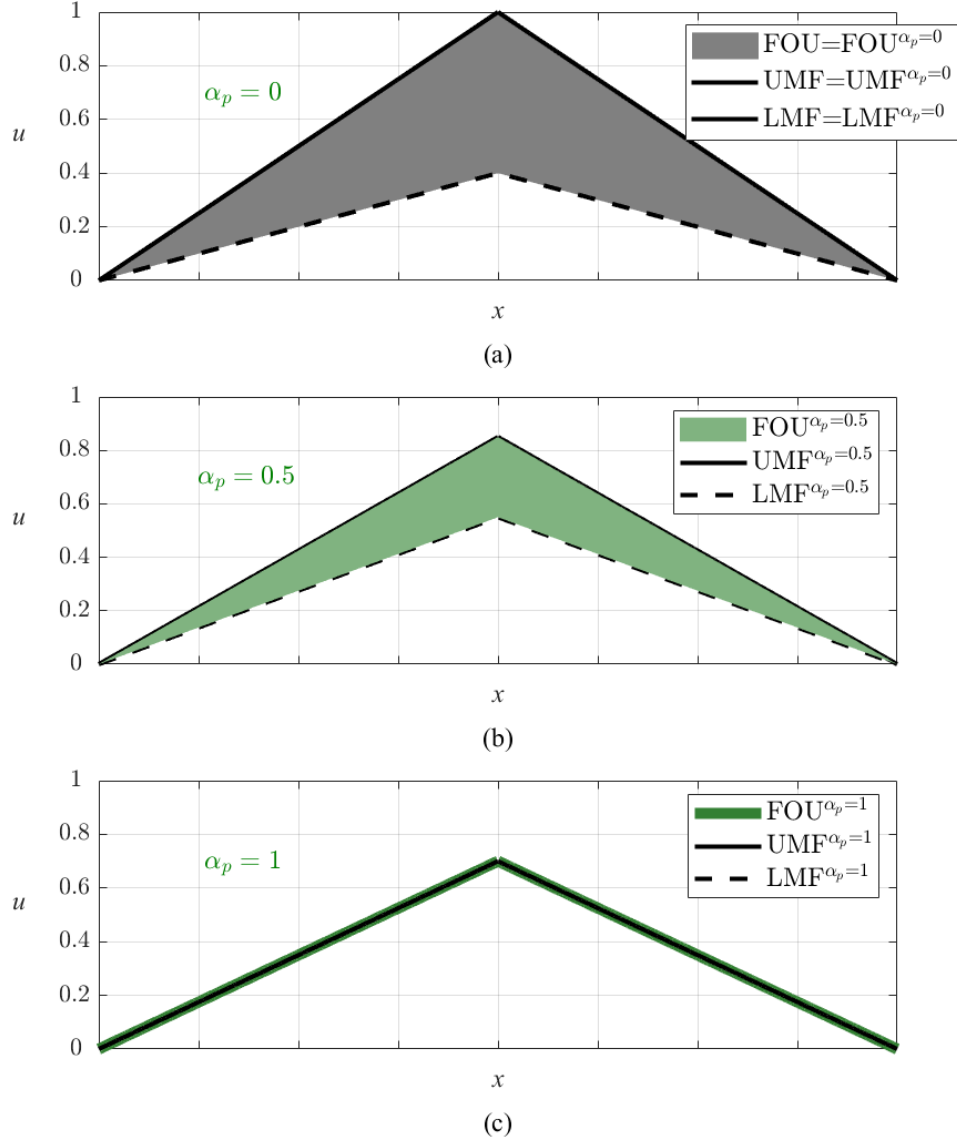


Figure 3.14 : Illustration of varying FOU sizes for different α -planes.

Also, Figure 3.15 shows the same triangular GT2-FS that is used in Figure 3.12, from another perspective. This view perspective shows various α -planes (\tilde{A}^{α_p}) with respect to their α -plane levels. This figure provides a better visual understanding of how GT2-FLC calculations are handled by the horizontal slice or the α -plane representation.

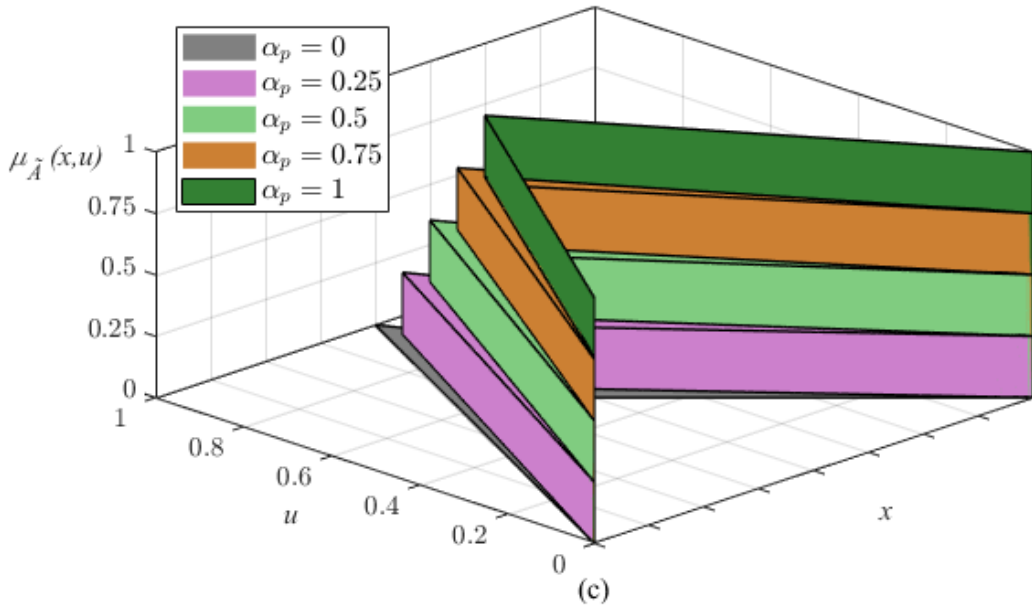
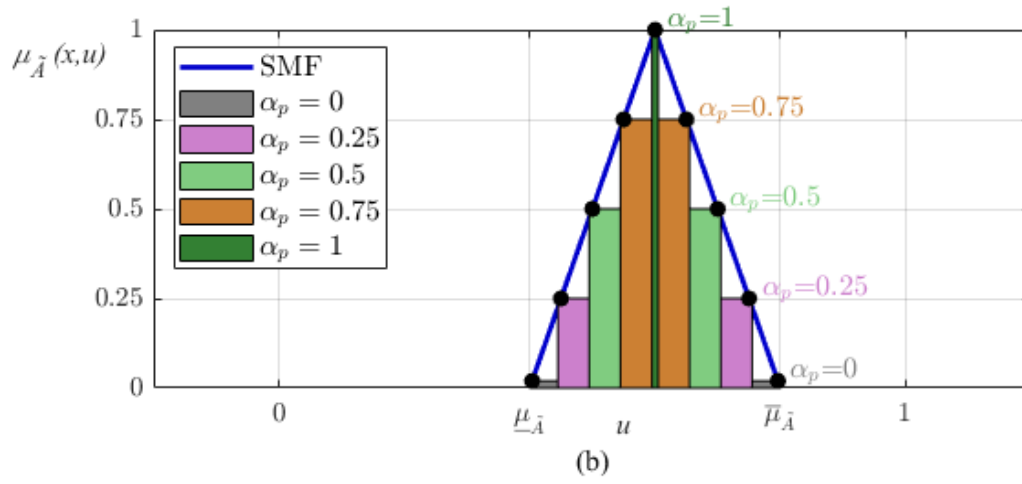
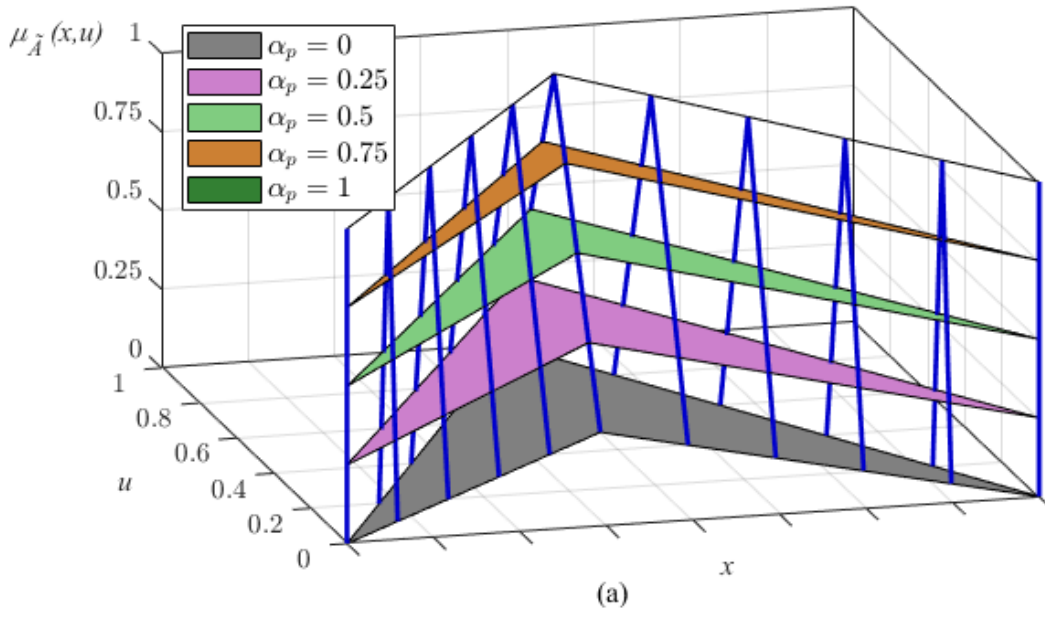


Figure 3.15 : Illustration of a horizontal-sliced GT2-FS by α -plane levels.

3.5 Computation of an α -Plane Output

The main calculation steps for the computation of an α -plane output for GT2-FLC is similar to the calculation steps for the computation of an IT2-FLC output. As shown in Figure 3.15, each α -plane of GT2-FLC represents an α -plane associated T2-FLC, in short α -T2-FLC, where the height of the secondary membership is α_p . So, each α -T2-FLC has its computations based on α -plane associated firing levels. Recalling Figure 2.9, an IT2-FLC has 5 main operations (fuzzifier, rules, inference, type-reducer, and defuzzifier), so does α -T2-FLC. Here, IT2-FLC and α -T2-FLC only differ at the fuzzifier part, since membership degrees and firings are changing with respect to α -plane levels. The system block diagram for α -T2-FLCs is given in Figure 3.16, where the fuzzifier is separated into two parts as Fuzzifier and Fuzzifier ^{α} to point out the α -T2-FLC calculations. The sub-operator Fuzzifier ^{α} calculates an α -plane associated interval set of lower and upper membership degrees for further α -T2-FLC calculations which are the same as in IT2-FLC. This interval set can be alternatively interpreted as α -plane associated LMF and UMF, denoted as $\underline{\mu}_A^\alpha$ and $\bar{\mu}_A^\alpha$, respectively.

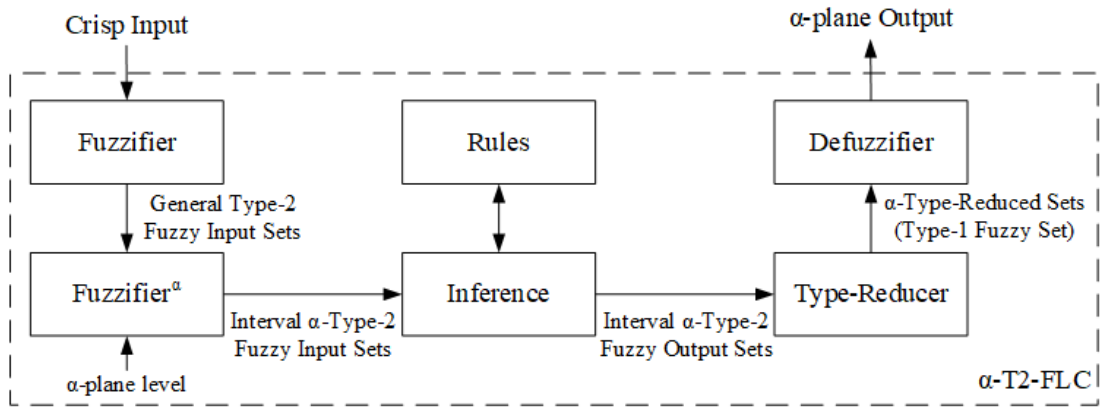


Figure 3.16 : Block diagram of α -plane associated type-2 fuzzy logic controllers.

For a triangle SMF defined in equation (3.9), the corresponding LMF and UMF of an α -T2-FLC (i.e. $\underline{\mu}_{\tilde{A}}^{\alpha_p}$ and $\bar{\mu}_{\tilde{A}}^{\alpha_p}$) are defined respectively as follows:

$$\underline{\mu}_{\tilde{A}}^{\alpha_p} = \underline{\mu}_{\tilde{A}} + w \left(\bar{\mu}_{\tilde{A}} - \underline{\mu}_{\tilde{A}} \right) \alpha_p \quad (3.25)$$

$$\bar{\mu}_{\tilde{A}}^{\alpha_p} = \bar{\mu}_{\tilde{A}} - (1 - w) \left(\bar{\mu}_{\tilde{A}} - \underline{\mu}_{\tilde{A}} \right) \alpha_p \quad (3.26)$$

where α_p is the α -plane level and w is the apex point location of the triangle.

For a trapezoid SMF defined in equation (3.13), the corresponding LMF and UMF of an α -T2-FLC (i.e. $\underline{\mu}_{\tilde{A}}^{\alpha_p}$ and $\overline{\mu}_{\tilde{A}}^{\alpha_p}$) are defined as follows:

$$\underline{\mu}_{\tilde{A}}^{\alpha_p} = \underline{\mu}_{\tilde{A}} + \text{Core}_L(u|x) (\overline{\mu}_{\tilde{A}} - \underline{\mu}_{\tilde{A}}) (\alpha_p) \quad (3.27)$$

$$\overline{\mu}_{\tilde{A}}^{\alpha_p} = \overline{\mu}_{\tilde{A}} - (1 - \text{Core}_R(u|x)) (\overline{\mu}_{\tilde{A}} - \underline{\mu}_{\tilde{A}}) (\alpha_p) \quad (3.28)$$

Once the α -plane associated LMF ($\underline{\mu}_{\tilde{A}}^{\alpha_p}$) and UMF ($\overline{\mu}_{\tilde{A}}^{\alpha_p}$) are calculated, then the membership grades of each α -T2-FLC are obtained, so that the output of α -plane (i.e. α -T2-FLC) is calculated straightforwardly, as illustrated in Figure 3.16.

3.6 Aggregation of α -Planes towards Fuzzy Logic Controller Output

According to α -plane based horizontal slice representation, the output of a GT2-FLC (y_{GT2}) can be defined as a weighted average aggregation of α -plane associated T2-FLC outputs over the α -planes as follows [7]:

$$y_{GT2} = \left(\sum_{p=1}^P y_{GT2}^{\alpha_p} \alpha_p \right) / \left(\sum_{p=1}^P \alpha_p \right) \quad (3.29)$$

where $y_{GT2}^{\alpha_p}$ is the output of α -T2-FLC, α_p is the α -plane level, $p \in \{1, \dots, P\}$ denotes corresponding α -plane index, and P ($p = 1, \dots, P$) is the total number of α -planes.

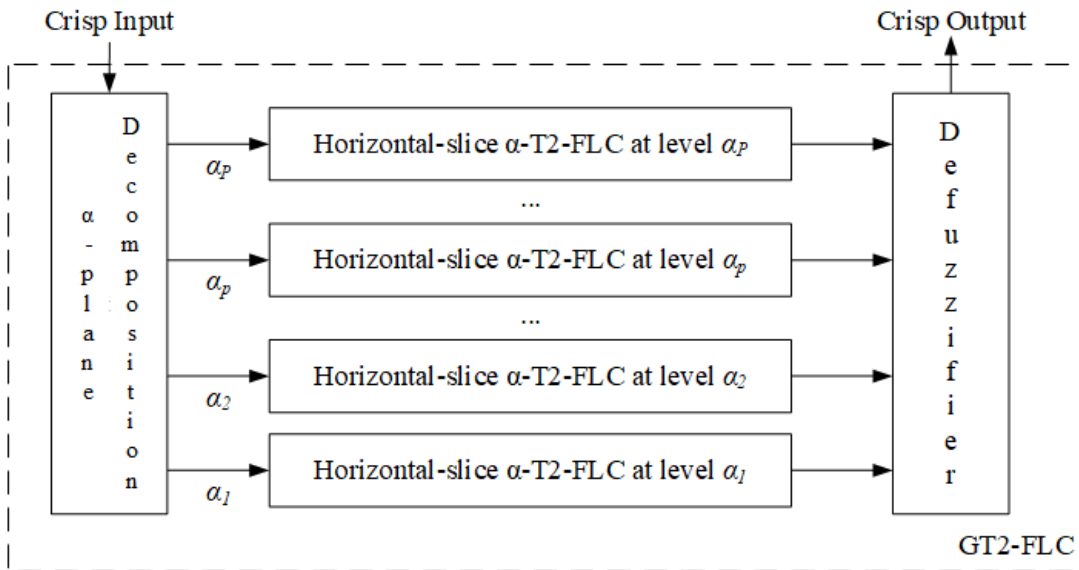


Figure 3.17 : Block diagram of the aggregation of α -plane based horizontal slices.

This representation allows defining the output of GT2-FLC (y_{GT2}) as an aggregation of α -plane outputs ($y_{GT2}^{\alpha_p}$) in terms of α -T2-FLCs which are principally the resulting T1-FLC or IT2-FLCs that are derived for α_p is the α -plane level [7, 75-76]. The weighted average aggregation of α -plane associated T2-FLC outputs is visualized in Figure 3.17. Here, the baseline IT2-FLC plane where $\alpha_0 = 0$ is excluded from the α -plane list since it has no impact on the GT2-FLC output calculation which is given in equation (3.29) [64]. It is worth mentioning that once the total number of α -planes increases, then the α -axis is sampled better in terms of granularity so that the collection of the α -T2-FLC outputs will approach a uniformly sampled set of sets; on the other hand, this high number of α -plane samples increases computational complexity and computation time.

3.7 Illustrative Numerical Example

In this section, a numerical example for the output calculation of GT2-FLCs will be presented. For illustration purposes, a simple, single-input (x), and 3-rule GT2-FLC structure that employs 5 α -planes ($\alpha_p = \{0, 0.25, 0.5, 0.75, 1\}$) is considered. So, the handled GT2-FSs are shaped similar to the example given in Figure 3.15. Here, the GT2-FLC is constructed with 3 antecedent and 3 consequent MFs. The antecedent part is defined with triangular GT2-FSs ($\tilde{A}_1, \tilde{A}_2, \tilde{A}_3$) with triangular SMFs (as the example given in Figure 3.12) and the consequent part is defined with singletons ($C_1 = -1, C_2 = 0, C_3 = 1$). The rules are given in equations (3.30) – (3.32) and the rule table is given in Table 3.1. The heights of the LMFs are selected as ($M_1 = 0.2, M_2 = 0.6, M_3 = 0.2$) and the apex point of the triangular SMF ($\text{Apex}(u|x)$) is set by the setting $w = 0.6$ as shown in Figure 3.18.

$$R_1: \text{ IF } x \text{ is } \tilde{A}_1 \text{ THEN } y \text{ is } C_1 \quad (3.30)$$

$$R_2: \text{ IF } x \text{ is } \tilde{A}_2 \text{ THEN } y \text{ is } C_2 \quad (3.31)$$

$$R_3: \text{ IF } x \text{ is } \tilde{A}_3 \text{ THEN } y \text{ is } C_3 \quad (3.32)$$

Table 3.1 : Rule base of the illustrative GT2-FLC.

x	\tilde{A}_1	\tilde{A}_2	\tilde{A}_3
y	$C_1 = -1$	$C_2 = 0$	$C_3 = 1$

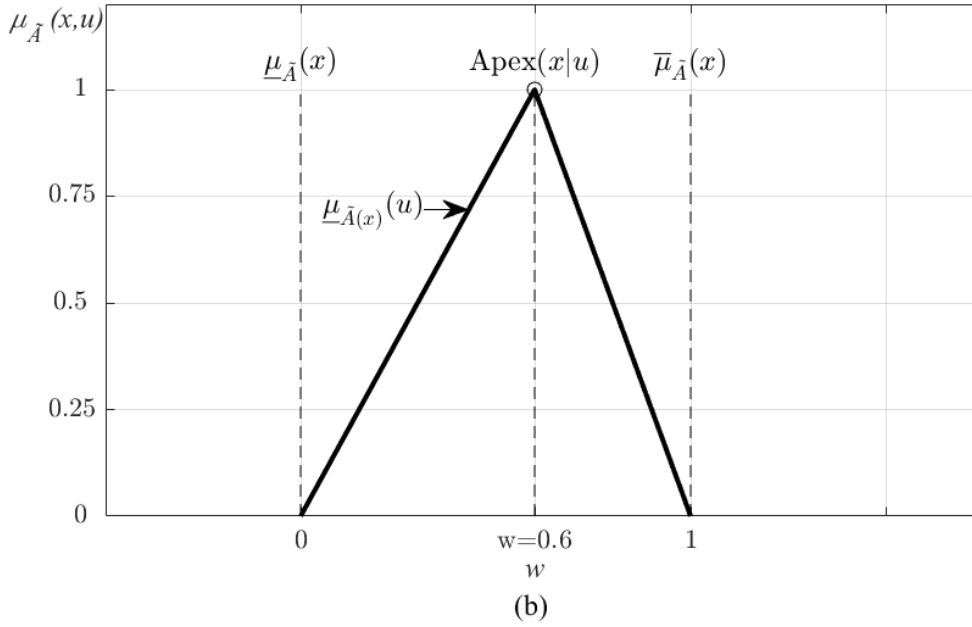
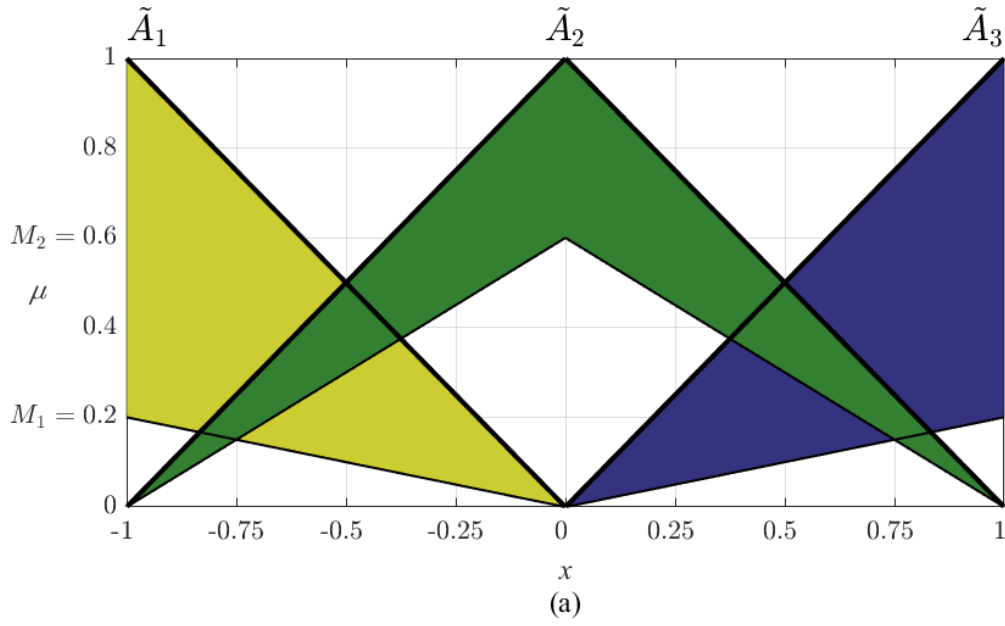


Figure 3.18 : Block diagram of the aggregation of α -plane based horizontal slices.

For illustration purposes, the input variable is applied as $x = 0.4$. For each α -plane ($\alpha_p = \{0, 0.25, 0.5, 0.75, 1\}$), α -T2-FLC calculations are performed according to α -plane horizontal slice representation. In this context, 1) α -plane associated membership degrees ($\underline{\mu}_{\tilde{A}^{\alpha_p}}$ and $\overline{\mu}_{\tilde{A}^{\alpha_p}}$), 2) α -plane associated firing intervals ($\underline{f}_n^{\alpha_p}$ and $\overline{f}_n^{\alpha_p}$), 3) α -plane associated left and right endpoints of the type-reduced sets ($y_L^{\alpha_p}$ and $y_R^{\alpha_p}$) by employing the KM center of sets calculation method, 4) defuzzified outputs of α -T2-FLCs ($y_{GT2}^{\alpha_p}$), and finally, 5) final output of GT2-FLC (y_{GT2}) are calculated based on IT2 mathematics. The obtained numerical values are collected in Table 3.2.

Table 3.2 : Calculation steps of illustrative GT2-FLC.

α_p	$\begin{bmatrix} \underline{\mu}_{\tilde{A}_1}^{\alpha_p} & \overline{\mu}_{\tilde{A}_1}^{\alpha_p} \\ \underline{\mu}_{\tilde{A}_2}^{\alpha_p} & \overline{\mu}_{\tilde{A}_2}^{\alpha_p} \\ \underline{\mu}_{\tilde{A}_3}^{\alpha_p} & \overline{\mu}_{\tilde{A}_3}^{\alpha_p} \end{bmatrix}$	$\begin{bmatrix} \underline{f}_1^{\alpha_p} & \overline{f}_1^{\alpha_p} \\ \underline{f}_2^{\alpha_p} & \overline{f}_2^{\alpha_p} \\ \underline{f}_3^{\alpha_p} & \overline{f}_3^{\alpha_p} \end{bmatrix}$	$[y_L^{\alpha_p} \quad y_R^{\alpha_p}]$	$y_{GT2}^{\alpha_p}$
$\alpha_p = 0$	$\begin{bmatrix} 0 & 0 \\ 0.36 & 0.6 \\ 0.08 & 0.4 \end{bmatrix}$	$\begin{bmatrix} 0 & 0 \\ 0.36 & 0.6 \\ 0.08 & 0.4 \end{bmatrix}$	$[0.1176 \quad 0.5263]$	0.3220
$\alpha_p = 0.25$	$\begin{bmatrix} 0 & 0 \\ 0.396 & 0.576 \\ 0.128 & 0.368 \end{bmatrix}$	$\begin{bmatrix} 0 & 0 \\ 0.396 & 0.576 \\ 0.128 & 0.368 \end{bmatrix}$	$[0.1818 \quad 0.4817]$	0.3317
$\alpha_p = 0.5$	$\begin{bmatrix} 0 & 0 \\ 0.432 & 0.552 \\ 0.176 & 0.336 \end{bmatrix}$	$\begin{bmatrix} 0 & 0 \\ 0.432 & 0.552 \\ 0.176 & 0.336 \end{bmatrix}$	$[0.2418 \quad 0.4375]$	0.3396
$\alpha_p = 0.75$	$\begin{bmatrix} 0 & 0 \\ 0.468 & 0.528 \\ 0.224 & 0.304 \end{bmatrix}$	$\begin{bmatrix} 0 & 0 \\ 0.468 & 0.528 \\ 0.224 & 0.304 \end{bmatrix}$	$[0.2979 \quad 0.3938]$	0.3458
$\alpha_p = 1$	$\begin{bmatrix} 0 & 0 \\ 0.504 & 0.504 \\ 0.272 & 0.272 \end{bmatrix}$	$\begin{bmatrix} 0 & 0 \\ 0.504 & 0.504 \\ 0.272 & 0.272 \end{bmatrix}$	$[0.3505 \quad 0.3505]$	0.3505

Here, Table 3.2 is filled according to the following membership function definitions:

$$\underline{\mu}_{\tilde{A}_i}^{\alpha_p} = \underline{\mu}_{\tilde{A}_i} + w (\overline{\mu}_{\tilde{A}_i} - \underline{\mu}_{\tilde{A}_i}) \alpha_p, \quad i = \{1,2,3\} \quad (3.33)$$

$$\overline{\mu}_{\tilde{A}_i}^{\alpha_p} = \overline{\mu}_{\tilde{A}_i} - (1 - w) (\overline{\mu}_{\tilde{A}_i} - \underline{\mu}_{\tilde{A}_i}) \alpha_p, \quad i = \{1,2,3\} \quad (3.34)$$

$$\overline{\mu}_{\tilde{A}_1} = \begin{cases} -x & x \leq 0 \\ 0 & x > 0 \end{cases}, \quad \underline{\mu}_{\tilde{A}_1} = \begin{cases} -x M_1 & x \leq 0 \\ 0 & x > 0 \end{cases} \quad (3.35)$$

$$\overline{\mu}_{\tilde{A}_2} = \begin{cases} 1 + x & x \leq 0 \\ 1 - x & x > 0 \end{cases}, \quad \underline{\mu}_{\tilde{A}_2} = \begin{cases} (1 + x) M_2 & x \leq 0 \\ (1 - x) M_2 & x > 0 \end{cases} \quad (3.36)$$

$$\overline{\mu}_{\tilde{A}_3} = \begin{cases} 0 & x < 0 \\ x & x \geq 0 \end{cases}, \quad \underline{\mu}_{\tilde{A}_3} = \begin{cases} 0 & x < 0 \\ x M_3 & x \geq 0 \end{cases} \quad (3.37)$$

It is worth noting that these membership degrees are the ones for α -T2-FLCs, including the base α -plane level ($\alpha_0 = 0$). The secondary grades of the input value ($x = 0.4$) are shown with circles in Figure 3.19. Accordingly, the GT2-FLC output, which is also shown in Figure 3.19, is calculated as a weighted average of α -T2-FLC outputs as:

$$y_{GT2} = \left(\sum_{p=1}^P y_{GT2}^{\alpha_p} \alpha_p \right) / \left(\sum_{p=1}^P \alpha_p \right) \quad (3.38)$$

$$= \frac{0.3220 \times 0 + 0.3317 \times 0.25 + 0.3396 \times 0.5 + 0.3458 \times 0.75 + 0.3505 \times 1}{0 + 0.25 + 0.5 + 0.75 + 1} = 0.3451$$

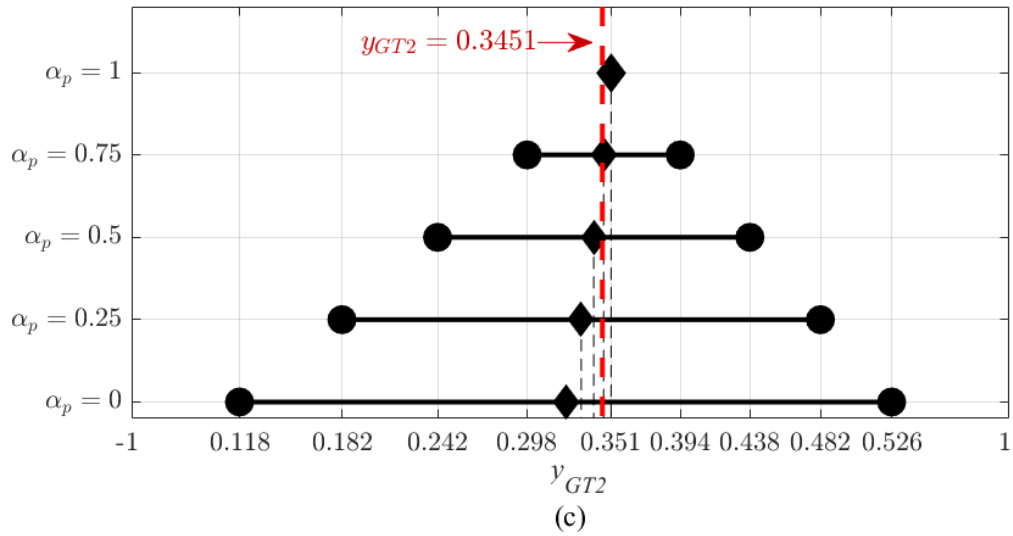
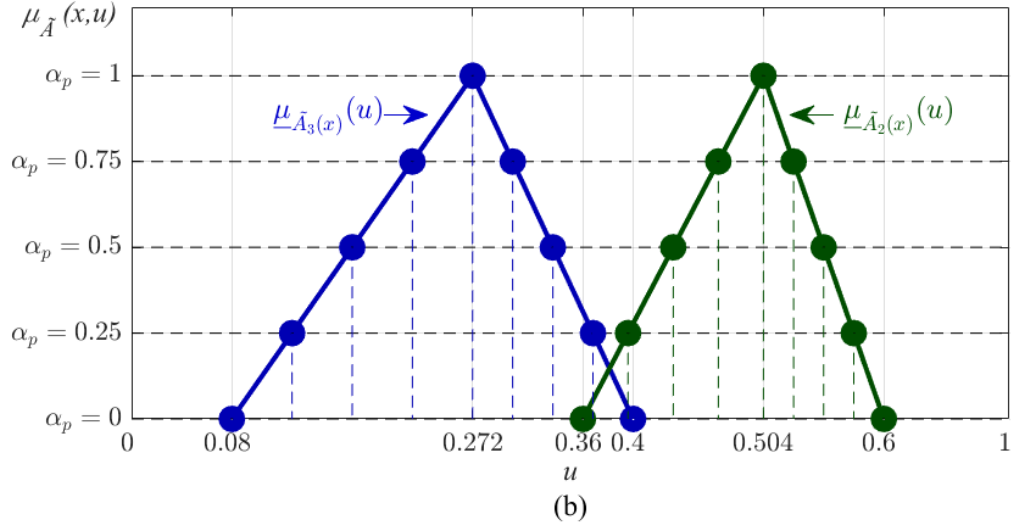
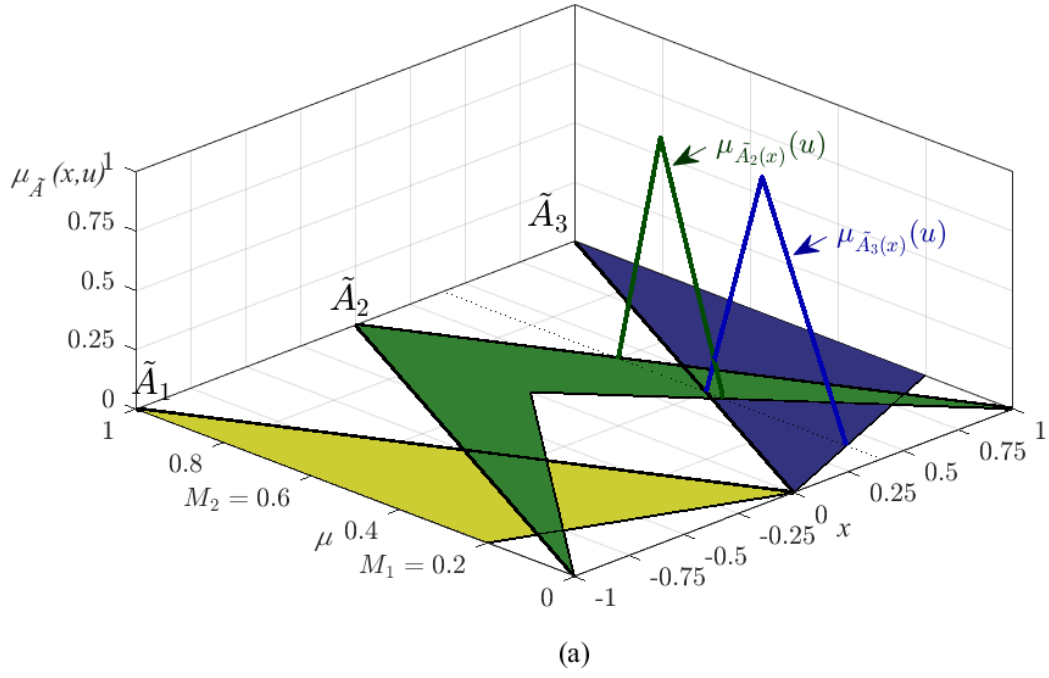


Figure 3.19 : Illustration of (a) antecedent MFs, (b) SMFs, (c) type-reduced sets.

As another example, if three α -planes ($\alpha_p = \{0, 0.5, 1\}$) are considered for the output calculation then the results are slightly different as follows:

$$y_{GT2} = \left(\sum_{p=1}^P y_{GT2}^{\alpha_p} \alpha_p \right) / \left(\sum_{p=1}^P \alpha_p \right) = \frac{0.3220 \times 0 + 0.3396 \times 0.5 + 0.3505 \times 1}{0 + 0.5 + 1} = 0.3469 \quad (3.39)$$

This example also shows the effect of the number and level of the α -planes. It is obvious that once the total number of slices increases (or α -plane grid fined down), then the calculation accuracy improves. Although it is not shown in this chapter, the computational time also rises with a high number of α -planes. In the literature, there is no unique methodology for the selection of α -planes, so the selection of alpha planes is still under investigation by the fuzzy community [7]. This topic will be addressed in the next chapters.



4. TOWARDS SYSTEMATIC DESIGN OF GENERAL TYPE-2 FUZZY LOGIC CONTROLLERS

In this chapter, the structural settings of the GT2-FLCs are investigated in order to provide a better and clear understanding on the design parameters and interpretations of these design parameters towards systematic design approaches for GT2-FLCs. As explained in “Chapter 3 - General Type-2 Fuzzy Logic Controllers”, the SMFs are the promising feature of GT2-FLCs. The SMFs, comparing to T1 and IT2 counterparts of GT2-FLCs, provide extra design flexibility and more design options such that various sophisticated fuzzy mappings can be achieved. On the contrary to these advantages, the SMFs also brings a high level of design complexity as the effect of SMF design or design parameters are not obvious.

4.1 Interactions between Fuzzy Logic Controllers

The GT2, IT2, and T1 FLCs are defined with respect to GT2, IT2, and T1 FSs used in their fuzzy inferences, respectively. In the most generic representation, GT2-FSs / GT2-FLCs include/cover corresponding IT2 counterparts, while IT2-FSs / IT2-FLCs include /cover corresponding T1 counterparts, as illustrated in Figure 4.1 based on a visual representation. This representation provides a pseudo-answer for a famous design question [55, 60]: “Why does improved performance occur as one goes from crisp, to T1, to IT2, to GT2 fuzzy systems?”. As illustrated in Figure 4.1, the outer category inherits the inner one, so it can be commented that the performance of the outer category is potentially higher than its inner category, if the design is proper.

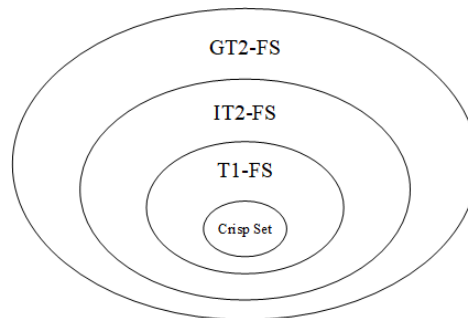


Figure 4.1 : Inclusions and interactions of fuzzy sets.

When an interaction (conversion) is considered, it is also possible to represent an inner FS in terms of its outer FS [54]. This is also a very useful operation since FLC calculations can involve a mixture of T1, IT2, and GT2-FSs [7]. In this context, the definitions of GT2-FS, IT2-FS, T1-FS, and crisp set can be summarized as follows:

- **GT2-FS**, the generic form, as defined in equations (2.11) and (3.2):

$$\tilde{A} = \left\{ (x, u), \mu_{\tilde{A}}(x, u) \mid x \in X, u = [\underline{\mu}_{\tilde{A}}(x), \bar{\mu}_{\tilde{A}}(x)] \in U \equiv [0, 1] \right\} \quad (4.1)$$

- **IT2-FS**, where all secondary grades are 1:

$$\tilde{A} = \left\{ (x, u), \mu_{\tilde{A}}(x, u) = 1 \mid x \in X, u = [\underline{\mu}_{\tilde{A}}(x), \bar{\mu}_{\tilde{A}}(x)] \in U \equiv [0, 1] \right\} \quad (4.2)$$

- **T1-FS**, where the primary grade is crisp value and secondary grade is 1:

$$A \rightarrow \tilde{A} = \left\{ (x, u), \mu_{\tilde{A}}(x, u) = 1 \mid x \in X, u = \mu_A(x) \in U \equiv [0, 1] \right\} \quad (4.3)$$

- **Crisp set**, where the primary grade is 0 or 1 and secondary grade is 1:

$$A \rightarrow \tilde{A} = \left\{ (x, u), \mu_{\tilde{A}}(x, u) = 1 \mid x \in X, u = \mu_A(x) = \{0, 1\} \right\} \quad (4.4)$$

These interaction relations that are given in equations (4.1) – (4.4) are quite helpful to connect different FSs during FLC calculations since the most outer FS covers all inner counterparts. Therefore, a similar idea can be employed during the controller design steps of GT2-FLCs, IT2-FLCs, T1-FLCs, such that the T1-FLCs extends the performance of non-fuzzy counterparts, the IT2-FLCs increase the performance of T1 counterparts, and the GT2-FLCs outperforms its IT2, T1 fuzzy counterparts.

The interactions between GT2, IT2, and T1 FSs are preserved in the SMF of GT2-FSs since only secondary grades are different as given in equations (4.1) – (4.4). This difference can be also defined in terms of SMFs (i.e. $\mu_{\tilde{A}(x)}(u)$). A SMF is represented by a collection of a membership grade function $f_x(u)$ that is calculated based on the primary variable x and the secondary variable u as follows:

$$\mu_{\tilde{A}(x)}(u) = \mu_{\tilde{A}(x)} = \mu_{\tilde{A}_x} = \int_{\underline{\mu}_{\tilde{A}(x)}}^{\bar{\mu}_{\tilde{A}(x)}} f_x(u)/u \quad (4.5)$$

where $f_x(u)$ is a slice from SMF and denoted as A_x . This function is defined for

$$A_x = \left\{ (u, \mu_{A_x}(u)) \mid u \in [\underline{\mu}_{\tilde{A}}(x), \overline{\mu}_{\tilde{A}}(x)] \right\} \quad (4.6)$$

$$A_x = \left\{ (u, \mu_{A_x}(u) = 1) \mid u \in [\underline{\mu}_{\tilde{A}}(x), \overline{\mu}_{\tilde{A}}(x)] \right\} \quad (4.7)$$

$$A_x = \{(u, \mu_{A_x}(u) = 1) \mid u = \mu_A(x) = \mu_{\tilde{A}}(x) = \bar{\mu}_{\tilde{A}}(x)\} \quad (4.8)$$

4.2 Novel Representation of Trapezoid Secondary Membership Function

Based on FS and SMF interactions given in equations (4.1) - (4.4) and (4.5) - (4.8), the SMFs can be defined in such a way that all properties of GT2, IT2, and T1 FSs can be preserved. For this purpose, the basic trapezoid SMF definition given in the previous chapter is extended and a novel representation of trapezoid SMF is proposed. A trapezoid SMF and its design parameters are given in Figure 4.2.

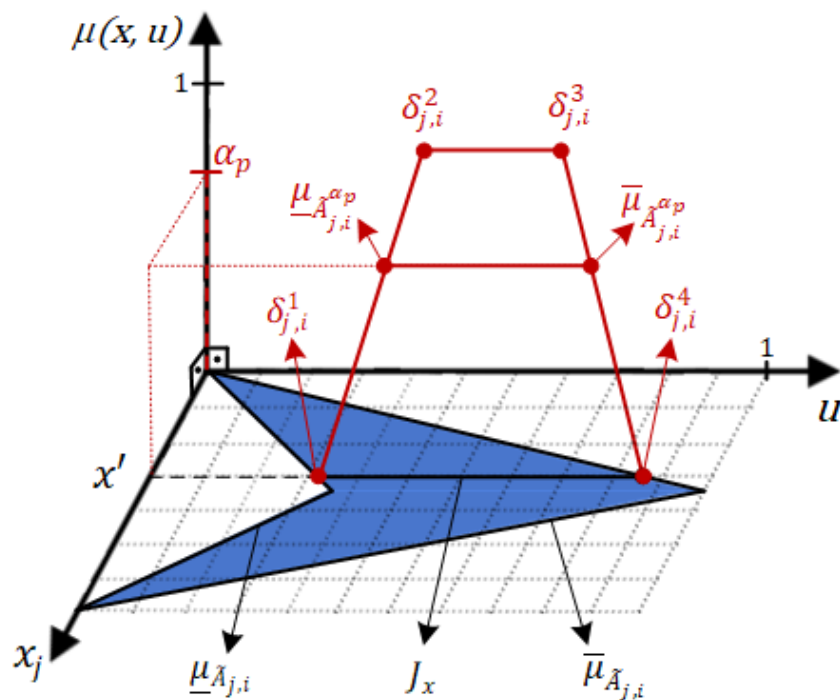


Figure 4.2 : Illustration of novel representation of trapezoid SMF.

In the design of GT2-FLCs, it is possible to obtain various FLC types based on the different shapes and supports of the trapezoid SMFs. The shape and support of the trapezoid SMF are determined by its left support (δ^1), left core (δ^2), right core (δ^3), and right support (δ^4) parameters.

The support of the trapezoid SMF is defined on the primary membership (i.e. J_x), if the following design condition is satisfied:

$$\delta^1 = 0 \quad \delta^2 = \text{free} \quad \delta^3 = \text{free} \quad \delta^4 = 1 \quad (4.9)$$

where the condition $\delta^1 = 0$ and $\delta^4 = 1$ indicates that the supports of trapezoid SMF are defined in the range of LMF and UMF, as formulated in equation (3.15).

The support of the trapezoid SMF is defined on a subset of the primary membership if one of the following design conditions is satisfied:

$$\delta^1 > 0 \quad \delta^2 = \text{free} \quad \delta^3 = \text{free} \quad \delta^4 = \text{free} \quad (4.10)$$

$$\delta^1 = \text{free} \quad \delta^2 = \text{free} \quad \delta^3 = \text{free} \quad \delta^4 < 1 \quad (4.11)$$

where the conditions $\delta^1 > 0$ and $\delta^4 < 1$ can be interpreted as resizing the FOU.

As the generic form of the trapezoid SMF, a trapezoidal shape is obtained if all design parameters are free and the following condition is satisfied:

$$0 \leq \delta^1 \leq \delta^2 \leq \delta^3 \leq \delta^4 \leq 1 \quad (4.12)$$

As the interval form of the trapezoid SMF, a rectangular shape is obtained when the following condition is satisfied:

$$\delta^1 = 0 \quad \delta^2 = 0 \quad \delta^3 = 1 \quad \delta^4 = 1 \quad (4.13)$$

As the crisp form of the trapezoid SMF, a spike shape is obtained when the following condition is satisfied:

$$\delta^1 = \xi, \quad \delta^2 = \xi, \quad \delta^3 = \xi, \quad \delta^4 = \xi \quad (4.14)$$

where $\xi \in [0,1]$ is a free design parameter. If the parameter $\xi = 0$, then the spike of the crisp SMF is located on the LMF. If the parameter $\xi = 1$, then the spike of the crisp SMF is located on the UMF.

As the triangle form of the trapezoid SMF, which is also a triangle SMF, a triangular shape is obtained when the following condition is satisfied:

$$\delta^1 = \text{free} \quad \delta^2 = \delta^3 \quad \delta^4 = \text{free} \quad (4.15)$$

Here, similar to the trapezoid case, the FOU resizing is also possible for the triangle SMFs based on the parameters δ^1 and δ^4 .

Even though the trapezoid T1-FSs provide more design options for the selection of the shape and support of the SMFs, the design is relatively more complex as there are 4 design parameters to be tuned [75, 76]. To overcome this design complexity of the trapezoid SMF, a simple parameter mapping (parameterization) is proposed.

The proposed novel parameterization determines the trapezoid SMF parameters (δ^t) with a single new design parameter as follows:

$$\delta^1 = \begin{cases} \theta - 1 & 1 \leq \theta \leq 2 \\ 0 & \theta < 1 \end{cases} \quad (4.16)$$

$$\delta^2 = \begin{cases} 1 & 1 < \theta \\ \theta & 0 \leq \theta \leq 1 \\ 0 & \theta < 0 \end{cases} \quad (4.17)$$

$$\delta^3 = \begin{cases} 1 & 0 < \theta \\ \theta + 1 & -1 \leq \theta \leq 0 \\ 0 & \theta < -1 \end{cases} \quad (4.18)$$

$$\delta^4 = \begin{cases} 1 & -1 < \theta \\ \theta + 2 & -2 \leq \theta \leq -1 \end{cases} \quad (4.19)$$

where $\theta \in [-2, 2]$ is the new design parameter of the trapezoid SMF. Once these parameter mapping equations are combined with respect to the design parameter value range (from -2 to 2), the following complete parameterization is obtained:

$$[\delta^1 \quad \delta^2 \quad \delta^3 \quad \delta^4] = \begin{cases} [0 & 0 & 0 & \theta + 2] & -2 \leq \theta \leq -1 \\ [0 & 0 & \theta + 1 & 1] & -1 \leq \theta \leq 0 \\ [0 & \theta & 1 & 1] & 0 \leq \theta \leq 1 \\ [\theta - 1 & 1 & 1 & 1] & 1 \leq \theta \leq 2 \end{cases} \quad (4.20)$$

where $[\delta^1 \quad \delta^2 \quad \delta^3 \quad \delta^4]$ is a vector of SMF parameters. The effect of the parameter θ on the shape of FSs as well as the shape and support of trapezoid SMFs for 9 design options is illustrated in Figures 4.3 - 4.12 (for $\theta = \{-2, -1.5, -1, -0.5, 0, 0.5, 1, 1.5, 2\}$).

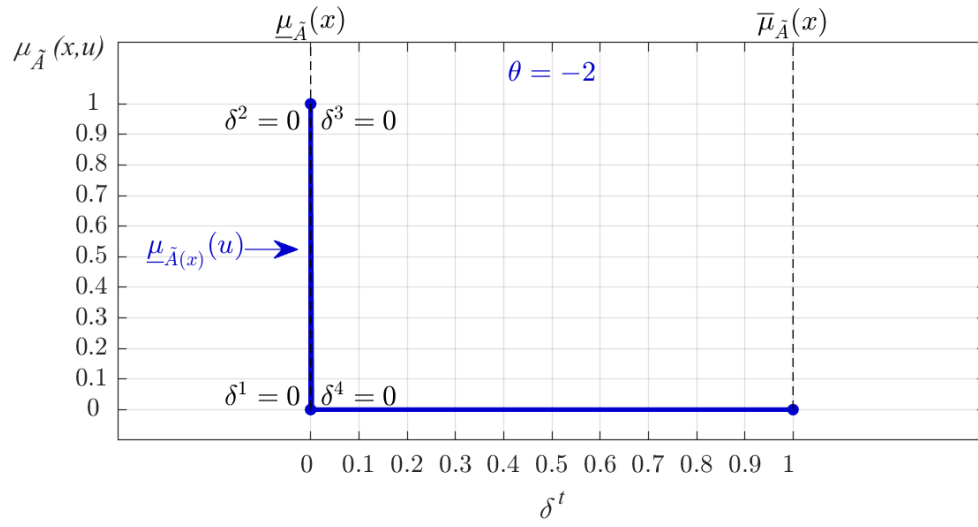


Figure 4.3 : Trapezoid SMF parameters for the design setting $\theta = -2$.

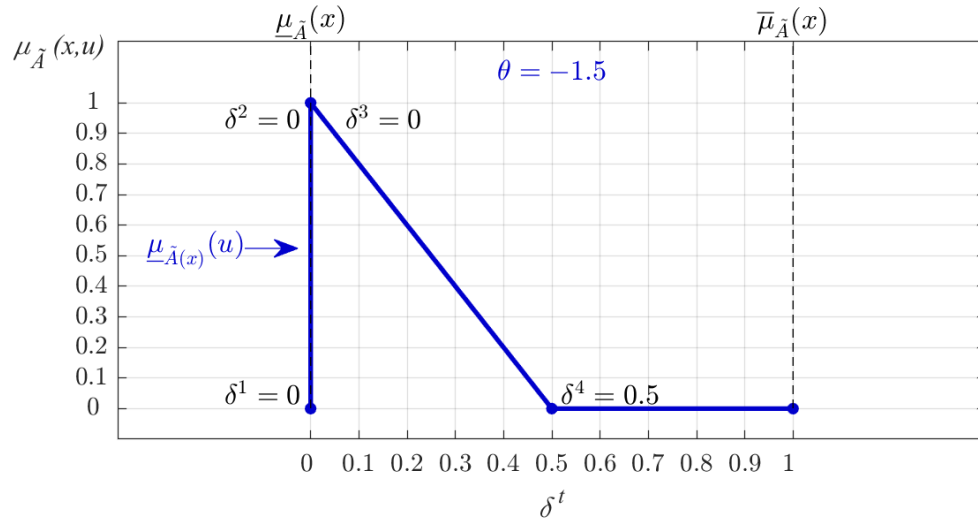


Figure 4.4 : Trapezoid SMF parameters for the design setting $\theta = -1.5$.

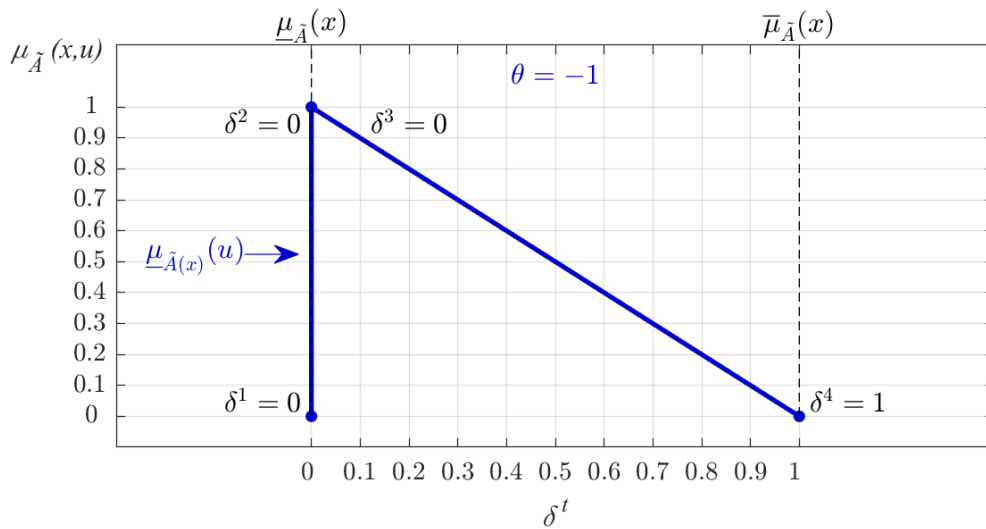


Figure 4.5 : Trapezoid SMF parameters for the design setting $\theta = -1$.

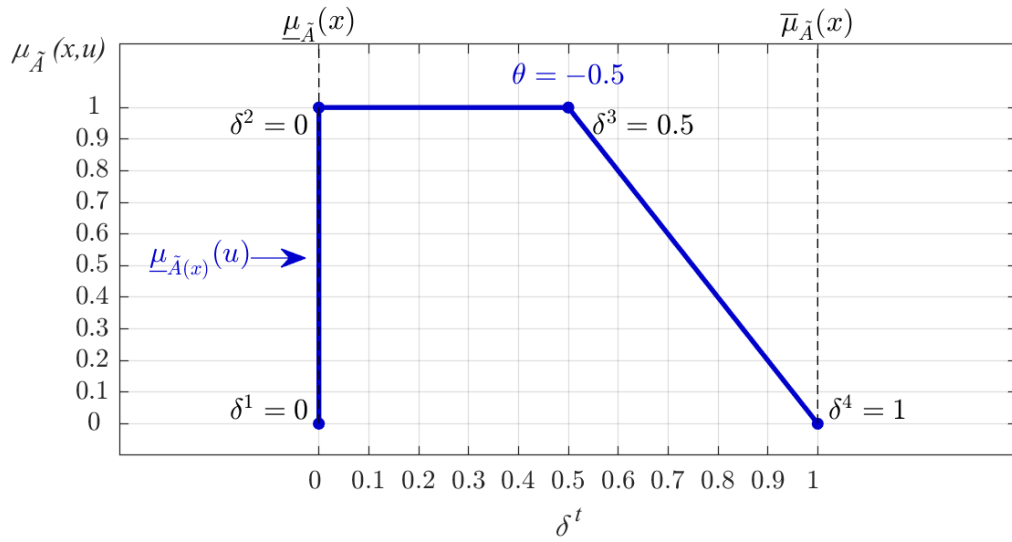


Figure 4.6 : Trapezoid SMF parameters for the design setting $\theta = -0.5$.

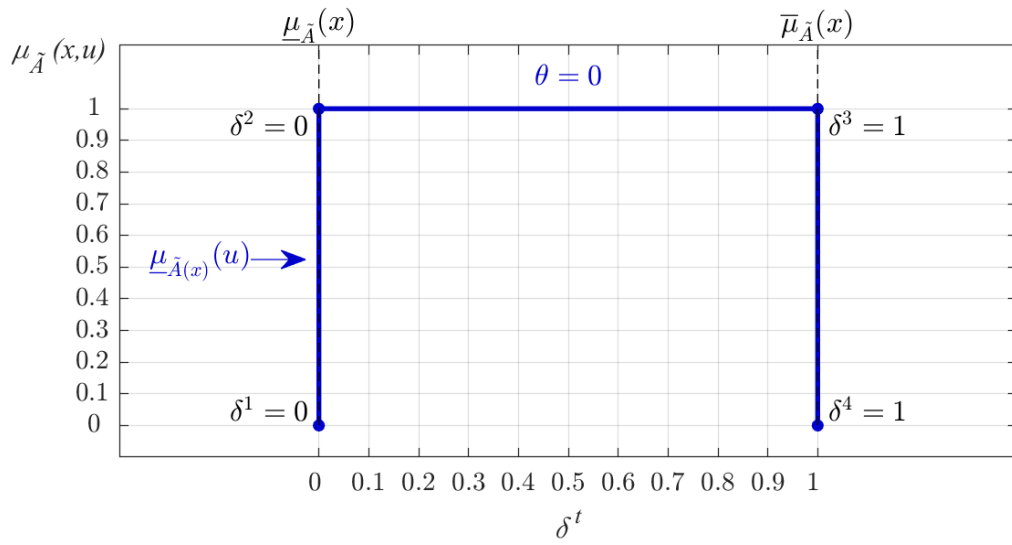


Figure 4.7 : Trapezoid SMF parameters for the design setting $\theta = 0$.

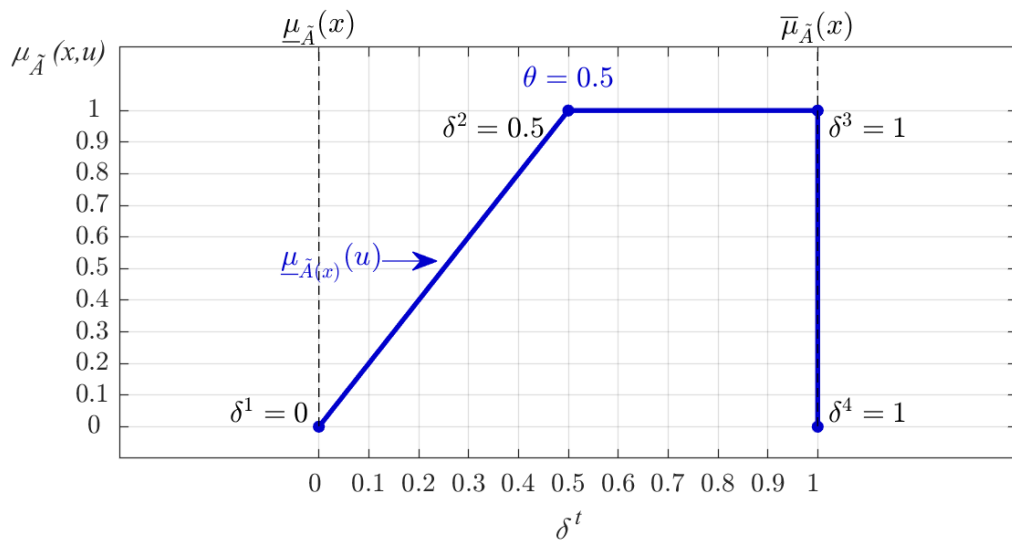


Figure 4.8 : Trapezoid SMF parameters for the design setting $\theta = 0.5$.

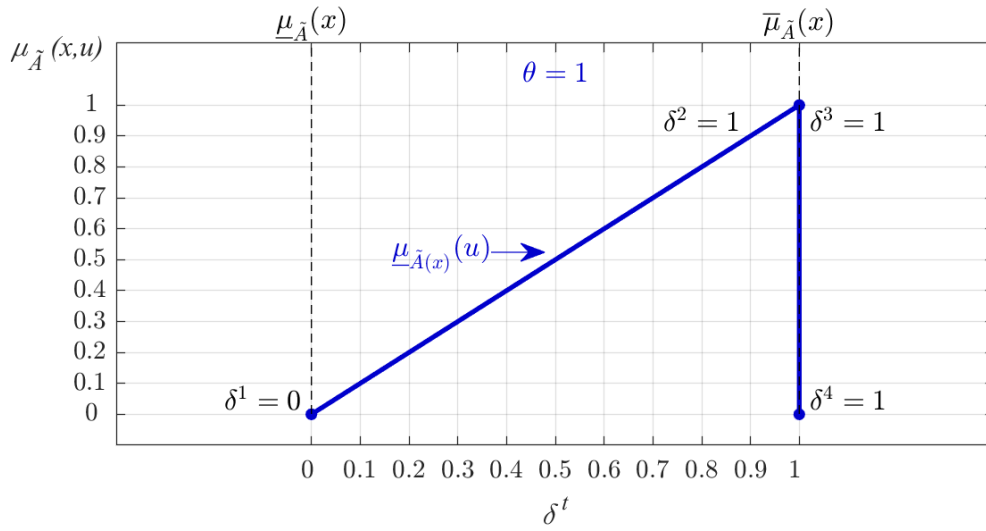


Figure 4.9 : Trapezoid SMF parameters for the design setting $\theta = 1$.

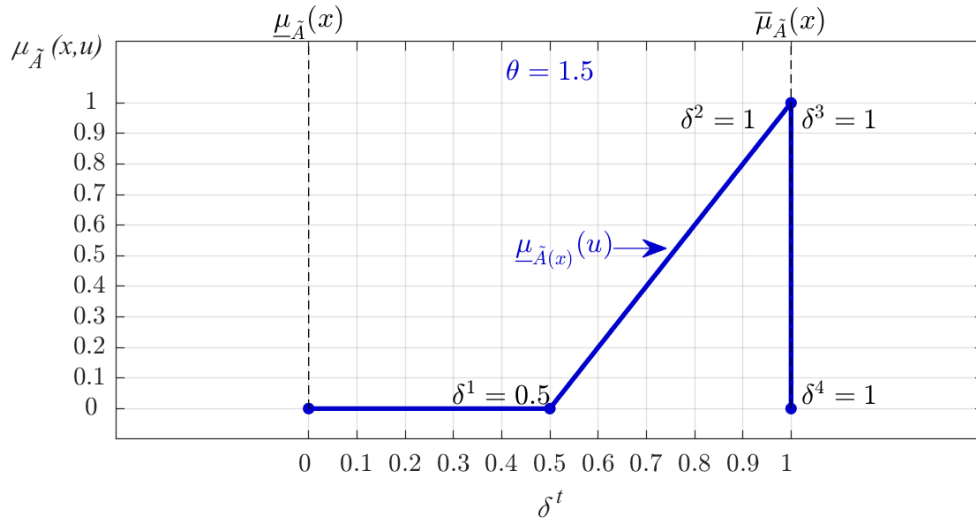


Figure 4.10 : Trapezoid SMF parameters for the design setting $\theta = 1.5$.

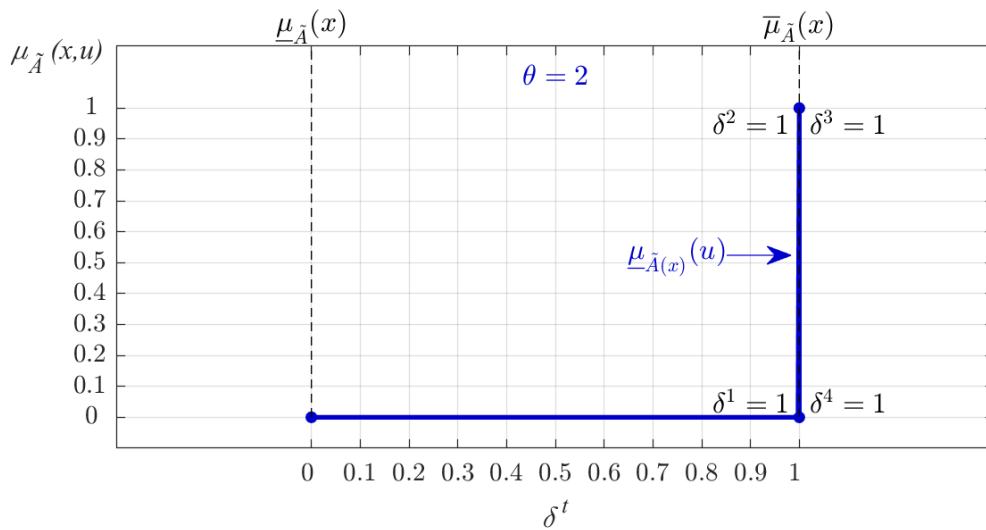


Figure 4.11 : Trapezoid SMF parameters for the design setting $\theta = 2$.

Although equation (4.20) gives a compact parameterization comparing to equations (4.16) – (4.19), it is not practical as it includes many piecewise if-else conditions. To eliminate these piecewise conditions, minimum and maximum functions are used so that the SMF parameterization can be handled by simple mapping functions (one function per design parameter) as follows [75, 76]:

$$\begin{aligned}\delta^1 &= \min(\max(\theta - 1, 0), 1) \\ \delta^2 &= \min(\max(\theta, 0), 1) \\ \delta^3 &= \min(\max(\theta + 1, 0), 1) \\ \delta^4 &= \min(\max(\theta + 2, 0), 1)\end{aligned}\tag{4.21}$$

where $\theta \in [-2, 2]$ is the proposed new design parameter of the SMF. It is concluded that it is possible to obtain various SMFs with this representation. Once the proposed trapezoid SMF representation is applied, then corresponding α -plane associated LMF and UMF ($\underline{\mu}_{\tilde{A}}^{\alpha_p}$ and $\overline{\mu}_{\tilde{A}}^{\alpha_p}$ respectively) for an α -T2-FLC (i.e. \tilde{A}^{α_p}) are calculated as:

$$\underline{\mu}_{\tilde{A}}^{\alpha_p} = \underline{\mu}_{\tilde{A}} + (\overline{\mu}_{\tilde{A}} - \underline{\mu}_{\tilde{A}}) \left(\delta_{j,i}^1 + \alpha_p (\delta_{j,i}^2 - \delta_{j,i}^1) \right)\tag{4.22}$$

$$\overline{\mu}_{\tilde{A}}^{\alpha_p} = \overline{\mu}_{\tilde{A}} - (\overline{\mu}_{\tilde{A}} - \underline{\mu}_{\tilde{A}}) \left(1 - \delta_{j,i}^4 + \alpha_p (\delta_{j,i}^4 - \delta_{j,i}^3) \right)\tag{4.23}$$

Here α -plane associated membership degrees, given in equations (4.22) and (4.23), are used for the α -plane output calculations as explained in the previous chapters.

4.3 Structural Design Recommendations and Design Parameters

Since a GT2-FLC inherits its IT2 and T1 counterparts according to FLC interactions summarized in “Section 4.1 - Interactions between Fuzzy Logic Controllers”, it is suggested constructing the GT2-FLCs by designing first the base T1 and IT2 FLCs in this thesis. The internal structures of baseline FLCs (single- and double- input) are presented in “Chapter 2 - Preliminaries on Fuzzy Logic Controllers”. These initial design settings provide a convenient starting point for the GT2-FLC design since the parameters of baseline FLCs (T1-FLC and IT2-FLC) are distinguished from the GT2-FLC ones. Therefore, in the design of GT2-FLCs, it is assumed that the baseline design parameters (the primary part of antecedent MFs and the consequents) and structural settings (rule base, aggregation/union operators, type-reduction) are tuned.

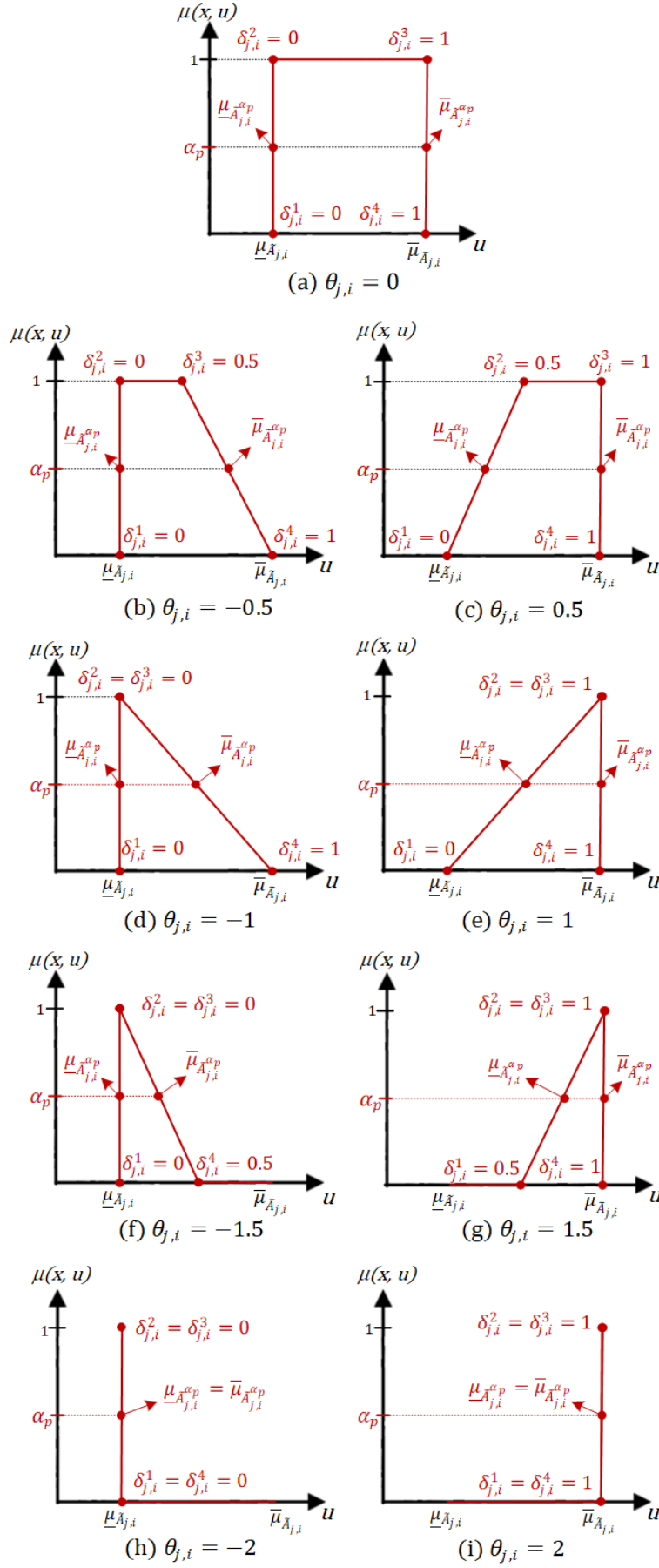


Figure 4.12 : Effect of shape design parameter on SMF shapes of GT2-FLCs.

The main design parameters of the GT2-FLCs are α -plane levels (α_p), the total number of α -planes (P), and the tuning parameters of the SMF. (Note: the design parameters of T1-FLCs and IT2-FLCs are summarized in Table 2.5 in “Chapter 2 - Preliminaries on Fuzzy Logic Controllers”). It is suggested handling these new GT2-FLC design parameters as follows:

- As given in equation (3.29), the output of the GT2-FLC is obtained based on a weighted average calculation of α -T2-FLC outputs. This calculation depends on the total number of α -planes (P) and α -plane levels (α_p) of α -T2-FLCs. In this thesis, the α -plane levels (α_p) are obtained with respect to the total number of α -planes (P). The level of p^{th} α -plane ($p = \{1, \dots, P\}$) is calculated as:

$$\alpha_p = p/P \quad (4.24)$$

such that the α -plane levels (α_p) excluded from the design parameters.

- The GT2-FLC output calculation given in equation (3.29) can be interpreted as granulation of continuous integration with respect to the total number of α -planes (P) and α -plane levels (α_p), which also depends on the total number of α -planes (P). The input-output mapping of GT2-FLC becomes closer to its continuous counterpart in terms of sensitivity/accuracy when the design parameter P increases. Therefore, it is concluded that the total number of α planes (P) is the sensitivity design parameter of the GT2-FLCs.
- As given in equations (4.22) and (4.23), the membership degrees of α -T2-FLCs are defined with respect to the parameters that define the shape and support of the SMFs according to equations (4.9) - (4.15). This directly influences the output of α -T2-FLCs ($y_{GT2}^{\alpha_p}$) and accordingly the output of the GT2-FLC (y_{GT2}) according to equation (3.29). Therefore, it is concluded that the parameters that define the SMF are the shape design parameters of the GT2-FLCs.

The design parameters of the GT2-FLCs can be assigned in various ways (similar to design options of T1 and IT2 counterparts). In Tables 4.1 and 4.2, the SMF design parameters and the total number of design parameters are tabulated for possible design configurations (Note: it is assumed that the baseline T1-FLC and IT2-FLC designs are completed and all T1 and IT2-FLC design parameters are fixed.).

Table 4.1 : Design parameters of GT2-SFLCs.

Assumptions	Total Number of Rules	Known Structural Parameters	Shape Design Parameters	Sensitivity Design Parameters	Total Number of Design Parameters
-	-	-	-	-	?
Unique SMF for each $\tilde{A}_{1,i}$	N	$I = N$	$\delta_{1,i}^t$	P	$4N + 1$
Same SMF for all $\tilde{A}_{1,i}$	N	$I = N$	$\delta_{1,i}$	P	$4 + 1$
Unique SMF for each $\tilde{A}_{1,i}$	N	$I = N$	$\theta_{1,i}$	P	$N + 1$
Same SMF for all $\tilde{A}_{1,i}$	N	$I = N$	θ^\dagger	P^\ddagger	2

?: Structure is not clear (too many design options).

†: The shape design parameter

‡: The sensitivity design parameter

Table 4.2 : Design parameters of GT2-DFLCs.

Assumptions	Total Number of Rules	Known Structural Parameters	Shape Design Parameters	Sensitivity Design Parameters	Total Number of Design Parameters
-	-	-	-	-	?
Unique SMF for each $\tilde{A}_{j,i}$	N	$I \times K = N$	$\delta_{1,i}^t, \delta_{2,k}^t$	P	$4(I + K) + 1$
Same SMF for all $\tilde{A}_{j,i}$	N	$I \times K = N$	$\delta_{j,i}^t$	P	$4 + 1$
Unique SMF for each $\tilde{A}_{j,i}$	N	$I \times K = N$	$\theta_{1,i}, \theta_{2,k}$	P	$(I + K) + 1$
Same SMF for all $\tilde{A}_{j,i}$	N	$I \times K = N$	θ^\dagger	P^\ddagger	2

?: Structure is not clear (too many design options).

†: The shape design parameter.

‡: The sensitivity design parameter

As shown in Tables 4.1 and 4.2, the proposed trapezoid SMF representation is very promising for the GT2-FLC design. Here it is worth underlying that trapezoid SMFs (rather than triangle SMFs) are preferred in this thesis since the trapezoid SMFs cover the triangular SMFs and also provide the flexibility to convert GT2-FLCs into T1 or IT2 FLC. The proposed trapezoid SMF representation is also easy-to-implement since it not only reduces the total number of design parameters but also provides flexibility to construct various shapes of SMFs based on the proposed parameterization [76]. In this thesis, all antecedent FSs of the handled GT2-FLCs are defined with the same SMF, as stated in [7], this option reduces the design complexity/effort.

According to these design recommendations, the GT2-FLCs can be designed (over the T1-FLC and IT2 FLC baselines), by simply tuning two design parameters:

- θ , the shape design parameter,
- P , the sensitivity design parameter.

The summary of the design parameters and the total number of design parameters of T1, IT2, and GT2 FLCs are listed in Table 4.3. Here, the consequent design parameter (C_n) is associated with T1-FLC design, the FOU design parameter ($M_{j,i}$) is related to IT2-FLC design, the SMF shape and sensitivity design parameters (θ and P) are associated with GT2-FLC design, while the total number of design parameters is related to the total number of the rules (N). In the next chapters, comprehensive comparative analyses are conducted to present the design recommendations/methods on how to tune the shape design parameter (θ) and the sensitivity design parameter (P) of the GT2-FLCs.

Table 4.3 : Summary of T1, IT2, and GT2 FLC design parameters.

FLC Type	Consequent Design Parameters	FOU Design Parameters	SMF Shape Design Parameters	Sensitivity Design Parameters	Total Number of Design Parameters
T1-SFLC	C_n	—	—	—	N
IT2-SFLC	—	$M_{1,i}$	—	—	N
GT2-SFLC	—	—	θ	P	2
T1-DFLC	C_n	—	—	—	N
IT2-DFLC	—	$M_{1,i}, M_{2,k}$	—	—	$I + K$
GT2-DFLC	—	—	θ	P	2



5. ANALYSIS AND DESIGN OF SHAPE DESIGN PARAMETER

In this chapter, the effect of the shape design parameter, (i.e. θ) on the control curve/control surface generation will be presented, the design recommendations for the GT2-FLCs are concluded, and new online scheduling mechanisms that tune the shape design parameter are proposed.

5.1 Structural Change Analysis

In this section, how the structure of the GT2-FLC changes with respect to the shape design parameter $\theta \in [-2, 2]$ will be investigated. In this context, the structure switching values of the shape design parameter ($\theta = \{-2, 0, 2\}$) will be examined.

- For the shape design parameter setting $\theta = 0$, all α -plane associated lower and upper membership degrees ($\underline{\mu}_{\tilde{A}^{\alpha p}}$ and $\overline{\mu}_{\tilde{A}^{\alpha p}}$) are equal for all α -planes slices as $\underline{\mu}_{\tilde{A}^{\alpha p}} = \underline{\mu}_{\tilde{A}^{\alpha_0}} = \underline{\mu}_{\tilde{A}}$ and $\overline{\mu}_{\tilde{A}^{\alpha p}} = \overline{\mu}_{\tilde{A}^{\alpha_0}} = \overline{\mu}_{\tilde{A}}$ respectively. Therefore, an interval SMF is obtained as illustrated in Figure 4.7. For this shape design parameter setting, the GT2-FLC transforms into its IT2-FLC counterpart from the input-output mapping point of view. Thus, the GT2-FLC results with an identical CC/CS with its IT2-FLC counterpart as follows:

$$U_{GT2} \Big|_{\theta=0} = U_{IT2} \quad (5.1)$$

- For the shape design parameter setting $\theta = -2$, all α -plane associated lower and upper membership degrees ($\underline{\mu}_{\tilde{A}^{\alpha p}}$ and $\overline{\mu}_{\tilde{A}^{\alpha p}}$) are equal to the one calculated for the LMF as $\underline{\mu}_{\tilde{A}^{\alpha p}} = \overline{\mu}_{\tilde{A}^{\alpha p}} = \underline{\mu}_{\tilde{A}^{\alpha_0}} = \underline{\mu}_{\tilde{A}}$. Therefore, a spike-shaped SMF is obtained as illustrated in Figure 4.3. For this shape design parameter setting, the GT2-FLC transforms into a particular T1-FLC that only utilizes the LMFs of the IT2-FSSs. Thus, from the input-output mapping point of view, the GT2-FLC results with the following CC/CS:

$$U_{GT2} \Big|_{\theta=-2} = \frac{\sum_{n=1}^N \underline{f}_n C_n}{\sum_{n=1}^N \underline{f}_n} \quad (5.2)$$

- For the shape design parameter setting $\theta = 2$, all α -plane associated lower and upper membership degrees ($\underline{\mu}_{\tilde{A}^{\alpha p}}$ and $\overline{\mu}_{\tilde{A}^{\alpha p}}$) are equal to the one calculated for the UMF as $\underline{\mu}_{\tilde{A}^{\alpha p}} = \overline{\mu}_{\tilde{A}^{\alpha p}} = \overline{\mu}_{\tilde{A}^{\alpha_0}} = \overline{\mu}_{\tilde{A}}$. Therefore, a spike-shaped SMF is obtained as illustrated in Figure 4.11. For this shape design parameter setting, the GT2-FLC reduces into its T1-FLC baseline from the input-output mapping point of view. Thus, the GT2-FLC results with the same CC/CS of its T1-FLC counterpart as follows:

$$U_{GT2} \Big|_{\theta=2} = U_{T1} \quad (5.3)$$

It can be concluded that, in addition to numerous GT2-FLC design options, T1-FLC and IT2-FLC design options are also possible by simply adjusting the shape design parameter θ . Here, the values of $\theta = \{-2, 0, 2\}$ are the structure switching values since they determine the resulting input-output mapping. The output of the GT2-FLC is over bounded by these structure switching values as follows:

$$\underline{U}_{GT2} \leq U_{GT2} \leq \overline{U}_{GT2} \quad (5.4)$$

where

$$\underline{U}_{GT2} = \min_{\theta=\{-2,0,2\}} U_{GT2} \Big|_{\theta} \quad (5.5)$$

$$\overline{U}_{GT2} = \max_{\theta=\{-2,0,2\}} U_{GT2} \Big|_{\theta} \quad (5.6)$$

where \underline{U}_{GT2} and \overline{U}_{GT2} are the lower and upper bounds of the GT2-FLC output, respectively.

5.2 Shape Analyses of Control Curves / Control Surfaces

In this section, the CCs/CSs of the GT2-FLCs will be analyzed for various shape design parameter settings. For all CC/CS analyses, the sensitivity design parameter is fixed as $P = 10$ (in other words the GT2-FLCs always employ 10 α -planes) and the

baseline FLCs (i.e. T1-FLC and IT2-FLC) are fixed as defined in Section 5.2.1, so that the resulting input-output mapping of the GT2-FLC is only determined by the shape design parameter θ . For this purpose, the resulting CCs of the GT2-SFLCs and CSs of the GT2-DFLCs are examined for 9 different shape design parameter settings in the definition range of $[-2, 2]$ as $\theta = \{-2, -1.5, -1, -0.5, 0, 0.5, 1, 1.5, 2\}$.

Moreover, for the demonstration of the potential impacts of the shape design parameter θ on the CC/CS generation clearly, two measures are defined to analyze the impact of the shape design parameter θ . The first measure is the Normalized Total Energy (*NTE*) of the CC/CS which is defined as follows:

$$NTE = \frac{\|U_{GT2}\|_2}{\|U_{T1}\|_2} \quad (5.7)$$

where $\|\cdot\|_2$ indicates the signal norm of FLC outputs, U_{GT2} and U_{T1} are the outputs of GT2-FLC and T1-FLC, respectively. The *NTE* measure provides useful information on the aggressiveness/smoothness of the CC/CS of GT2-FLC comparing to the T1 counterpart. For instance, if $NTE > 1$, then the CC/CS of the GT2-FLC is relatively more aggressive since it has more energy than its T1 counterpart, whereas the CC/CS surface of the GT2-FLC becomes smoother when $NTE < 1$. For the CCs/CSs with the measure $NTE > 1$, it is expected that the fuzzy control system achieves faster system responses in the transient state, but this aggressive action might result in overshoots/oscillations. The second measure is the Noise Ratio (*NR*), which is defined to examine the robustness of the handled FLCs around the steady-state. The *NR* measure is calculated based on a zero-mean Gaussian noise input with a standard deviation of $\sigma_{in} = 0.2$ as follows:

$$NR = \frac{\sigma_{out}^2}{\sigma_{in}^2} \quad (5.8)$$

where σ_{out} is the standard deviation of the GT2-FLC output. The *NR* measure provides useful information about how the GT2-FLC amplifies the zero-mean noise signal around the steady-state so that the system reaction of the GT2-FLC in terms of the control effort or the robustness against noises can be investigated in the time domain numerically. For instance; if $NR = 1$, then it means that the GT2-FLC has a unit mapping from input to output (e.g. $y = f(x)$, where $f(x) = x$); when $NR < 1$, the

GT2-FLC is potentially more robust against noises and uncertainties, since it does not amplify the noisy signal, if $NR > 1$, then the GT2-FLC potentially produces relatively more control action against noises and uncertainties around the state, which might end up with faster system response compromising overshoots/oscillations.

5.2.1 Baseline FLCs used in shape analyses

In this section, the baseline FLCs which are examined in the analyses of the next chapters (single/double-input T1/IT2-FLCs), will be presented. These employed controllers; particularly T1-SFLC, T1-DFLC, IT2-SFLC, and IT2-DFLC, are assumed as the baselines for the GT2-FLC design, as explained in previous sections. For this purpose, the CCs of SFLCs and the CSs of DFLCs are wisely constructed for the sake of clear GT2-FLC design.

The T1-SFLC and T1-DFLC are designed in a way that an aggressive CC and CS can be achieved, respectively. The T1-FLC design aims to obtain a faster system response in the transient state, although this might result in overshoot in some cases. To this end, the T1-FLCs are determined based on the consequent design parameters (C_n) by excluding the scaling factors which are set according to the control application. The baseline T1-SFLC and baseline T1-DFLC are determined according to the comments in [41, 40] via the consequent design parameter settings, which are denoted as CONS-1 and CONS-2 respectively, as follows:

- **CONS-1:** $C_1 = -1, C_2 = 0, C_3 = 1.$
- **CONS-2:** $C_1 = -1, C_2 = 0.8, C_3 = 0,$
 $C_4 = -0.8, C_5 = 0, C_6 = 0.8,$
 $C_7 = 0, C_8 = 0.8, C_9 = 1.$

The IT2-SFLC and IT2-DFLC can be designed in numerous ways such that smooth or aggressive CCs and CSs can be achieved, respectively. To this end, four IT2-FLCs are designed in this thesis; a smooth IT2-SFLC that employs FOU-1 which results with relatively smoother CC than T1 counterpart, an aggressive IT2-SFLC that employs FOU-2 which results with relatively more aggressive CC, a smooth IT2-DFLC that employs FOU-3 which results with relatively smoother CS around the origin, an aggressive IT2-SFLC that employs FOU-4 which results with relatively more aggressive CS around the origin. For the IT2-SFLC designs, the recommendations in

[41] are followed. For the IT2-DFLC designs, the analyses in previous works [40, 43, 44] are considered. The design parameters of the baseline IT2-FLCs are as follows:

- **FOU-1:** $M_{1,1} = 0.2, M_{1,2} = 0.9, M_{1,3} = 0.2.$
- **FOU-2:** $M_{1,1} = 0.9, M_{1,2} = 0.2, M_{1,3} = 0.9.$
- **FOU-3:** $M_{1,1} = 0.2, M_{1,2} = 0.9, M_{1,3} = 0.2,$
 $M_{2,1} = 0.2, M_{2,2} = 0.9, M_{2,3} = 0.2.$
- **FOU-4:** $M_{1,1} = 0.9, M_{1,2} = 0.3, M_{1,3} = 0.9,$
 $M_{2,1} = 0.9, M_{2,2} = 0.3, M_{2,3} = 0.9.$

5.2.1.1 Baseline type-1 single-input FLC

The internal structure of the baseline T1-SFLC is constructed according to Section 2.4 and the baseline T1-SFLC is composed of $N = 3$ rules. The T1-SFLC employs the design parameter setting CONS-1 in its rule base as shown in Table 5.1.

Table 5.1 : Rule base of baseline T1-SFLC.

$x_1 = E$	$A_{1,1}$	$A_{1,2}$	$A_{1,3}$
	$c_1 = -1$	$c_2 = 0$	$c_3 = 1$

The antecedent MFs ($A_{1,1}$, $A_{1,2}$, and $A_{1,3}$) are defined with triangle FSs and the cores are selected as $c_{1,1} = -1$, $c_{1,2} = 0$, and $c_{1,3} = 1$. Here, the cores are represented with $c_{j,i}$ instead of b (as given in equation (2.6)) in order to have a similar label convention with the MF $A_{j,i}$. The antecedent MFs and resulting CC of the baseline T1-SFLC are given in Figure 5.1 and Figure 5.2 in comparison with IT2 counterparts.

5.2.1.2 Baseline smooth interval type-2 single-input FLC

The internal structure of the baseline smooth IT2-SFLC is constructed according to Section 2.4. The IT2-SFLC shares the same rule of its T1 counterpart as given in Table 5.2, it only differs that the IT2- SFLC uses IT2-FSs instead of T1-FSs.

Table 5.2 : Rule base of baseline IT2-SFLCs.

$x_1 = E$	$\tilde{A}_{1,1}$	$\tilde{A}_{1,2}$	$\tilde{A}_{1,3}$
	$c_1 = -1$	$c_2 = 0$	$c_3 = 1$

The antecedent MFs ($\tilde{A}_{1,1}$, $\tilde{A}_{1,2}$, and $\tilde{A}_{1,3}$) are defined with triangle IT2-FSs and the core points of these antecedent MFs are selected as the ones used for T1 counterpart ($c_{1,1} = -1$, $c_{1,2} = 0$, and $c_{1,3} = 1$), while the FOU design parameters of the baseline smooth IT2-SFLC are set to FOU-1. The antecedent MFs and resulting CC of the baseline smooth IT2-SFLC are illustrated in Figure 5.1.

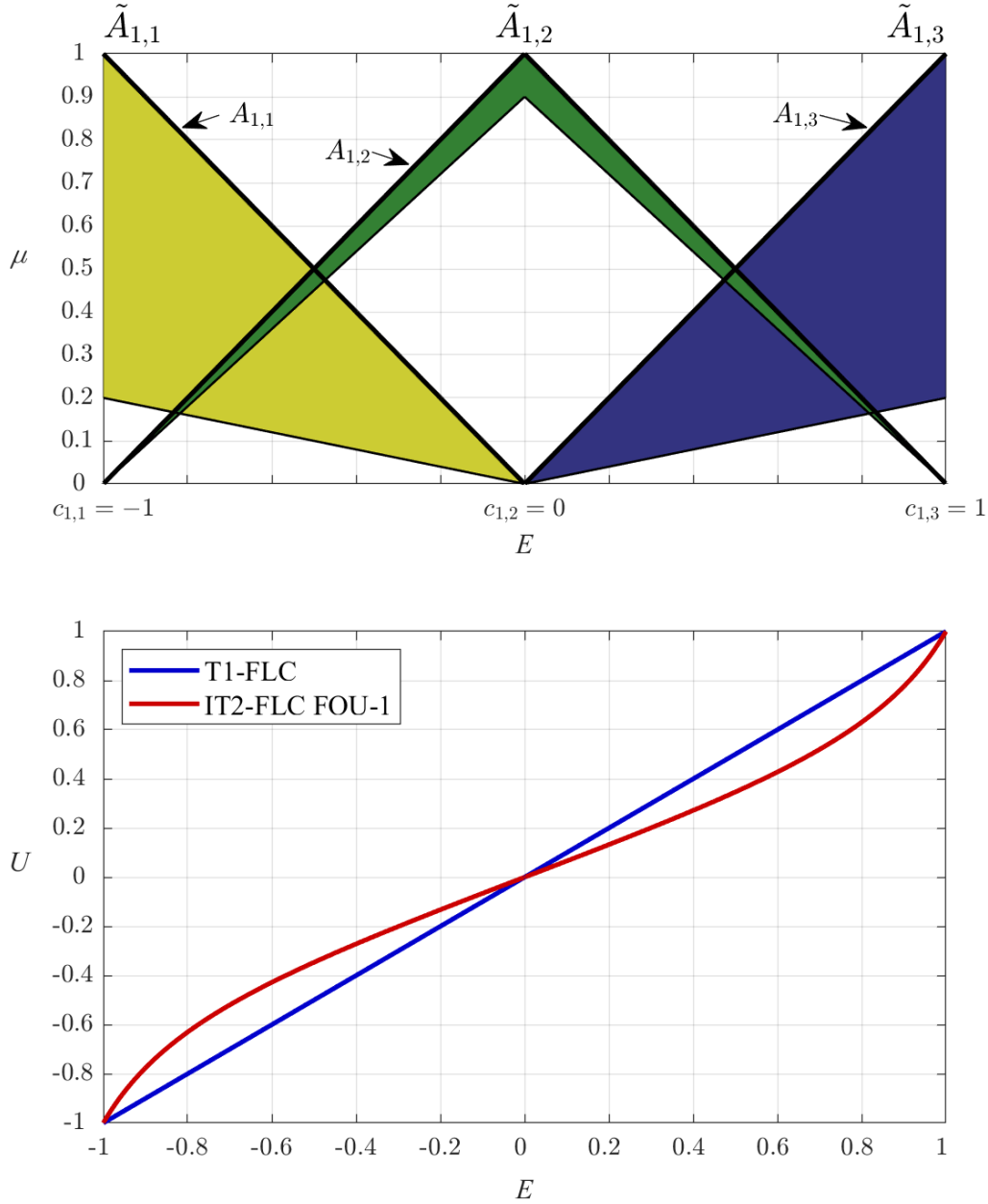


Figure 5.1 : Baseline T1-SFLC and baseline IT2-SFLC employing FOU-1.

5.2.1.3 Baseline aggressive interval type-2 single-input FLC

The internal structure of the baseline aggressive IT2-SFLC is constructed according to Section 2.4 and it employs the same rule base and antecedent MFs of its smooth counterpart (given in Table 5.2). It only differs on the FOU design, as the baseline aggressive IT2-SFLC employs the parameter setting FOU-2, while the smooth IT2-SFLC employs the parameter setting FOU-1. As shown in [36, 41], an aggressive or a smooth CC can be achieved by proper tuning of the FOU design parameters. The antecedent MFs and resulting CC of the baseline aggressive IT2-SFLC are illustrated in Figure 5.2 in comparison with the T1 counterpart.

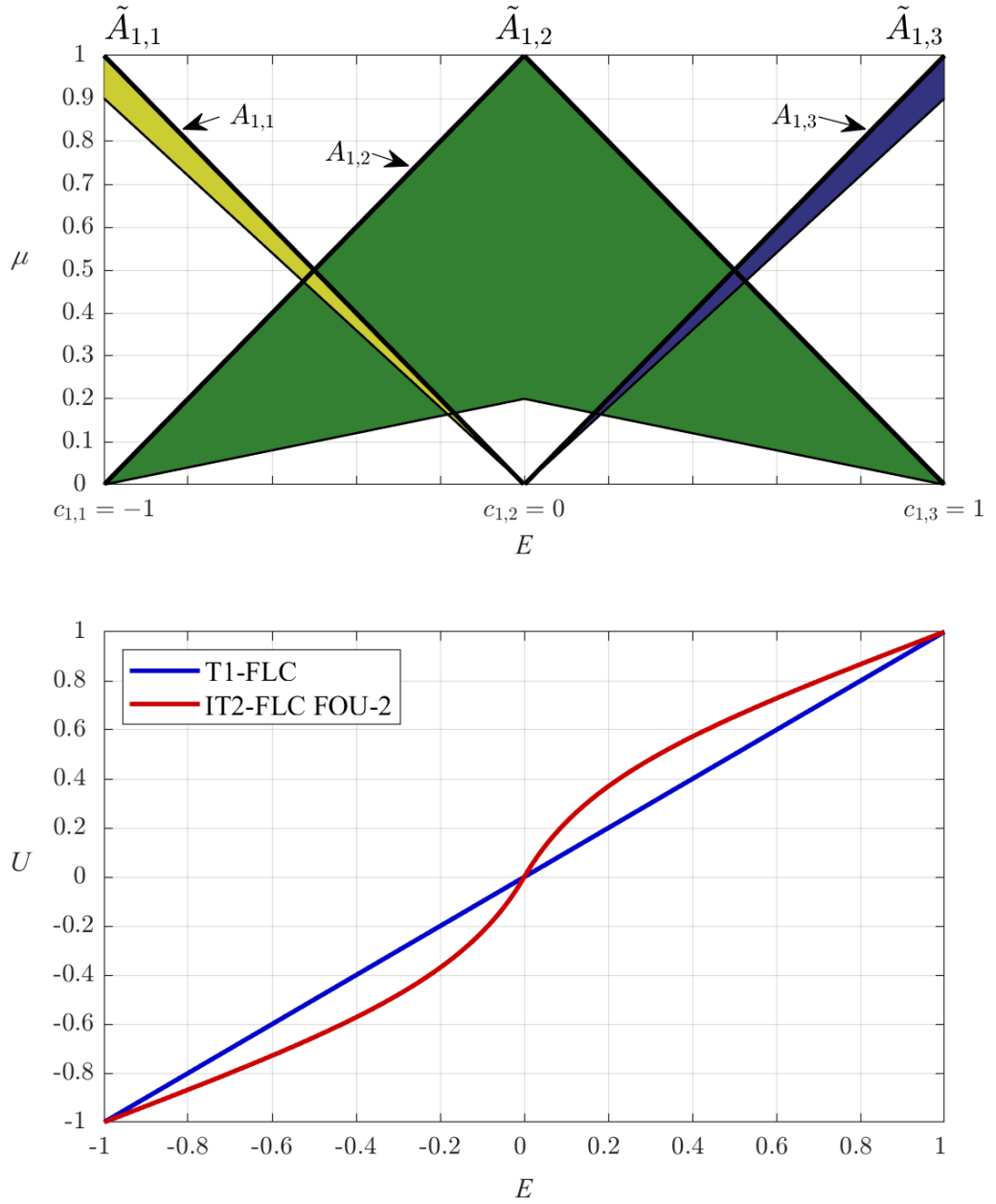


Figure 5.2 : Baseline T1-SFLC and baseline IT2-SFLC employing FOU-2.

5.2.1.4 Baseline type-1 double-input FLC

The internal structure of the T1-DFLC is constructed according to Section 2.5 and the T1-SFLC, which is used for the analyses in this thesis, is composed of $N = 3 \times 3 = 9$ rules. The T1-DFLC employs the design parameter setting CONS-2 as in Table 5.3.

Table 5.3 : Rule base of baseline T1-DFLC.

$x_2 = \Delta E \quad \backslash \quad x_1 = E$	$A_{1,1}$	$A_{1,2}$	$A_{1,3}$
$A_{2,1}$	$C_1 = -1$	$C_2 = -0.8$	$C_3 = 0$
$A_{2,2}$	$C_4 = -0.8$	$C_5 = 0$	$C_6 = 0.8$
$A_{2,3}$	$C_7 = 0$	$C_8 = 0.8$	$C_9 = 1$

The antecedent MFs ($A_{1,1}$, $A_{1,2}$, $A_{1,3}$, $A_{2,1}$, $A_{2,2}$, and $A_{2,3}$) are defined with triangle FSs and the core points are $c_{1,1} = c_{2,1} = -1$, $c_{1,2} = c_{2,2} = 0$, and $c_{1,3} = c_{2,3} = 1$. The resulting CS differences between the baseline T1-DFLC and the baseline smooth IT2-FLCs is given in Figure 5.3, and the differences between the baseline T1-DFLC and the baseline aggressive IT2-FLC is given in Figure 5.4.

5.2.1.5 Baseline smooth interval type-2 double-input FLC

The internal structure of the smooth IT2-DFLC is constructed according to Section 2.5 and the baseline smooth IT2-DFLC is composed of $N = 3 \times 3 = 9$ rules. Similar to its T1 counterpart, the smooth baseline IT2-DFLC also employs the design parameter setting CONS-2 as shown in Table 5.4.

Table 5.4 : Rule base of baseline IT2-DFLCs.

$x_2 = \Delta E \quad \backslash \quad x_1 = E$	$\tilde{A}_{1,1}$	$\tilde{A}_{1,2}$	$\tilde{A}_{1,3}$
$\tilde{A}_{2,1}$	$C_1 = -1$	$C_2 = -0.8$	$C_3 = 0$
$\tilde{A}_{2,2}$	$C_4 = -0.8$	$C_5 = 0$	$C_6 = 0.8$
$\tilde{A}_{2,3}$	$C_7 = 0$	$C_8 = 0.8$	$C_9 = 1$

The antecedent MFs ($\tilde{A}_{1,1}$, $\tilde{A}_{1,2}$, $\tilde{A}_{1,3}$, $\tilde{A}_{2,1}$, $\tilde{A}_{2,2}$, and $\tilde{A}_{2,3}$) are defined with triangle IT2-FSs and the core points are the same as the T1 counterparts; $c_{1,1} = c_{2,1} = -1$, $c_{1,2} = c_{2,2} = 0$, and $c_{1,3} = c_{2,3} = 1$. Here, the baseline smooth IT2-DFLC employs the design parameter setting FOU-1, which provides a smoother CS in comparison to its T1 counterpart (as shown in previous analyses works [42-44]). The antecedent MFs of the IT2-FLC and the CS differences between the baseline T1-DFLC, and the baseline smooth IT2-SFLC (i.e. $y_{T1} - y_{IT2}$) are illustrated in Figure 5.3.

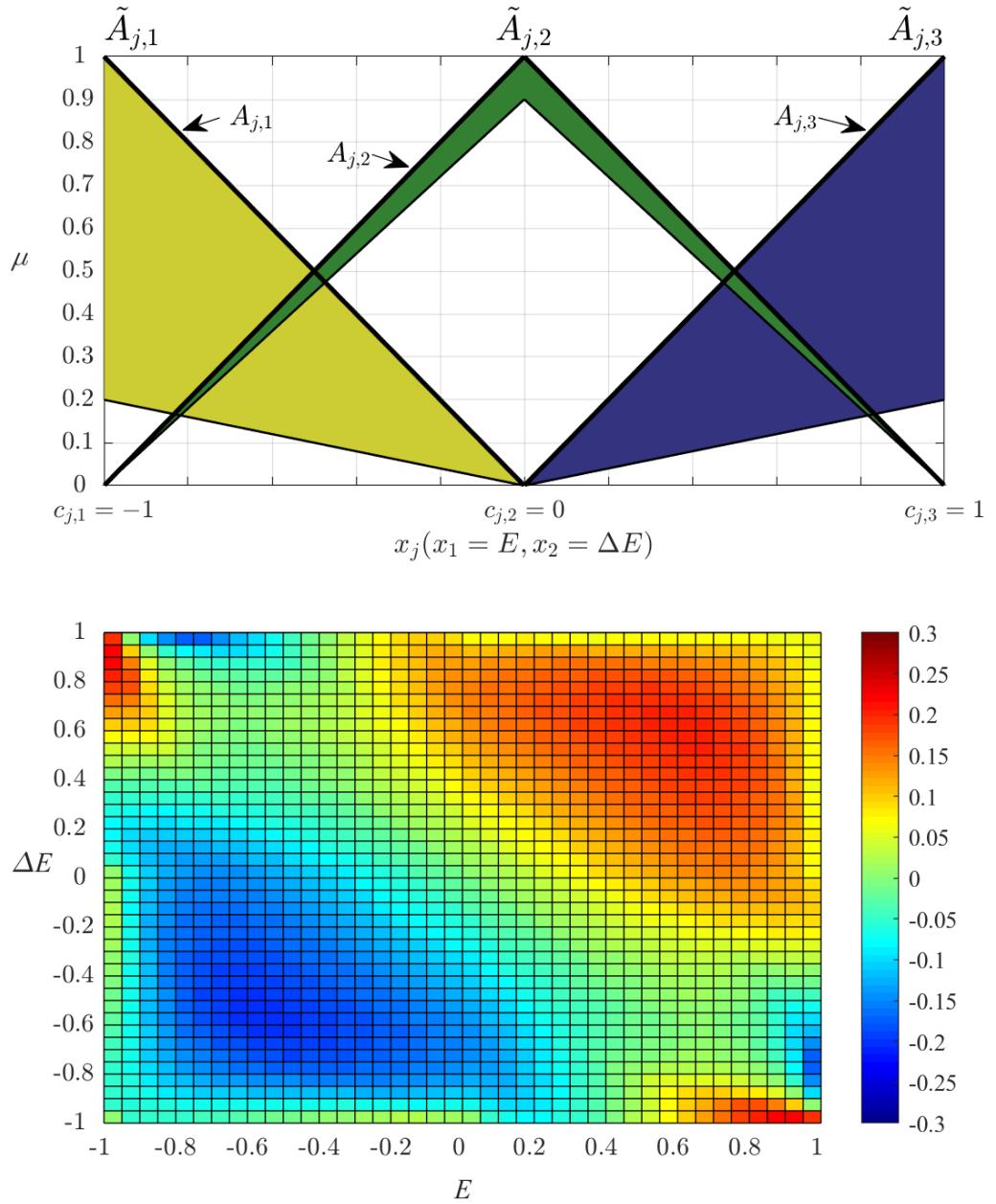


Figure 5.3 : Baseline T1-DFLC and baseline IT2-DFLC employing FOU-3.

5.2.1.6 Baseline aggressive interval type-2 double-input FLC

The internal structure of the baseline aggressive IT2-DFLC is constructed according to Section 2.5. The baseline aggressive IT2-DFLC employs $N = 3 \times 3 = 9$ rules and the design parameter setting CONS-2 as shown in Table 5.4. The antecedent MFs are selected as the ones used for the smooth IT2 counterpart, and the baseline aggressive IT2-DFLC uses the design parameter setting FOU-4, which provides an aggressive CS. As it is shown in previous analyses works [42-44], it is possible to generate both smooth and aggressive IT2 CS via proper FOU parameter design. The antecedent MFs

of the IT2-FLC and the CS differences between the baseline T1 and the baseline aggressive IT2 DFLCs (i.e. $y_{T1} - y_{IT2}$) are illustrated in Figure 5.4.

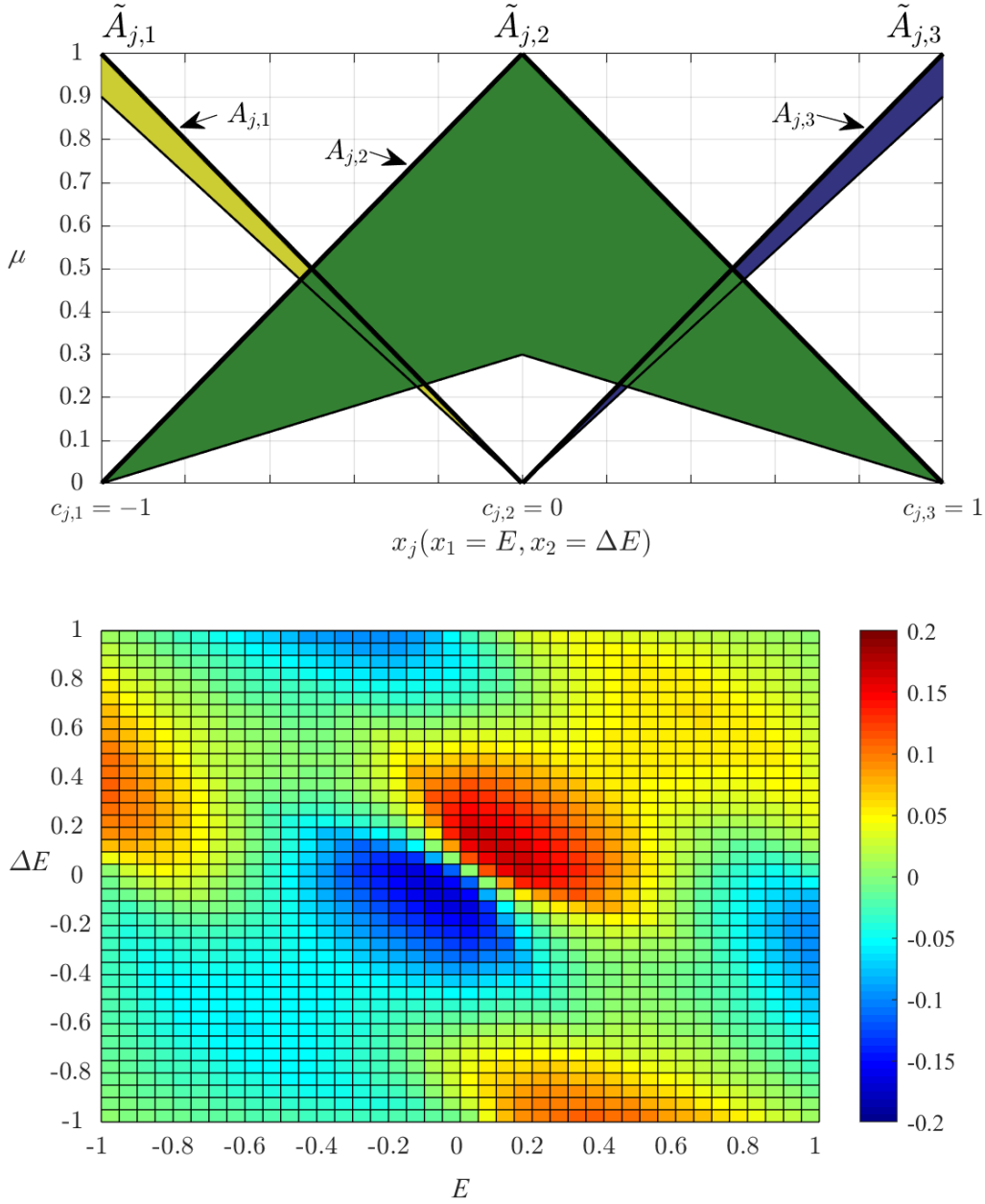


Figure 5.4 : Baseline T1-DFLC and baseline IT2-DFLC employing FOU-4.

5.2.2 Control curves of GT2-SFLCs

In this section, the shape analyses over the CCs of the GT2-SFLCs are presented for 9 shape design parameter settings, $\theta = \{-2, -1.5, -1, -0.5, 0, 0.5, 1, 1.5, 2\}$. In this context, the resulting CCs of the GT2-SFLCs are firstly calculated for each shape design parameter configuration, and the CCs of the handled GT2-SFLCs with FOU-1 and FOU-2 are illustrated in Fig. 5.5 and Fig. 5.6, respectively. For easier understanding

of how the shape design parameter affects the CCs, the CCs are given in two-fold; the CC window where $E \in [0, 1]$ and the complete CC where $E \in [-1, 1]$.

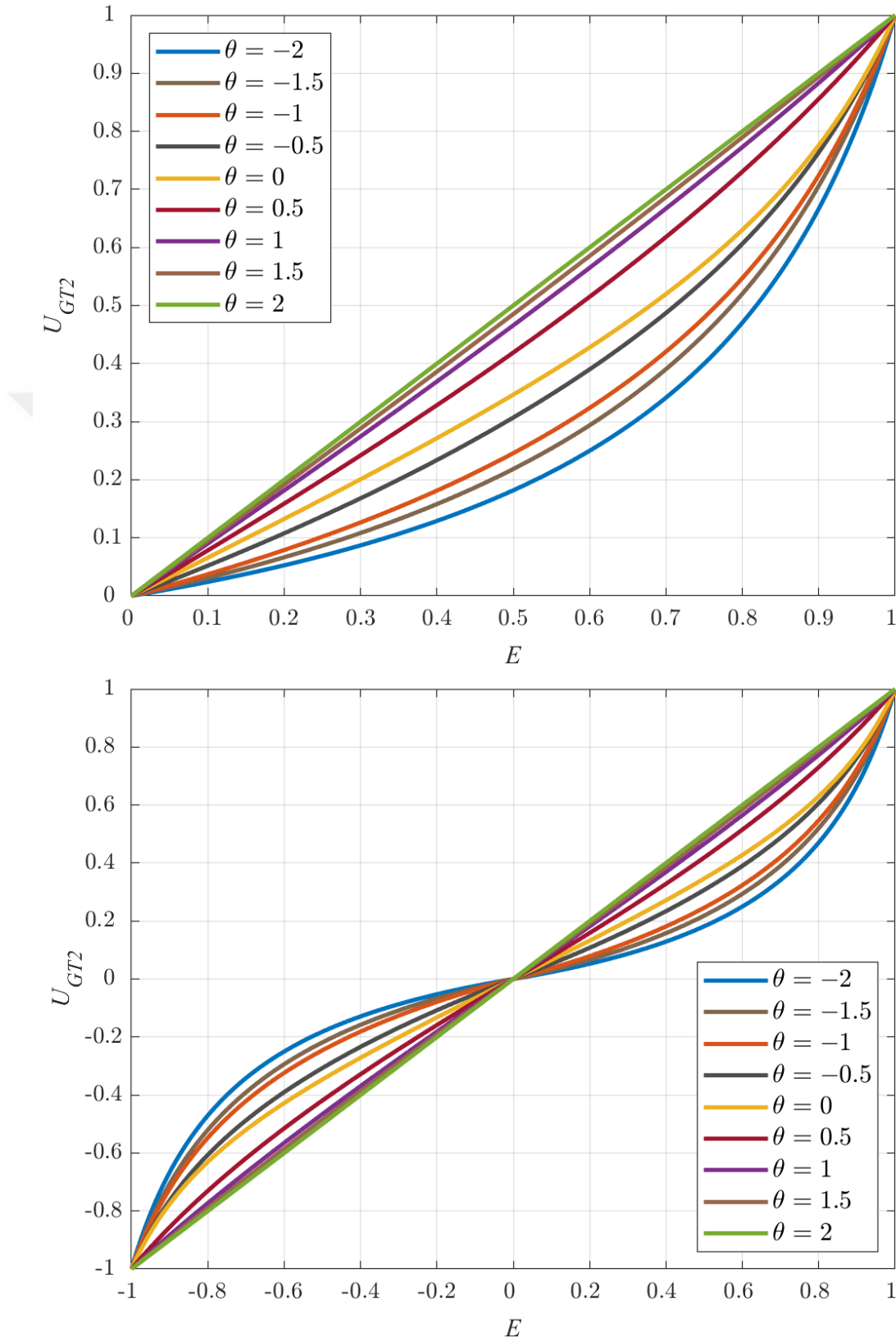


Figure 5.5 : Effect of shape design parameter on CCs of GT2-SFLCs with FOU-1.

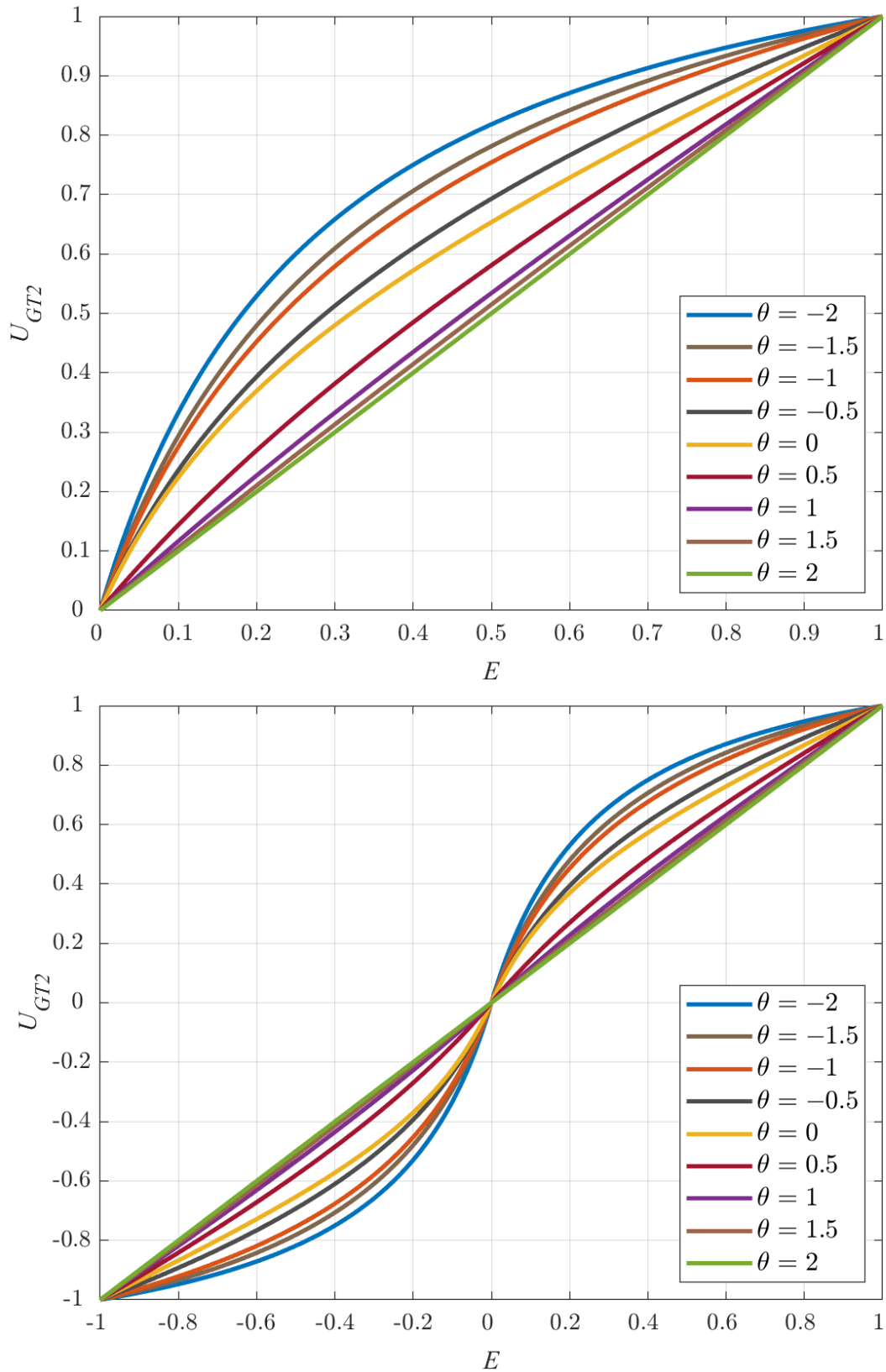


Figure 5.6 : Effect of shape design parameter on CCs of GT2-SFLCs with FOU-2.

As illustrated in Figure 5.5 and Figure 5.6, the shape design parameter θ not only defines the shape of the SMF (as explained in Section 4.2) but also shapes the resulting

CC of the GT2-SFLC. The numerical *NTE* and *NR* measures are tabulated in Table 5.5. For the smooth design option FOU-1, as shown in Figure 5.5, the resulting CC becomes smoother when the shape design parameter θ decreases from 2 to -2. Here, the shape design parameter settings $\theta = 2$ and $\theta = 0$ result with the baseline T1-SFLC and the baseline smooth IT2-SFLC, which are defined in Section 5.2.1, respectively. By decreasing the shape design parameter θ , the CC of the GT2-SFLC transforms from an aggressive mapping (the mapping of T1 counterpart) to a smoother mapping. This coincides with the *NTE* and *NR* measures. For this design, the lowest *NR* value is achieved for the GT2-SFLC with $\theta = -2$ design. Therefore, the GT2-SFLC with $\theta = -2$ design setting is potentially more robust since it is less sensitive to the noise in comparison to its GT2 counterparts. The *NTE* values are always less than 1, so it can be interpreted that any GT2-SFLC design ends up with a potentially smoother fuzzy controller than its T1-SFLC counterpart. For the aggressive design option FOU-2, as shown in Figure 5.6, the resulting CC becomes more aggressive when the shape design parameter θ decreases from 2 to -2. Here, the shape design parameter settings $\theta = 2$ and $\theta = 0$ result with the baseline T1-FLC and the baseline aggressive IT2-FLC, which are defined in Section 5.2.1, respectively. By decreasing the shape design parameter θ , the CC of the GT2-SFLC transforms from the mapping of its T1 counterpart to a more aggressive mapping. This also coincides with the *NTE* and *NR* measures. For this design, the highest *NTE* value is obtained for the GT2-SFLC with $\theta = -2$ design. Therefore, the resulting GT2-SFLC with $\theta = -2$ design setting has the potential to improve transient system response as its CC is aggressive.

Table 5.5 : Performance measures of shape analyses for GT2-SFLCs.

θ	FOU-1		FOU-2	
	<i>NTE</i>	<i>NR</i>	<i>NTE</i>	<i>NR</i>
-2	0.633	0.093	1.341	5.272
-1.5	0.679	0.141	1.297	4.420
-1	0.707	0.189	1.266	3.978
-0.5	0.772	0.324	1.199	3.091
0	0.805	0.455	1.156	2.733
0.5	0.910	0.658	1.079	1.627
1	0.963	0.841	1.033	1.230
1.5	0.985	0.925	1.015	1.088
2	1.000	1.000	1.000	1.000

5.2.3 Control surfaces of GT2-DFLCs

In this section, the shape analyses over the CSs of the GT2-DFLCs are presented for 9 shape design parameter settings, $\theta = \{-2, -1.5, -1, -0.5, 0, 0.5, 1, 1.5, 2\}$. In this context, the resulting CSs of the GT2-DFLCs with FOU-3 and FOU-4 are firstly calculated for each shape design parameter configuration. The CSs of the GT2-DFLCs with FOU-3 and FOU-4 are illustrated in Fig. 5.7 and Fig. 5.8, respectively. As the analysis on the shapes of resulting CSs is not straightforward as the one for CCs; the CS differences between the GT2-FLC and the baseline T1-FLC (i.e. $U_{GT2} - U_{T1}$), and the CS differences between GT2-FLC and baseline IT2-FLCs (i.e. $U_{GT2} - U_{IT2}$) are examined by varying the shape design parameter θ , for FOU-3 and FOU-4 settings respectively.

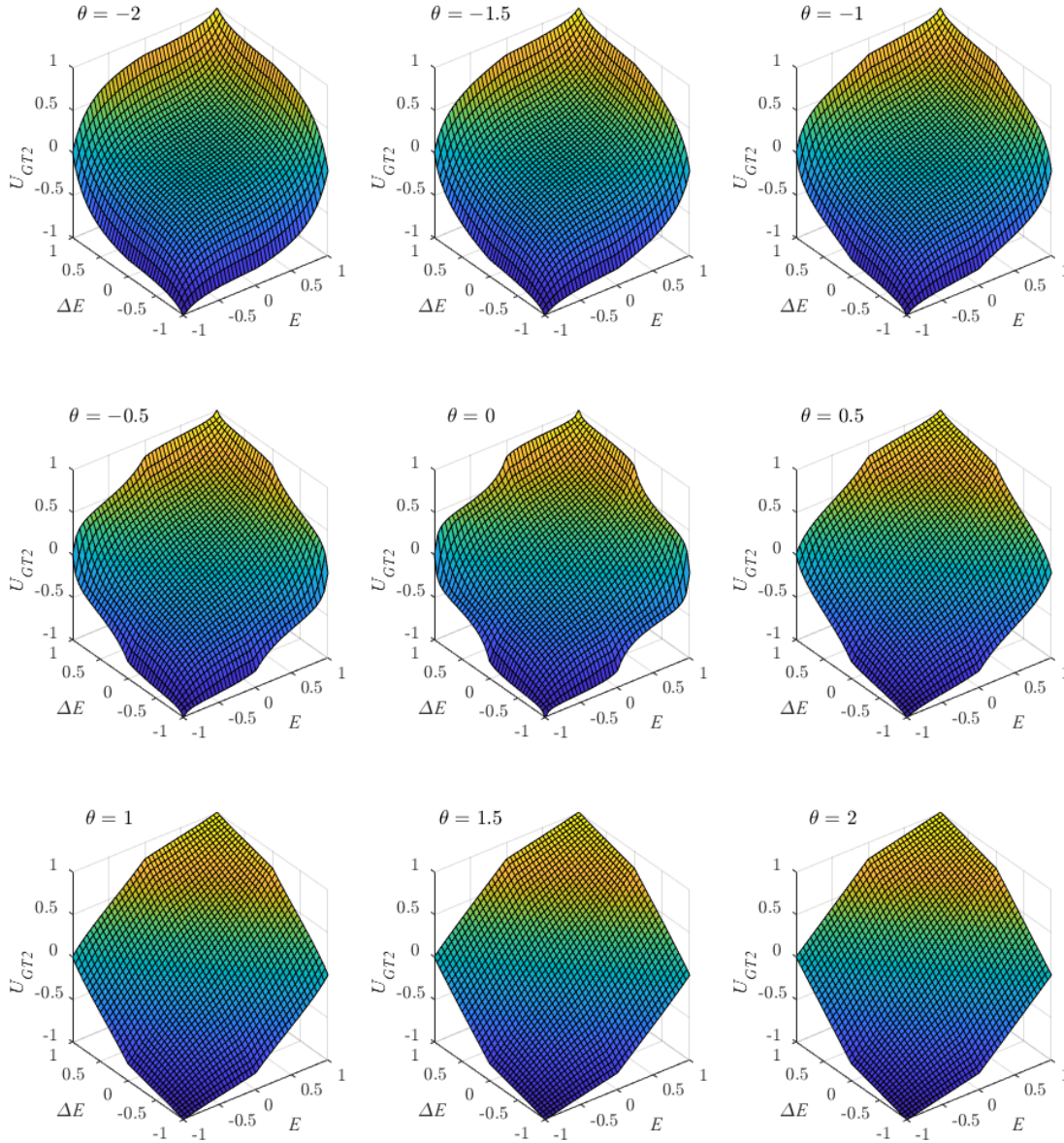


Figure 5.7 : Effect of shape design parameter on CSs of GT2-DFLCs with FOU-3.

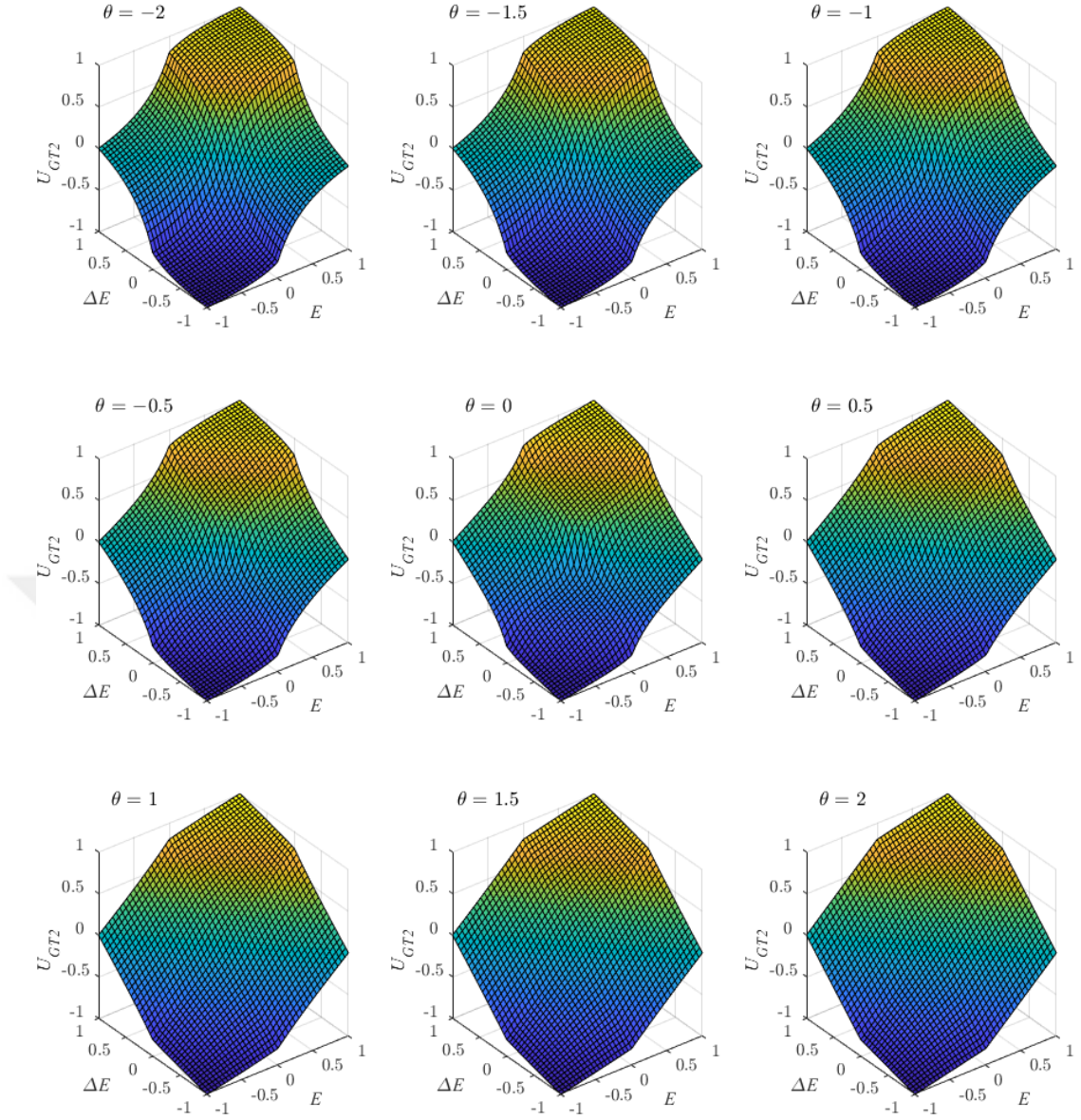


Figure 5.8 : Effect of shape design parameter on CSs of GT2-DFLCs with FOU-4.

For the smooth design option FOU-3, the CS differences between the GT2-DFLC and the baseline T1-DFLC ($U_{GT2} - U_{T1}$) is presented in Figure 5.9, and the CS differences between the GT2-DFLC and the baseline smooth IT2-DFLC (i.e. $U_{GT2} - U_{IT2}$) is presented in Figure 5.10. For the aggressive design option FOU-4, the CS differences between the GT2-DFLC and the baseline T1-DFLC ($U_{GT2} - U_{T1}$) is presented in Figure 5.11, and the CS differences between the GT2-DFLC and the baseline aggressive IT2-DFLC (i.e. $U_{GT2} - U_{IT2}$) is presented in Figure 5.12. The calculated numerical *NTE* and *NR* measures for the employed GT2-DFLCs are tabulated in Table 5.6.

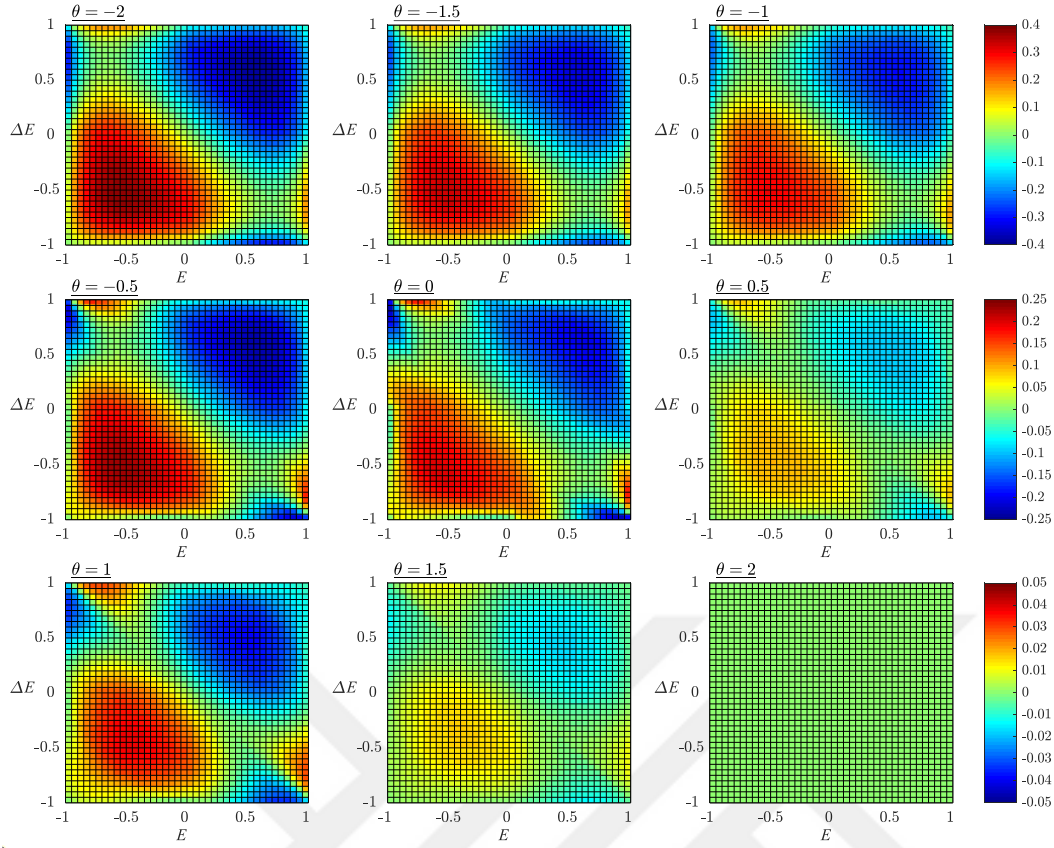


Figure 5.9 : CS differences between GT2 and T1 FLCs with FOU-3.

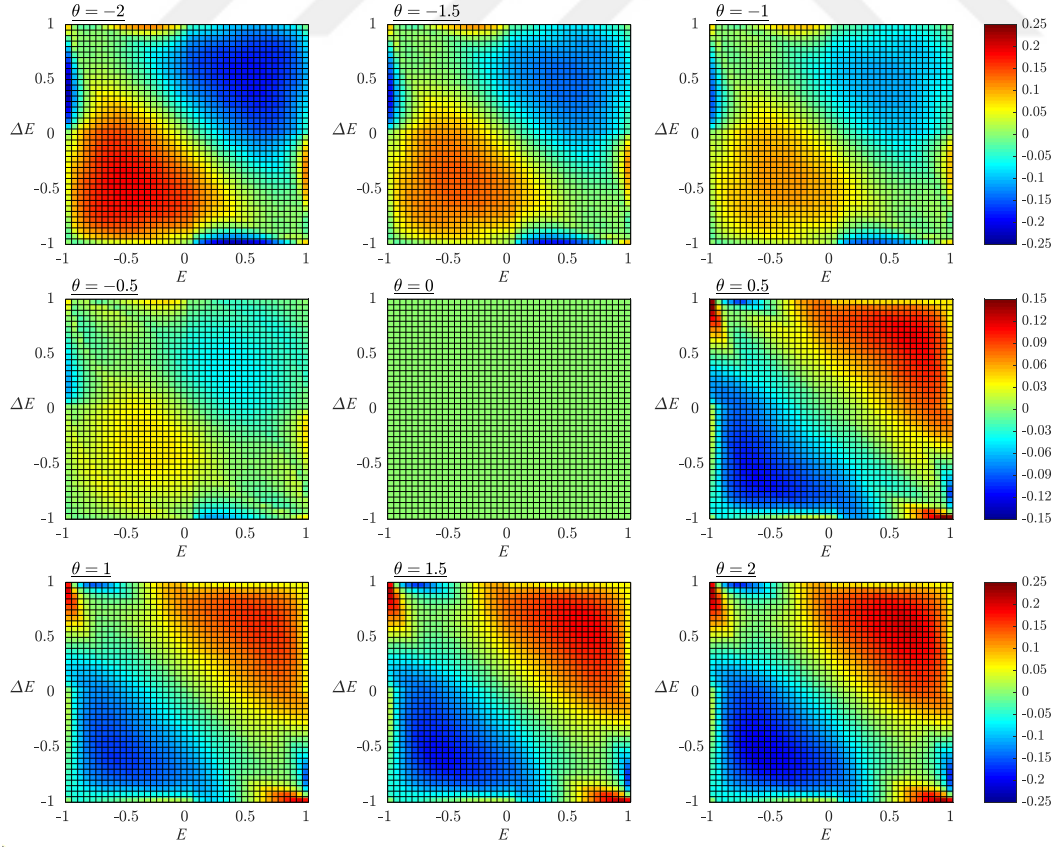


Figure 5.10 : CS differences between GT2 and IT2 FLCs with FOU-3.

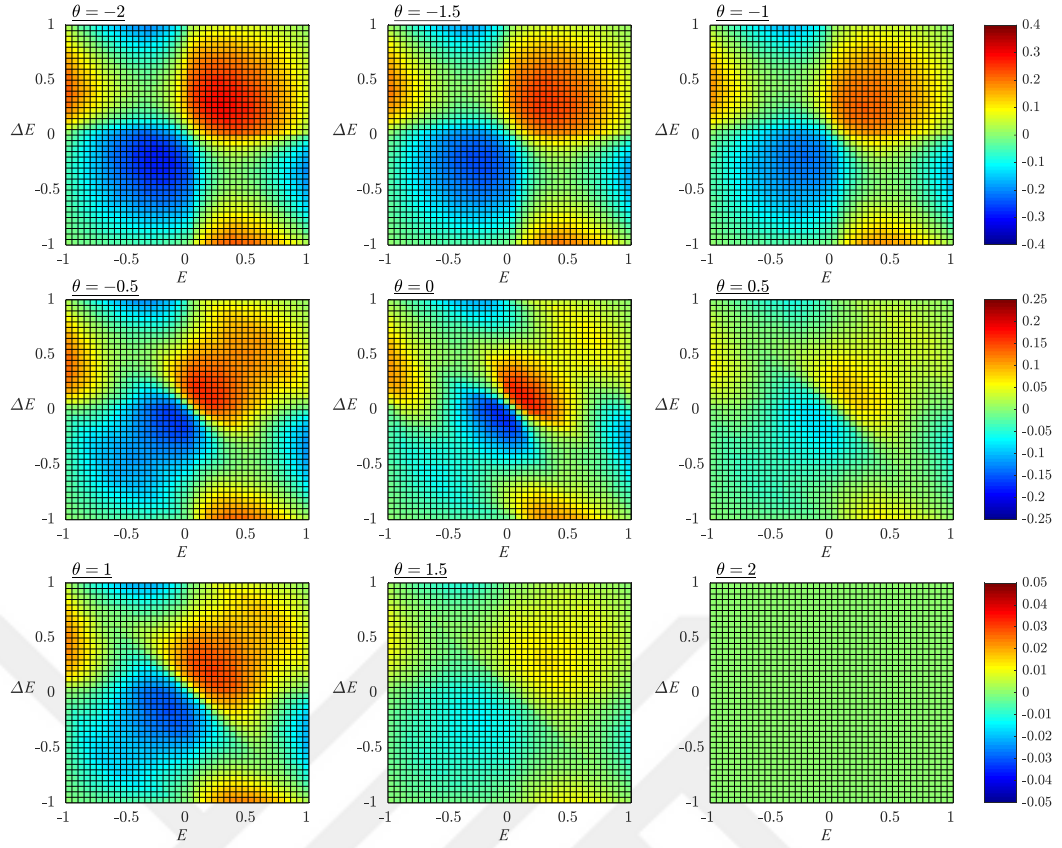


Figure 5.11 : CS differences between GT2 and T1 FLCs with FOU-4.

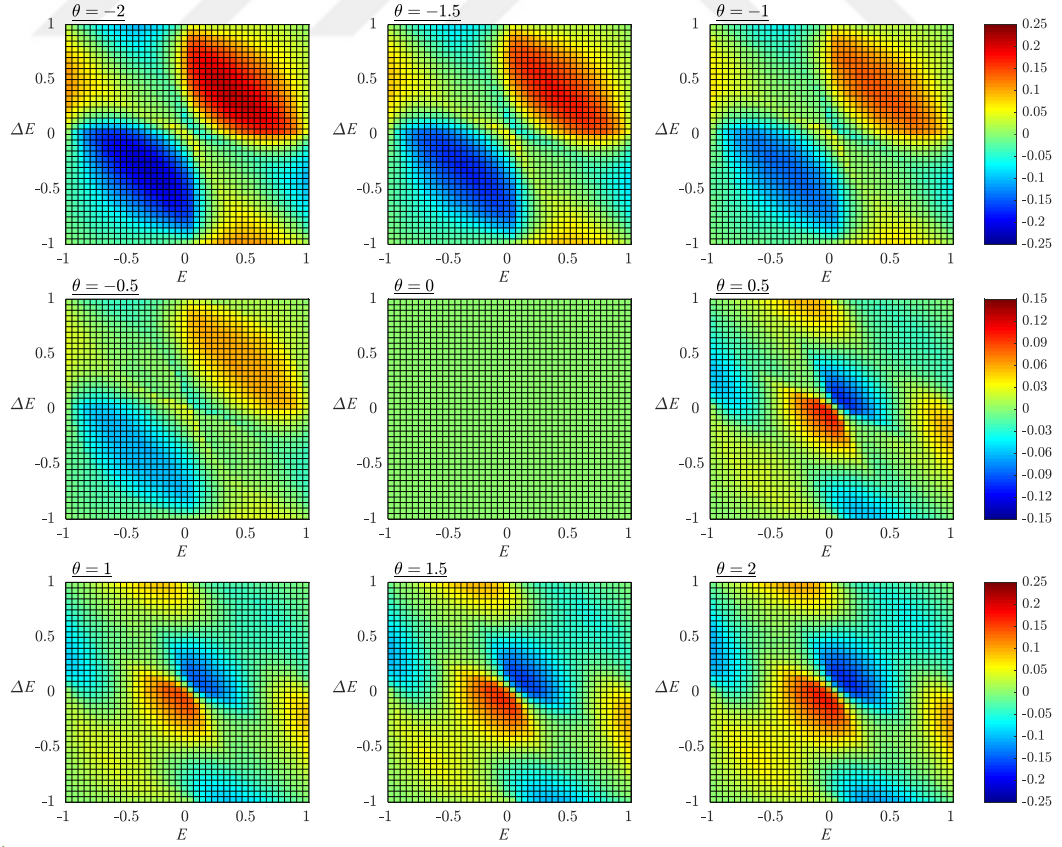


Figure 5.12 : CS differences between GT2 and IT2 FLCs with FOU-4.

Table 5.6 : Performance measures of shape analyses for GT2-DFLCs.

θ	FOU-3		FOU-4	
	<i>NTE</i>	<i>NR</i>	<i>NTE</i>	<i>NR</i>
-2	0.736	0.344	1.143	6.638
-1.5	0.770	0.485	1.125	5.970
-1	0.787	0.609	1.106	5.502
-0.5	0.829	0.948	1.065	4.542
0	0.846	1.230	1.028	4.063
0.5	0.935	1.743	1.025	3.308
1	0.974	2.154	1.012	2.818
1.5	0.990	2.337	1.007	2.633
2	1.000	2.491	1.000	2.491

As illustrated in Figures 5.7 – 5.12 and listed in Table 5.6, the shape design parameter θ not only defines the shape of the SMF (as explained in Section 4.2) but also shapes the resulting CS of the GT2-DFLC, similar to its SFLC counterpart.

For the smooth design option FOU-3, the resulting CS becomes smoother when the shape design parameter θ decreases from 2 to -2. Here, the shape design parameter settings $\theta = 2$ and $\theta = 0$ result with the baseline T1-DFLC and the baseline smooth IT2-DFLC, which are defined in Section 5.2.1, respectively. By decreasing the shape design parameter θ , the CC of the GT2-SFLC transforms from an aggressive mapping (the mapping of its T1 counterpart) to a smoother mapping (a mapping smoother than its smooth IT2 counterpart). This coincides with the *NTE* and *NR* measures. For this design, the lowest *NTE* and *NR* values are achieved for the GT2-DFLC with $\theta = -2$. Thus, the performance of the resulting GT2-DFLC is potentially more robust than its counterparts as it is more capable to mitigate the noise. For the aggressive design option FOU-4, the resulting CS becomes more aggressive when the shape design parameter θ decreases from 2 to -2. Here, the shape design parameter settings $\theta = 2$ and $\theta = 0$ result with the baseline T1-FLC and the baseline aggressive IT2-FLC, which are defined in Section 5.2.1, respectively. By decreasing the shape design parameter θ , the CC of the GT2-DFLC transforms from the mapping of its aggressive T1 counterpart to a more aggressive mapping. This also coincides with the *NTE* and *NR* measures. For this design, the highest *NTE* value is achieved for the GT2-SFLC with $\theta = -2$ design. Therefore, the resulting CS of the GT2-DFLC with $\theta = -2$ is aggressive and the fuzzy controller has the opportunity to improve system response, although the robustness level of the resulting GT2-DFLC might reduce against noise, as the *NR* value increases.

5.3 Comments and Suggestions on Shape Design Parameter

In this section, in the light of the structural change analysis that is given in Section 5.1 and the shape analyses that are given in Section 5.2, the design comments and suggestions on the shape design parameter θ will be given for the sake of systematic GT2-FLC design.

It is observed from previous analyses that the shape design parameter θ defines the resulting CC/CS of the GT2-FLC. In this context, the tuning of this parameter might be an efficient and convenient technique to design GT2-FLCs, as the properties of the baseline T1 and IT2 FLCs can be conserved. Since the impact of the shape design parameter on the CC/CS generation is strongly connected to the baseline T1 and IT2 FLCs (in terms of smooth or aggressive design options as mentioned in Section 5.2.1), this starting point (or design baseline) should be considered for the GT2-FLC design too. In this context, it is suggested designing the T1-FLC first, then the IT2-FLC, and finally the GT2-FLC, by introducing new design parameters to improve the previous results of the base FLC.

In the design of the GT2-FLC, it is suggested designing the T1 and IT2 FLC baselines (i.e. $U_{GT2} \big|_{\theta=2} = U_{T1}$ and $U_{GT2} \big|_{\theta=0} = U_{IT2}$) with aggressive and smooth CCs/CSs, respectively. Here, the design of the baseline IT2-FLC is constructed over its T1-FLC counterpart, so that the baseline IT2-FLC has additional FOU design parameters than its T1 counterpart. This design setting is very convenient as usually followed in various fuzzy control studies [6, 7, 10, 12, 40-44] since the performance of IT2-FLC mostly outperforms its T1 counterpart thanks to the extra degree of freedom provided by the FOU. Thus, this initial design of “Aggressive T1-FLC & Smooth IT2-FLC” provides a useful condition $|U_{IT2}| < |U_{T1}|$ for all input values (or almost all), and then the boundaries of structure switch conditions, given in (5.4), can be revisited as follows:

$$\left| U_{GT2} \big|_{\theta=-2} \right| \leq |U_{GT2}| \leq \left| U_{GT2} \big|_{\theta=2} \right| \quad (5.9)$$

which can be also observed from Figure 5.5, in which the CCs of the GT2-SFLCs with FOU-1 are illustrated for different shape design parameter settings. For example, the GT2-SFLC employing $\theta = -2$ generates the smoothest curve since the magnitude of the signal is lower than its counterparts. Although the aggressive IT2-FLC design is

not followed in this thesis, similar observations can be made for this design option. In this case, the boundaries of structure switch conditions, given in (5.4), transforms to:

$$\left| U_{GT2} \right|_{\theta=2} \leq |U_{GT2}| \leq \left| U_{GT2} \right|_{\theta=-2} \quad (5.10)$$

which can be also observed in Figure 5.6.

For the suggested baseline design setting; “Aggressive T1-FLC & Smooth IT2-FLC”, the following comments can be made:

- A change in the shape design parameter θ from 2 to 0 converts the CC/CS of the GT2-FLC from the baseline T1-FLC to the baseline IT2-FLC, since the shape of the SMF transforms from a crisp value to an interval set (as explained in Section 4.2). Thus, the performance and robustness of the GT2-FLC with a shape design parameter setting in the range of $\theta \in [0, 2]$ will always lie between the baseline T1-FLC and the baseline IT2-FLC.
- A change in the shape design parameter θ from 0 to -2 converts the CC/CS of the GT2-FLC from the baseline IT2-FLC to a T1-FLC that only executes the LMFs as defined in equation (5.2). Thus, the design of a GT2-FLC with a shape design parameter setting in the range of $\theta \in [-2, 0]$ gives a chance to construct GT2-FLCs that are relatively more robust than its IT2-FLC baseline according to the boundaries of structure switch condition in equation (5.9).

In conclusion, it can be underlined that “the shape design parameter $\theta \in [-2, 2]$ provides not only a design simplicity as only baseline T1 and IT2 FLCs are needed, but also convenient design flexibility since various GT2 CCs / CSs can be generated straightforwardly by simply tuning a single parameter θ ” [76]. The following sections will provide the proposed tuning steps with a systematic design perspective.

5.4 Systematic Tuning of Shape Design Parameter

In this section, the proposed systematic tuning methods for the shape design parameter will be presented. In this context, in the light of the structural change analysis given in Section 5.1, the shape analyses that are given in Section 5.2, and the design comments and suggestions on the shape design parameter (given in Section 5.3), the tuning steps of the shape design parameter is summarized in Table 5.7. The systematic design of

the CC/CS of the GT2-FLC, in other words, a systematic GT2-FLC design from the baseline FLCs towards a desired CC/CS generation, can be achieved by following three tuning steps. In Step-1, the baseline T1-FLC is designed such that the system response is fast and satisfactory (i.e. the baseline T1-FLC has an aggressive CC/CS). This can be accomplished by the selections of 1) the type of FLC (single or double), 2) the number of rules (N), 3) the antecedent MFs ($A_{j,i}$), 4) the consequent MFs (C_n), 5) the rules in rule base (R_n), and the fuzzy operators. For this purpose, the structural design recommendations given in Section 2.6, where the design parameters of the T1-FLCs are also summarized in Table 2.5, can be followed. In Step-2, the baseline IT2-FLC is designed by converting the baseline T1-FLC to the baseline IT2-FLC by tuning the FOU design parameters ($M_{j,i}$) to result in a potentially robust controller (i.e. the baseline IT2-FLC has a smooth CC/CS). For this purpose, the structural design recommendations that are given in Section 2.6 and the guidelines/suggestions in [12, 18-20, 40-44] can be followed. In Step-3, the GT2-FLC is designed over the baseline FLCs. For this purpose, the baseline T1-FLC (from Step-1) and the baseline IT2-FLC (from Step-2) are considered as initial settings to construct the GT2-FLC. Then, the shape design parameter θ (in online or offline manner) is tuned based on a compromise between robustness (i.e. like IT2-FLC) and control system performance (i.e. like T1-FLC). The tuning steps of the shape design parameter are summarized in Table 5.7.

Table 5.7 : Tuning steps of the shape design parameter.

Step-1:	Design a baseline T1-FLC such that the system response is fast and satisfactory (i.e. aggressive CC/CS).
Step-2:	Convert the baseline T1-FLC to a baseline IT2-FLC by tuning the FOU design parameters ($M_{j,i}$) to end up with a potentially robust controller (i.e. smooth CC/CS).
Step-3:	Use the designed baseline T1-FLC (from Step-1) and the designed baseline IT2-FLC (from Step-2) as initial settings to construct the GT2-FLC. Then, tune the shape design parameter θ (in online or offline manner) by providing a tradeoff between robustness (i.e. like IT2-FLC) and control system performance (i.e. like T1-FLC).

5.5 Online Scheduling Mechanisms for Shape Design Parameter

In this section, two online scheduling mechanisms will be proposed to tune the shape design parameter in an online manner. The generic design steps for the tuning of the shape design parameter (given in Table 5.7) can be easily accomplished in an offline manner by numerous design options such as; prior knowledge of system experts or optimization-based design via neural networks or genetic algorithms. However, the resulting control system performance (in transient and steady states) of the GT2-FLC for a fixed shape design parameter θ value closely depends on the operating points in which the system is controlled/designed/optimized, especially for nonlinear systems. Thus, the performance of a fuzzy control system might be optimal or satisfactory at a certain operating point where the GT2-FLC is tuned, yet its performance might be unacceptable at other points. This is expected since the dynamics of nonlinear systems might change at different operating points and/or environmental conditions. In control theory, this problem is usually addressed by gain-scheduled controllers designed at various operating points and schedule a collection of controllers at the corresponding steady-states [76]. Thus, on top of the offline-tuning of the shape design parameter, it is proposed tuning the shape design parameter in an online manner by providing a tradeoff between performance and robustness. This online update of the shape design parameter can be easily achieved by the proposed SMF parameterization in Section 4.2 since the shape of the CC/CS of GT2-FLC is changed by the shape design parameter as given in Sections 5.2 and 5.3.

The first proposed scheduling mechanism is denoted as SM-1 and it tunes the shape design parameter in an online manner with respect to the steady-state operating points. In this context, the SM-1 determines the shape design parameter values (θ_r) that are associated with steady-state operating points or references (r). Accordingly, the SM-1 calculates the value of the shape design parameter as follows:

$$\text{SM-1:} \quad \theta = \theta_r = f_r(r) \quad (5.11)$$

where $f_r(r)$ is a mapping (i.e. $r \rightarrow \theta_r$) that provides the updated value of the shape design parameter (θ_r) with respect to the reference signal (r) of the operating point. Here, if there is only one operating point, then the SM-1 is not required so that the GT2-FLC design can be accomplished as explained in Table 5.7. If there are multiple steady-state operating points, the values of the shape design parameters are stored in

the shape design parameter vector $\theta_r = [\theta_{r_1}, \theta_{r_2}, \dots, \theta_{r_k}]$ with respect to the reference signal vector $r = [r_1, r_2, \dots, r_k]$. For each operating point (i.e. r_k), the corresponding value of the shape design parameter (i.e. θ_k) is defined. To accomplish this goal in terms of the systematic way of the GT2-FLC design, the Step-3 of Table 5.7 can be followed to determine the appropriate values (θ_{r_k}) of the shape design parameter. Besides, if an interpolation method for the mapping function $f_r(r)$ is defined, then the GT2-FLC can also work for the intermediate operating points of the control system. The design steps of the SM-1 are summarized in Table 5.8.

Table 5.8 : Design steps of the online SM-1.

Step-1:	Define the steady-state operating points/references of the control system as $r = [r_1, r_2, \dots, r_k]$.
Step-2:	For each operating point (i.e. r_k), determine the corresponding shape design parameter value (i.e. θ_{r_k}). For this purpose, the Step-3 of Table 5.7 can be followed to tune the GT2-FLCs.
Step-3:	Define an interpolation method (e.g. linear, cubic, polynomial, fuzzy) for the mapping function $f_r(r)$.

Although tuning the shape design parameter as given in (5.11) is a simple method, the scheduling sometimes might not be adequate to achieve a good transient-state control performance because only steady-state operating points are considered. To overcome this, the handling of the transient system dynamics during reference changes might be an efficient way to update the shape design parameter. In this context, the second online scheduling mechanism (SM-2) is proposed to update the shape design parameter in an online manner with respect to the transient states of the control system as well as the steady-state operating points, as follows:

$$\text{SM-2:} \quad \theta = \theta_r + \gamma \theta_t \quad (5.12)$$

where γ is a weighting coefficient and θ_t is the varying parameter during the transient state to enhance the performance of the GT2-FLC while the control system approaches the steady-state operating point. Here, the value of θ_r is determined with respect to the steady-state operating points (r), as explained in the SM-1 part, while the value θ_t is

updated based on the transient states of the control system. As a transient state, various signal information can be processed; for example, the error signal, the change of the error signal, the rate of the control signal, the system output, etc. In this thesis, the following design guidelines are followed to shape the value of θ_t :

- If the transient state response is fast, then the control signal or control action should be smoothened to prevent overshoots and oscillations. Hence, the value of the varying parameter (θ_t) is set to $\theta_t < 0$, so that the value of the shape design parameter θ decreases, according to SM-2 definition in equation (5.12). With this design option, the CC/CS of the GT2-FLC becomes smoother as it bends towards its boundary T1-FLC defined in equation (5.2).
- If the transient state response is slow, then the aggressiveness of the control signal should be increased to increase the convergence speed of the control system. Therefore, the value of the varying parameter (θ_t) is set to $\theta_t > 0$, so that the value of the shape design parameter θ increases, based on SM-2 definition in equation (5.12). With this design option, the CC/CS of the GT2-FLC becomes more aggressive as it bends towards its boundary baseline T1-FLC defined in equation (5.3).
- At the steady-state of the control system, the value of the varying parameter (θ_t) should be set to $\theta_t = 0$ in order to assign the shape design parameter θ to its nominal value θ_r at the steady-state operating point r .

Since these online scheduling mechanism design guidelines can be easily transformed into fuzzy rules, as a part of SM-2, a fuzzy scheduling mechanism, denoted as $f_t(h)$, is also proposed. This fuzzy scheduling mechanism provides a mapping (i.e. $h \rightarrow \theta_t$) that generates the θ_t as follows:

$$\theta_t = f_t(h) \quad (5.13)$$

where h denotes the inputs of the fuzzy mapping $f_t(h)$, and it indicates the transient state signals of the system. In this thesis, these signals are selected as $h = [E, \Delta E]$ (the error signal and the change of error signal) to process the transient state dynamics of the control system, as it has been widely done in self-tuning FLC structures [16, 18, 22]. Here, the fuzzy scheduling mechanism is defined with the same antecedent MFs and the fuzzy rules of the T1-DFLC presented in Section 5.2.1. According to the given

design guidelines for the scheduling mechanisms, the rule base of the $f_t(h)$ fuzzy mapping is constructed as given in Table 5.9. As given in Table 5.9, the rules are symmetric on the left diagonal axis so that a symmetric CS is obtained, while the rule consequents are mostly set to 0 and -1 values, to avoid the risk of overshoots and oscillations. At the steady-state where $E = \Delta E = 0$, only the rule R_5 is activated with $C_5 = 0$, and this provides the fuzzy mapping output becomes $\theta_t = 0$ and $\theta = \theta_r$, so the value of the shape design parameter converges to its nominal value. It is worth underlying that the consequents are the design parameters of the fuzzy scheduling mechanism $f_t(h)$, and these parameters are suggested tuning according to the transient dynamics of the control system. In this thesis, the following rule table is used as it has resulted in satisfactory enhancements in experiments.

Table 5.9 : Rule table of fuzzy mapping of online SM-2.

$x_2 = \Delta E \quad \backslash \quad x_1 = E$	$A_{1,1}$	$A_{1,2}$	$A_{1,3}$
$A_{2,1}$	$C_1 = 1$	$C_2 = 0$	$C_3 = -1$
$A_{2,2}$	$C_4 = 0$	$C_5 = 0$	$C_6 = -1$
$A_{2,3}$	$C_7 = -1$	$C_8 = -1$	$C_9 = -1$

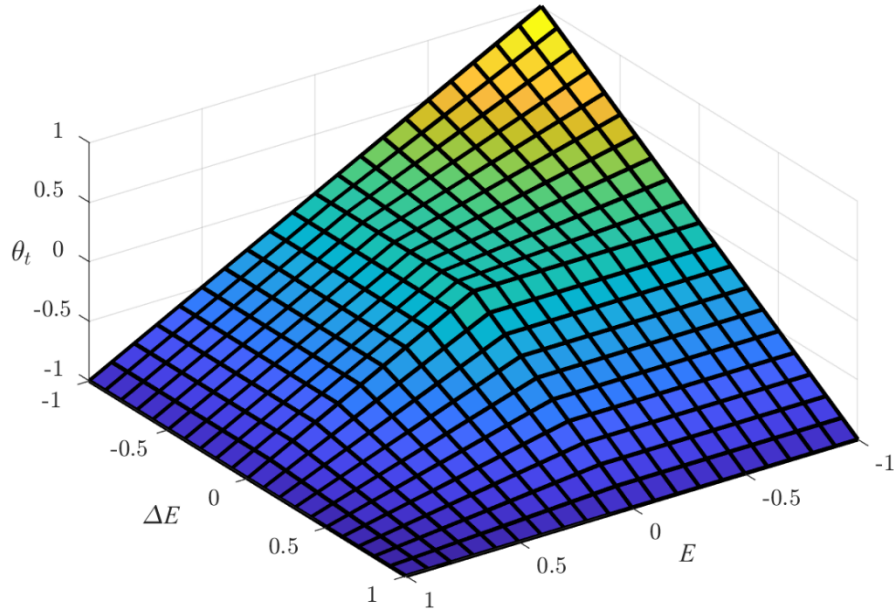


Figure 5.13 : Surface of fuzzy mapping of online SM-2.



6. ANALYSIS AND DESIGN OF SENSITIVITY DESIGN PARAMETER

In this chapter, the effect of the sensitivity design parameter (i.e. P) on the control curve and control surface generation will be investigated, and a practical tuning algorithm is proposed for the selection of the sensitivity design parameter P .

6.1 Sensitivity Analyses of Control Curves / Control Surfaces

In this section, the CCs/CSs of the GT2-FLCs will be analyzed for various sensitivity design parameter settings in order to provide a practical insight into how to tune the sensitivity design parameter P . In this context, the sensitivity/accuracy of the resulting CCs/CSs and their computation burden are examined. For all CC/CS generation and time analyses, the shape design parameters are fixed, which means that the shapes of the CCs/CSs of the GT2-FLCs are fixed, so that any difference that occurs on the resulting input-output mapping of the GT2-FLC is only related to the different settings of the sensitivity design parameter P that is the total number of α -planes. For this purpose, the results of the GT2-FLCs employing different number of α -planes are analyzed for the settings $P = \{2, 3, 4, 10, 25, 100\}$ in terms of three measures; the Maximum Value of Errors (MVE) and the Mean Absolute Error (MAE) and the average Computation Time (CT). These comparison measures are defined as:

$$MVE(\varepsilon_a^b) = \max_{v=1, \dots, V} (\varepsilon_a^b[v]) \quad (6.1)$$

$$MAE(\varepsilon_a^b) = \sum_{v=1}^V |\varepsilon_a^b[v]| / V \quad (6.2)$$

$$\varepsilon_a^b[v] = U_a[v] - U_b[v] \quad (6.3)$$

Here, V is the total number of samples, $U_a[v]$ and $U_b[v]$ denote samples from U_a and U_b outputs of the GT2-FLCs employing $P = a$ and $P = b$ α -planes, respectively. As a part of the sensitivity analyses, the average CT values are calculated over 10 trials, by changing the input variables with 0.001 and 0.01 step sizes for GT2-SFLC and

GT2-DFLC, respectively. The CT values are calculated with tic and toc functions of the MATLAB. Similar to the shape analyses, the sensitivity analyses are performed for the CC of the GT2-SFLC and the CS of the GT2-DFLC separately. During these analyses, the following GT2-FLCs are considered;

- GT2-SFLC with FOU-2 and $\theta = -1$,
- GT2-DFLC with FOU-3 and $\theta = -1$.

In the comparisons, it is assumed that the output of a continuous GT2-FLC (U_C) can be approximated with a GT2-FLC employing $P=1000$ α -planes (i.e. U_{1000}). This high number of α -planes provides a high level of granularity on the GT2-FLC computations as mentioned in Section 3.6. Thus, for the comparative sensitivity analyses on the CCs/CSs of the GT2-FLCs, it is assumed that $U_C = U_{1000}$. The effect of the sensitivity design parameter P is firstly examined by comparing the outputs of the handled GT2-SFLCs and GT2-DFLCs with the continuous ones. The resulting CCs of the GT2-SFLCs and the CC differences to continuous the GT2-SFLC are illustrated in Figures 6.1 and Figure 6.2, while the CS differences between the GT2-DFLCs and the continuous one is given in Figure 6.3. The comparison measures are given in Tables 6.1 and 6.2 for GT2-SFLCs and GT2-DFLCs, respectively.

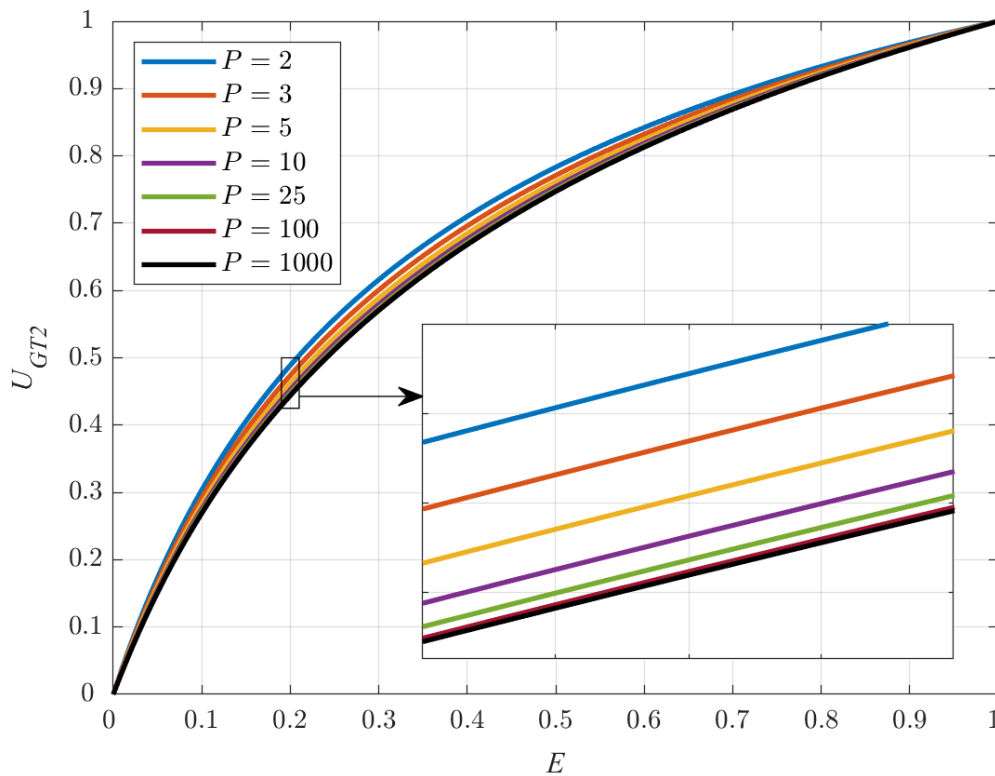


Figure 6.1 : Effect of sensitivity design parameter on CCs of GT2-SFLCs.

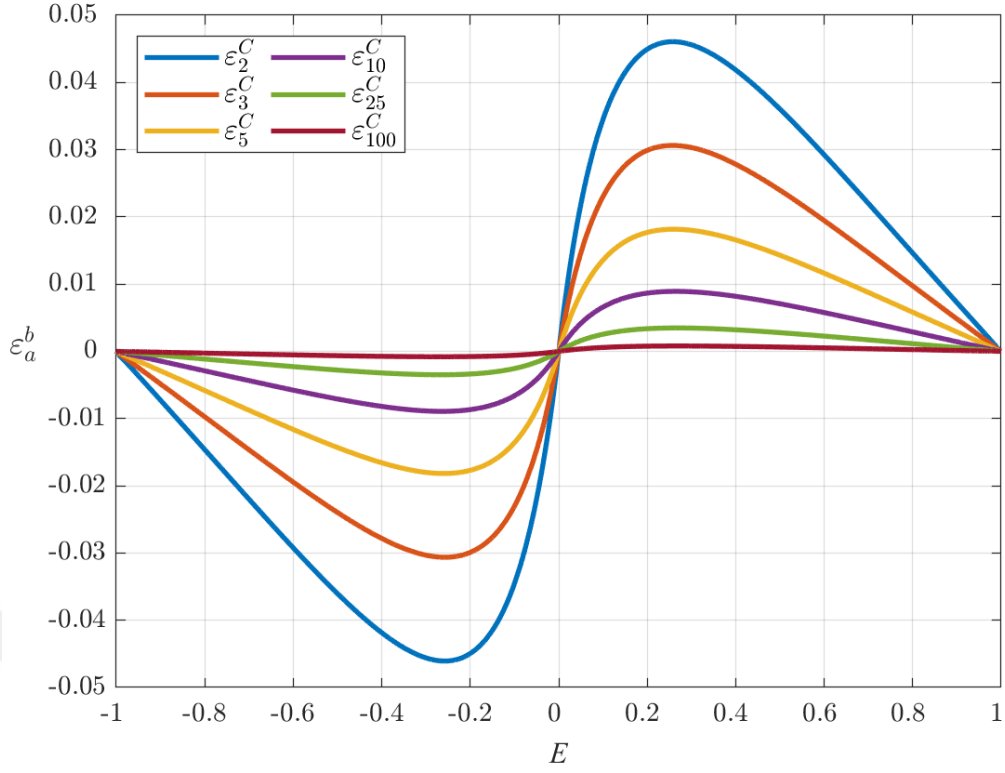


Figure 6.2 : CC differences between U_C and U_P for $P = \{2, 3, 4, 10, 25, 100\}$.

As illustrated in Figure 6.1 and Figure 6.2, the input-output mappings of the GT2-SFLCs are almost identical, although the sensitivity design parameter P varies through a wide range from 2 to 1000, and the CS differences of the GT2-DFLCs are relatively low as illustrated in Figure 6.3. These can be numerically observed from Table 6.1 for the GT2-SFLCs and from Table 6.2 for the GT2-DFLCs.

It is worth underlying that the employed GT2-FLCs resulted in relatively low MVE and MAE measures, independent from the value of the sensitivity design parameter P . However, the total number of α -planes, in order words the sensitivity design parameter P , has a significant effect on the average CT as expected. Accordingly, it can be argued that the realization of a GT2-FLC (in a hardware element such as microcontroller) employing high values of P (constructing by high numbers of α -planes) might be a challenging problem in real-time applications that usually require a short computation window (due to the high sampling frequencies). For instance, when the value of the sensitivity design parameter P increases from 10 to 100, which means that the GT2-SFLC employs 90 α -planes more, then the MVE measure of the GT2-SFLC reduces from 8.925×10^{-3} to 0.798×10^{-3} but accordingly the average CT value increases approximately 9 times.

Table 6.1 : Sensitivity measures for GT2-SFLCs.

P	$MVE(\varepsilon_P^C)$	$MAE(\varepsilon_P^C)$	Average CT (ms)	$MVE(\varepsilon_P^{P+1})$	$MAE(\varepsilon_P^{P+1})$
2	46.067	28.120	0.039±0.001	15.435	9.406
3	30.632	18.714	0.052±0.001	7.798	4.743
5	18.167	11.128	0.076±0.003	3.099	1.890
10	8.925	5.483	0.133±0.003	0.831	0.509
25	3.482	2.143	0.315±0.016	0.138	0.0805
100	0.798	0.492	1.257±0.077	0.009	0.006

* The sensitivity measures (MVE and MAE) values are normalized by 10^{-3} .

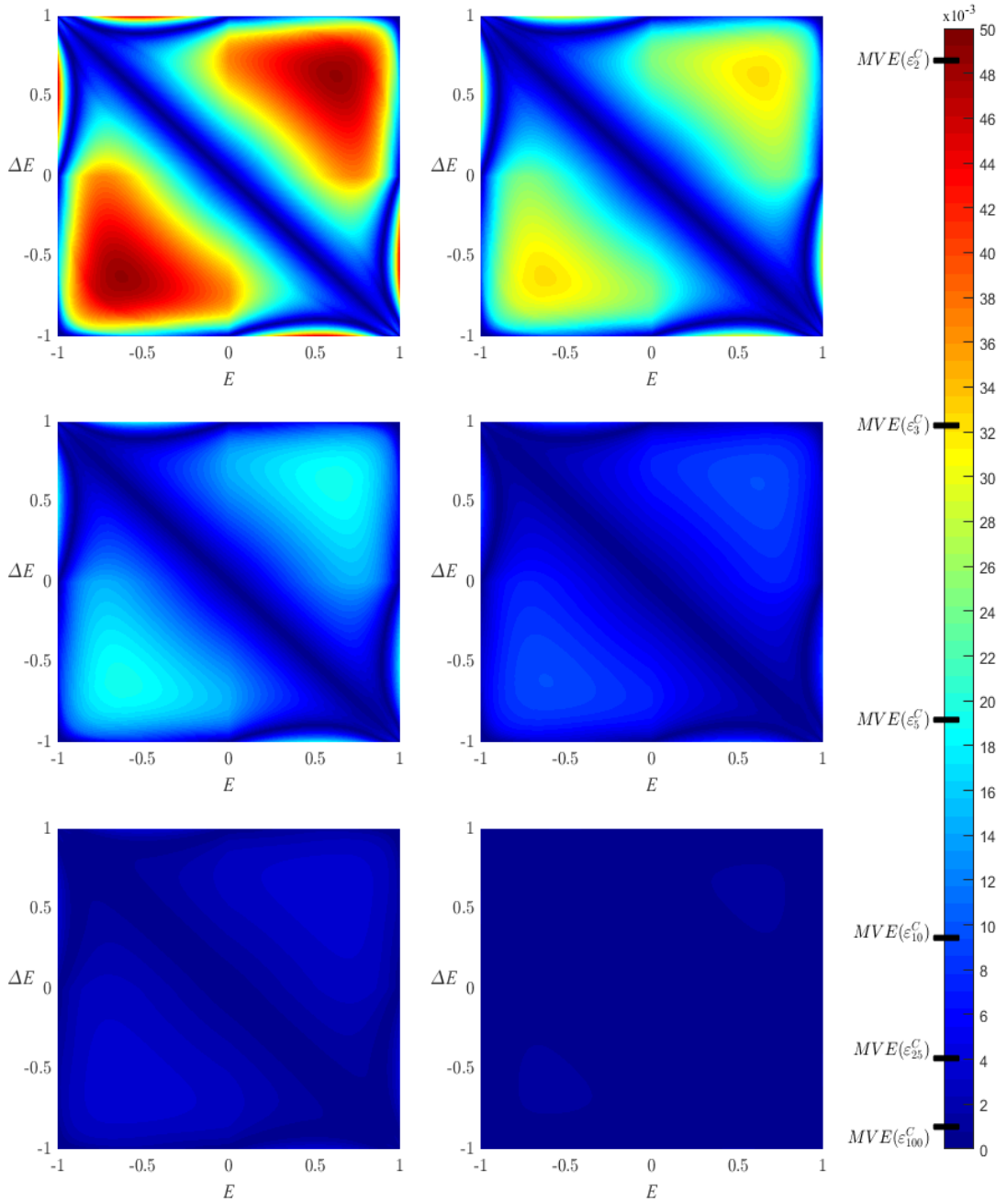


Figure 6.3 : Effect of sensitivity design parameter on GT2-FLCs' ε_P^C values.

In the second part of the sensitivity analyses, how the sensitivity of the CCs/CSs changes with respect to the increments of the number of α -planes, (i.e. the increment of the sensitivity design parameter from P to $P + 1$) is analyzed. In this context, the resulting CC/CS differences between U_P (a GT2-FLC employing P α -planes) and U_{P+1} (a GT2-FLC employing $P+1$ α -planes) are examined and the sensitivity measures; MVE_P^{P+1} and MAE_P^{P+1} , are calculated. These differences are illustrated in Figure 6.4 for GT2-SFLCs and Figure 6.5 for GT2-DFLCs. The sensitivity measures are given in Table 6.1 and Table 6.2 for GT2-SFLCs and GT2-DFLCs, respectively. Similar to the first part of the analyses, the CCs/CSs are almost identical for various sensitivity design parameter settings. On the other hand, increasing the value of the sensitivity design parameter from $P = 3$ to $P = 4$ resulted in a relatively bigger improvement in terms of the MVE and MAE measures when it is compared to the results in which the value of P is increased from $P = 100$ to $P = 101$. The levels of the differences are relatively lower than the differences to the continuous CC/CS. Thus, it can be concluded that the relative CC/CS difference per increment on the P value decreases when the total number of α -planes (or the value of the sensitivity design parameter) is getting bigger.

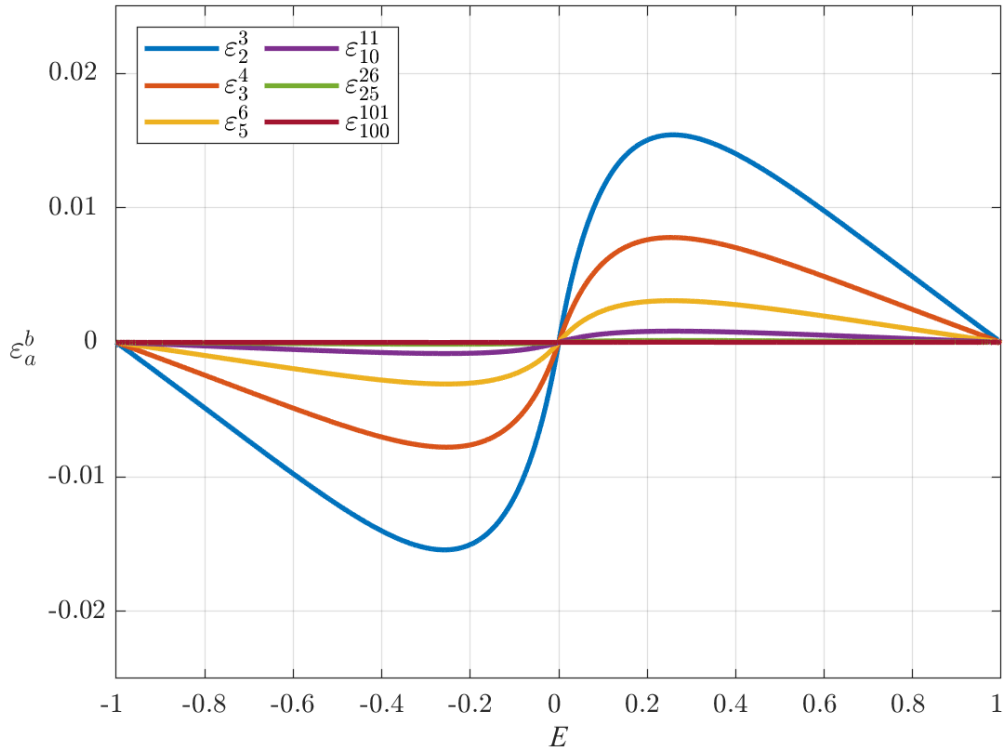


Figure 6.4 : CC differences between U_{P+1} and U_P for $P = \{2, 3, 4, 10, 25, 100\}$.

Table 6.2 : Sensitivity measures for GT2-DFLCs.

P	$MVE(\varepsilon_P^C)$	$MAE(\varepsilon_P^C)$	Average CT (ms)	$MVE(\varepsilon_P^{P+1})$	$MAE(\varepsilon_P^{P+1})$
2	48.577	23.783	0.133±0.012	16.295	7.975
3	32.281	15.814	0.147±0.014	8.342	4.022
5	19.140	9.393	0.169±0.014	3.299	1.598
10	9.407	4.625	0.224±0.015	0.878	0.430
25	3.701	1.808	0.356±0.017	0.146	0.072
100	0.860	0.415	1.017±0.051	0.010	0.005

* The sensitivity measures (MVE and MAE) values are normalized by 10^{-3} .

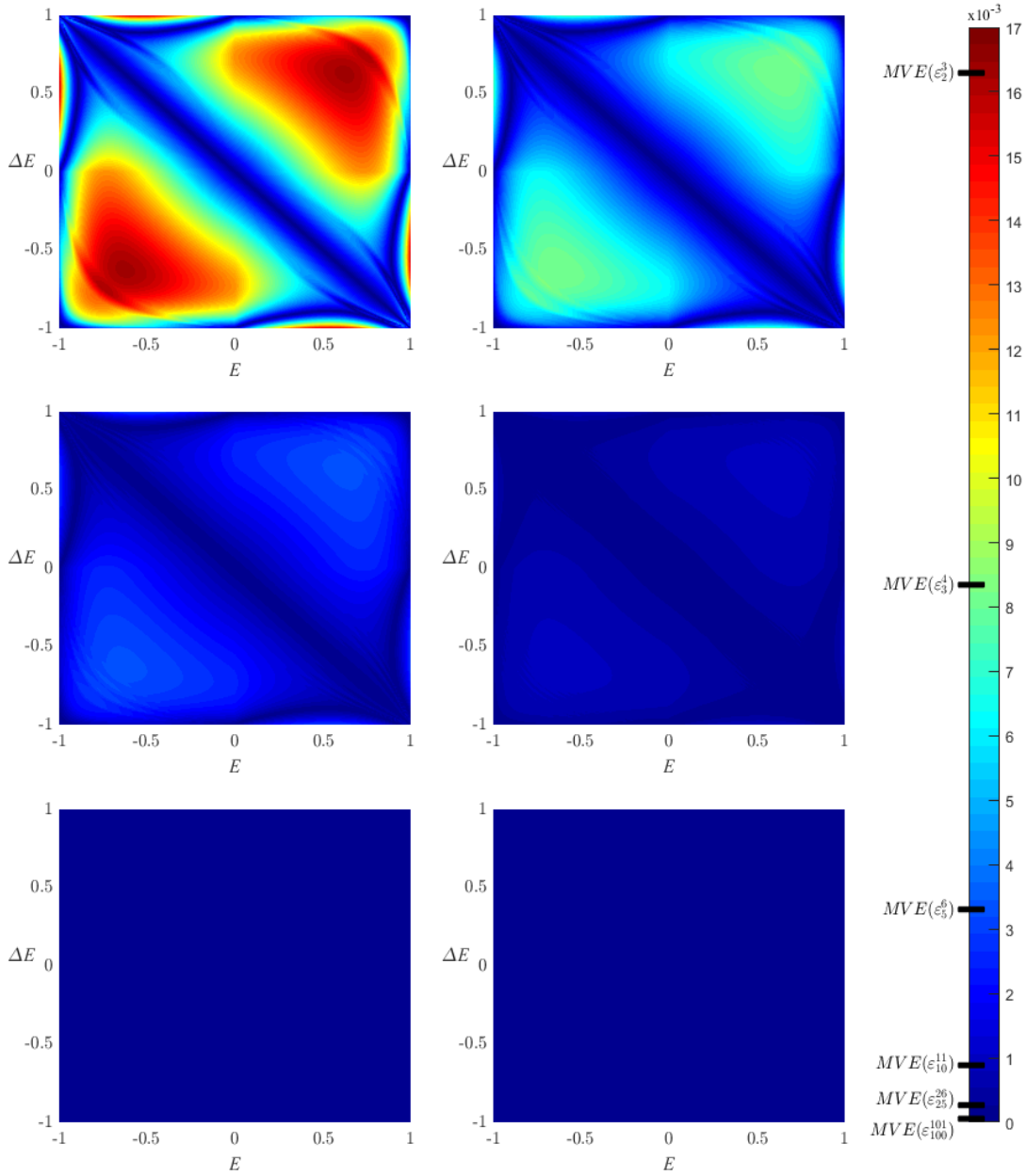


Figure 6.5 : Effect of sensitivity design parameter on GT2-FLCs' ε_P^{P+1} values.

6.2 Comments and Suggestions on the Sensitivity Design Parameter

In this section, in the light of the sensitivity analyses given in Section 6.1, the design comments and suggestions on the sensitivity design parameter P will be given for the sake of systematic and practical GT2-FLC design. The performed sensitivity analyses clearly demonstrated that the sensitivity design parameter does not change the shape of the CC/CS alike its shape design parameter counterpart, but it closely defines the CC/CS accuracy/sensitivity of the GT2-FLCs. The results also demonstrate that there is a strong tradeoff between computational time and CC/CS precision. In other words, a high number of α -planes means accurate precision on the computation of the control signal of the GT2 fuzzy system, but a huge computation burden at the same time. Thus, a practical technique is necessary to balance the time compromise of the CC/CS sensitivity of the GT2-FLCs to be deployed.

In real-time control applications, the designed GT2-FLCs are usually implemented on microcontroller-based hardware components that have finite precision (e.g. fixed or floating data types) and limited processing power (e.g. function execution time) in practice. Moreover, the GT2-FLCs do not only process quantized/sampled signals from the environment, but also generate quantized/sampled signals to be deployed to the actuators in the environment. This is due to fact that the feedback signals of the system are captured by sensing elements (like resolvers, voltage/speed/position sensors, cameras, IMUs, ...), while the control signal of the control system is realized by physical actuators (like engines, electric machines, charging units, heaters, ...). In this context, a continuous signal S , used in real-time applications, is usually defined by a quantization operation as follows:

$$\hat{S} = \lfloor S/\Delta \rfloor \Delta \quad (6.4)$$

where \hat{S} is the quantized/sampled signal that is derived from the continuous signal S , Δ is quantization level (or quantization interval) and $\lfloor \cdot \rfloor$ denotes floor function happens during the quantization. Then the quantization error (Q_S) is defined as follows:

$$Q_S = \hat{S} - S \quad (6.5)$$

Here, it is worth underlying that the quantization error might happen at the inputs and outputs of GT2-FLCs in real-time applications. So, the magnitude and characteristic

of the quantization error have an impact on the real-time control performance of the GT2-FLC, since it changes the accuracy of the designed CC/CS of the GT2-FLC. Thus, the quantization intervals or quantization errors of the fuzzy control system should be considered in the design of GT2-FLCs. In this context, it is suggested adjusting the sensitivity design parameter P by considering the quantization level Δ and the required computational time on the target hardware element.

6.3 Tuning of Sensitivity Design Parameter

In this section, how the sensitivity design parameter P can be tuned from a practical real-time implementation perspective is presented. Based on the sensitivity analyses given in Section 6.1, and the design comments and suggestions on the sensitivity design parameter P given in Section 6.2, a novel iterative tuning algorithm for the sensitivity design parameter is proposed. The new algorithm determines the sensitivity design parameter so that it addresses the problem of the selection of α -planes.

The proposed tuning algorithm of the sensitivity design parameter takes into account the hardware limits of the real-time control system; quantization intervals that occur in input/output signals, in terms of the sensitivity measures. The aim of the proposed tuning algorithm is to determine the best P value, the number of α -planes, in a way that the designed CC/CS can be realized with a reasonable compromise from the sensitivity and the computation time. It is worth noting that the hardware limits are very important factors for real-time control problems, in which the sensitivity and the computational time are limited. The pseudo-code of the proposed tuning algorithm is given in Table 6.3. The proposed tuning algorithm is constructed with two main steps: Forward Calculation and Backward Calculation, as follows:

1. **Forward Calculation:** The goal of the forward calculation is to find the best (in terms of sensitivity/accuracy) GT2-FLC output under given sensitivity constraints and quantization levels of the input/output signals. In the forward calculation step, the value of P is increased by 1 in each iteration step, until the improvement per increment is lower than a stopping threshold. In this context, the CC/CS differences of two consecutive GT2-FLCs (i.e. U_P : the GT2-FLC employing P α -planes and U_{P+1} : the GT2-FLC employing $P + 1$ α -planes) are calculated in the search space $[P_{min}, P_{max}]$ where $P_{min} = 2$ and P_{max} is defined

by the designer. The algorithm updates the candidate solution of the forward calculation ($P^* = P$) until the following stopping condition is satisfied:

$$MAE(\varepsilon_P^{P-1}) < \varepsilon_1 \quad (6.6)$$

where ε_1 is the threshold value that defines the improvement limit per α -plane increment. Since a chattering effect is highly possible, when a floor operator is executed for the quantization of a signal; then it is verified if the stopping condition in equation (6.6) is satisfied in the next P_f iteration for the interval of $[P^*, P^* + P_f]$, so that the iteration can be stopped at the point P^* as it is the solution of the forward calculation. This extra procedure is a kind of local search mechanism to handle the chattering effects on the MAE measure. Then the solution P^* is stored to be used in the next step. Here it should be noted that if the resulting CTs of the GT2-FLC employing P^* α -planes is suitable for the real-time application (in terms of the time), the next step can be skipped.

2. **Backward Calculation:** The goal of the backward calculation is to find the best (in terms of sensitivity and time) GT2-FLC output under given constraints of the signals, as well as the computation time limits of the hardware elements. As mentioned the calculated P^* solution in the forward calculation might result in a GT2-FLC with a very high computation time which may not be practicable for a realization. In order to handle this bottleneck, an error threshold (ε_2), which defines the precision tolerance, is defined to reduce the total number of α -planes which unsurprisingly reduces the average CT measure (as shown in Section 6.2). This is accomplished by decreasing the value of P^* by 1 in each iteration step until the MVE value satisfies the following stopping condition:

$$MVE(\varepsilon_P^{P^*}) > \varepsilon_2 \quad (6.7)$$

Here, the backward iteration stops at P^{**} , when the condition (6.7) cannot be satisfied anymore. This condition gives a compromise (between sensitivity and computation time) by finding a solution satisfying $P^{**} < P^*$. Note that, if there is no feasible solution for the real-time application (e.g. the average CT of the GT2-FLC employing P^{**} α -planes is too high), then the threshold ε_2 should be increased and the backward calculation should be re-executed.

Table 6.3 : Tuning algorithm of the sensitivity design parameter.

Forward Calculation
<p>Define input and output quantization levels: Δ_{in} and Δ_{out}</p> <p>Quantize input values based on Δ_{in} according to (6.4)</p> <p>Define hyperparameter ε_1 to be used in the stopping criteria</p> <p>Define hyperparameters P_f, P_{min}, and P_{max} to be used for iteration limits</p> <p>Initialize the parameters used in iteration loops as: $P_i = 0$ and $P^* = P_{max}$</p> <p>Start iteration</p> <pre> FOR $P = P_{min} : 1 : P_{max}$ Calculate the input-output mapping of the GT2-FLC employing P α-planes (i.e. U_p by gridding the inputs) considering the input quantization level Δ_{in} Calculate the quantized output signal of the GT2-FLC (i.e. \hat{U}_p) via (6.4) considering the output quantization level Δ_{out} IF $P > 2$ Calculate the measure $MAE(\varepsilon_p^{P-1})$ with \hat{U}_p and \hat{U}_{p-1} using (6.2) IF $MAE(\varepsilon_p^{P-1}) < \varepsilon_1$ IF $P_i == P_f$ $P^* = P - P_f$ BREAK END $P_i = P_i + 1$ ELSE $P_i = 0$ END END END END </pre>
Backward Calculation
<p>Take P^* and \hat{U}_p^* as calculated in the Forward Calculation step</p> <p>Define hyperparameter ε_2 to be used in the stopping criteria</p> <p>Initialize the parameters used in iteration loops as: $P^{**} = P_{min}$</p> <pre> FOR $P = P^* - 1 : -1 : P_{min}$ Calculate the input-output mapping of the GT2-FLC employing P α-planes (i.e. U_p by gridding the inputs) considering the input quantization level Δ_{in} Calculate the quantized output signal of the GT2-FLC (i.e. \hat{U}_p) via (6.4) considering the output quantization level Δ_{out} Calculate the measure $MVE(\varepsilon_p^{P^*})$ with \hat{U}_p and \hat{U}_{p^*} using (6.1) IF $MVE(\varepsilon_p^{P^*}) > \varepsilon_2$ $P^{**} = P + 1$ BREAK END END END </pre>

In this section, a numerical example will be also presented in order to clearly show the forward and backward calculation steps of the proposed tuning algorithm. In this context, a GT2-DFLC is constructed over the rule base defined in Table 5.4 and by employing the FOU design parameters as $M_{1,1} = 0.05$, $M_{1,2} = 0.95$, $M_{1,3} = 0.05$,

$M_{2,1} = 0.15$, $M_{2,2} = 0.85$, $M_{2,3} = 0.15$, and the shape design parameter as $\theta = 0.1$. The quantization intervals of the inputs and output are defined as $\Delta_{in} = 0.01$ and $\Delta_{out} = 0.001$, respectively. The hyperparameters used in iterations of the proposed tuning algorithm as $P_{min} = 2$, $P_{max} = 100$, and $P_f = 20$. The error thresholds of the stopping conditions are selected as $\varepsilon_1 = 0.025 \times 10^{-3}$ and $\varepsilon_2 = 0.01$. The variation of the *MAE* measure with respect to the sensitivity design parameter P (or the total number α -planes) is illustrated in Figure 6.6, the calculated execution times during the iterations are illustrated in Figure 6.7, and the variation of the *MVE* measure with respect to the sensitivity design parameter P is illustrated in Figure 6.8.

In the forward calculation step of the proposed tuning algorithm, the iteration starts by varying the sensitivity design parameter from $P_{min} = 2$ to $P_{max} = 100$. The forward calculation iteration stops at the iteration $P = 43$ with the solution $P^* = 23$, since the improvement on the $MAE(\varepsilon_P^{P-1})$ the measure becomes less than the ε_1 stopping condition for more than P_f trials, which are executed to handle the chattering effect.

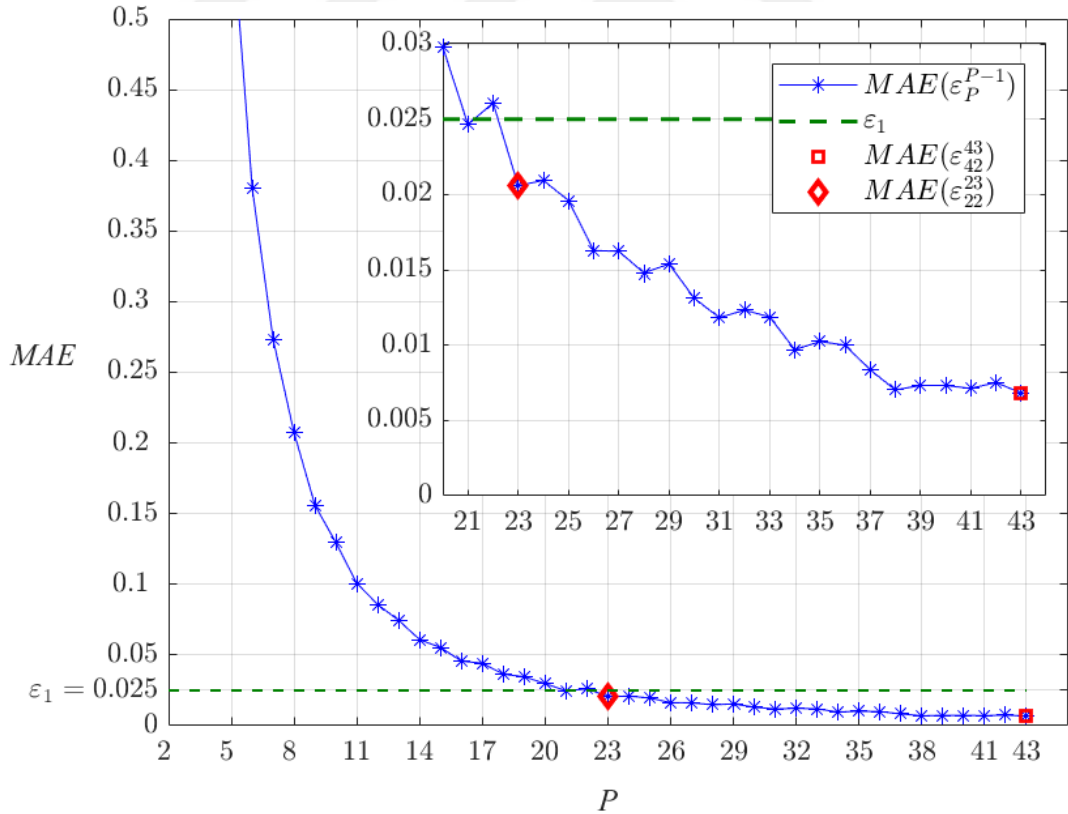


Figure 6.6 : Variation of *MAE* measure with respect to the P values.

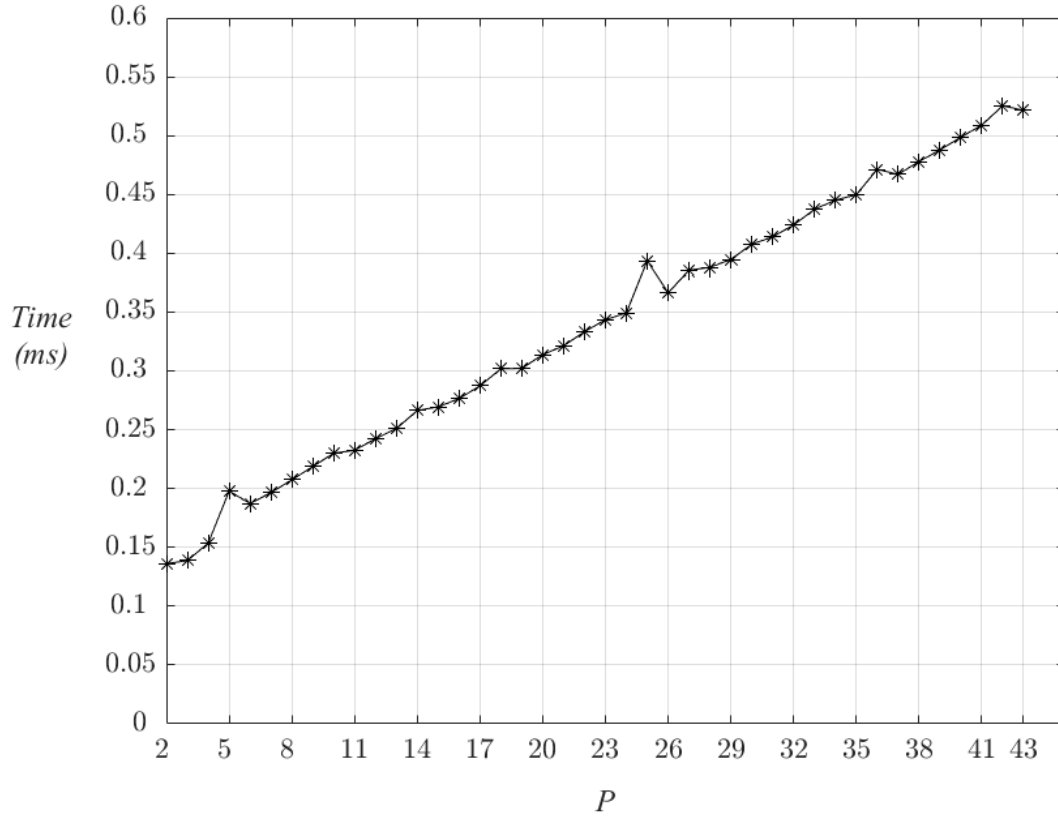


Figure 6.7 : Variation of execution time with respect to the P values.

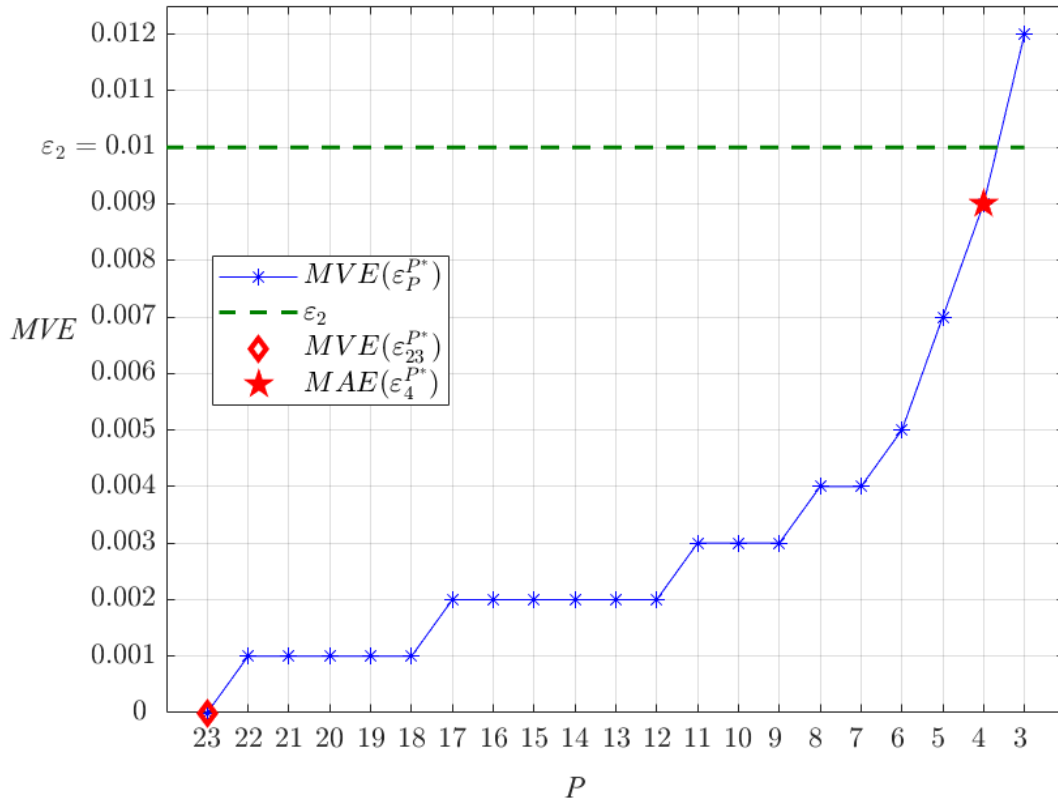


Figure 6.8 : Variation of MVE measure with respect to the P values.

In the backward calculation step of the proposed tuning algorithm, the iteration starts from the solution of the forward calculation $P^* = 23$ towards the $P_{min} = 2$. Then the backward calculation iteration stops at the solution $P^{**} = 4$, since the value of the $MAE(\varepsilon_P^{P^*})$ measure reaches the level of the ε_2 stopping condition. The variation of the MVE measure with respect to the sensitivity design parameter P (or the total number α -planes) and the final solution of the proposed tuning algorithm are illustrated in Figure 6.8. In order to show the effects of other candidate solutions, the differences between GT2-FLCs are illustrated in terms of the difference $\varepsilon_a^{P^*}[v]$ for each data sample of the handled GT2-DFLCs in Figure 6.9. Here the total number of samples is $V = 40401 = 201 \times 201$, since the inputs are sampled with $\Delta_{in} = 0.01$ quantization interval such that 201 points are obtained for each input. As it is shown, the error values for the solution $P^{**} = 4$ is always below the $\varepsilon_2 = 0.01$ boundary.

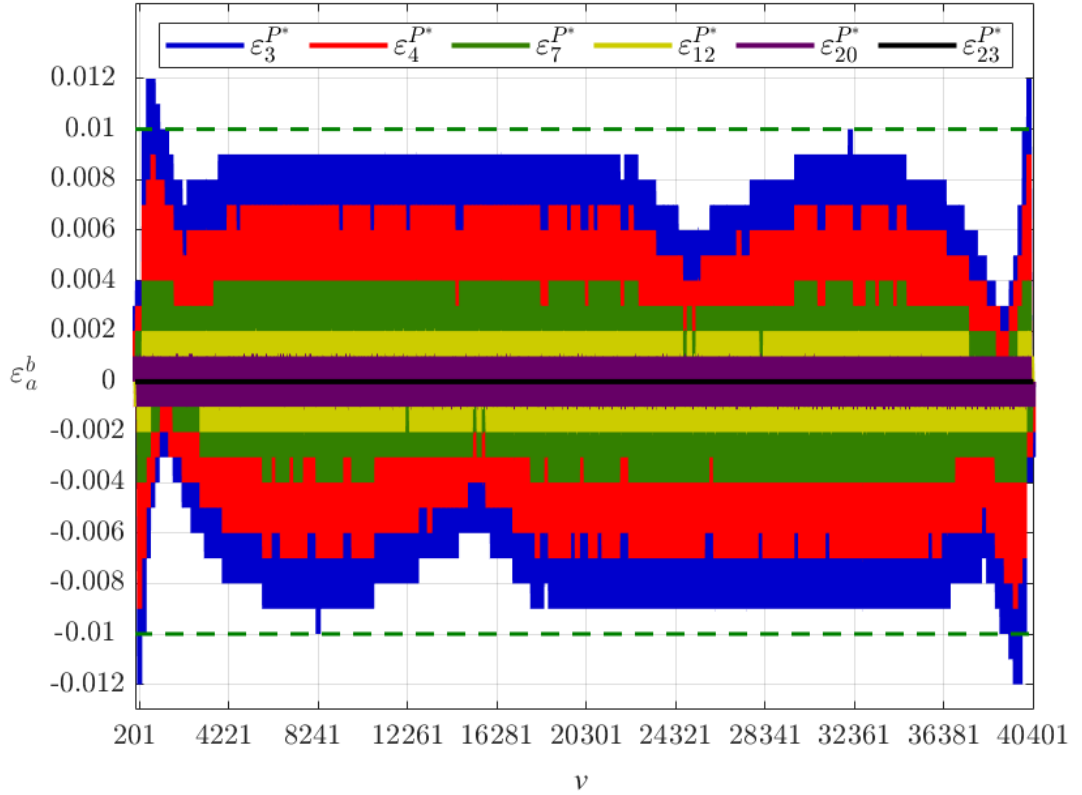


Figure 6.9 : Output differences of GT2-FLCs with different P values.



7. SIMULATION STUDIES AND REAL-TIME APPLICATIONS

In this chapter, simulation studies and real-time applications will be presented in order to evaluate the effectiveness and the impact of the proposed interpretations, design recommendations, and tuning methods for the GT2-FLCs.

7.1 Simulation Study on a Second-Order Nonlinear System

In this section, a simulation study [75] on a second-order nonlinear benchmark control system will be presented to show how the GT2-FLC design can be accomplished based on the proposed guides for a control problem.

7.1.1 Simulation environment

The benchmark control system, second-order nonlinear process model [14, 75] is defined as follows:

$$\frac{d^2y}{dt^2} + \frac{dy}{dt} + \frac{y^2}{4} = u(t - L) \quad (7.1)$$

where y is the output of the system, u is the input of the system, and L is the time delay which is $L = 0.5s$. Here, the gain of the second-order nonlinear system changes with respect to the output of the system (i.e. y), so the system dynamic varies at different operating points. When the system output is relatively low, then the gain of the nonlinear process increases so that the system response is relatively faster; whereas if the system output is relatively high, then the gain of the nonlinear process decreases so that the system response is relatively slower. Due to this challenging nature of the nonlinear system, a controller might result in very satisfactory performances for an operating point, but this performance cannot be maintained for other operating points. For the designs of the DFLCs, four steady-state operating points $\mathbf{r} = [r_1, r_2, r_3, r_4] = [0.6, 0.8, 1, 1.2]$ are considered, and these references are applied in sorted order during the simulation. Moreover, the PID type DFLC structure (given in Section 2.5) is used for all fuzzy controllers during the simulation study.

7.1.2 Controller design

In the design of the T1, IT2, and GT2 FLCs, the systematic tuning steps presented in Section 5.4 are followed and the controllers are tuned according to three performance measures; the rise time (T_r), the settling time (T_s), and the overshoot ($OS\%$). In this context, according to Step-1 of Table 5.7, the baseline T1-FLC is first designed for the reference change from r_3 to r_4 . The baseline T1-FLC is constructed with the fuzzy rule base given in Table 5.3 and the design parameters T1-FLC, the scaling factors of the T1-FPID controller structure are selected as

- T1-FLC: $K_e = 1, K_{\Delta e} = 0.8, K_a = 0.15, K_b = 2.5$

such that desired system performance (aggressive transient response) can be achieved in terms of T_r , T_s , and $OS\%$ performance measures. Then, according to Step-2 of Table 5.7, the baseline IT2-DFLC is designed for the reference change from r_1 to r_2 . The IT2-FPID controller is constructed by using the same design parameters of the T1-FPID counterpart and the FOU design parameters are selected as

- IT2-FLC: $M_{1,1} = 0.02, M_{1,2} = 0.90, M_{1,3} = 0.02,$
 $M_{2,1} = 0.30, M_{2,2} = 0.80, M_{2,3} = 0.30$

such that desired system performance (smooth transient response) can be achieved in terms of T_r , T_s , and $OS\%$ performance measures. Then, as the last step of Table 5.7, the GT2-DFLCs are designed; the GT2-DFLC with a fixed θ value (called as GT2-DFLC in simulation), the GT2-DFLC with online SM-1 (called as GT2-DFLC-SM). The GT2-DFLC is first designed for the reference change from r_2 to r_3 , and the shape design parameter of the GT2-DFLC is selected as

- GT2-DFLC: $\theta = 0.1$

such that a tradeoff between performance and robustness (i.e., a tradeoff between an aggressive T1-FPID controller and a smooth IT2-FPID controller) is obtained by reducing the T_r and T_s measures while compromising from $OS\%$ performance within acceptable limits. Then, in the design of GT2-DFLC-SM, according to the tuning steps in Table 5.8, the shape design parameters ($\theta_r = [\theta_1, \theta_2, \theta_3, \theta_4]$) that are associated with the target references ($r = [r_1, r_2, r_3, r_4] = [0.6, 0.8, 1, 1.2]$) are obtained as

- GT2-DFLC-SM: $\theta_1 = -1.2, \theta_2 = -0.8, \theta_3 = 0.1, \theta_4 = 0.4$

such that different system responses can be achieved for each operating point.

7.1.3 Simulation results

The simulation results of the employed T1-DFLC, IT2-DFLC, GT2-DFLC, and GT2-DFLC-SM are compared with respect to performance measures: the rise time (T_r), the settling time (T_s), and the overshoot ($OS\%$). The results are illustrated in Figure 7.1 and the performance measures are given in Table 7.1. The outcomes of the simulations showed that an acceptable tradeoff between robustness and system performance can be achieved by tuning the shape design parameter θ . Besides, the proposed online scheduling mechanism SM-1 provides an opportunity to improve the overall system performance since the shape design parameter θ is effectively online-adjusted with respect to the operating points.

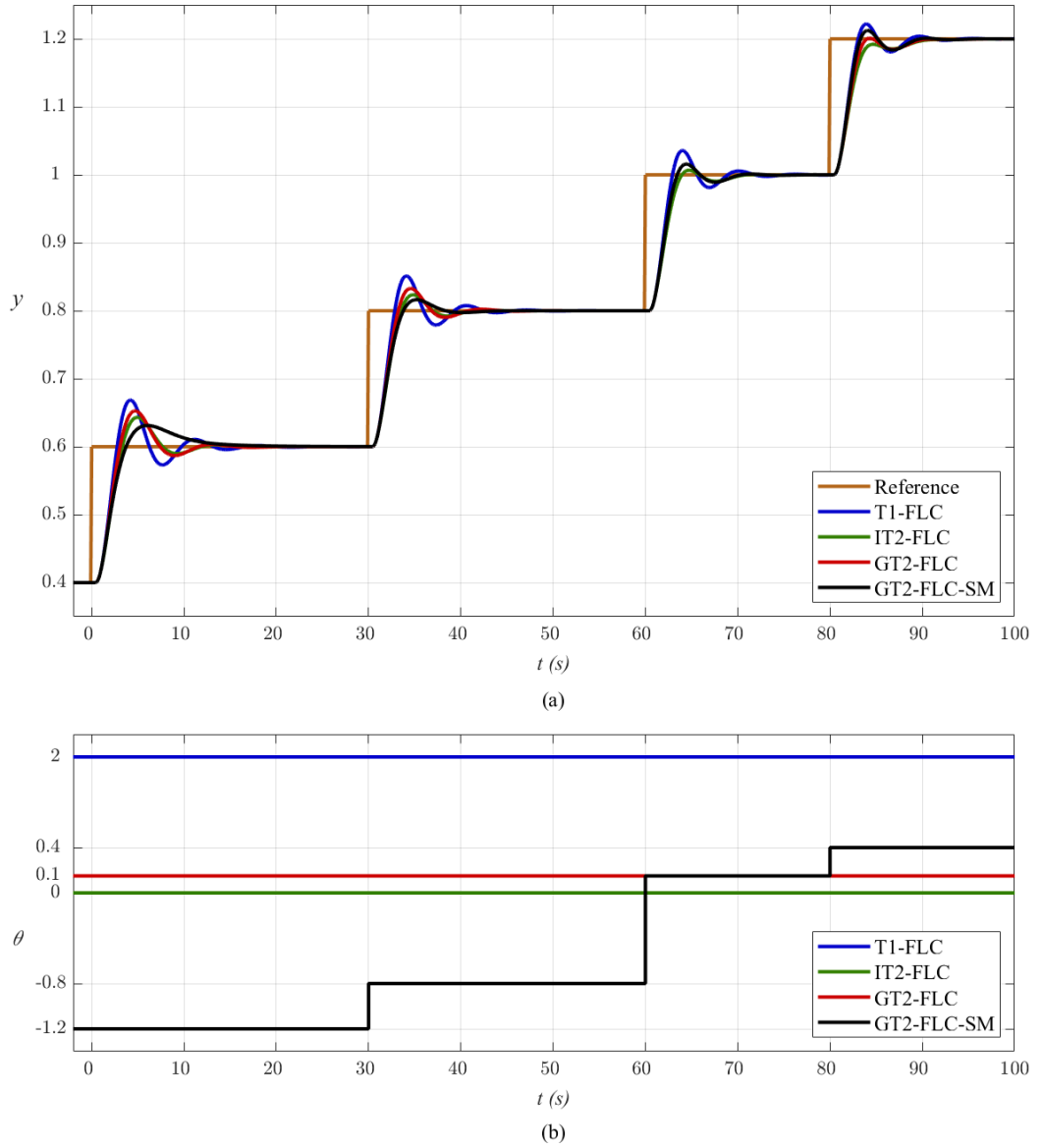


Figure 7.1 : Control performances of T1, IT2, and GT2 FLCs.

As shown in Figure 7.1, the GT2-FLC-SM ended up with a robust system response for the reference variation to the operating point $r_1 = 0.6$, since it obtained the best OS% value without oscillations but the highest T_r value in contrast. For the reference variation to the operating point $r_4 = 1.2$, the online scheduling mechanism tuned the value of the shape design parameter from 0.1 to 0.4 at 80s such that the aggressiveness of the control surface is increased which eventually speeds up the system response. The resulting T_r value is smaller than its IT2 and GT2 counterparts. For the reference variation to the operating point $r_2 = 0.8$ where the baseline IT2-FLC was designed, the GT2-FLC-SM reduced the T_s and OS% performance measures by employing the shape design parameter θ value to -0.8. In summary, it can be concluded that the proposed online tuning mechanism is highly efficient in the tuning of the shape design parameter to enhance the control system performance.

Table 7.1 : Performance measures of T1, IT2, and GT2 FLCs.

Operating Point	Performance Measure	T1-FLC	IT2-FLC	GT2-FLC	GT2-FLC-SM
r_1	T_r	1.538	1.962	1.776	2.221
	T_s	14.98	10.98	10.86	12.96
	OS%	34.35	21.67	26.38	15.08
r_2	T_r	1.587	2.095	1.869	2.189
	T_s	11.78	9.967	9.916	7.484
	OS%	25.90	11.75	16.37	8.196
r_3	T_r	1.648	2.268	1.983	1.983
	T_s	10.90	9.456	9.335	9.335
	OS%	18.05	3.380	7.915	7.915
r_4	T_r	1.721	2.552	2.143	1.863
	T_s	8.256	9.490	9.212	8.880
	OS%	10.99	0.0	0.514	6.241

7.2 Real-Time Application on Parrot Mambo Drone

In this section, the real-time experimental results [76] will be presented to validate the proposed design interpretations, design recommendations, and tuning methods.

7.2.1 Experimental setup

The real-time experiments are conducted on the Parrot Mambo drone that is a commercial product equipped with sophisticated software/hardware ingredients such as an ARM 9 416 MHz processor, 6-degree of freedom IMU, pressure and ultrasonic

sensors, and a downward-facing camera with a 60 FPS measurement [76]. The Parrot Mambo drone has a MATLAB/Simulink support package that makes the system as a proof-of-concept experimental setup. This drone has an efficient built-in preliminary flight control structure, which contains low-level PID controllers and state estimators, to stabilize the attitude and altitude dynamics, and the sampling time of this flight control system is defined as $T = 5 \text{ ms}$, so that the flight control algorithms run in every 5ms cycle. The Parrot Mambo drone is illustrated in Figure 7.2

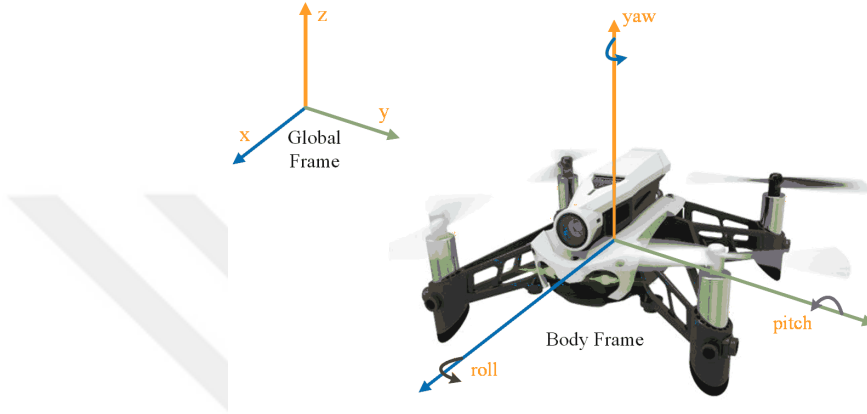


Figure 7.2 : Illustration of Parrot Mambo drone.

For the real-time control experiments on the drone, the controllers are designed for the x-axis position tracking problem. In this context, the y-axis reference is set to 0m, and the yaw angle reference is set to 0° and the z-axis altitude reference is set to 1m from the ground, moreover the low-level built-in controllers are utilized for the control of physical actuators. Then the DFLCs are designed to generate the pitch angle reference signal with respect to the x-axis position reference changes. It is preferred to use a PI type fuzzy controller that is formed by a DFLC (i.e. T1, IT2, or GT2) with an integrator [3, 9] as explained in Section 2.5. In the PI type DFLC structure, there are two input scaling factors used to normalize the inputs (K_e , $K_{\Delta e}$) and one output scaling factor (K_b) to denormalize the output of the DFLC. The x-axis reference positions are considered as $\mathbf{r} = [r_1, r_2, r_3] = [1 \text{ m}, 0.75 \text{ m}, 1.5 \text{ m}]$.

7.2.2 Design of the shape design parameter

In the design of the shape design parameter (θ), the systematic tuning steps presented in Section 5.4 are followed. In this context, according to Step-1 and Step-2 of Table 5.7, the baseline DFLCs are first designed for the first x-axis reference, which is the steady-state operating point $r_1 = 1 \text{ m}$. According to Step-1 of Table 5.7, the baseline

T1-DFLC is designed by employing the fuzzy rule base given in Table 5.3 and the remaining design parameters (i.e. input/output scaling factors) are selected as

- T1-DFLC: $K_e = 1, K_{\Delta e} = 0.68, K_b = 2.5$

such that an aggressive CS is obtained. Then, based on Step-2 of Table 5.7, the baseline IT2-DFLC is designed by using the same design parameters of its T1 counterpart and assigning the remaining FOU design parameters as

- IT2-DFLC: $M_{1,1} = 0.05, M_{1,2} = 0.95, M_{1,3} = 0.05,$
 $M_{2,1} = 0.15, M_{2,2} = 0.85, M_{2,3} = 0.15$

such that a smooth CS is achieved. As the last step of Table 5.7, the GT2-DFLCs are designed in 3 ways; the GT2-DFLC with a fixed θ value (called as GT2-DFLC in order to distinguish from the online-tuned counterparts), the GT2-DFLC with SM-1 (called as GT2-DFLC-SM-1), and the GT2-DFLC with SM-2 (called as GT2-DFLC-SM-2). The GT2-DFLC, similar to its T1 and IT2 counterparts, is designed for the steady-state operating point $r_1 = 1 \text{ m}$ by providing a tradeoff between the aggressive T1-DFLC baseline and the smooth IT2-DFLC baseline. The shape design parameter of the GT2-DFLC is founded experimentally as

- GT2-DFLC: $\theta = 0.1$

such that a tradeoff between performance and robustness is obtained. Then, the GT2-DFLC-SM-1 is designed for each steady-state operating point, where $\mathbf{r} = [r_1, r_2, r_3] = [1 \text{ m}, 0.75 \text{ m}, 1.5 \text{ m}]$, by following the tuning steps in Table 5.8 (besides the generic GT2-FLC design steps given in Table 5.7). The shape design parameters associated with an operating point ($\boldsymbol{\theta}_r = [\theta_1, \theta_2, \theta_3]$) is obtained as

- GT2-DFLC-SM1: $\theta_1 = 0.1, \theta_2 = -0.8, \theta_3 = 1$

such that moderate, smooth, and aggressive CSs can be achieved for the operating points r_1, r_2 , and r_3 , respectively. The linear interpolation is used to define the mapping given in equation (5.11). Then, the GT2-DFLC-SM-2 is designed for the same steady-state operating points of its SM-1 counterpart ($\mathbf{r} = [r_1, r_2, r_3]$) by using the same steady-state shape design parameters ($\boldsymbol{\theta}_r = [\theta_1, \theta_2, \theta_3]$) and further employing the online update rule given in equation (5.12). Here, the transient part of the shape design parameter (i.e. the parameter θ_t) is handled by the fuzzy mapping defined in equation (5.13) and Table 5.9 with the weighting coefficient $\gamma = 0.5$.

7.2.3 Comments on the control surfaces of the designed DFLCs

In this section, the CSs of the DFLCs that are employed for the real-time experiments will be examined to provide a better understanding of how the proposed design methods result. The resulting CSs of the designed DFLCs are illustrated in Figure 7.3. The CS differences between “IT2-DFLC versus T1-DFLC, GT2-DFLC versus T1-DFLC, and GT2-DFLC versus IT2-DFLC” are also examined in Figure 7.4.

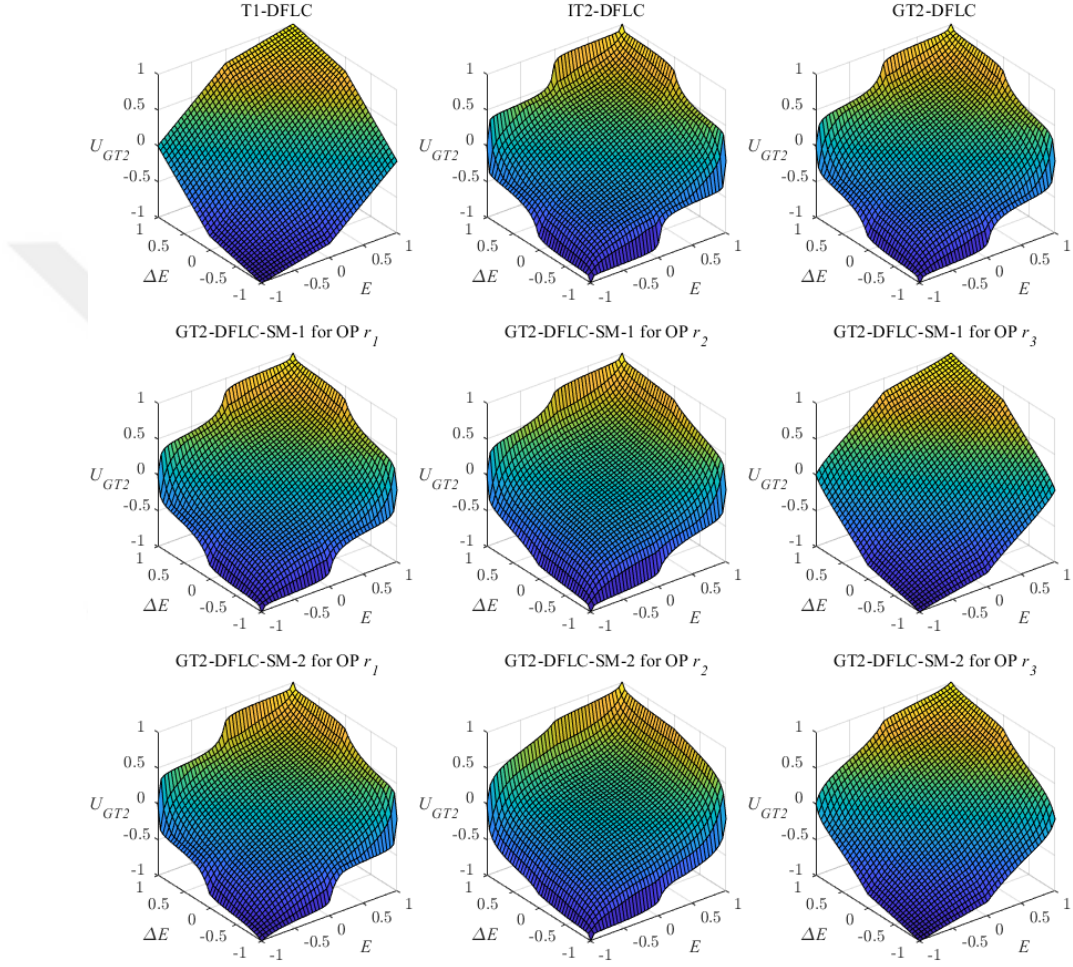


Figure 7.3 : The CSs of the designed T1, IT2, and GT2 DFLCs.

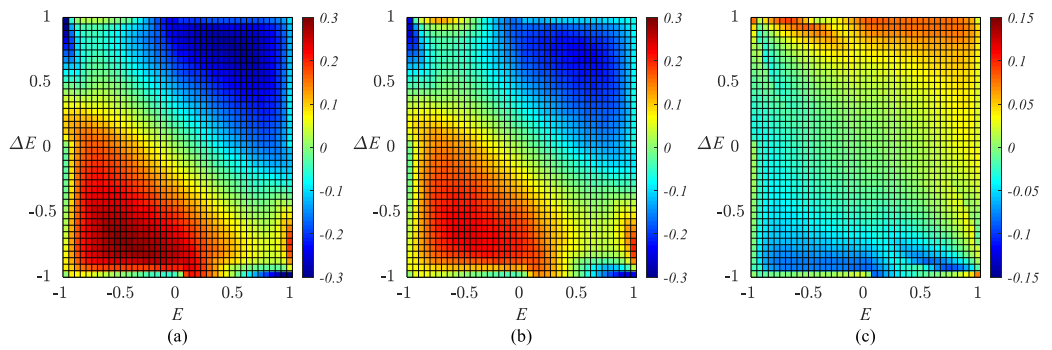


Figure 7.4 : The CS differences between the designed T1, IT2, and GT2 DFLCs.

The CS differences between GT2-DFLC and baseline controllers are illustrated in Figure 7.4. In subfigures of Figure 7.4, the CS differences are shown by subtracting the controller outputs which means that the CS differences calculated by “ $U_{IT2} - U_{T1}$ ”, “ $U_{GT2} - U_{T1}$ ”, and “ $U_{GT2} - U_{IT2}$ ” in subplots (a), (b), and (c), respectively. Here, as the baseline fuzzy controllers (T1-DFLC and IT2 DFLC) are designed with smooth and aggressive CSs, there are larger and deeper blue and red areas in Figure 7.4a (the blue area for the region where $E > 0$ and $\Delta E > 0$, and the red area for the region where $E < 0$ and $\Delta E < 0$). This is an expected outcome of the prior design because IT2-DFLC generates a relatively lower control signal due to its smooth CS. Figure 7.4b and Figure 7.4c also show that the designed GT2-DFLC is relatively smoother and more aggressive than its T1 and IT2 baseline counterparts, respectively.

The CSs of the designed online controllers (i.e. GT2-DFLC-SM-1 and GT2-DFLC-SM-2) are compared with their fixed T1, IT2, and GT2 DFLC counterparts for each operating point. The CS differences for GT2-DFLC-SM-1 and GT2-DFLC-SM-2 (in comparison to T1, IT2, and GT2 DFLCs) are illustrated in Figures 7.5 – 7.7 and Figures 7.8 – 7.10, respectively.

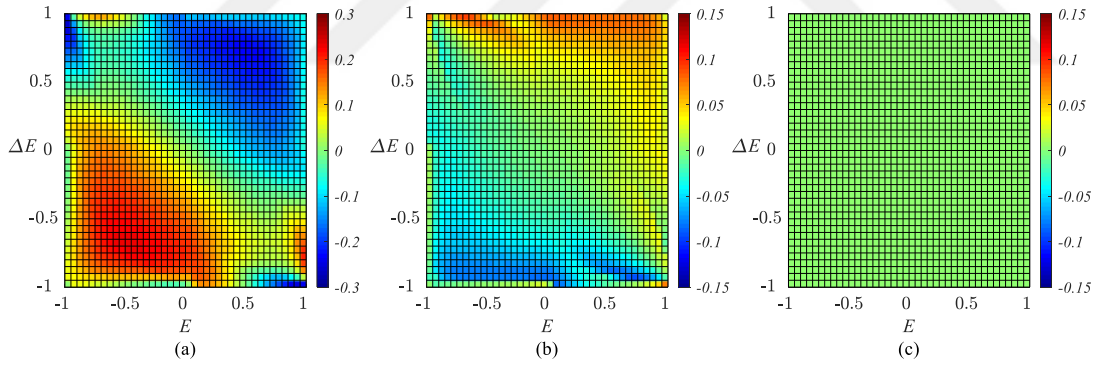


Figure 7.5 : OP r_1 : CS differences between SM-1 and (a) T1 (b) IT2 (c) GT2.

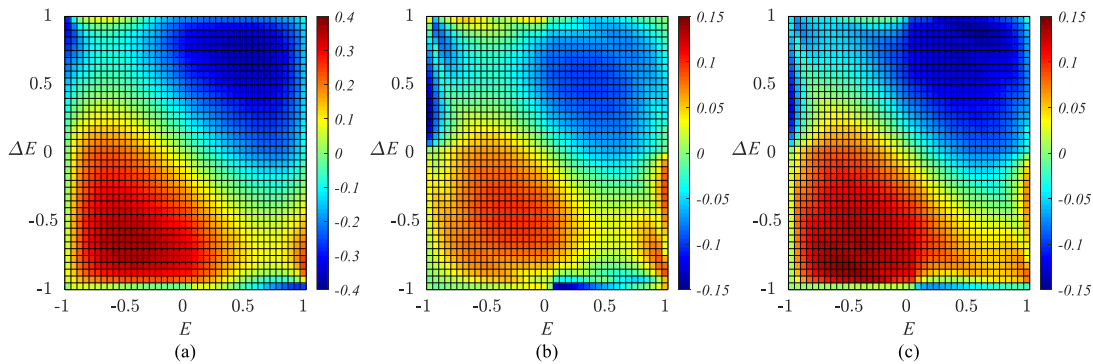


Figure 7.6 : OP r_2 : CS differences between SM-1 and (a) T1, (b) IT2, (c) GT2.

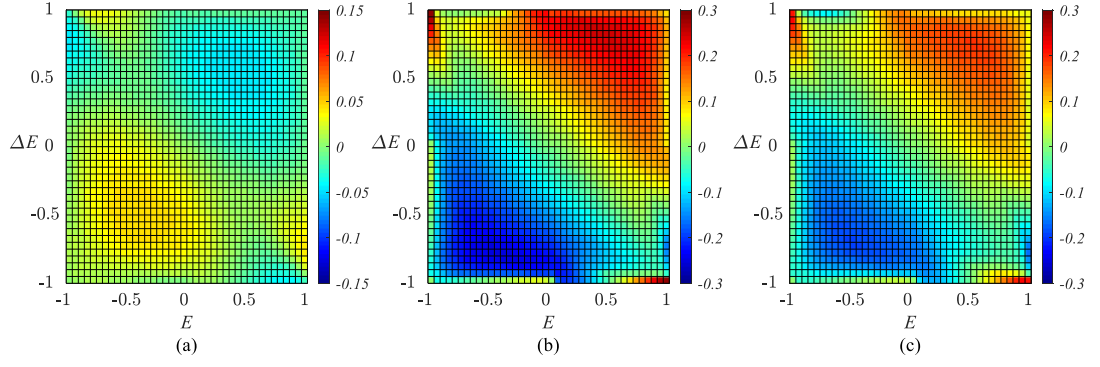


Figure 7.7 : OP r_3 : CS differences between SM-1 and (a) T1, (b) IT2, (c) GT2.

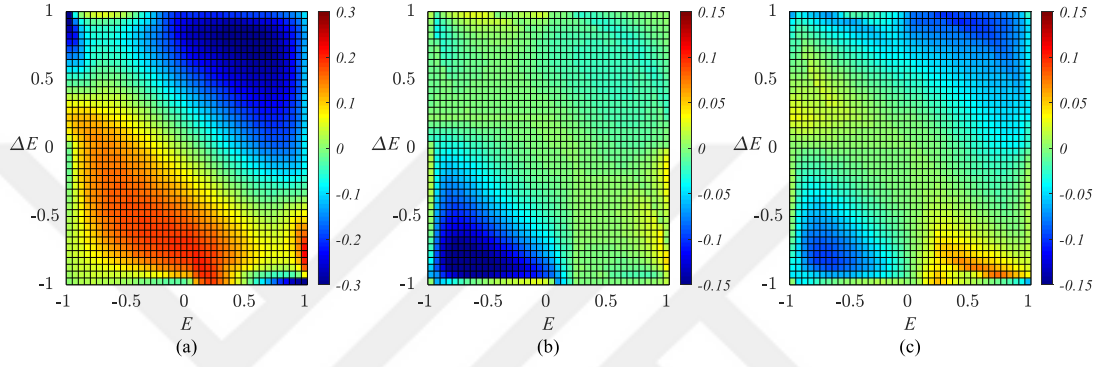


Figure 7.8 : OP r_1 : CS differences between SM-2 and (a) T1, (b) IT2, (c) GT2.

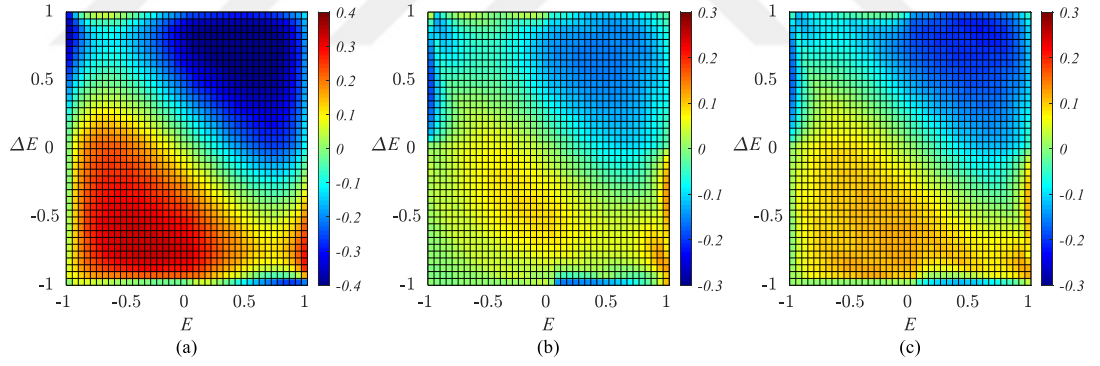


Figure 7.9 : OP r_2 : CS differences between SM-2 and (a) T1, (b) IT2, (c) GT2.

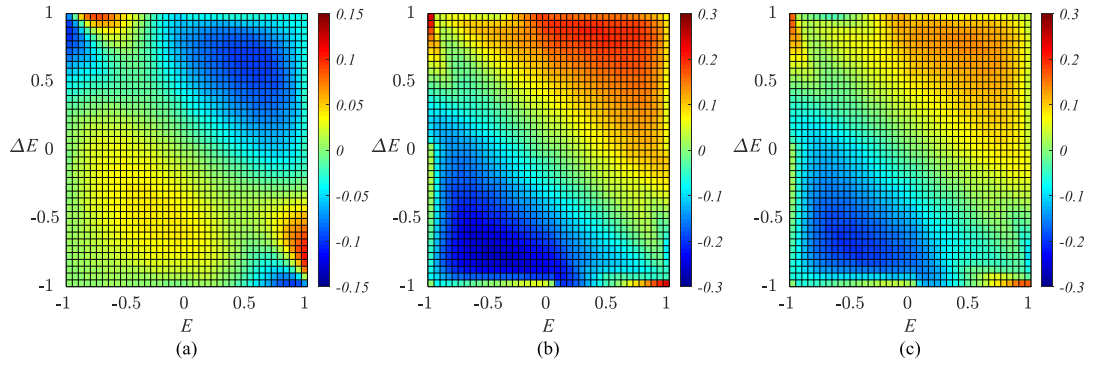


Figure 7.10 : OP r_3 : CS differences between SM-2 and (a) T1, (b) IT2, (c) GT2.

It can be commented that the CSs of the GT2-DFLC-SM-1 and the GT2-DFLC-SM-2 can transform both smoother CS (for example in Figures 7.6c and 7.9c for the operating point r_2) and more aggressive CS (for example in Figures 7.7c and 7.10c for the operating point r_3) for different operating points. This also coincides with the corresponding NTE and NR values given in Table 7.2. It is observed that:

- For the first operating point r_1 , the GT2-DFLC-SM-2 has a relatively high NTE value and a NR value that is close to the baseline IT2 counterpart. So, without comprising the robustness property of the designed IT2-DFLC around the steady-state significantly, the SM-2 structure will increase the response of the system in comparison to its IT2 and GT2 DFLC counterparts.
- For the second operating point r_2 , the GT2-DFLC-SM-2 has the lowest NR value and thus the robustness around the steady-state is risen by transforming the CS of the GT2-DFLC that is smoother than its baseline IT2-DFLC. This is an expected design to result in a system response without oscillations.
- For the third operating point r_3 , the GT2-DFLC-SM-2 has a high NTE value, which is close to its baseline T1-DFLC counterpart, and a relatively lower NR value. Thus, the SM-2 structure will smoothen CS around the steady-state to eliminate overshoots while increasing the aggressiveness of the CS to speed up the system response like its T1 fuzzy counterpart.

Table 7.2 : Performance measures of the designed CSs of the DFLCs.

Controller	OP	NTE	NR
T1-DFLC	r_1, r_2, r_3	1.000	2.491
IT2-DFLC	r_1, r_2, r_3	0.820	1.044
GT2-DFLC	r_1, r_2, r_3	0.858	1.175
GT2-DFLC-SM-1	r_1	0.858	1.175
	r_2	0.795	0.547
	r_3	0.975	2.107
GT2-DFLC-SM-2	r_1	0.876	1.108
	r_2	0.804	0.484
	r_3	0.978	1.999

As mentioned in the previous sections, that tuning the shape design parameter with respect to the operating points via the proposed SMs in an online manner gives the opportunity to provide a good tradeoff between robustness and performance.

7.2.4 Design of the sensitivity design parameter

In the design of the shape design parameter (P), the systematic tuning steps presented in Section 6.3 are followed. In this context, the hardware limits of the real-time Parrot Mambo drone experimental setup are considered in terms of quantization levels (i.e. Δ) and computational time. These two terms are quite essential for an effective real-time application on a flying drone since it is equipped with various sensors with different scalings and available resources of the onboard computation power. Then the average quantization levels of the real-time application are assumed as $\Delta_{in} = 0.01$ and $\Delta_{out} = 0.001$ approximately. In order to verify the feasibility of the designed GT2-DFLCs, the average computational time of the built-in controllers of the Parrot Mambo drone is examined by using the MATLAB Simulink Profiler toolbox. Then the average computational time is found as $T_{FC} \approx 3.7 \text{ ms}$, which leaves $T - T_{FC} \approx 1.3 \text{ ms}$ for the computations of the designed GT2-DFLCs. Based on this system information, the iterative algorithm given in Table 6.3 is employed. The forward calculation is stopped at $P^* = 23$ for the stopping criteria and hyperparameter setting $\varepsilon_1 = 0.025 \times 10^{-3}$, $P_f = 20$, and $P_{max} = 100$ (The numerical example that is given in Section 6.3 can be visited for further details, as it uses the same GT2-DFLC structure.). Then, in order to conclude if the obtained forward calculation result, $P^* = 23$, is feasible for the real-time application, the average computation time of the GT2-DFLC with $P^* = 23$ α -planes is examined. In this context, the average computation time on the computer's processor, which is used for DFLC designs, is firstly calculated and then this value is projected into the microprocessor of the drone by multiplying by 6.25 which is the clock speed ratio between the computer (2.6 GHz) and the Parrot Mambo drone (416 MHz). Here, a buffer time ($T_B = 0.3 \text{ ms}$) is also considered for computational time calculation, since this rough conversion might include some errors. The average computation time of the GT2-DFLC with $P^* = 23$ α -planes on the computer (T_{GT2}^{Comp}) and the drone (T_{GT2}) are calculated as $T_{GT2}^{Comp} = 0.348 \text{ ms}$ and $T_{GT2} = 2.176 \text{ ms}$, respectively. Then it is concluded that the solution of the forward calculation ($P^* = 23$) is not feasible for the target real-time application, since the total required time is higher than the sampling time of the Parrot Mambo drone ($T_{FC} + T_{GT2} + T_B > T = 5 \text{ ms}$). Thus, the backward calculation of Table 6.3 is performed, and the iteration is stopped at $P^{**} = 4$ for the stopping criteria setting $\varepsilon_2 = 0.01$ (The numerical example that is given in Section 6.3 can be visited for further details, as it uses the same GT2-

DFLC structure.). The average calculation time of the GT2-DFLC with $P^{**} = 4$ for is calculated as in the forward calculation and obtained as $T_{GT2} = 0.978 \text{ ms}$. Accordingly, it is concluded that the solution $P^{**} = 4$ is feasible for the real-time application on the drone so that all GT2-DFLCs are constructed with 4 α -planes (excluding $\alpha_0 = 0$) as $\alpha_1 = 0.25$, $\alpha_2 = 0.5$, $\alpha_3 = 0.75$, and $\alpha_4 = 1$.

7.2.5 Experimental results

The experimental result performances of the employed T1, IT2, and GT2 fuzzy PI controllers are compared with respect to three performance measures: the rise time (T_r), the settling time (T_s), and the overshoot ($OS\%$). The performances of the fuzzy controllers are compared in two parts; the GT2-DFLC is first compared with the baseline T1 and IT2 DFCLCs (for this case, all design parameters are tuned and fixed in an offline manner) in Figure 7.11, then the performance improvements of the proposed online SMs, which change the shape design parameter during the flight, are compared with the fixed GT2-DFLC in Figures 7.12, 7.13, and 7.14 for the operating points r_1 , r_2 , and r_3 , respectively. The performance measures are given in Table 7.2.

Table 7.3 : Performance measures of T1, IT2, and GT2 FLCs.

Operating Point	Performance Measure	T1-FLC	IT2-FLC	GT2-FLC	GT2-FLC-SM-1	GT2-FLC-SM-2
OP-1 r_1	T_r	0.79	1.12	0.85	0.85	0.88
	T_s	3.54	2.01	2.44	2.44	1.79
	$OS\%$	10.13	1.39	7.22	7.22	3.39
OP-2 r_2	T_r	0.65	0.79	0.75	0.69	0.74
	T_s	5.85	4.86	3.75	5.78	4.05
	$OS\%$	30.47	9.38	15.87	9.39	6.64
OP-3 r_3	T_r	1.23	1.64	1.39	1.18	1.15
	T_s	2.25	2.84	2.54	2.16	2.16
	$OS\%$	4.80	0.92	2.20	4.84	2.91

It is observed that the lowest $OS\%$ measures are obtained for the IT2-DFLC that is designed as the smooth baseline with a smooth CS, whereas the lowest T_r measure is calculated for the T1-DFLC that is designed as the aggressive baseline with an aggressive CS. As shown in Figure 7.4, the designed GT2-DFLC has a CS that is smoother and aggressive than its T1 and IT2 baselines respectively, so the resulting controller behavior lies in between these baselines. As a result of the shape design parameter setting the value of $\theta = 0.1$ for the steady-state operating point r_1 , the GT2-

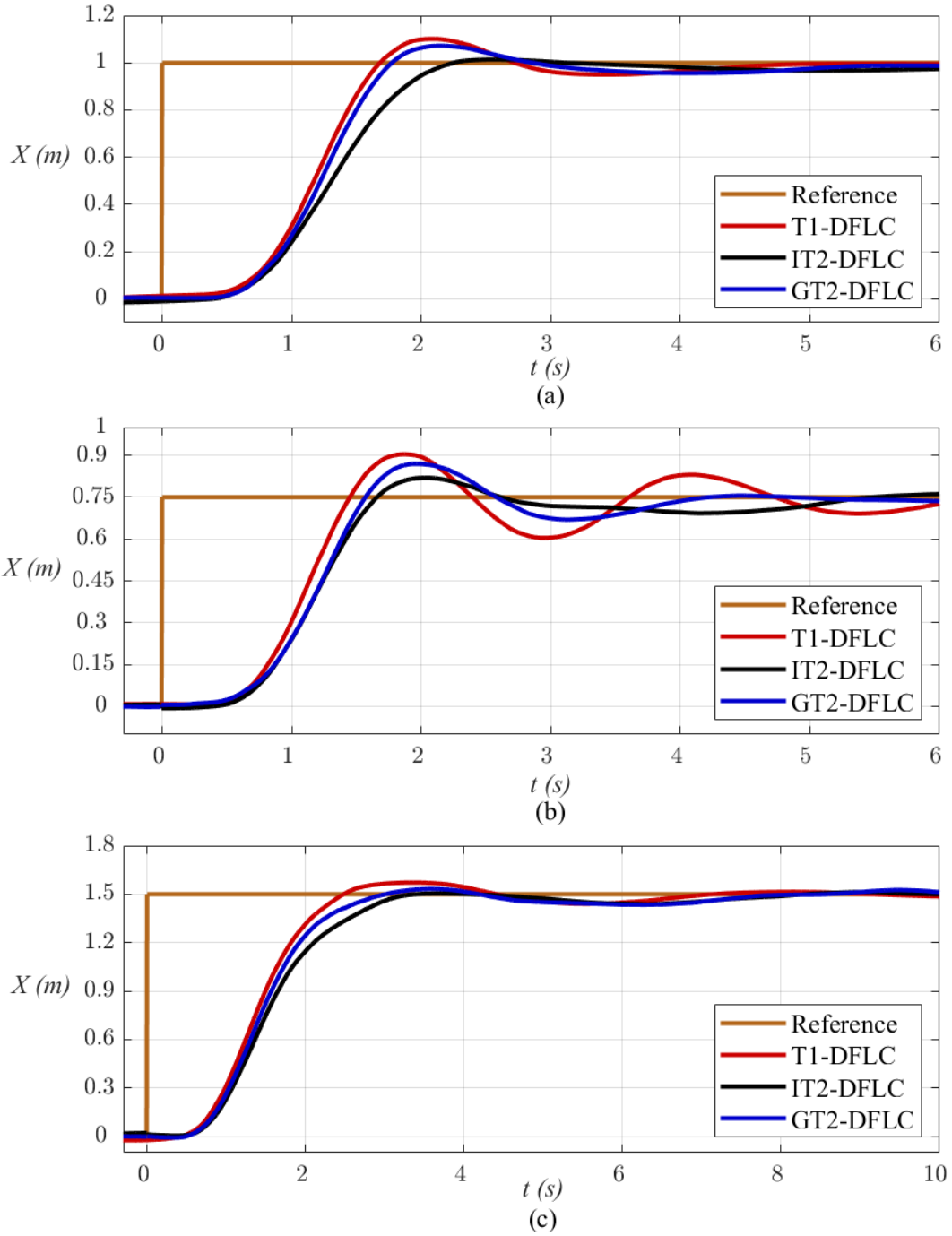


Figure 7.11 : Real-time experiment results of the T1, IT2 and GT2 DFLCs.

DFLC improves the T_r performance measure of the baseline IT2-DFLC by 0.27s by compromising the OS% value by 5.83%, on the other side, the GT2-DFLC improves the OS% performance measure of the baseline T1-DFLC by 2.91% by compromising 0.06 s from the T_r value. Moreover, for the steady-state operating point r_2 , the performances of the baseline T1 and IT2 DFLCs (given in Figure 7.11b) decrease in comparison to the results for the first operating point r_1 (given in Figure 7.11a), so the performance of the GT2-DFLC is also degraded for this operating point. This is an

expected outcome of the proposed systematic controller design since the GT2-DFLC combines the outputs of the baseline T1 and IT2 DFLCs, so the GT2 fuzzy controller performance also depends on the performances of the initial baseline controllers. For the steady-state operating r_3 , the GT2-DFLC performs a moderate and superior system response which results in among the performances of the baseline T1 and IT2-DFLCs in terms of performance measures; T_s , T_r , and OS%.

The system responses of the GT2-DFLCs with SMs are compared with the GT2-DFLC with a fixed shape design parameter $\theta = 0.1$ in Figures 7.12, 7.13, and 7.14 for the operating points r_1 , r_2 , and r_3 respectively. It is observed that the online update of the shape design parameter θ (per the steady-state operating points) ends up with very efficient system responses in terms of control performance and robustness.

As illustrated in Figure 7.12, the online tuning mechanism SM-2 changes the shape design parameter dynamically based on the transient states (E and ΔE) of the control system. Accordingly, the GT2-DFLC-SM-2 changes the shape design parameter from -0.4 to a nominal design value $\theta_1 = 0.1$ according to the fuzzy scheduling mechanism defined in Table 5.9 and the update rule defined in equation (5.12).

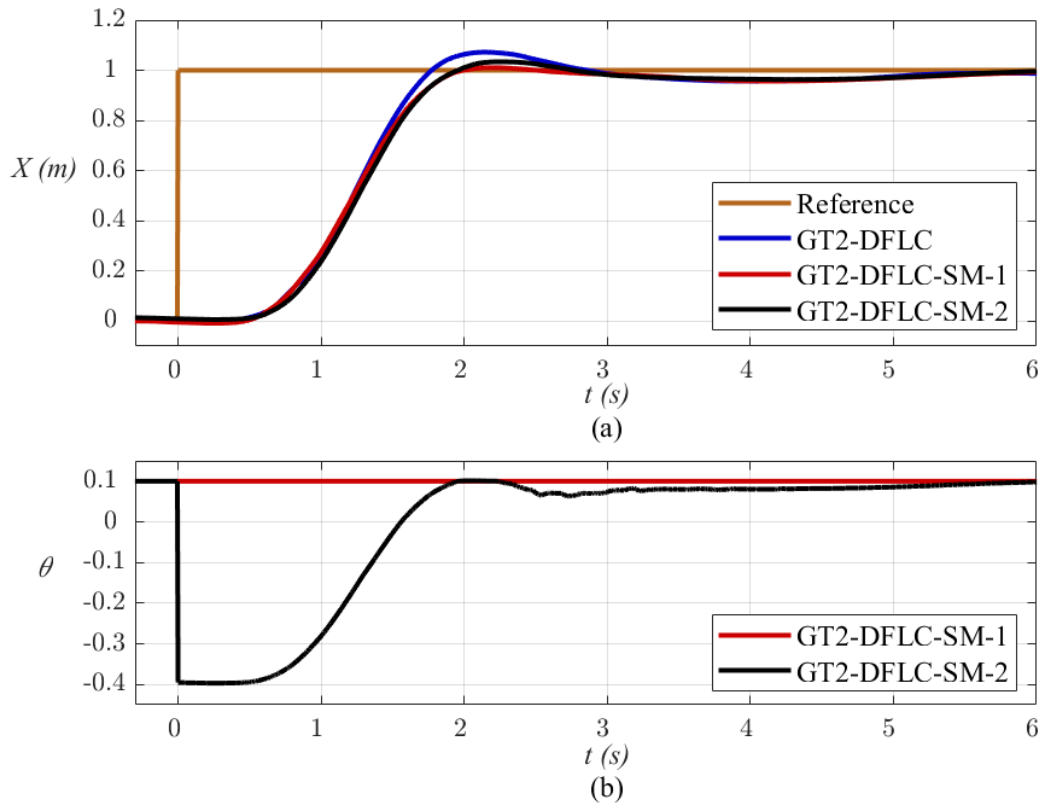


Figure 7.12 : Real-time experiment results of the GT2 DFLCs for r_1 .

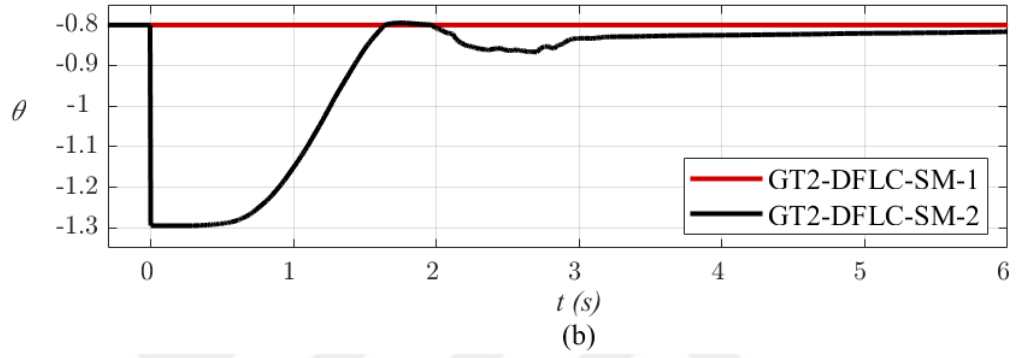
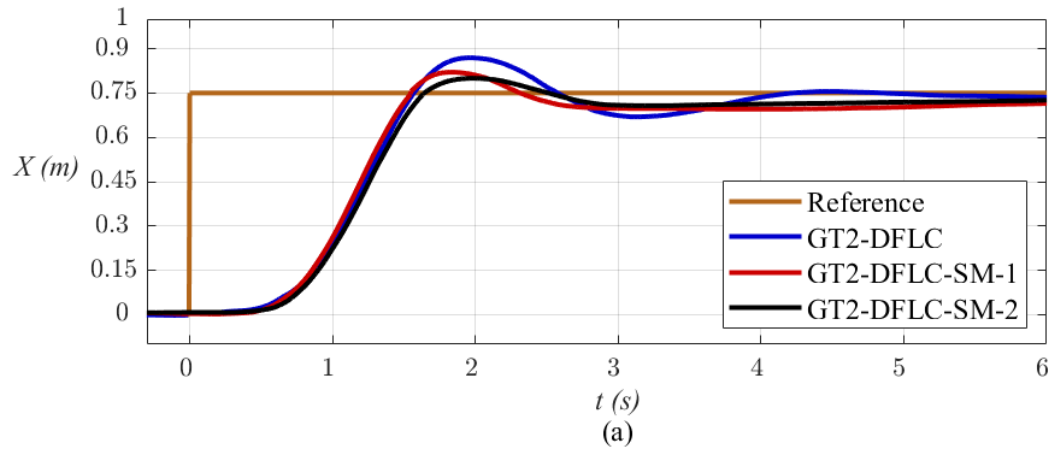


Figure 7.13 : Real-time experiment results of the GT2 DFLCs for r_2 .

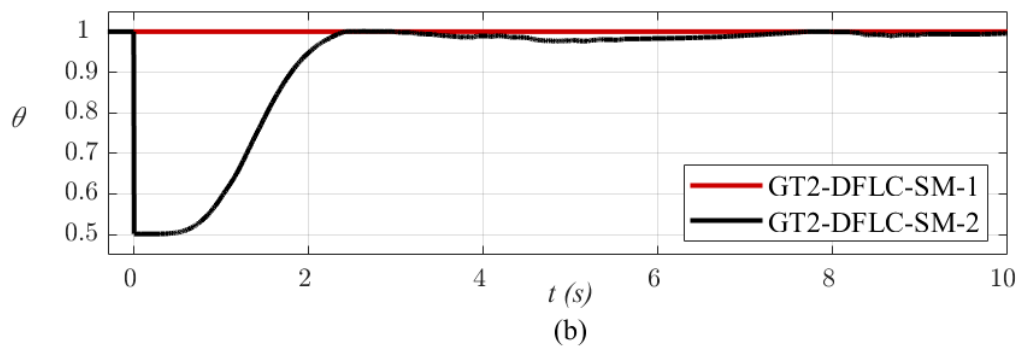
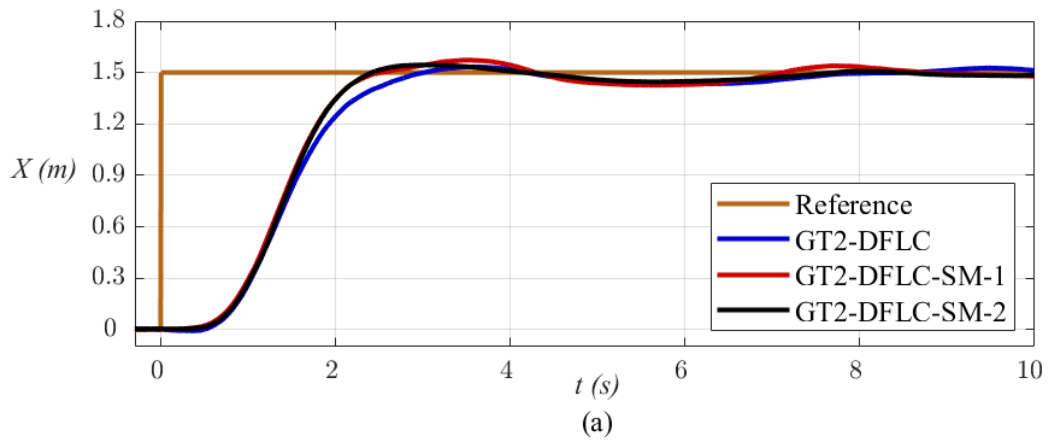


Figure 7.14 : Real-time experiment results of the GT2 DFLCs for r_3 .

As illustrated in Figure 7.13, the SM-2 reduces the shape design parameter θ value to -1.3 (i.e. the smoothness of the CS is increased) and then dynamically increases the value of the shape design parameter θ to its nominal design value $\theta_2 = -0.8$ at the operating point $r_2 = 0.75 \text{ m}$. As given in Table 7.3, this ends up with non-oscillating performance and less overshoot comparing to its T1, IT2, and GT2 counterparts. For example, the GT2-DFLC-SM-2 reduces the values of OS% and T_s performance measures by 2.64% and 0.81s respectively, because the online SM transforms the CS as smoother than its baseline IT2 counterpart. As illustrated in Figure 7.14 for the steady-state operating point $r_3 = 1.5 \text{ m}$, the shape design parameter of the GT2-DFLC-SM-2 is changed from 0.5 to $\theta_3 = 1$ gradually, and thus the aggressiveness of the GT2 CS is increased gradually to result in a faster transient system response in comparison to the GT2-DFLC with a fixed shape design parameter.

In conclusion, it is worth underlying that both online SMs; SM-1 and SM-2, enhance the control system performance, while SM-2, which considers the transient state dynamics and operating points to tune the shape design parameter, is capable to achieve superior control performances for operating points in overall.

8. CONCLUSIONS

In this thesis, the internal structures of GT2-FLCs are examined, the design parameters are analyzed to provide new interpretations for these GT2-FLC design parameters, the systematic controller design approaches for GT2-FLCs are presented and novel tuning methods/algorithms are proposed. This thesis also shows new perceptions of how the design of GT2-FSs affect the CC/CS of GT2-FLCs and how the design of GT2-FLCs can be accomplished in straightforward and practical manners.

As the first part of the structural analyses, the GT2-FSs are investigated. It is shown that a GT2-FS can transform into its IT2 fuzzy, T1 fuzzy, or crisp counterparts based on the settings of the SMF of the antecedent GT2-FS. This structural analysis on the types of FSs clearly shows that the superiority of the GT2-FLCs mostly lies in the definitions of the SMFs of the GT2-FSs. It is shown that the trapezoid SMF has design superiorities over its counterparts since the trapezoid SMF allows constructing not only trapezoid but also triangle, interval, and singleton shapes. A new parameterization is also proposed to represent/tune the trapezoid SMFs with a single parameter. Hence, it is suggested the usage of trapezoid SMFs with the proposed parameterization of the trapezoid SMFs such that the GT2-FS design can be accomplished with a single parameter. Then, the general suggestions on the structural settings of GT2-FLCs are provided not only to construct GT2-FLCs straightforwardly but also to ease the design of the GT2-FLCs with few design parameters. The main design parameters of the GT2-FLCs are presented as the shape design parameter and the sensitivity design parameter with respect to their interpretable effects on the resulting CCs/CSs of the GT2-FLCs. The tuning parameter of the GT2-FLCs is interpreted as the shape design parameter and the total number of α -planes is interpreted as the sensitivity design parameter. It is suggested to initialize GT2-FLCs over their T1 and IT2 counterparts by tuning the new GT2-FLC design parameters.

The role of the shape design parameter is investigated via the shape analyses conducted for two types of GT2-FLC structure with various design options. The effects of the shape design parameter on the CCs/CSs of the GT2-FLCs show that the shape design

parameter changes the shape of the fuzzy input-output mapping remarkably. This observation provides explanations on the role of the shape design parameters on the potential improvements to performance and robustness. It is shown that the GT2-FLCs can achieve much complex CCs/CSs than their baseline T1 and IT2 counterparts in terms of aggressiveness and smoothness of the fuzzy system. Therefore, it is suggested to tune the CCs/CSs of the GT2-FLCs (via the shape design parameter) based on the tradeoff between robustness and performance. It is concluded that the shape design parameter provides not only design simplicity as only baseline T1 and IT2 FLCs are needed, but also convenient design flexibility as the tradeoff between performance (like T1-FLC) and robustness (like IT2-FLC) can be fulfilled. In order to accomplish the controller design task in a systematic way, the design recommendations are given for the easy design of the shape parameter. Two novel online scheduling mechanisms are also proposed for online-adjustment of the shape design parameter to enhance the system performance for different steady-state operating points and transient-state dynamics of the control system.

The role of the sensitivity design parameter is investigated via the sensitivity analyses conducted for two GT2-FLC structures with various design options. The effects of the sensitivity design parameter on the CCs/CSs of the GT2-FLCs show that the sensitivity design parameter has a minor impact on the shape of the fuzzy mapping but has a major impact on the accuracy of the mapping and computational time. This provides practical explanations on the role of the sensitivity design parameters on the calculation accuracy and the computational time. It is shown that the GT2-FLCs result in almost identical CCs/CSs, although the sensitivity design parameter changes in a wide range. Consequently, it is suggested tuning the sensitivity design parameter by considering the limitations of hardware components such as quantization level (e.g. resolutions) and processing speed. It is shown that this design approach provides a compromise between the calculation accuracy and computational time. It is shown that the proposed iterative algorithm provides a practical solution to tune the sensitivity design parameter, especially for real-time applications.

The simulation and real-time applications show the deployment of the proposed design approaches on benchmark control systems, while the controller design phases validate that the design of the GT2-FLCs is accomplished by simply following the proposed design methods. These control applications also show that the presented analyses and

the proposed design methods are applicable for different control problems. The real-time experiments present a comprehensive design (for both shape and sensitivity design parameters) and a comparative, as well as a complete application (among T1, IT2, and GT2 FLCs) to evaluate the proposed systematic design approaches (the tuning steps of shape and sensitivity design parameters) for the GT2-FLCs. The results of the real-time control application show that the GT2-FLCs achieve better performance measures comparing to the T1 and IT2 counterparts. This is an expected outcome of the proposed GT2-FLC designs since the GT2-FLCs use a collection of T1 and IT2 FLCs. The real-time application results also show the proposed online tuning methods for the shape design parameter provides satisfactory performances for all operating conditions (since the shape design parameter is updated in an online manner), while the proposed tuning method for the sensitivity design parameter provides a practical solution to real-time applications.

It is believed that this thesis will open the doors for wider usage of GT2-FLCs in real-time applications thanks to the presented interpretations on the design parameters of the GT2-FLCs, the proposed design and tuning approaches for the GT2-FLCs, and the presented analyses of the design parameters on the GT2-FLC's performance, robustness, sensitivity, and computational time.



REFERENCES

- [1] **Zadeh, L. A.** (1965). Fuzzy sets, *Information and Control*, 8(3), 338-353.
- [2] **Zadeh, L. A.** (1973). Outline of a new approach to the analysis of complex systems and decision processes, *IEEE Transactions on Systems, Man, and Cybernetics*, 3(1), 28-44.
- [3] **Mamdani, E. H.** (1974). Application of fuzzy logic algorithms for control of simple dynamic plant, *Proceedings of the Institution of Electrical Engineering*, 121(12), 1585-1588.
- [4] **Mamdani, E. H. and Assilian, S.** (1975). An experiment in linguistic synthesis with a fuzzy logic controller, *International Journal of Man-Machine Studies*, 7(1), 1-13.
- [5] **Takagi, T. and Sugeno, M.** (1985). Fuzzy identification of systems and its application to modeling and control. *IEEE Transactions on Systems, Man, and Cybernetics*, 15(1), 116-132.
- [6] **Sugeno, M. and Kang, G. T.** (1988). Structure identification of fuzzy model. *Fuzzy Sets and Systems*, 28(1), 15-33.
- [7] **Mendel, J. M.** (2017). *Uncertain Rule-Based Fuzzy Systems, Introduction and New Directions*, Second Ed., Springer, Cham, Switzerland.
- [8] **Sugeno, M. and Yasukawa, T.** (1993). A fuzzy-logic-based approach to qualitative modeling. *IEEE Transactions on Fuzzy Systems*, 1(1), 7-31.
- [9] **Galichet, S. and Foulloy, L.** (1995). Fuzzy controllers: synthesis and equivalences, *IEEE Transactions on Fuzzy Systems*, 3(2), 140-148.
- [10] **Mizumoto, M.** (1995). Realization of PID controls by fuzzy control methods, *Fuzzy Sets and Systems*, 70(2-3), 171-182.
- [11] **Qiao, W. Z. and Mizumoto, M.** (1996). PID type fuzzy controller and parameters adaptive method, *Fuzzy Sets and Systems*, 78(1), 23-35.
- [12] **Li, H. X. and Gatland, H. B.** (1996). Conventional fuzzy control and its enhancement, *IEEE Transactions on Systems, Man, and Cybernetics, Part B*, 26(5), 791-796.
- [13] **Li, H. X., Gatland, H. B., and Green, A. W.** (1997). Fuzzy variable structure control, *IEEE Transactions on Systems, Man, and Cybernetics, Part B*, 27(2), 306-312.
- [14] **Mudi, R. K. and Pal, N. R.** (1999). A robust self-tuning scheme for PI- and PD-type fuzzy controllers, *IEEE Transactions on Fuzzy Systems*, 7(1), 2-16.
- [15] **Xu, J. X., Hang, C. C., and Liu, C.** (2000). Parallel structure and tuning of a fuzzy PID controller. *Automatica*, 36(5), 673-684.

- [16] **Woo, Z. W., Chung, H. Y., and Lin, J. J.** (2000). A PID type fuzzy controller with self-tuning scaling factors, *Fuzzy Sets and Systems*, 115(2), 321-326.
- [17] **Guzelkaya, M., Eksin, I., and Yesil, E.** (2003). Self-tuning of PID-type fuzzy logic controller coefficients via relative rate observer, *Engineering Applications of Artificial Intelligence*, 16(3), 227-236.
- [18] **Yesil, E., Guzelkaya, M., and Eksin, I.** (2004). Self-tuning fuzzy PID type load and frequency controller, *Energy Conversion and Management*, 45(3), 377-390.
- [19] **Duan, X. G., Li, H. X., and Deng, H.** (2008). Effective tuning method for fuzzy PID with internal model control, *Industrial & Engineering Chemistry Research*, 47(21), 8317-8323.
- [20] **Ahn, K. K. and Truong, D. Q.** (2009). Online tuning fuzzy PID controller using robust extended Kalman filter, *Journal of Process Control*, 19(6), 1011-1023.
- [21] **Yesil, E., Sakalli, A., Ozturk, C., and Kumbasar, T.** (2013). Online fuzzy rule weighting method for fuzzy PID controllers via big bang - big crunch optimization, *IEEE International Conference on Fuzzy Systems*.
- [22] **Zadeh, L. A.** (1975). The concept of a linguistic variable and its application to approximate reasoning, *Information Science*, 19(3-4), 829-841.
- [23] **Karnik, N. N., Mendel, J. M., and Liang, Q.** (1999). Type-2 fuzzy logic systems, *IEEE Transactions on Fuzzy Systems*, 7(6), 643-658.
- [24] **Liang, Q. and Mendel, J. M.** (2000). Interval type-2 fuzzy logic systems: theory and design, *IEEE Transactions on Fuzzy Systems*, 8(5), 535-550.
- [25] **Wu, H., and Mendel, J. M.** (2002). Uncertainty bounds and their use in the design of interval type-2 fuzzy logic systems, *IEEE Transactions on Fuzzy Systems*, 10(5), 622-639.
- [26] **Hagras, H.** (2004). A hierarchical type-2 fuzzy logic control architecture for autonomous mobile robots, *IEEE Transactions on Fuzzy Systems*, 12(4), 524-539.
- [27] **Wu, D. and Tan, W. W.** (2006). Genetic learning and performance evaluation of interval type-2 fuzzy logic controllers. *Engineering Applications of Artificial Intelligence*, 19(8), 829-841.
- [28] **Wu, D. and Tan, W. W.** (2006). A simplified type-2 fuzzy logic controller for real-time control. *ISA Transactions*, 45(4), 503-516.
- [29] **Mendel, J. M.** (2007). Type-2 fuzzy sets and systems: an overview. *IEEE Computational Intelligence Magazine*, 2(1), 20-29.
- [30] **Castillo, O. and Melin, P.** (2008). *Type-2 Fuzzy Logic Theory and Applications*. Springer-Verlag, Berlin, Germany.
- [31] **Mendel, J. M., Hagras, H., Tan, W. W., Melek, W. W., and Ying, H.** (2014). *Introduction to Type-2 Fuzzy Logic Control*. John Wiley and IEEE Press, Hoboken, NJ.

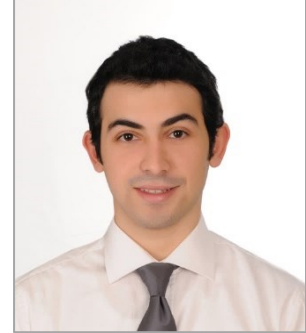
- [32] **Wu, D. and Tan, W. W.** (2010). Interval type-2 fuzzy PI controllers: why they are more robust. *IEEE International Conference on Granular Computing*, 802-807.
- [33] **Wu, D.** (2012). On the fundamental differences between type-1 and interval type-2 fuzzy logic controllers. *IEEE Transactions on Fuzzy Systems*, 20(5), 832-848.
- [34] **Kumbasar, T., Eksin, I., Guzelkaya, M., and Yesil, E.** (2011). Interval Type-2 Fuzzy Inverse Controller Design in Nonlinear IMC Structure. *Engineering Applications of Artificial Intelligence*, 24(6), 996-1005.
- [35] **Kumbasar, T., Eksin, I., Guzelkaya, M., and Yesil, E.** (2012). Type-2 fuzzy model based controller design for neutralization processes. *ISA Transactions*, 51(2), 277-287.
- [36] **Kumbasar, T.** (2013). A simple design method for interval type-2 fuzzy PID controllers, *Soft Computing*, 18, 1293-1304.
- [37] **Kumbasar, T. and Hagrass, H.** (2014). Big Bang–Big Crunch optimization based interval type-2 fuzzy PID cascade controller design strategy. *Information Sciences*, 282(20), 277-295.
- [38] **Sakalli, A., Kumbasar, T., Dodurka, M. F., and Yesil, E.** (2014). The simplest interval type-2 fuzzy PID controller: structural analysis. *IEEE International Conference on Fuzzy Systems*.
- [39] **Yesil, E.** (2014). Interval type-2 fuzzy PID load frequency controller using Big Bang-Big Crunch optimization. *Applied Soft Computing*, 15, 100-112.
- [40] **Sakalli, A., Kumbasar, T., Yesil, E., and Hagrass, H.** (2014). Analysis of the performances of type-1, self-Tuning type-1 and interval type-2 fuzzy PID controllers on the magnetic levitation system. *IEEE International Conference on Fuzzy Systems*.
- [41] **Kumbasar, T.** (2016). Robust stability analysis and systematic design of single-input interval type-2 fuzzy logic controllers. *IEEE Transactions on Fuzzy Systems*, 24(3), 675-694.
- [42] **Sakalli, A., Beke, A., and Kumbasar, T.** (2016). Gradient descent and extended Kalman filter based self-tuning interval type-2 fuzzy PID controllers. *IEEE International Conference on Fuzzy Systems*.
- [43] **Sakalli, A. and Kumbasar, T.** (2017). On the design and gain analysis of IT2-FLC with a case study on an electric vehicle. *IEEE International Conference on Fuzzy Systems*.
- [44] **Sakalli, A., Beke, A., and Kumbasar, T.** (2018). Analyzing the control surfaces of type-1 and interval type-2 FLCs through an experimental study. *IEEE International Conference on Fuzzy Systems*.
- [45] **Sarabakha, A., Fu, C., and Kayacan, E.** (2019) Intuit before tuning: type-1 and type-2 fuzzy logic controllers, *Applied Soft Computing*, 81.
- [46] **Karnik, N. N. and Mendel, J. M.** (2001). Centroid of a type-2 fuzzy set. *Information Sciences*, 132(1-4), 195-220.
- [47] **Wu, D. and Mendel, J. M.** (2009). Enhanced Karnik-Mendel algorithms. *IEEE Transactions on Fuzzy Systems*, 17(4), 923-934.

- [48] **Dodurka, M. F., Kumbasar, T., Sakalli, A., and Yesil, E.** (2014). Boundary function based Karnik-Mendel type-reduction method for interval type-2 fuzzy PID controllers. *IEEE International Conference on Fuzzy Systems*.
- [49] **Sakalli, A. and Kumbasar, T.** (2015) On the fundamental differences between the NT and the KM center of sets calculation methods on the IT2-FLC performance. *IEEE International Conference on Fuzzy Systems*.
- [50] **Mendel, J. M. and John, R. I.** (2002). Type-2 fuzzy sets made simple. *IEEE Transactions on Fuzzy Systems*, 10(2), 808-821.
- [51] **Mendel, J. M., John, R., and Liu, F.** (2006). Interval type-2 fuzzy logic systems made simple. *IEEE Transactions on Fuzzy Systems*, 14(6), 808-821.
- [52] **Coupland, S. and John, R. I.** (2007). Geometric type-1 and type-2 fuzzy logic systems. *IEEE Transactions on Fuzzy Systems*, 15(1), 3-15.
- [53] **Aisbett, J., Rickard, J. T., and Morgenthaler, D. G.** (2010). Type-2 fuzzy sets as functions on spaces. *IEEE Transactions on Fuzzy Systems*, 18(4), 3-15.
- [54] **Bustince, H., Fernandez, J., Hageras, H., Herrera, H., Pagola, M., and Barrenechea, E.** (2015). Interval type-2 fuzzy sets are generalization of interval-valued fuzzy sets: towards a wide view on their relationship. *IEEE Transactions on Fuzzy Systems*, 23(5), 1876–1882.
- [55] **Mendel, J. M.** (2018). Explaining the performance potential of rule-based fuzzy systems as a greater sculpting of the state space*, *IEEE Transactions on Fuzzy Systems*, 26(4), 2362-2373.
- [56] **Lam, H. K. and Seneviratne, L. D.** (2008). Stability analysis of interval type-2 fuzzy-model-based control systems, *IEEE Transactions on Systems, Man and Cybernetics Part B: Cybernetics*, 38(3), 617-628.
- [57] **Biglarbegian, M., Melek, W. W., and Mendel, J. M.** (2010). On the stability of interval type-2 TSK fuzzy logic control systems, *IEEE Transactions on Systems, Man and Cybernetics Part B: Cybernetics*, 40(3), 798-818.
- [58] **Du, X. and Ying, H.** (2010). Derivation and analysis of the analytical structures of the interval type-2 fuzzy-PI and PD controllers, *IEEE Transactions on Fuzzy Systems*, 18(4), 802-814.
- [59] **Nie, M. and Tan, W. W.** (2010). Analytical structure and characteristic of symmetric Karnik-Mendel type-reduced interval type-2 fuzzy PI and PD controllers, *IEEE Transactions on Fuzzy Systems*, 20(3), 416-430.
- [60] **Mendel, J. M.** (2019). Comparing the performance potentials of interval and general type-2 rule-based fuzzy systems in terms of sculpting the state space. *IEEE Transactions on Fuzzy Systems*, 27(1), 58-71.
- [61] **Liu, F.** (2008). An efficient centroid type-reduction strategy for general type-2 fuzzy logic system. *Information Sciences*, 178(9), 2224-2236.
- [62] **Mendel, J. M., Liu, F., and Zhai, D.** (2009) α -plane representation for type-2 fuzzy sets: Theory and applications. *IEEE Transactions on Fuzzy Systems*, 17(5), 1189-1207.

- [63] **Wagner, C. and Hagrass, H.** (2008) zSlices-Towards bridging the gap between interval and general type-2 fuzzy logic. *IEEE International Conference on Fuzzy Systems*.
- [64] **Wagner, C. and Hagrass, H.** (2010). Toward general type-2 fuzzy logic systems based on zSlices, *IEEE Transactions on Fuzzy Systems*, 18(4), 637-660.
- [65] **Mendel, J. M.** (2010) Comments on “ α -plane representation for type-2 fuzzy sets: theory and applications”. *IEEE Transactions on Fuzzy Systems*, 18(1), 229-230.
- [66] **Zhai, D. and Mendel, J. M.** (2012). Comment on “toward general type-2 Fuzzy logic systems based on zSlices”. *IEEE Transactions on Fuzzy Systems*, 20(5), 996-997.
- [67] **Mendel, J. M.** (2014). General type-2 fuzzy logic systems made simple: A tutorial. *IEEE Transactions on Fuzzy Systems*, 22(5), 1162-1182.
- [68] **Kumbasar, T., and Hagrass, H.** (2015) A self-tuning zSlices based general type-2 fuzzy PI controller. *IEEE Transactions on Fuzzy Systems*, 23(4), 991-1013.
- [69] **Sanchez, M. A., Castillo, O., and Castro J. R.** (2015). Generalized type-2 fuzzy systems for controlling a mobile robot and a performance comparison with interval type-2 and type-1 fuzzy systems. *Expert Systems with Applications*, 42(14), 5904-5914.
- [70] **Castillo, O., Angulo, L. A., Castro, J. R., and Valdez, M. G.** (2016). A comparative study of type-1 fuzzy logic systems, interval type-2 fuzzy logic systems and generalized type-2 fuzzy logic systems in control problems. *Information Sciences*, 354, 257-274.
- [71] **Mohammadzadeh, A., Ghaemi, S., Kaynak, O., and Khanmohammadi, S.** (2016). Observer-based method for synchronization of uncertain fractional order chaotic systems by the use of a general type-2 fuzzy system. *Applied Soft Computing*, 49, 554-560.
- [72] **Khooban, M. H., Vafamand, N., Liaghat A., and Dragicevic, T.** (2017) An optimal general type-2 fuzzy controller for urban traffic network. *ISA Transactions*, 66, 335-343.
- [73] **Castillo, O. and Angulo, L. A.** (2018). A generalized type-2 fuzzy logic approach for dynamic parameter adaptation in bee colony optimization applied to fuzzy controller design. *Information Sciences*, 460-461, 476-496.
- [74] **Shi, J. Z.** (2020). A fractional order general type-2 fuzzy PID controller design algorithm. *IEEE Access*, 8, 52151-52172.
- [75] **Sakalli, A., Kumbasar, T., and Mendel, J. M.** (2020). A design approach for general type-2 fuzzy logic controllers with an online scheduling mechanism. *IEEE International Conference on Fuzzy Systems*.
- [76] **Sakalli, A., Kumbasar, T., and Mendel, J. M.** (2020). Towards systematic design of general type-2 fuzzy logic controllers: analysis, interpretation and tuning, *IEEE Transactions on Fuzzy Systems (early access)*.



CURRICULUM VITAE



Name Surname : Ahmet SAKALLI
Place and Date of Birth : Söke/Aydın, 04.09.1989
E-Mail : sakallia@itu.edu.tr

EDUCATION:

- **B.Sc.** : 2012, Istanbul Technical University, Faculty of Electrical and Electronics Engineering, Control and Automation Engineering Department
- **M.Sc.** : 2014, Istanbul Technical University, Graduate School of Science Engineering and Technology, Department of Control and Automation Engineering

PUBLICATIONS, PRESENTATIONS AND PATENTS ON THE THESIS:

- **Sakalli, A.** and Kumbasar, T. (2017). On the design and gain analysis of IT2-FLC with a case study on an electric vehicle. *IEEE International Conference on Fuzzy Systems*.
- **Sakalli, A.,** Beke, A., and Kumbasar, T. (2018). Analyzing the control surfaces of type-1 and interval type-2 FLCs through an experimental study. *IEEE International Conference on Fuzzy Systems*.
- **Sakalli, A.,** Kumbasar, T., and Mendel, J. M. (2020). A design approach for general type-2 fuzzy logic controllers with an online scheduling mechanism. *IEEE International Conference on Fuzzy Systems*.
- **Sakalli, A.,** Kumbasar, T., and Mendel, J. M. (2020). Towards systematic design of general type-2 fuzzy logic controllers: analysis, interpretation and tuning, *IEEE Transactions on Fuzzy Systems (early access)*.

OTHER PUBLICATIONS, PRESENTATIONS AND PATENTS:

- **Sakalli, A.**, Kumbasar, T., Yesil E., ad Hagraş, H. (2014). Analysis of the performances of type-1, self-Tuning type-1 and interval type-2 fuzzy PID controllers on the magnetic levitation system. *IEEE International Conference on Fuzzy Systems*.
- **Sakalli, A.**, Kumbasar, T., Dodurka M. F., and Yesil, E. (2014). The simplest interval type-2 fuzzy PID controller: structural analysis. *IEEE International Conference on Fuzzy Systems*.
- Dodurka, M. F., Kumbasar, T., **Sakalli, A.**, and Yesil, E. (2014). Boundary function based Karnik-Mendel type-reduction method for interval type-2 fuzzy PID controllers. *IEEE International Conference on Fuzzy Systems*.
- Yesil, E., Dodurka, M. F., Kumbasar, T., and **Sakalli, A.** (2014). Peak observer based self-tuning of type-2 fuzzy PID controllers. *International Conference on Artificial Intelligence Applications and Innovations*.
- **Sakalli, A.**, and Kumbasar, T. (2015) On the fundamental differences between the NT and the KM center of sets calculation methods on the IT2-FLC performance. *IEEE International Conference on Fuzzy Systems*.
- **Sakalli, A.**, Beke, A., and Kumbasar, T. (2016). Gradient descent and extended Kalman filter based self-tuning interval type-2 fuzzy PID controllers. *IEEE International Conference on Fuzzy Systems*.
- Aktekin, O., **Sakalli, A.**, Ongun, M. A., Palaz, C., Hacıoglu, F., and Altin, I. (2017). System design of a human electric hybrid vehicle. *European Automotive Congress*.
- Ongun, M. A., Aktekin, O., and **Sakalli, A.** (2017). Functional safety analysis of a human electric hybrid vehicle. *European Automotive Congress*.
- Hacıoglu, F., Altin, I., Aktekin, O., and **Sakalli, A.** (2017). Predictive rule based optimization techniques for series hybrid electric vehicle. *25th Mediterranean Conference on Control and Automation*.
- **Sakalli, A.**, Aktekin, O., and Kiran, U. (2018). Hardware in the Loop (HiL) testing of a human electric hybrid vehicle. *IEEE 19th International Conference on Industrial Technology*.
- Yesilyurt, A. Y., **Sakalli, A.**, Hacıoglu, F., and Mungan, M. A. (2019). Fuzzy Logic Controller and Load Point Selection Based Fuel-Efficient Hybrid Controller for PSHEVs. *International Conference on Electrical and Electronics Engineering*.
- Ongun, M. A., Kiran, U., and **Sakalli, A.** (2020). System design and simulation of a human electric hybrid vehicle in AVL CRUISE. *IEEE International Symposium on Systems Engineering*.